CANADIAN THESES ON MICROFICHE

I.S.B.N.

THESES CANADIENNES SUR MICROFICHE

National Library of Canada
Collections Development Branch

Canadian Theses on
Microfiche Service

Ottawa, Canada
K1A 0N4

Bibliothèque nationale du Canada
Direction du développement des collections

Service des thèses canadiennes
sur microfiche

NOTICE

The quality of this microfiche is heavily dependent upon the quality of the original thesis submitted for microfilming. Every effort has been made to ensure the highest quality of reproduction possible.

If pages are missing, contact the university which granted the degree.

Some pages may have indistinct print especially if the original pages were typed with a poor typewriter ribbon or if the university sent us a poor photocopy.

Previously copyrighted materials (journal articles, published tests, etc.) are not filmed.

Reproduction in full or in part of this film is governed by the Canadian Copyright Act, R.S.C. 1970, c. C-30. Please read the authorization forms which accompany this thesis.

THIS DISSERTATION
HAS BEEN MICROFILMED
EXACTLY AS RECEIVED

AVIS

La qualité de cette microfiche dépend grandement de la qualité de la thèse soumise au microfilmage. Nous avons tout fait pour assurer une qualité supérieure de reproduction.

S'il manque des pages, veuillez communiquer avec l'université qui a conféré le grade.

La qualité d'impression de certaines pages peut laisser à désirer, surtout si les pages originales ont été dactylographiées à l'aide d'un ruban usé ou si l'université nous a fait parvenir une photocopie de mauvaise qualité.

Les documents qui font déjà l'objet d'un droit d'auteur (articles de revue, examens publiés, etc.) ne sont pas microfilmés.

La reproduction, même partielle, de ce microfilm est soumise à la Loi canadienne sur le droit d'auteur, SRC 1970, c. C-30. Veuillez prendre connaissance des formules d'autorisation qui accompagnent cette thèse.

LA THÈSE A ÉTÉ
MICROFILMÉE TELLE QUE
NOUS L'AVONS REÇUE

NL-339 (r. 82/08)

Canada

National Library of Canada
Canadian Theses Division
Ottawa, Canada
K1A 0N4

Bibliothèque nationale du Canada
Division des thèses canadiennes

0-315-06112-X

54032

PERMISSION TO MICROFILM — AUTORISATION DE MICROFILMER

- Please print or type — Écrire en lettres moulées ou dactylographier

Full Name of Author — Nom complet de l'auteur
JOHN VINCENT SIMMONS

Date of Birth — Date de naissance
16 MAY 1980

Country of Birth — Lieu de naissance
AUSTRALIA

Permanent Address — Résidence fixe
53 Raglan Street
St Lucia Queensland, 4067
AUSTRALIA

Title of Thesis — Titre de la thèse
SHEARBAND YIELDING AND STRAIN WEAKENING

University — Université
UNIVERSITY OF ALBERTA

Degree for which thesis was presented — Grade pour lequel cette thèse fut présentée
Ph. D.

Year this degree conferred — Année d'obtention de ce grade
1981 (Fall)

Name of Supervisor — Nom du directeur de thèse
PROF. N. R. MORGENSTERN

Permission is hereby granted to the NATIONAL LIBRARY OF CANADA to microfilm this thesis and to lend or sell copies of the film.

The author reserves other publication rights, and neither the thesis nor extensive extracts from it may be printed or otherwise reproduced without the author's written permission.

L'autorisation est, par la présente, accordée à la BIBLIOTHÈQUE NATIONALE DU CANADA de microfilmer cette thèse et de prêter ou de vendre des exemplaires du film.

L'auteur se réserve les autres droits de publication; ni la thèse ni de longs extraits de celle-ci ne doivent être imprimés ou autrement reproduits sans l'autorisation écrite de l'auteur.

Date
16 October 1981

Signature
JV Simmons

NL-91 (4/77)

THE UNIVERSITY OF ALBERTA

SHEARBAND YIELDING AND STRAIN WEAKENING

by

© JOHN VINCENT SIMMONS

A THESIS

SUBMITTED TO THE FACULTY OF GRADUATE STUDIES AND RESEARCH

IN PARTIAL FULFILMENT OF THE REQUIREMENTS FOR THE DEGREE

OF DOCTOR OF PHILOSOPHY

CIVIL ENGINEERING

EDMONTON, ALBERTA

FALL 1981

THE UNIVERSITY OF ALBERTA

RELEASE FORM

NAME OF AUTHOR JOHN VINCENT SIMMONS

TITLE OF THESIS SHEARBAND YIELDING AND STRAIN WEAKENING

DEGREE FOR WHICH THESIS WAS PRESENTED DOCTOR OF PHILOSOPHY

YEAR THIS DEGREE GRANTED FALL 1981

Permission is hereby granted to THE UNIVERSITY OF ALBERTA LIBRARY to reproduce single copies of this thesis and to lend or sell such copies for private, scholarly or scientific research purposes only.

The author reserves other publication rights, and neither the thesis nor extensive extracts from it may be printed or otherwise reproduced without the author's written permission.

(SIGNED) ...JV Simmons...

J.V. Simmons

PERMANENT ADDRESS:

53 Raglan Street,
St Lucia, Queensland 4067,
AUSTRALIA

DATED: 9th of October, 1981

THE UNIVERSITY OF ALBERTA

FACULTY OF GRADUATE STUDIES AND RESEARCH

The undersigned certify that they have read, and recommend to the Faculty of Graduate Studies and Research, for acceptance, a thesis entitled SHEARBAND YIELDING AND STRAIN WEAKENING submitted by JOHN VINCENT SIMMONS in partial fulfilment of the requirements for the degree of DOCTOR OF PHILOSOPHY.

....
N.R. Morgenstern
Supervisor

....
Z. Eisenstein

....
T.M. Hrudey

J.R. Colbourne
....
J.R. Colbourne

....
H.-Y. Ko
Boulder, Colorado
External Examiner

Date: 9th of October, 1981

ABSTRACT

The mechanics of postpeak yielding of dense-structured soils (and to a limited extent, rocks) has been examined. In most instances, yielding of these materials tends to localize along shearzones. The behaviour of shearzones is examined and a mechanistic approach has been found suitable for describing the postpeak yield process. Under natural conditions, depositional and environmental factors often lead to controls on shearzone location which greatly simplify analysis of the yielding process.

Suitable one-dimensional closed-form models and finite element analytical procedures are examined and, where necessary, developed, in order to carry out deformation analysis of shearzone yielding. Application of these techniques to simple problems met with limited success, and obviously further development work is required before a wide range of shearzone yielding problems can be confidently managed.

Two important case histories are examined. The progressive failure postulated to have developed at the Saxon Clay Pit seems unlikely in light of the deformation analysis results. The behaviour of the foundation shearzones of Gardiner Dam demonstrates some limitations of design based on limit-equilibrium techniques, and the deformation analysis has helped to clarify the mechanisms of movement in the foundation.

ACKNOWLEDGEMENTS

This thesis is the outcome of a sustained period of research effort. The guidance, support, and interest of Dr. N.R. Morgenstern, who supervised this work, is gratefully appreciated.

Financial assistance provided by a Natural Sciences and Engineering Research Council postgraduate scholarship, and later a scholarship from the Alberta Oil Sands Technology and Research Authority, is acknowledged with thanks.

Close consultation with Dr. Morgenstern and the Geotechnical Division of the Prairie Farm Rehabilitation Administration was of great benefit in determining the outcome of the analyses of Gardiner Dam. Mr. J.L. Jaspar and Mr. N. Peters are particularly thanked for their assistance in carrying out this work.

This thesis was completed while the writer was employed by Golder Associates in Edmonton. The support, encouragement, and understanding of Dr. J.M. Laing during this period was a great inspiration.

Particular appreciation is extended to Oldrich Hungr, who assisted in the development of the CWX model discussed in Chapter 3. Bryan Watts, Kevin Sterne, and Don Sargent used the writer's computer programs and thus acted as willing test subjects whose advice and comments were greatly valued. Discussions with Dr. D.H. Trollope during the early formative stages of this research in Townsville, Australia, were also of great assistance.

Thesis writing is not an easy task. Editorial assistance is even less easy, and so the efforts and contributions of John Root and Dr. Maurice Dusseault have been particularly appreciated. Data entry assistance from Mireille Dubreuil and Linda Neilsen is acknowledged with thanks, and the drafting services of Jerry Comeau, Andy Tsang, and Gerry Cyre have been most helpful.

Geotechnical research at the University of Alberta takes place in an exceptional environment. Technical and social interactions with fellow students and staff have been a major part of the writers life for many years, and no individual details will ever justly record the value of these relationships. My friends know who they are.

DEDICATION

This work could not have been accomplished without the love and patient support of my wife Claudia Baldwin, and the cheerful acceptance of my infant son Christopher.

Additionally, my parents Dorothy and Vince Simmons and my brother Hugh have steadfastly supported me through the "thesis years", despite the ravages of international communications. During the "thesis years" I acquired Canadian parents-in-law, Lois and Clif Baldwin, who have become my enthusiastic supporters.

To all these people I owe a special debt of gratitude. They all believe unquestionably in basic human qualities of faith, charity, hope and kindness.

This thesis is dedicated to Claudia and to Christopher in the faith that, as a family, we will grow together. We have, through our family ties, the best possible examples to follow.

Table of Contents

Chapter Page

1. INTRODUCTION 1
   1.1 PROGRESSIVE FAILURE 2
   1.2 DEFINITIONS OF SHEARZONE YIELDING BEHAVIOUR 7
   1.3 AIMS OF RESEARCH PROGRAM 12
2. A MECHANISTIC VIEW OF SHEARZONE YIELDING 15
   2.1 PHYSICAL VIEWPOINT 16
   2.2 MECHANISTIC VIEWPOINT 32
   2.3 LOCALIZATION MECHANICS 47
   2.4 MODELLING SHEARZONES AND PROGRESSIVE FAILURE 55
   2.5 SUMMARY OF THE MECHANISTIC VIEWPOINT 72
3. ANALYTICAL MODELS 76
   3.1 ONE-DIMENSIONAL ANALYTICAL MODELS 77
   3.2 NONLINEAR ELASTIC CONSTITUTIVE MODELLING 85
   3.3 ELASTOPLASTIC CONSTITUTIVE MODELLING 89
   3.4 ROWE'S STRESS-DILATANCY MODEL 101
   3.5 A POST-PEAK PLASTICITY MODEL 114
   3.6 REVIEW OF ANALYTICAL CONCEPTS 117
4. FINITE ELEMENT ANALYTICAL TECHNIQUE 119
   4.1 REVIEW OF DESIGN CRITERIA 119
   4.2 COMPUTATIONAL ASPECTS 132
   4.3 COMPUTER PROGRAM CHOICES 140
   4.4 REVIEW OF PROGRAM DESIGN 147
   4.5 TEST PROBLEM: ACCURACY OF THE Q48 ELEMENT 158
5. BEHAVIOUR OF COMPUTATIONAL MODELS 164
   5.1 DERIVATION OF MODEL PARAMETERS 165
   5.2 SIMPLE PLANE STRAIN TEST SIMULATION 179

5.3 BEHAVIOUR OF A NONHOMOGENEOUS TEST 187

5.4 BEARING-CAPACITY PROBLEMS 199

5.5 CONCLUSIONS CONCERNING COMPUTATIONAL MODELS 212

6. SHEARBAND PROPAGATION IN THE SAXON CLAY PIT WALL 214

6.1 REVIEW OF FIELD BEHAVIOUR 215

6.2 APPLICATION OF ONE-DIMENSIONAL MODELS 230

6.3 FINITE ELEMENT ANALYSIS PROCEDURES 243

6.4 SIMULATION OF EXCAVATION BEHAVIOUR 258

6.5 CONCLUSIONS REGARDING BEHAVIOUR 272

7. SHEARBAND BEHAVIOUR IN GARDINER DAM FOUNDATIONS 286

7.1 REVIEW OF FIELD BEHAVIOUR 287

7.2 FINITE ELEMENT ANALYSIS PROCEDURES 292

7.3 SIMULATION OF CONSTRUCTION 309

7.4 SIMULATION OF OPERATION 319

7.5 SUMMARY AND CONCLUSIONS 336

8. SUMMARY, CONCLUSIONS, AND RECOMMENDATIONS 339

8.1 PERFORMANCE OF THE NUMERICAL MODELS 339

8.2 ROLE OF DEFORMATION ANALYSIS 341

8.3 AREAS MOST WARRANTING FURTHER RESEARCH 342

8.4 RECOMMENDATIONS FOR FUTURE WORK 344

REFERENCES 346

APPENDIX A 364

APPENDIX B 373

APPENDIX C 378

APPENDIX D 384

List of Tables

Table Page

5.1 Model Parameters for SD, CRD, and PPP Analyses 180

6.1 Parameters Used in Saxon Clay Pit Deformation Analysis 250

7.1 Parameters Used for Nonlinear Elastic Loading 311

7.2 Parameters Used for Elastic Unloading 327

List of Figures

Figure Page

1.1 Stress-Deformation and Strength Response 9

2.1 Prepeak Microstructure and Response Characteristics 22

2.2 Postpeak Granular Shearzone Characteristics 26

2.3 Postpeak Cohesive Shearzone Characteristics 27

2.4 Evolution of Shearzone Structure for Cohesive Material 33

2.5 Phenomenological Block Models for Strain Weakening 35

2.6 Fracture Modes, with Applications to Rock Mechanics 37

2.7 Simplified Postpeak Model Behaviour 42

2.8 Kinematic Discontinuity Conditions 45

2.9 Predictions of Localization in Elastoplastic Material 49

2.10 Localization Modes for Biaxial Tests on Sand 53

2.11 Time-Dependent Progressive Failure in a Slope 58

2.12 Substructuring Technique for Failure Modelling 61

2.13 Schematic View of Antiplane Shear Model of Faulting 63

2.14 Example Applications of Boundary Integral Methods 65

2.15 Hybrid Element Scheme for Shearband Development 67

2.16 Wedge Style Slope Failure Mechanism 71

3.1 Typical One-Dimensional Progressive Failure Model 78

Figure Page

3.2 Terminology and Results, CW Model 80

3.3 Characteristics of PR Model 81

3.4 Terminology and Results, CWX Model 84

3.5 Transverse-Isotropic Material 86

3.6 Schematic Nonlinear Elastic Shearband Material 88

3.7 Constant-Rate-Of-Dilation Elastoplastic Material 92

3.8 Stress and Strain Increments and Stress-Dilatancy Relationship 104

3.9 R-D Plot for Typical Triaxial Test 105

3.10 R-D Plots for Plane Strain Tests with Variable Sand Fabrics 107

3.11 Schematic Post-Peak-Plasticity Elastoplastic Material 116

4.1 Examples of Finite Elements for Localization Research 122

4.2 Elements for Representing Shearbands 125

4.3 Higher-Order Isoparametric Elements 127

4.4 Nonlinear Elastic and Elastoplastic Model Capabilities 133

4.5 Nonlinear Elastic Computational Procedure 137

4.6 Elastoplastic Computational Procedure 139

4.7 Q48 Element Configurations 149

4.8 Isoparametric Element Gauss Points 153

4.9 Simplified Elastoplastic Response 156

4.10 Double-Edge-Cracked Plate Problem 159

4.11 Analytical Solutions for D.E.C. Plate Problem 161

4.12 Results of F.E. Analysis of D.E.C. Plate

Figure Page

Problem 162

5.1 R-D Path Plots for Brasted Sand Tests 167

5.2 Comparison of R-D Plots at Peak Strength 168

5.3 Dilatancy Rate Function for Brasted Sand 170

5.4 Effect of Stress Regime on Dilatancy Rate 172

5.5 Comparison of Predicted and Measured Strengths 173

5.6 Dilatancy Rates Consistent with Measured Strengths 175

5.7 Elastic Moduli Derived from Tests 176

5.8 Interpretation of Elastic Behaviour Component 177

5.9 Simple Plane Strain Test Simulation 181

5.10 Measured and Simulated Tests on Dense Sand 182

5.11 Measured and Simulated Tests on Loose-Medium Sand 183

5.12 Void Ratio Changes During Simulated Tests 185

5.13 Simple Plane Strain Test with Shearband 188

5.14 Stress Sampling Points for Shearband Simulation 189

5.15 Lack of Convergence for Shearband Simulations 192

5.16 Convergence Characteristics for Shearband Simulations 195

5.17 Deformations During Shearband Simulation 196

5.18 Bearing Capacity Problem on Cohesive Soil 201

5.19 Load-Deformation Response for Bearing Capacity Problem 203

5.20 Yield Zones for Bearing Capacity Problem 204

Figure Page

5.21 Convergence Characteristics for Bearing Capacity Problem 205

5.22 Load-Deformation Problem on Frictional Soil 208

5.23 Results of Load-Deformation Problem 209

5.24 Yielding Zones at Collapse for Load-Deformation Problem 210

5.25 Convergence Characteristics for Load-Deformation Problem 211

6.1 Plan View of Excavation Face, Saxon Clay Pit 217

6.2 Geology and Excavation Cross-Section 218

6.3 Summary Geotechnical Properties 220

6.4 Direct Shear Test Summary Data 222

6.5 Typical Overthrust Gauge Movements 225

6.6 Vertical Extension Pattern Variation with Time 227

6.7 Summary Surface Displacements 228

6.8 Inferred Surface Displacement Trajectories 229

6.9 Inferred Shearband Yield Mechanism 231

6.10 Idealized Slope for Analysis 233

6.11 One-Dimensional Model Predictions for E = 200Mpa 236

6.12 One-Dimensional Model Predictions for E = 400Mpa 237

6.13 Postpeak Stiffness Derivation for CWX Model 241

6.14 Simulation of Construction Procedure 246

6.15 Assessment of Optimum Shearband Thickness 252

6.16 Shearband Tip Detailing 253

Figure Page

6.17 Uniform Elastic Notch Stresses 255

6.18 Outline of Finite Element Mesh 257

6.19 Improved Convergence Technique 261

6.20 Horizontal Displacements at Stage I of Excavation 263

6.21 Boundary Stresses for Stage II Unloading 264

6.22 Stress-Deformation Response, CRD Elastoplastic Model 267

6.23 Incremental Displacements, CRD Elastoplastic Model 268

6.24 Stress-Deformation Response, Nonlinear Elastic Model 270

6.25 Incremental Displacements, Nonlinear Elastic Model 271

6.26 Schematic Interpretations of Response 274

6.27 Comparison of Measured and Predicted Incremental Behaviour 277

7.1 General Layout of Gardiner Dam 289

7.2 Selected Postconstruction Displacements 291

7.3 Coteau Creek Section Performance Summary 293

7.4 Simplified Coteau Creek Embankment Cross-Section 296

7.5 Finite Element Mesh Detail Showing Elements 297

7.6 Finite Element Mesh Detail Showing Nodes 298

7.7 Construction Loading Procedure 303

7.8 Loading Schemes for Simulating Reservoir Impounding 306

7.9 Schematic Unloading/Reloading Response 308

7.10 Displacement Patterns, First Trial

Figure Page

Construction 312

7.11 Location of Movement Measurement Lines 315

7.12 Total Horizontal Movement Predictions for E.O.C. 316

7.13 Shearband Strength Mobilization Predictions for E.O.C. 318

7.14 Shearband Slip Predictions During Construction 320

7.15 Incremental Horizontal Movement Predictions for Impounding 322

7.16 Shearband Slip Predictions During Impounding 323

7.17 Shearband Strength Mobilization Predictions for Impounding 324

7.18 Predictions of Cumulative Slip for Cyclic Loading 328

7.19 Typical Shearband Slip Prediction for Reservoir Load Cycle 329

7.20 Average Slip Per Cycle for Cyclic Loading 330

7.21 Geometry of Crest Modifications 333

7.22 Average Slip Per Cycle for Modified Crest 334

1. INTRODUCTION

"Yielding" of soil or rock masses refers to the processes by which irrecoverable deformations develop. It is a consequence of the constitutive properties of the materials, and response to particular conditions of loading and deformation. In practice, yielding processes are complex and are generally difficult to predict accurately.

"Failure", on the other hand, refers to a qualitative or quantitative assessment of the *consequences* of yielding. Depending on the nature of the risks involved, on the economic factors applicable to the situation, and on the experience of the participants, failure defines the situation where tolerable conditions become intolerable.

This thesis deals with aspects of a class of problems referred to in the geotechnical literature as "progressive failure". This is the yielding process by which a soil or rock mass fails without fully mobilizing throughout the maximum available strength. Such failure states are generally observed to involve discrete surfaces of intense shearing, and it is the post-peak strain weakening associated with such localized shearzones which permits progressive failure to develop.

From a practical viewpoint, time-dependent yielding processes cannot rigorously be separated from progressive failures. Effects such as pore pressure equilibration, weathering, and long-term available strength reductions give rise to "delayed failure". In the literature, aspects of delayed and progressive failure are often interrelated. It is beyond the scope of this research to examine time-dependent behaviour in any detail; however, such matters are discussed where pertinent.

The yielding behaviour of discrete shearzones is examined herein. A mechanistic approach to yielding and strain-weakening is considered, and computational procedures for realistic deformation analysis of shearzone problems are developed. Case histories of shearzone yielding are examined, and some further contributions made to the on-going debate over progressive failure.

In this chapter, the literature on progressive failure is briefly reviewed. Concepts necessary for definition of shearzone problems are discussed, and the objectives of the research program are introduced.

1.1 PROGRESSIVE FAILURE

Terzaghi (1936) described a progressive weakening phenomenon in clay slopes: stress changes and removal of lateral support allowed fissures to open, moisture ingress then caused nonuniform weakening; this allowed further cracks to develop; and so on. This classical description of a delayed failure process is equally relevant today. Terzaghi and Peck (1948) and Taylor (1948) were particularly concerned that under certain conditions, nonuniform straining of strain-weakening materials would not allow full simultaneous development of maximum strength. This latter observation is at the heart of the progressive failure problem, and forms the basis of all further discussion.

As field evidence from slope failures accumulated in the 1950's, it became apparent in most field situations that full peak strength was not being mobilized at failure. Some early observations that weathering and softening lead to loss of the cohesive peak strength component were made, but Skempton (1964) clarified knowledge to that time by introducing the concept of residual strength. This lead to a problem in slope analysis: on what strength basis should slopes be designed, to allow for progressive failure development which reduces peak strength towards residual? The "residual factor" introduced to account for progressive failure implied a proportional loss of cohesive and frictional strength components (James, 1970).

A more precise description of nonuniform stress and strain conditions, and progressive failure, was given by Bjerrum (1967). A necessary precondition was the existence of a discontinuity in the soil mass or at its boundary, where yielding could initiate and subsequently localize. Then, in order for progressive failure to occur,

1. Local shear stresses tend to exceed the maximum available strength;
2. The advance of the failure surface must be

accompanied by local differential strains in the shearzone sufficient to strain the material beyond maximum strength;

3. The material must show a large and rapid strength decrease after maximum strength is exceeded.

The existence of relatively high lateral stresses, relieved by this progressive yielding, were cited as a prime cause of development of the excessive shear stresses in the first instance. Bjerrum also distinguished between materials which had stored strain energy "locked-in" by means of diagenetic bonds, and weathered material where bond destruction allowed the stored energy to flow and aggravate the stress concentration effect. Consequently, Bjerrum regarded weathered material as being most susceptible to progressive failure. This implicit linkage of progressive and delayed failure elements was maintained by most subsequent researchers.

The importance of geological processes had been realized by the time Skempton's and Bjerrum's contributions had been made. Amongst the case histories in the literature at that time, good alternative explanations of behaviour could be found without progressive failure being a critical element. The search for first-time slides which could definitely be attributed to progressive failure was intensified. James (1970) examined more than 50 slope failures, and could not find evidence for progressive failure. However, his studies conclusively demonstrated the following points:

1. Delayed failure processes result in the loss of any cohesive strength component in the field, while peak frictional strength is maintained;
2. Very large displacements in first-time slides are required to develop residual strength by the progressive failure mechanism;
3. Delayed failure processes and activation of presheared surfaces are sufficient to explain the range of slope behaviour observed.

Progressive failure in overconsolidated clays and clay shale slopes has not been substantiated by field experience to date. Delayed failure, particularly softening of the cohesive strength component and pore pressure equilibration, has been quite well documented. Morgenstern (1977) discussed the state-of-the-art for these failure conditions at some length, and drew attention to three basic concerns for further research work.

Firstly, geological conditions in such materials control failure geometry. Residual strength is much more rapidly attained by shear along bedding than across it. Geological factors associated with the stress history of many materials virtually assure the development of insitu pre-shearing along bedding planes irrespective of whether any slip failures develop.

Secondly, delayed failure processes are difficult to separate from the progressive failure mechanism. This means that exceptionally careful and complete investigation is required of any field record which suggests progressive failure of a first-time slide.

Thirdly, residual strength in the field is only obtained after sufficient straining has developed along thin, localized shearzones. Analytical treatment of the progressive failure problem thus requires careful attention to the geometrical constraints of shearzones as well as correct treatment of representative constitutive behaviour.

The above discussion is specific to slope behaviour in overconsolidated clays or clay shales, where indeed most of the engineering concerns regarding progressive failure are centred. However, progressive failure mechanisms may develop in any dense-structured material which is subjected to nonuniform strain development once peak strength is attained. Such situations commonly are found in laboratory testing beyond peak strength, where an *overall* stress-strain response is recorded even though nonuniform straining ("shear planes") are observed to evolve (for example Cornforth, 1964). When combined with the path-dependency of stress-strain response, progressive failure is difficult or impossible to isolate and measure. Bearing capacity problems and underground excavations are other areas where progressive failure can be expected to develop if material properties are suitable. These matters can not be discussed in this thesis. However it is pertinent to state that, as for slope stability behaviour, geotechnical design and construction economies are available in such areas if suitable understanding of the progressive failure process can be developed and analysed.

1.2 DEFINITIONS OF SHEARZONE YIELDING BEHAVIOUR

The term *shearzone* will be used to refer to the physical zone where localized post-peak yielding occurs. In analytical models of such processes, the model shearzone will be referred to as a *shearband* . These terms have been used somewhat interchangeably in the past, but there are conveniences in adhering to the above distinctions here. Physically the shearzone may be a complex set of structures on various scales, of great point-to-point variations. The processes operating in such a shearzone are intended to be encapsulated in a shearband by appropriate constitutive laws.

Yielding refers to processes such as particle crushing or reorientation, fracture, frictional slip, and so on which are not reversible upon removal of the causative forces. This is distinct from elastic behaviour, which may or may not accompany yielding and which will be significant or insignificant depending on particular circumstances.

Weakening and *strengthening* refer to modifications to the current available strength as a function of microstructural changes brought about by yielding. Strain-weakening thus describes the strength-envelope reduction from peak to residual conditions, and necessarily takes place in the *post-peak* yield regime. Strain-strengthening typically develops during drained yielding of normally consolidated clays or initially loose sands. In each case strain is the most convenient measure of yielding since it avoids non-uniqueness associated with weakening of strength in particular.

It is important to note the reservation of the terms weakening and strengthening in relation to the description of material strength. On the other hand, *softening* and *stiffening* refer to the loading and unloading stress-deformation characteristics. Historically, strain-weakening has usually been referred to as strain-softening, but it is more rational now to use a terminology which distinguishes the processes involved. Figure 1.1 is an illustration of the meaning of all of the above terms in context.

As a comment, "softening" has become associated with the time-dependent reduction of peak cohesive strength in the field. This is out-of-step with the above notions, but for historical reasons must now be accepted into the geotechnical terminology even as residual strength has been.

The *inception* of localized shear yielding is a most complex issue. Needless to say, the simplistic Mohr-Coulomb rupture surfaces which can be predicted at peak strength are far from a complete description of the yielding process. However they do have significance for the evolution of a shearzone, as will be discussed in Chapter 2. Some elegant

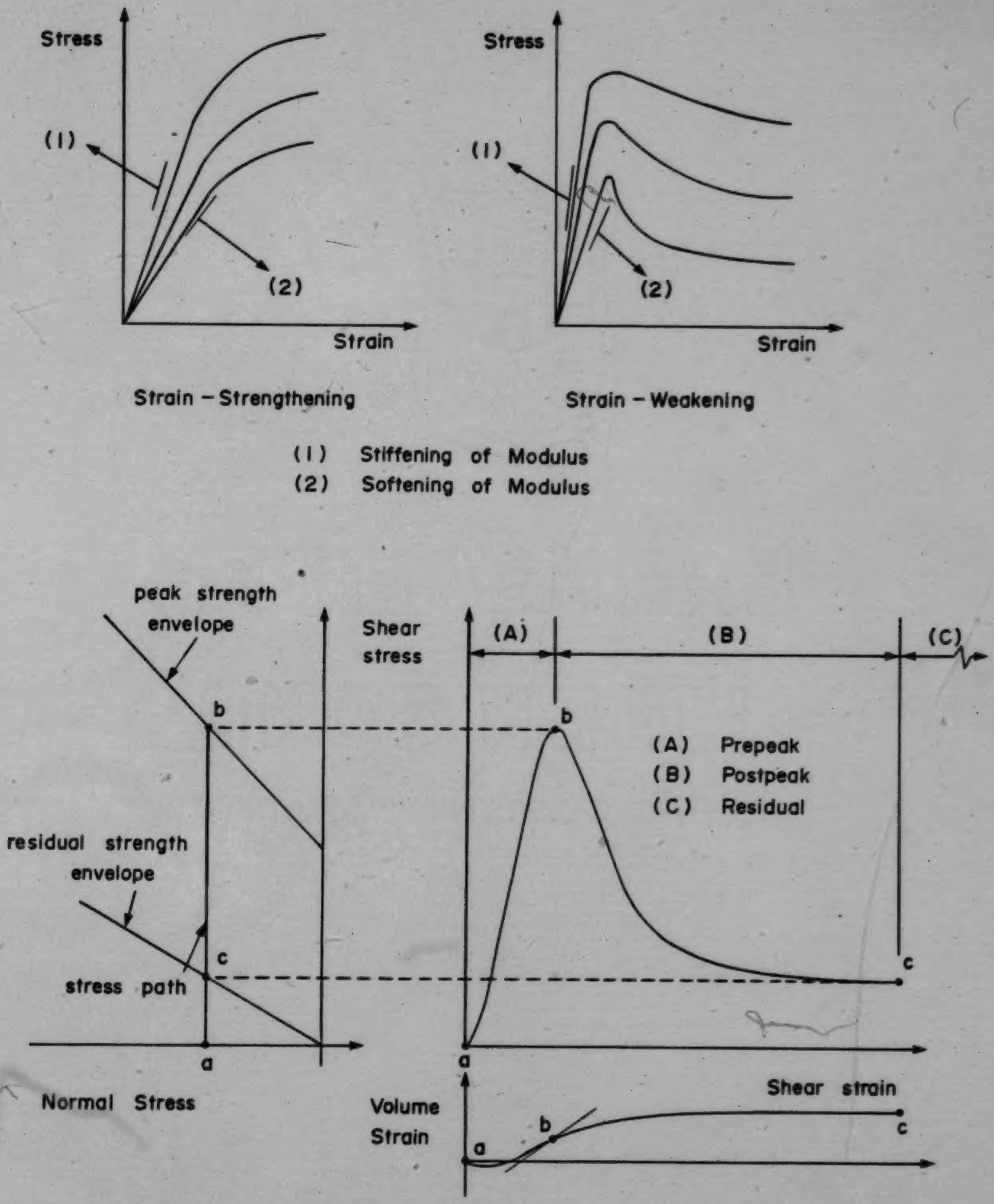
Stress
(1)
(2)
Strain
Strain – Strengthening
Stress
(1)
(2)
Strain
Strain – Weakening
(1) Stiffening of Modulus
(2) Softening of Modulus
peak strength envelope
b
residual strength envelope
c
stress path
a
Normal Stress
Shear stress
(A)
(B)
(C)
b
(A) Prepeak
(B) Postpeak
(C) Residual
c
a
Shear strain
Volume Strain
b
a
c

FIGURE 1.1 IDEALIZED STRESS DEFORMATION AND STRENGTH RESPONSE

research has been conducted into the prediction of inception as a bifurcation solution of the equilibrium conditions. This demands complicated and extensive mathematical treatment and has not matured to the stage of practical utilization at the time of writing. A review of some concepts of the bifurcation approach is also provided in Chapter 2.

Fortunately, geological conditions greatly simplify the understanding of inception in the field. Natural materials are invariably anisotropic on account of depositional conditions and stress history. Preferred particle orientation thus *controls* inception, along microstructural zones of weakness. This is the reason for observations that residual strength is obtained parallel to bedding planes with least straining (James, 1970; and others; see Morgenstern, 1977). It will be shown in Chapter 2 that preferred particle orientation is developed by stress changes of any nature. For the inception of shearzone yielding, it can be tentatively concluded that first development will occur parallel to bedding. Subsequent straining and tension cracking (delayed failure processes contributing as well) may eventually lead to shearzones across bedding, as with the maturing of a slope failure in overconsolidated clay.

It naturally follows that the *propagation* of shearzones be examined. Again, geological and environmental factors in nature favour controls such as bedding orientation and material inhomogeneity. However, shearzones which propagate under laboratory test conditions are most probably controlled by the kinematic constraints of the test. As will be shown in Chapters 2 and 3, control under these conditions is undoubtedly exercised by other factors besides microstructural fabric, and these are not amenable to simple analysis. Therefore, the *direction* of shearzone propagation in field problems can be more conveniently analysed than that for the shearzones which evolve in laboratory testing. In this respect, though, the direct shear test is of great value since it constrains the direction of shearzone growth and hence enables the effects of geological controls to be evaluated with considerable insight.

Finally, the *constitutive laws* which bridge the gap from shearzone to analytical shearband must be noted. The concepts of microstructural control have already been introduced, and it may be concluded that whatever laws are used in a model must reflect the microstructural influences at play. In this respect the direct shear test loses its value because parameters for constitutive laws cannot be determined. Generally speaking, it is impossible to evaluate all the required microstructural parameters from any test. Therefore (conveniently) it is best to adopt an "averaging" approach, applying to the shearband a simple, appropriate law or laws which respect above all else the microstructural behaviour expected.

1.3 AIMS OF RESEARCH PROGRAM

The basic aim was to develop analytical procedures for predicting deformation response of soil (or rock) masses which are influenced by shearzone yielding and strain weakening. The basic tools are one-dimensional yield models and two-dimensional finite element analysis. The former case treats the shearband as a displacement discontinuity whereas the latter employs a suitable thin element, with displacement compatibilities along its boundary but considerable freedom for strain discontinuities.

Necessary steps in developing these procedures included development of suitable constitutive laws in a form amenable to economical numerical analysis. Following are the steps necessary to achieve this goal:

1. An examination and assessment of the microstructural processes in shearzones;
2. Assessment of available treatments of the inception of yielding and shearzone response;
3. Assessment of shearzone propagation and development of yielding processes;
4. A statement of the features necessary if the modelling procedure is to be adequate.

These steps are discussed in Chapter 2, or (if more appropriate) Chapter 3.

Discussion of the one-dimensional analytical models and the two-dimensional constitutive laws is provided in Chapter 3, while in Chapter 4 the development of suitable computational procedures for finite element analysis is presented.

Any new analytical procedures have to be evaluated under simple conditions. Ideally, comparison with closed-form analytic solutions is a necessary step in this process, but it is not generally possible when significant nonlinearities are invoked. In Chapter 5, the behaviour of the computational models is discussed.

Two case histories were examined using the analytical procedures available. The interpretation of shearzone propagation in response to excavation of a steep slope is examined in Chapter 6. This has been discussed as an example of a progressive failure mechanism (Burland *et.al*. 1977) but the analysis presented suggests that only residual strength was developed along bedding surfaces in the field. The behaviour of shearzones in the foundation of Gardiner Dam (Jaspar and Peters, 1979) is evaluated in Chapter 7, as an illustration of the interactions that develop between a structure and a zone of localized yielding.

The question of progressive failure remains elusive. While the analytical tools developed should prove to be valuable in further research or in practical design problems, they do not address the interactions of delayed failure processes with the progressive failure mechanism. Likewise, there is still a lack of field experience proving that progressive failure can develop in first-time slope failures in overconsolidated clay or clay shale. These matters, and some suggested avenues of research into other materials and problems are discussed in Chapter 8.

2. A MECHANISTIC VIEW OF SHEARZONE YIELDING

The central theme of this thesis concerns the relationship between the deforming structural components of a shearzone and the constitutive description of the yielding process. Certain common features of shearzone response for a wide variety of natural materials and structural scales are noted. Many of the more subtle but nevertheless important aspects of detailed response of a given material at a given scale are deliberately set aside, in order to reach workable conclusions for the modelling of shearzone yielding.

Of paramount interest are the common physical features of localized yielding in different materials, at different scales and at successive stages of the yielding process. The observations of a number of researchers are summarized and a working hypothesis of microstructural control of the yielding process is developed. (In this context "microstructural" refers to structure within the shearzone, whatever physical scale this happens to represent.)

Certain aspects of applied mechanics are potentially important to the consideration of localized shearing. Treatments which specifically recognize shearband behaviour are examined in order to extract concepts useful for this research. Unfortunately, most of this subject matter is not yet developed to the stage of practical implementation.

This thesis is by no means the first attempt to deal with the mechanics of progressive failure. Other work on the subject, and particularly that dealing with the modelling of post-peak yielding, is presented and discussed.

Finally, the mechanistic approach is summarized in its component aspects, and the direction of this research program is defined.

2.1 PHYSICAL VIEWPOINT

The character of a typical strain-weakening material response was shown on Figure 1.1. Three important phases of successive deformation may be identified from this figure:

1. Prepeak response,
2. Postpeak strength modifications, and
3. Residual or steady-state deformation.

In each case the following discussion is conveniently separated into the behaviour of unbonded granular aggregates and the extra complications of cohesive material. "Cohesion" may be a physical reality, as for intergranular bonding of rock grains, or an apparent effect due to certain characteristics of fine-grained soils.

Prepeak Response, Granular Material:

Theoretical arguments (Horne, 1965) and experimental observation (Oda, 1972 a,b,c) clarify and confirm the basic hypotheses of Rowe (1962) concerning an incremental sliding between favourably oriented *groups* of particles. If appreciable grain-to-grain crushing, or intergranular and intragranular elastoplastic processes take place, the relationship becomes more approximate (Rowe, 1972). Slip increments between any two groups may be quite small before other, more favourably-arranged groups assume the next movement increment. Oda was able to determine physically that the particles themselves undergo insignificant rotations, rather it is the orientation of the interparticle contact surfaces which is adjusted during the slippage process. Horne concluded that

> "...particle rotations do not appear to constitute an important feature of the total deformation state at stresses below the peak stress ratio."

The agreement between these two distinct approaches is quite remarkable.

Oda (1972b) examined the fabric change mechanism in detail by comparing the response of two otherwise identical samples, prepared by tapping and by plunging respectively. Tapping during sedimentation resulted in a greater degree of particle preferred orientation. The initial fabric, characterised by particle shape, grading, and compaction method, was subjected to deviatoric stress increments. This caused *preferred orientation of grain-to-grain contact surface orientations*, perpendicular to the direction of greatest compressive principal stress. It can therefore be concluded that *the primary component of prepeak fabric* *change is the development of a highly anisotropic grain contact fabric* . Peak sustainable deviatoric stress is reached when the maximum possible fabric orientation has been developed. Concurrently, the maximum possible friction angle is maintained between particles. Further fabric deformation must then involve gross particle slippage and reorientation, on a more individual particle basis.

Further evidence for the grain-contact mechanisms was provided by Oda and Konishi (1974a,b) for simple shear tests. In this case, principal stress axis rotation is enforced. The same incremental reorientation of contact surfaces, by minor slips of particle groups, was observed.

The deformation behaviour of such assemblies can be approximated to some degree by elastic theory. This usually results in an adequate choice of deformation modulus (for example, Young's modulus) but an inadequate value of a complementary modulus (as given, for example, by the use of Poisson's ratio). This is because the dilatancy rates which develop in denser particle packings violate the assumptions of linear isotropic elastic theory. The prepeak deformations are generally small, particularly in denser packings, hence the elastic simplifications are usually adequate for practical purposes unless significant volumes of material are strained close to their peak strength.

Prepeak Response, Cohesive Material:

A distinction has to be made between interparticle bonding, as in a typical rock, and apparent cohesion of a fine-grained soil mass. The latter behaves as an unbonded aggregate if allowance is made for interparticle electrochemical forces which may be significant.

In *bonded* materials, a certain element of true elastic behaviour can be sustained until the point is reached where bond fracture commences (Bieniawski, 1967). Further deviatoric stress increases can be tolerated during a phase of stable microcrack growth. At peak strength, microcrack growth becomes unstable and further deformations result in larger-scale coalescence of fractures, This process has been observed experimentally in a variety of materials (Peng and Johnson, 1972, in granite; Sangha *et.al.* 1974, in sandstone; Tapponnier and Brace, 1976, in granite). Associated with microfracture growth is the onset of dilatant volume changes, which were earlier thought to be a result of shear displacements and propping along the crack faces but are now recognized as non-recoverable crack face separations. The prepeak fracture field is oriented with the fracture elongation direction parallel to the maximum compressive principal stress.

Deformation behaviour in such materials typically requires very small strains to attain peak strength. Thus, elastic deformation moduli can conveniently be used to model this aspect of response. However, the growth of microcracks typically results in significant dilatancy, even into the more ductile stress ranges (Edmond and Paterson, 1972) and the linear isotropic elastic Poisson's ratio cannot be used as a suitable model. Because the strains involved are small, practical disadvantages of prepeak elastic assumptions are unlikely to be significant.

In *fine-grained soils* , response is similar to that in granular soils except that individual particles are less likely to respond than "packets" of particles. The prepeak deformation phase is characterized by development of crenulations and kink-band structures (Tchalenko, 1968; Maltman, 1977). Much the same conclusions arise: peak strength occurs where the maximum sustainable fabric re-orientation is developed, without gross rearrangement of particle "packets". Again, the deformation behaviour consists of generally small strains with dilatancy developing to its maximum extent at peak strength. The primary dilatant mechanism is the volume increase associated with particle-packet rotation to form the kink bands or crenulations. Typically, much larger strains are involved than for rock microfracture.

These mechanisms refer to drained conditions, where all of the external stress is carried by the particulate skeleton. In undrained conditions, the tendency to dilate is inhibited by pore fluid pressure drops and skeletal stress increase, and the overall strength may be significantly increased. Evidence exists for other mechanisms such as tensile fracturing or hydrofracturing in unbonded fine grained soils (Sibson, 1981) as a cause of fabric dilatancy. In such cases, the fabric evolution closely parallels that for bonded materials.

Prepeak Response Summary:

In all materials, the characteristic of prepeak response is statistically homogeneous deformation with low overall strains. The microfabric mechanisms all involve structural adjustments to align interparticle contact surfaces predominantly perpendicular to the maximum compression. Full development requires significant volumetric expansion (dilatancy) of dense-structured materials. (This is the most suitable definition for a dense-structured material). Figure 2.1 shows typical prepeak behaviour for the materials described above. The most interesting aspects of microstructural control are the stress-induced anisotropy which results, and the apparent coincidence of maximum dilatancy rate with peak strength. A qualitative assessment of the effects of principal stress rotation, different stress paths to failure, influence of intermediate principal stress and so on can be made in terms of microstructure behaviour. For example, plane strain deformation is the most kinematically restrictive for the microfabric. Hence, stiffness and strength should be higher than for conventional triaxial tests under the same stress conditions.

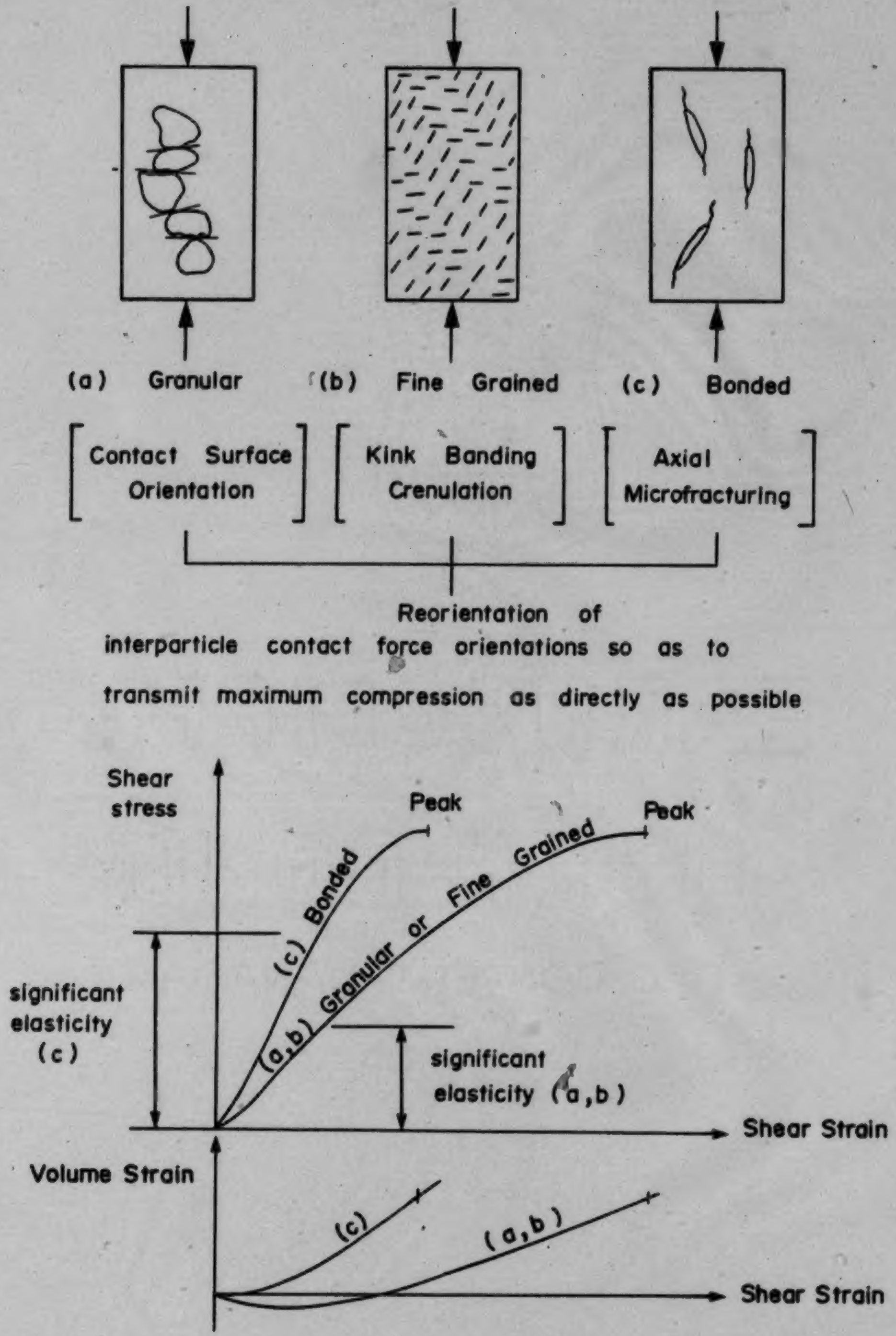
(a) Granular
(b) Fine Grained
(c) Bonded
Contact Surface Orientation
Kink Banding Crenulation
Axial Microfracturing
Reorientation of interparticle contact force orientations so as to transmit maximum compression as directly as possible
Shear stress
Peak
Peak
(c) Bonded
(a,b) Granular or Fine Grained
significant elasticity (c)
significant elasticity (a,b)
Shear Strain
Volume Strain
(c)
(a,b)
Shear Strain

FIGURE 2.1 PREPEAK MICROSTRUCTURE AND RESPONSE CHARACTERISTICS

Postpeak Response, Granular Material:

Further straining of the peak microfabric can only take place with significant intergranular slip and reorientation, since the (statistically) maximum sustainable contact shear forces have been attained. The mean orientation of the contact planes is preserved in relation to the principal compression, but the dilating, slipping fabric results in statistically fewer contacts and hence lower sustainable stress. This is the primary cause of postpeak strain weakening. Oda (1972a) was able to show clearly that triaxial test samples deformed towards a unique microfabric in the zone of postpeak weakening. This may be compared with Taylor's (1948) inference of a unique ultimate condition he called the *critical void ratio* .

Unfortunately, the postpeak structural processes are extremely sensitive to displacement conditions. Grains near the boundaries of laboratory test specimens are easily restricted in movement by restraints of friction or different stiffness at the contact with other materials. For an unloading system undergoing monotonic strain, it has been shown (Vardoulakis *et.al.* 1978) that the equilibrium of the overall deforming system may be met by alternative internal mechanisms. Very careful attention to removal of boundary restraints may permit homogeneous weakening, but localized weakening and a heterogeneous sample mechanism is more realistic. Oda (1972a,b,c) and Oda *et.al.* (1978) were able to demonstrate this clearly.

Mandl *et.al.* (1977) conducted a thorough study of postpeak shearzones in granular materials using a specially constructed ring shear apparatus. This permitted physical examination of shearzone evolution as well as continuous monitoring of stress conditions both inside and outside the zone. Dilatancy could only be suppressed at very high stress levels, with severe grain crushing as a consequence of shearing. In common with Oda (1972a) they observed no shearzone development until after peak strength had been achieved. (Again on theoretical grounds, Horne (1965) was also able to justify why shearzone development could not proceed until after peak strength was mobilized).

Evolution of the granular shearzones was described in considerable detail, and the structure of the postpeak shearzones in the ring shear tests was clarified in two ways. Direct observations showed principal shear surfaces along the boundaries. Within the shearzone, and in some cases extending into the unyielded material on either side, were *en echelon* shear surfaces inclined at approximately $\frac{\phi}{2}$ to the principal shear directions, where ϕ was the currently available frictional strength. The material within the shearband dilated, reaching a constant-volume condition only after large shear displacements had occurred. During this dilation, there was some adjustment of the minor slip surfaces to maintain angles of approximately $\frac{\phi}{2}$ with the principal shear direction. Stress orientation measurements enabled the principal shear surfaces to be identified as directions of maximum shear stress, while the minor shears corresponded closely with Mohr-Coulomb rupture orientations. The granular shearzone microstructural interpretation is shown in Figure 2.2. Response of individual grains was not closely documented, except for recording the severe cataclasis which accompanied suppression of dilation. Grain sizes were between 0.1mm and 2.0mm and shearband thickness grew during dilatant shearing to a maximum thickness between 8mm and 20mm. Thus, shearzones approximately 20 to 50 times thicker than average particle size were observed. By comparison, Bridgwater (1980) used stochastic mechanics to predict a minimum shearzone thickness of 10 particle diameters.

Postpeak Response, Cohesive Material:

Tchalenko (1970) summarized the microfabrics of shearzones over a large range of scales, from micrometres (individual shears within a direct shear test shearzone) to tens of metres (surface expression of regional strike-slip faulting). The similarities are strikingly obvious. Three stages of evolution of the microfabrics were recognized. The first stage, coincident with peak strength developement, consists of preferred orientations of particle "packets" and an incipient set of Riedel and conjugate Riedel shears, as defined in Figure 2.3. It is important to note that localized shearing, a consequence of the deformation of this shear structure, does not develop until peak strength is

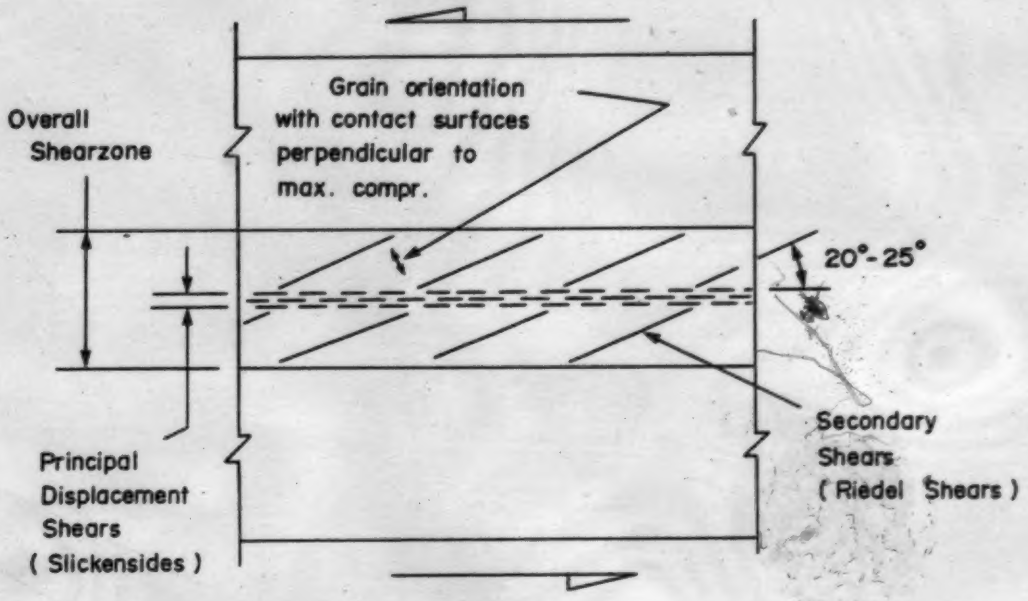
Grain orientation
with contact surfaces
perpendicular to
max. compr.
Overall
Shearzone
20°-25°
Secondary
Shears
(Riedel Shears)
Principal
Displacement
Shears
(Slickensides)

Character of Overall Shearzone depends upon :

(1) Dilatancy Allowed : (Grain Overriding)

Migration of fines under gravity or pore fluid transport ; Principal Displacement Shears formed in zone of accumulated fines , at either margin of Shearzone.

(2) Dilatancy Suppressed : (Cataclasis)

Fines accumulate in centre of shearzone , with active crushing of margins ; then Principal Displacement Shears develop in central fine-grained zone.

FIGURE 2.2 POSTPEAK GRANULAR SHEARZONE CHARACTERISTICS (after Mandl et. al. 1977)

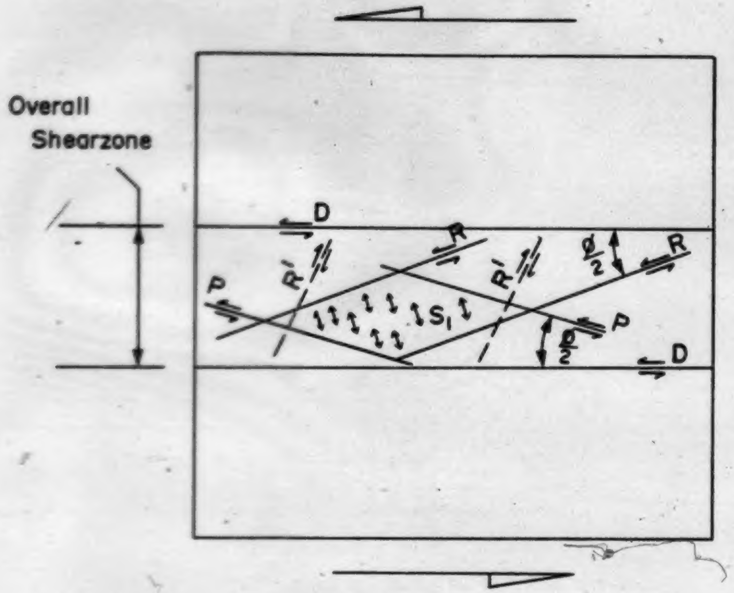

Composite View of Cohesive Microstructures:

	Component	Deformation Stage
S_1	Compression Texture	Grain axis perpendicular to maximum compression. Starts as limb of kink-band prior to peak strength
R	Riedel Shear	Appears at peak strength as a modification of kink-band limb
R'	Conjugate Riedel Shear	Subdued relative to R, appears at peak
P	Thrust Shears	Appears after peak as microstructure deforms
D	Principal Displacement Shears	Appears at shearzone margins as residual strength is approached

All microstructural shears have internal shear fabric like D

FIGURE 2.3 POSTPEAK COHESIVE SHEARZONE CHARACTERISTICS
(after Tchalenko, 1968)

attained. (Morgenstern and Tchalenko, 1967a, did find however that the influence of boundary conditions in the direct shear test induced "edge structure" shears prior to peak). The shear lenses formed by Riedel shears are not conducive to large-scale fabric deformation, and other structures are produced when postpeak deformations increase. Most obvious are the thrust shears of the second, postpeak stage of shearzone evolution. Tchalenko (1968) showed how these conjugate shears developed from the prepeak kinkband structures. The "compression texture", of oriented particle packets within the shear lenses, remained with long axes essentially perpendicular to the maximum compression. The microstructural stress distribution during this phase is exceedingly complex but can be overlooked. However, the overall effect is to maintain planes of maximum average shear stress parallel to the shearing direction, in complete accordance with the observations for granular shearzones described above. As might be expected, the dilatancy rate for the shearzone is a maximum at peak strength conditions, where the shear lenses are in a state of maximum potential movement. There is a close agreement of microstructural processes, for materials of different grain size and for a shearzone scale range of several orders of magnitude. The third stage, residual structure, is described separately below.

For *bonded materials*, other complicating factors arise. Bond failure may arise from stress corrosion, dislocation migration, or other weathering effects in addition to local stress and temperature regimes. The axial splitting mechanism may be continued after peak strength, but inclined, throughgoing shear fractures are more commonly observed. Opinion varies as to reasons for development of the shear fractures, most likely they are a response to boundary restraint conditions and the postpeak stiffness of the loading system (Bieniawski *et.al.* 1969). It is probable that different microstructural histories, which evolve from the axial splitting mechanism under different loading and displacement conditions, may result in different postpeak microfabrics and hence, different ultimate strength characteristics (Krahn and Morgenstern, 1979). A particulate shearzone is eventually formed if shear deformations localize, the infilling material usually being referred to as "gouge". Behaviour of the gouge/bonded system is dependent on the stiffness of the overall loading system (Jaeger and Gay, 1974; Byerlee and Summers, 1976). Of particular interest, postpeak microstructural processes in gouge were observed directly by Byerlee *et.al.* (1978). Stick-slip behaviour was more noticeable at higher confining pressures, and was caused by episodic slip on component Riedel shears within the overall microstructural assembly of the shearzone. In summary, the bonded materials undergo much more substantial postpeak microfabric changes than do originally particulate materials. This leads to some nonuniqueness of the ultimate shearzone characteristics, but if essentially particulate gouge is formed, the general conclusions for shearzones in granular or cohesive soils still apply.

Postpeak Response Summary:

In the majority of materials, postpeak strain weakening is accompanied by the development of heterogeneous deformation in shearzones (Cornforth, 1964; Lee, 1970). This may be as much a response to the deformation and loading conditions as to inherent microfabric characteristics, and in bonded materials gives rise to nonunique ultimate conditions. The microstructure of the shearzones, however, consists of shear surfaces inclined to the overall direction of shearing. As slippage takes place on these, other shear surfaces are forced to develop and eventually principal displacement surfaces are formed along the shearzone boundaries. Within the shearzones, a compression texture is developed with interparticle contact surfaces inclined perpendicular to the maximum compression. The principal shear surfaces are planes of maximum shear stress, not Mohr-Coulomb rupture. Microstructural evidence (Tchalenko, 1970) indicates a unique fabric development in cohesive materials. Further evidence from plane strain tests (Oda *et.al.* 1978) suggests that granular soils are also remoulded to a unique fabric, and this is discussed further in Section 3.4.

Ultimate, Residual, and Steady State Response:

Residual strength was established by Skempton (1964) as the ultimate strength which can be mobilized along shearzones. The term "ultimate" has a unique meaning for particulate materials, but is not necessarily unique for initially bonded materials as noted above (Krahn and Morgenstern, 1979). For particulate material, residual strength is primarily a function of mineralogical composition (Kenney, 1967). This is hardly surprising in light of the unique microstructural fabric of principal displacement shears which are, in practical effect, discrete sliding surfaces. Taylor's (1948) concept of critical void ratio is realistic, for given stress conditions, because the dilatant shearzone evolves in the limit to a condition of no volume change.

Poulos (1981) introduced the term *steady state of deformation* to define, in addition to the static conditions of microstructure fabric, the concept of constant velocity of deformation of that fabric. The steady state condition is thus continuous deformation of a flow structure, consistent with but not necessarily identical to a residual microfabric. While it is a useful distinction for problems involving flow, the steady state concept has no further relevance here.

Tchalenko (1970) described the evolution of postpeak microfabric to the residual condition. The major changes were the alignment of compression texture to the residual direction of maximum compression, and the dominance of the principal displacement shears, parallel to the shearing direction as shown on Figure 2.3. Because of strain weakening, the residual condition involves a substantial realignment of the component shear structures. This is summarized in Figure 2.4, adapted from Tchalenko's work. The same general conclusions were obtained from granular shearzones (Mandl *et.al.* 1977).

2.2 MECHANISTIC VIEWPOINT

Obviously there are two aspects of strain weakening of shearzones which have to be accounted for: localized deformations, and postpeak yielding behaviour.
Time-dependent behaviour is an additional aspect beyond the scope of this research.

Phenomenological and mechanistic viewpoints may be taken with respect to localization and yielding. The phenomenological viewpoint does not consider the geometrical constraints and controls of the localization process, and until proven otherwise (by application to field problems) must remain limited in its practical applicability. However, a brief review of excellent phenomenological models is presented here for completeness.

The mechanistic viewpoint stresses both the geometrical and constitutive aspects of shearzone phenomena. The constitutive aspect can be treated in a phenomenological

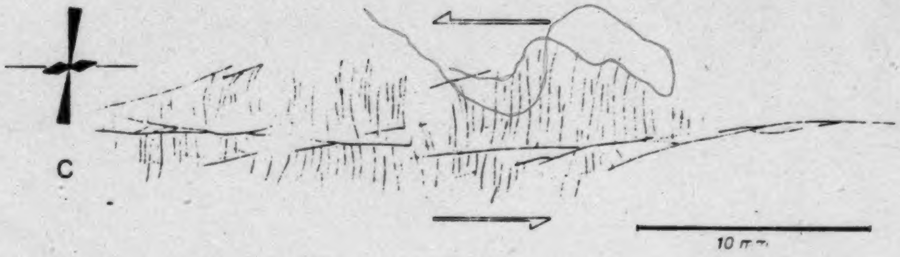

Direct Shear Test : Microstructure at Peak Condition

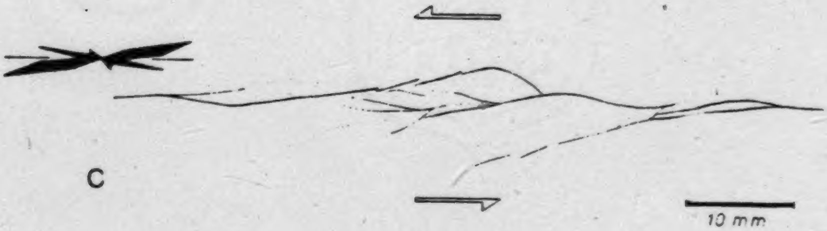

Direct Shear Test : Microstructure at Postpeak Condition

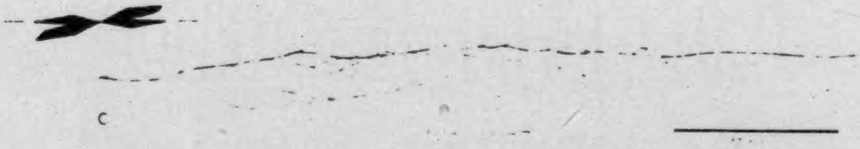

Direct Shear Test : Microstructure at Residual Condition

Rose Diagrams	show orientations of R and R' at peak , R and P orientations at postpeak , and R, P, and D orientations at residual

FIGURE 2.4 EVOLUTION OF SHEARZONE MICROSTRUCTURE FOR COHESIVE MATERIAL (after Tchalenko, 1970)

sense, and some useful examples are mentioned. The geometrical aspect is difficult, but can be treated in a number of ways which are reviewed below. Significant developments of localization mechanics, which recognize the inception and development of shearzones with yielding, are discussed more completely in Section 2.3.

Phenomenological Models:

No attempt is made to deal physically with microstructural aspects of yielding. A suitable "black box" provides insight into the external load deformation response characteristics by employing suitable elementary analogues. Kovari (1977 and 1979) developed such models to account for observed strain weakening response of rock specimens under laboratory test conditions. Figure 2.5 shows some of the elementary analogues. "Blocks" were constructed by assembling elementary analogues having continuously varying properties, allowing smoothed response to be obtained. Extending this approach, Kaiser and Morgenstern (1981) included aspects of time-dependent deformation using additional analogue elements. They were able to conclude that, after failure initiation, deformation behaviour depended on the loading rate. This implies that crack initiation and propagation are time-dependent processes, and laboratory test evidence supporting this view was discussed.

Fracture Mechanics Concepts:

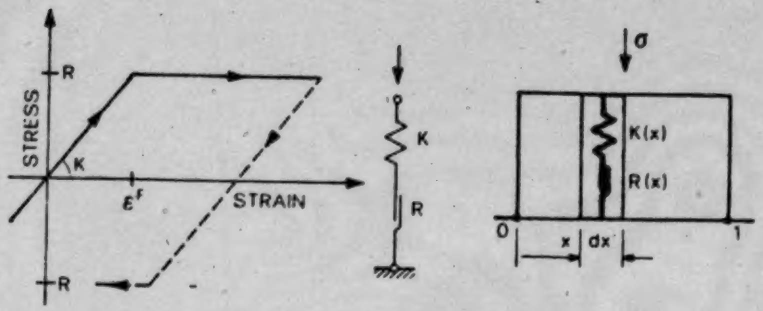
R
STRESS
K
ε^F
STRAIN
R
K
R
σ
K(x)
R(x)
0
x
dx
1

(Left) Elastic and Slip elements in series forming a Unit, and continuous distribution of Units forming a Block

LOAD DEFORMATION DIAGRAM	BLOCK COM-POSITION	SYMBOL
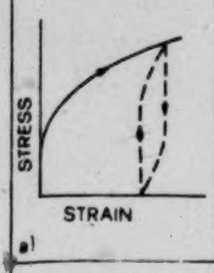 a)	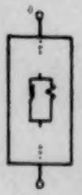	BEP
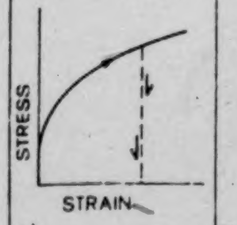 b)	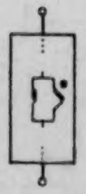	BR
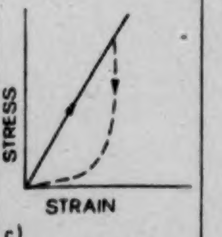 c)	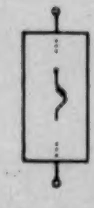	BH

LOAD DEFORMATION DIAGRAM	BLOCK COMBINATIONS
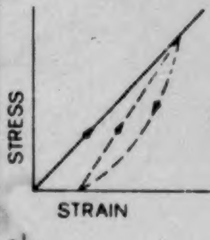 a)	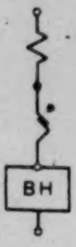
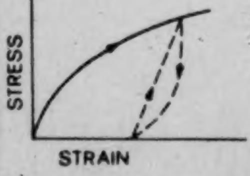 b)	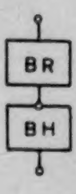
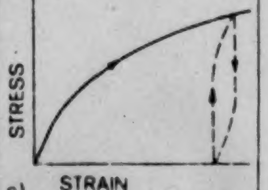 c)	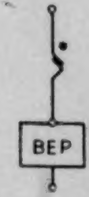
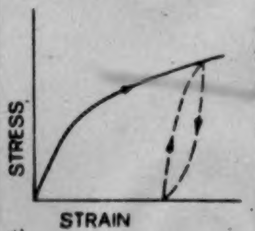 d)	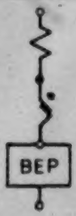

FIGURE 2.5 PHENOMENOLOGICAL BLOCK MODELS FOR SIMULATING YIELDING AND WEAKENING (after Kovari, 1977 and 1979)

Fracture Mechanics deals with localized stress and strain concentration points such as crack tips, notches, dissimilar or geometrically complex boundaries. The basic concepts surround criteria for growth or extension of flaws, which can be expressed in terms of the energy release rate at the tips of such flaws. This approach enables a locally unbounded stress field (for example, at a crack tip) to be studied in terms of *effects* rather than *quantities* . The introductory text of Lawn and Wilshaw (1975) is an excellent guide to the present state of this subject.

Three modes of fracture behaviour can be identified, as shown in Figure 2.6. Any general response is a combination of these modes. The *effects* of cracks are measured by *Stress Intensity Factors* which are scale-dependent and which can be calculated for given materials, geometries, and loading conditions. Fracture mechanics was originally developed in an elastic-perfectly brittle sense. However, the development by Rice of the path-independent J-Integral for measuring the work of virtual crack extension has enabled general application to be made to problems of elastoviscoplasticity (Rice, 1976; Landes and Begley, 1976).

Fracture mechanics has become a mainstay of design for fatigue and service-life in critical technologies of the aircraft, power turbine, and nuclear industries. Ever since Griffith's original analyses, fracture mechanics has also had potential application to rock mechanics. Mode I fracture (axial microcrack growth) of granite was studied by

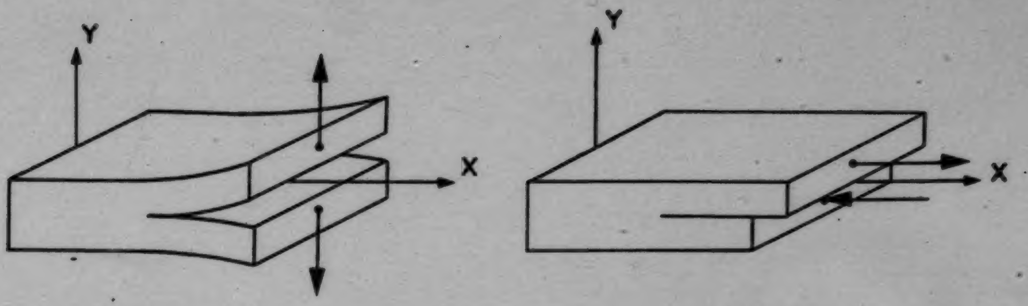

MODE I

(in-plane opening)

MODE II

(in - plane shear)

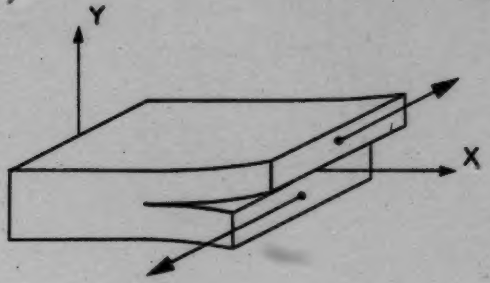

MODE III

(out-of - plane shear)

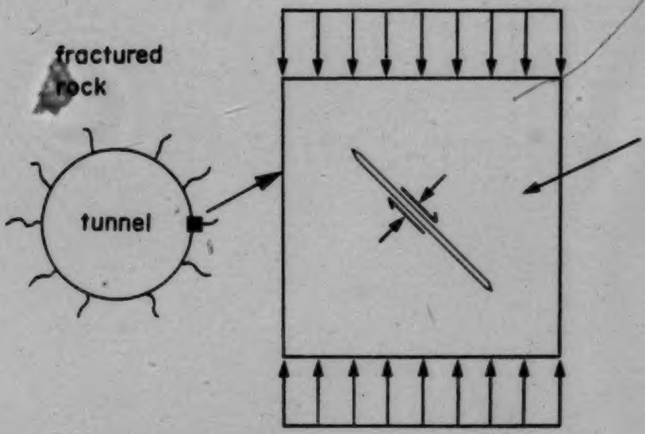

Uniaxial compression of rock containing a crack of arbitrary orientation (after Ingraffea , 1977)

Example of Mixed Mode I / Mode II Conditions

FIGURE 2.6 FRACTURE MODES, WITH APPLICATIONS TO ROCK MECHANICS.

Holzhausen (1977) while Ingraffea (1977) studied mixed Mode I/Mode II fracture of rock in the laboratory as well as by numerical analysis. Ingraffea's work contains an excellent description of modern theories of crack development and extension, and is very clearly written.

All of the studies of classical fracture mechanics ignore significant interactions of the crack surfaces. The Mode II (in-plane shear) mechanism is, however, analogous to a shearband if extra terms are introduced to account for the normal and shear stresses acting accross the band. Such adaptations were made by Palmer and Rice (1973) in a study of progressive failure conditions in an idealized slope cut into overconsolidated clay. This study is reviewed in Section 3.1 and is applied to a case history in Chapter 6.

Solutions for stress intensity factors have been obtained for a variety of simple loadings and geometries (Tada *et.al.* 1973), but closed-form analytic solutions are not generally feasible. The finite element method has proved to be a powerful tool for obtaining fracture mechanics solutions by numerical means. Difficulties which arise in trying to apply such techniques to shearzone yield problems lie not so much with the computational procedures as with terminology and constitutive descriptions of the yielding process.. The writer remains convinced about the potential applicability of fracture mechanics ideas. However, the J-Integral, stress intensity factors, and fracture toughness are not concepts immediately applicable to geotechnical problems, particularly in unbonded materials where the existence of fracture is debatable. Therefore, until such time as determined (and probably exhaustive) research efforts bring fracture mechanics concepts closer to geotechnical viewpoints, fracture mechanics remains a tempting but inapplicable tool for studying shearzone yield problems.

Constitutive Modelling:

The widespread adoption of numerical analysis in geotechnical engineering has spawned a tremendous variety of nonlinear constitutive models capable of describing certain features of soil behaviour. From a physical appreciation of shearing behaviour, it is important to understand that no tractable model can be expected to cope with nonlinearity, path dependency, anisotropy, and natural statistical variability simultaneously. What is required for current research purposes is a tractable model of the close relationship between strength and shearzone microfabric evolution. The Stress-Dilatancy theory (Rowe, 1962; Horne, 1965) is satisfactory for this purpose if certain features are exploited in a manner consistent with observed behaviour: this is discussed more fully in Section 3.4.

Some other pertinent models are reviewed here for completeness. De Josselin de Jong (1959) demonstrated that for constant-volume yielding, there was an indefiniteness in the direction of subsequent plastic strain increments. The same conditions were more rigorously examined by Mandl and Fernandez Luque (1970), who also supported restricted noncoaxiality of principal stress and principal strain increments. The indefiniteness has not been resolved by subsequent research, so coaxiality has to be assumed until a more suitable elaboration is established.

Experiments with truly-triaxial testing of sand have provided some insight as to the role of intermediate principal stress and general strain conditions. Green and Bishop (1969) referred to the advantages of simple idealized particulate models (Parkin, 1964) for interpreting three-dimensional stress and strain conditions. Such simple models will be discussed below, for another reason. From cubical triaxial tests, Lade and Duncan (1975) were able to verify the behaviour of an elastoplastic model for sand. This was modified to account for plastic all-around compression by Evgin and Eisenstein (1980) and forms the basis of a finite element analytical scheme (Evgin, 1981). Arthur *et.al.* (1977) discussed qualitatively the performance of a "double-hardening" model which could reflect both pre-peak *strengthening* and postpeak *weakening*. Roscoe and Burland (1968) introduced a two-component plasticity model which accounted separately for shear and volumetric yielding, and this was developed by Vermeer (1980) into a tool for analysis of sand behaviour to include strengthening and weakening under static and cyclic load conditions. Such models are complex, and beyond the scope of immediate practical implementation. They require evaluation of a large number of material parameters which are not yet meaningful to geotechnical practice.

Many elastoplastic formulations have been developed to include strain weakening. Nayak and Zienkiewicz (1972) developed a very general model based upon classical plasticity theory. Weakening was accomplished by using a negative hardening modulus. Prevost and Hoeg (1975) discussed a similar model and included a rigorous justification for the violation of certain stability and uniqueness postulates (Drucker and Prager, 1952). In neither case was general, practical *implementation* of the weakening procedures documented, and it is concluded that a simpler, microstructural-mechanical approach may be more fruitful at present.

Returning briefly to the subject of simple particulate models, both Leussink and Wittke (1963) and Lee (1970) utilized an elastic prepeak/plastic postpeak model based on regular packings of spheres to investigate the causes of strength differences in plane strain and conventional triaxial testing. The packings were assumed to undergo grain slip *after* peak strength was developed, and the differences in packing conditions and kinematic freedom caused different peak strength and postpeak weakening to develop. Lee's predictions are shown on Figure 2.7. It is obvious that, for the same initial packing and equivalent prepeak elastic parameters, the plane strain test is both stiffer and

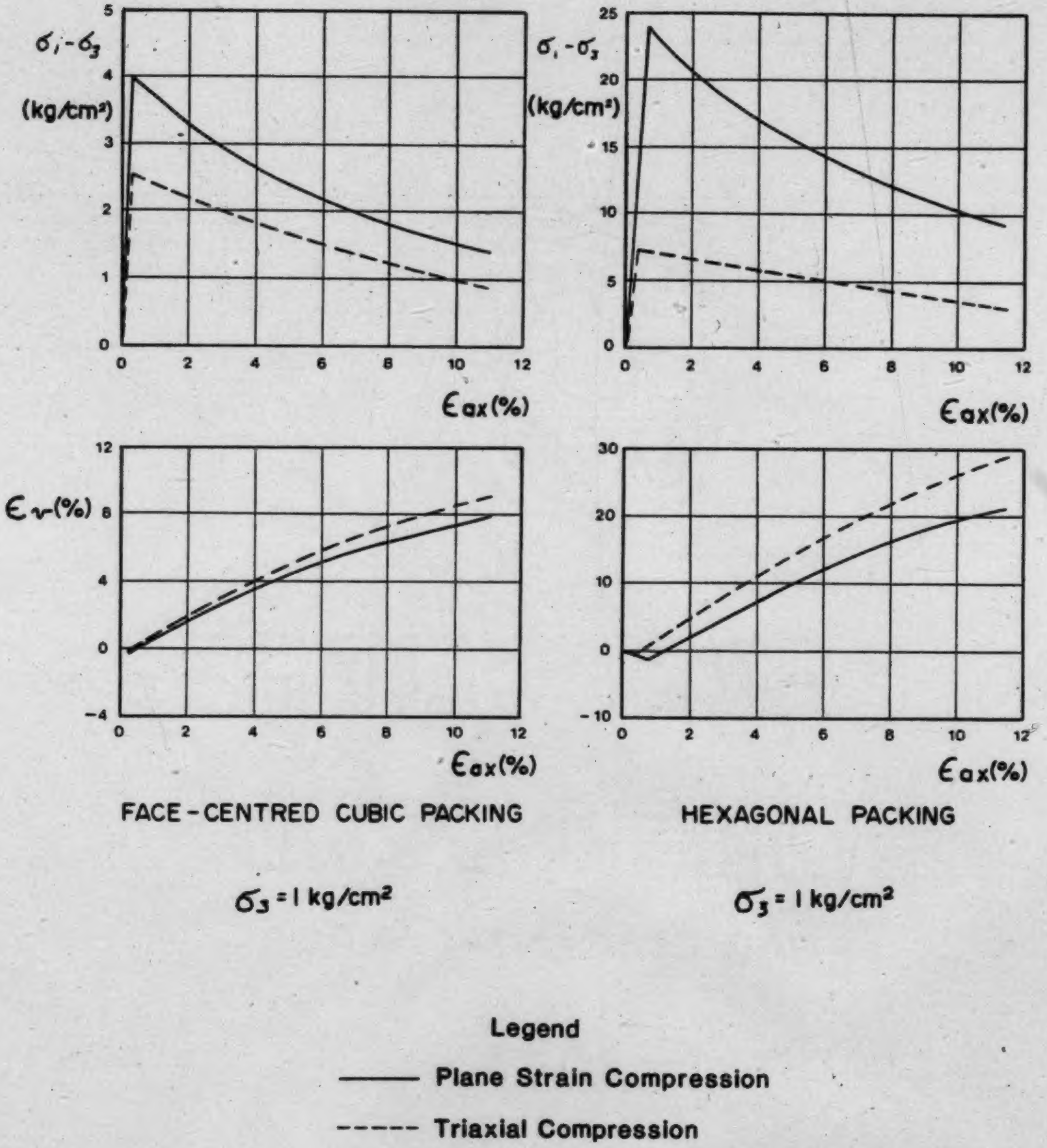

FIGURE 2.7 SIMPLIFIED POSTPEAK MODEL BEHAVIOUR
(after Lee, 1970)

stronger. In postpeak conditions, the plane strain test weakens more rapidly and undergoes less overall dilation. Laboratory tests validate the general conclusions regarding postpeak response, but laboratory plane strain tests indicate peak strength development at smaller strains than for equivalent triaxial test conditions. This suggests that the prepeak deformation parameters in these different tests are not elastically equivalent.

These experiments were duplicated by the writer using Rowe's Stress-Dilatancy theory. It was found that the constant-volume condition was obtained only after at least 80% plastic shear strain. Such large strains require large-displacement and/or large-strain theory, as discussed below.

Physical Representation of Shearzones:

It can be shown that small-strain small-displacement mechanics leads to errors in strain terms of greater than 5% when maximum shear strains exceed about 30%, so that rigorous study of shearzone strains should logically require finite strain theory, as described by Cobbold (1977a,b). Ramsay and Graham (1970) applied finite strain theory to shearzones in rocks, and were able to estimate magnitudes of discrete shearing episodes in addition to all-around compression. Finite-strain theory introduces geometric nonlinearities into analysis and so it was decided that the extra refinement gained in this manner would not be worthwhile, given other sources of error in analysis at this stage.

Strain and displacement discontinuities in soil were rigorously examined by Houlsby and Wroth (1980), who developed a classification for kinematic discontinuities under plane strain conditions. These range from complete continuity to complete separation, as shown on Figure 2.8. The velocity discontinuity, type (c), is a shearband in the usage of this thesis, while a rupture line, type (d), is the limiting case of a shearband of zero thickness. One troublesome result of the application of plasticity theory to geotechnical problems using classical mechanics has been confusion in terminologies among "stress characteristics", "velocity characteristics", "slip lines", and "rupture surfaces". The view has become widely held that a velocity discontinuity (shearband) must form along a stress characteristic (a trajectory line in the stress field indicating a yielding stress state). Houlsby and Wroth pointed out that this is not necessary, and that inferences from other research that this must be so are based on constitutive-law limitations rather than geometrical relationships. Considerable debate was also raised in the past over the shearbands having to be lines of zero extension. Again, this was shown to be a consequence only of constitutive-law assumptions.

Houlsby and Wroth also discussed dilatant shearbands, pointing out the limitations of the classical mechanics

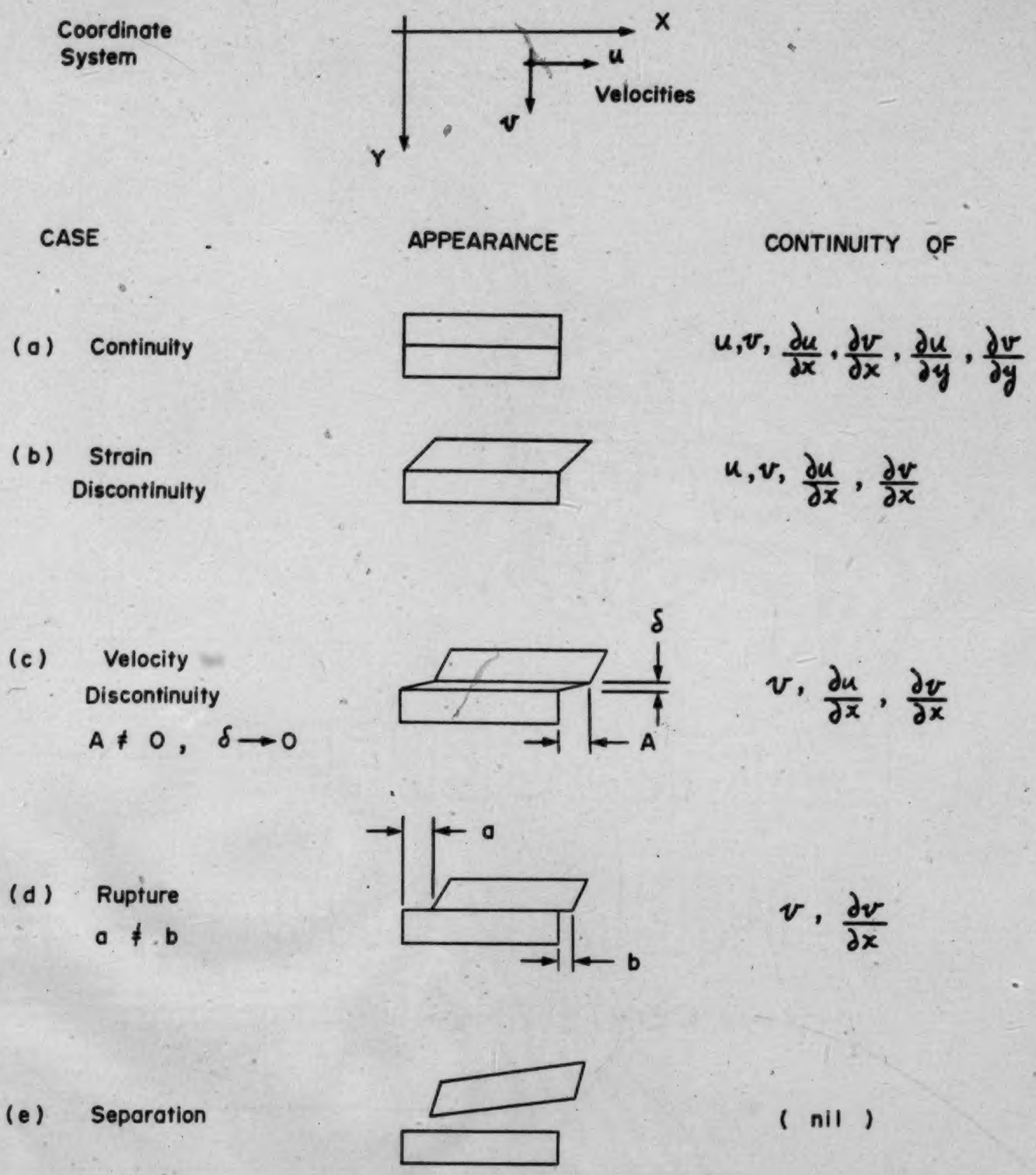
Coordinate System
X
u
Velocities
v
Y
CASE
APPEARANCE
CONTINUITY OF
(a) Continuity
$u, v, \frac{\partial u}{\partial x}, \frac{\partial v}{\partial x}, \frac{\partial u}{\partial y}, \frac{\partial v}{\partial y}$
(b) Strain Discontinuity
$u, v, \frac{\partial u}{\partial x}, \frac{\partial v}{\partial x}$
(c) Velocity Discontinuity
$A \neq 0, \delta \rightarrow 0$
δ
A
$v, \frac{\partial u}{\partial x}, \frac{\partial v}{\partial x}$
(d) Rupture
$a \neq b$
a
b
$v, \frac{\partial v}{\partial x}$
(e) Separation
(nil)

FIGURE 2.8 KINEMATIC DISCONTINUITY CONDITIONS
(after Houlsby and Wroth, 1980)

approach by comparing real material (whose dilatancy rate varies as a function of strain) with analytic model material which (for tractability) must have a constant dilatancy rate of zero. After considering possible effects of associated- and and nonassociated-plasticity constitutive laws on the equilibrium conditions across the shearband, they then discovered that shearzones *must* have different material properties. Outside the band, peak strength and finite dilatancy are possible. For analytic simplicity, inside the band the strength should correspond to constant volume shearing with zero dilatancy rate. The unfortunate aspect of these studies is that closed-form analytic solutions require such sweeping simplifications of material model behaviour. The microstructural evolution of a shearzone during weakening is profound, and in a field problem even as simple as an idealized retaining wall, generalizations such as Houlsby and Wroth proposed are too simplistic.

It is concluded that numerical analysis, recognizing the microstructural processes, is *essential* for further understanding of shearband problems. The only reasonable alternative is physical modelling, which is unrealistic for practical reasons.

2.3 LOCALIZATION MECHANICS

Specific attention is now focussed on analyses which *predict* the formation of localized yielding. The procedure followed is to specify constitutive response (if necessary, different responses in different zones of material) and kinematic compatibility, and to write the full equations of equilibrium. It can be demonstrated that under certain kinematic and constitutive conditions, alternative equilibrium deformation states are possible. The conditions for this *bifurcation* of equilibrium can be examined in terms of the material parameters specified. In simplest terms, it is the negative incremental stiffness of the weakening zone which governs this behaviour. In physical terms, it involves the interchange of strain energy and frictional work inside and outside any such zones.

Localization phenomena are by no means confined to soil and rock. Luders bands and necking in steel have been widely observed, and prompted initial study of localization mechanics by structural and mechanical engineers. The frictionless plastic behaviour displayed simplified the requirements for constitutive models used for these studies. Rudnicki and Rice (1975) adopted frictional, dilatant material behaviour appropriate to rock in the prepeak stress regime and derived conditions for bifurcation into a planar shearband. This was expressed in terms of a modulus of deformation for the overall sample, at which localization could occur. Although exact values depend upon the choice of frictional and dilatancy-rate parameters, the trend of results is interesting because localization can be predicted while in the prepeak overall stress regime. This is shown in Figure 2.9 as a plot of critical tangent modulus versus field stress conditions.

Some aspects of the localization solution require careful examination. *Firstly*, a generally nonassociated flow rule was adopted (an explanation of such constitutive terms is assumed to be unnecessary for most readers here, but may be found in Section 3.3). Nonassociated flow rules are in much better agreement with observed material behaviour than the classically-preferred associated flow rules. If the special case of associated conditions is assumed, the critical modulus is everywhere negative (postpeak). If no dilatancy takes place, localization is predicted in the prepeak regime over a wide range of stress states. *Secondly*, the microstructural evolution of rock results in a stress-induced, highly anisotropic condition by the stage of peak strength development. This was incorporated into Rudnicki and Rice's analysis by the construction of yield-direction-dependent vertex structures in the plastic yield surface. Curve 4 of Figure 2.9 may be compared with curve 2 as being representative of realistic rock conditions, with curve 4 showing the effect of incorporating "vertex effects" into the analysis.

A number of tentative conclusions may be drawn from this analysis. Firstly, in agreement with experimental

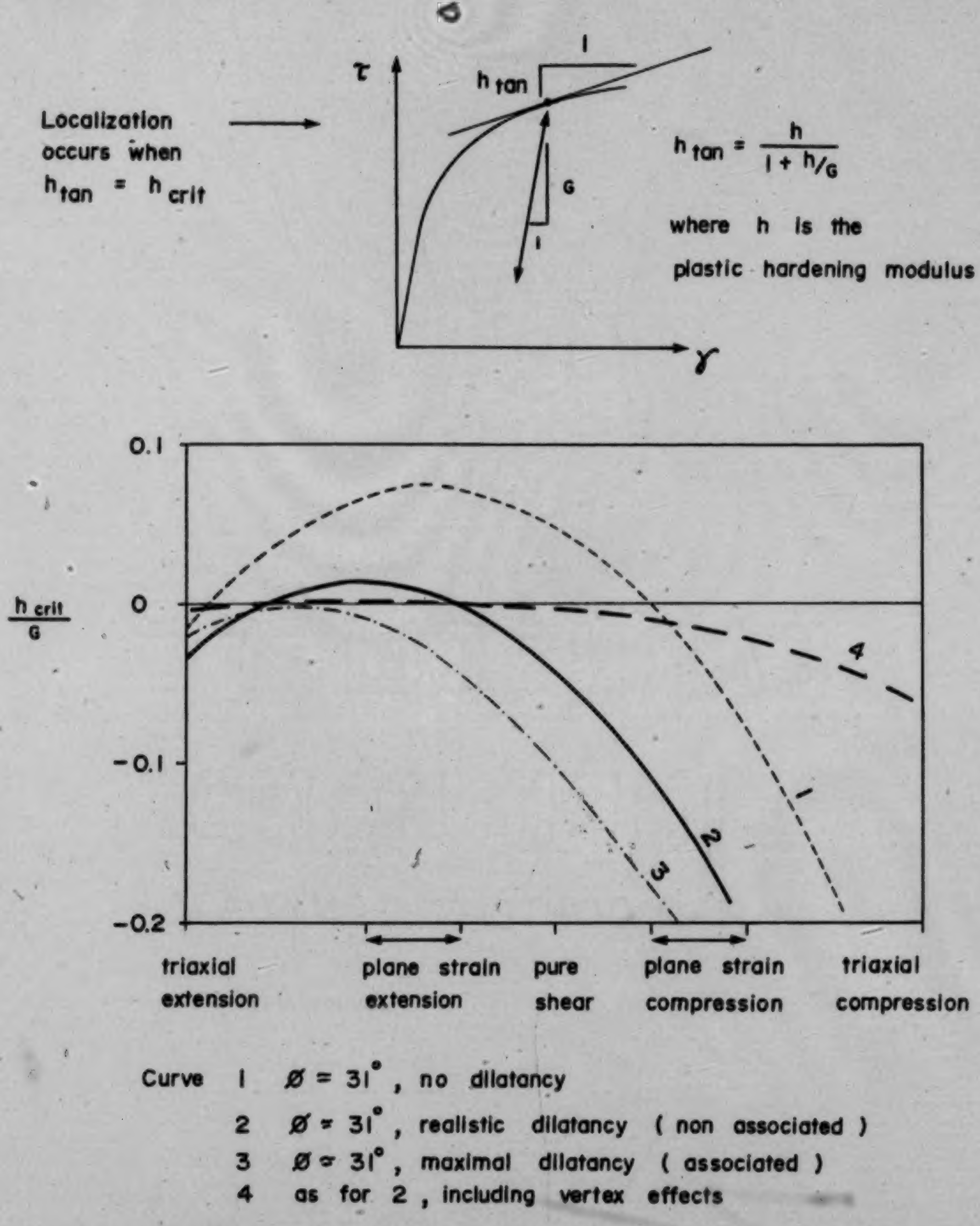

FIGURE 2.9 PREDICTIONS OF LOCALIZATION
(after Rudnicki and Rice, 1975)

observations in compression tests, localization is unlikely to develop in an otherwise uniform isotropic mass until peak strength has been more-or-less obtained. Secondly, localization seems to be relatively insensitive to strain conditions (compression versus extension) if account is taken of likely stress-induced fabric anisotropy. Thirdly, localization can be predicted just prior to peak strength development especially if extensional strain paths are being followed. There is some experimental evidence for this in the observations by Morgenstern and Tchalenko (1967a) of minor precursory shear structures in direct shear tests, and it is certainly substantiated by the early growth of "edge structures" in their tests.

The analysis of Rudnicki and Rice (1975) was confined to continuous bifurcation solutions, that is, elastoplastic deformations continuing both inside and outside the shearband. Rudnicki (1977) extended the analysis to account for inclusions, in otherwise elastic material, which obeyed similar elastoplastic behaviour. By flattening ellipsoidal inclusions, he was able to describe the inception of faulting in a weakened zone. Coupled with any dilatant behaviour in fluid-saturated porous media is a discussion of the effects of pore-fluid behaviour. Stabilizing effects were examined by Rice and Simons (1976), and their analysis was extended to weakened zones by Rice and Rudnicki (1979). It was concluded that a range of observed earthquake precursory events could be qualitatively explained in this manner. Of particular interest was the observation that, sufficiently close to the tip of an advancing fault, deformation always took place under drained conditions. This has implications for the analysis of shearband propagation under general conditions, and is utilized in the analysis presented in Chapter 6.

Of further practical interest is the development of discontinuous bifurcation solutions, where plastic yielding is maintained in the shearband but elastic unloading takes place outside. This is most relevant to rock testing and behaviour since the recognition of the need for stiff testing machines. An initial analysis (Rice and Rudnicki, 1980) showed that localization first develops as a continuous bifurcation, but for realistic geometries elastic deformation outside the shearband may develop after an infinitessimally small amount of continuous bifurcation. In other words, the elastic unloading takes place *after* development of localization by plastic deformations. This concurs with the physical interpretation of postpeak microstructural response.

In a completely separate study of shearzones in sand, bifurcation solutions were obtained for two overall deformation modes by Vardoulakis *et.al.* (1978). From a review of previous predictions of shearband orientation, they concluded that bifurcation behaviour would depend on whether or not the principal stress axes were rotating physically during yielding. Solutions were developed using hypoelastic-form nonlinear constitutive equations for the homogeneous deformation state. The two deformation modes are shown on Figure 2.10.

Mode C11 represents irrotational compression, and the bifurcation solution predicts an inclination for the shearband equivalent to that predicted by Mohr-Coulomb theory. The shearband boundaries represent planes of maximum strength mobilization in this case. At the shearband boundary, the deviation angle between principal stress and principal strain increment axes is as predicted by de Josselin de Jong (1959), but includes a correction for nonzero dilation at peak strength. (Bifurcation was assumed to develop at peak strength, to obtain this solution). In order to obtain the solution, geometric correction terms to account for finite strain and displacement compatibility had to be introduced along the shearband boundary. The shearband mechanism specifically requires that rotational strain components be considered. This is not normally done using small-strain and engineering-notation shear strains, which ignore rotations by smearing them out.

Mode C12 represents uniform bending and compression, so that the principal stress axes are continuously rotated. Under these conditions, coaxial principal stress and principal strain increments are obtained for bifurcation at peak strength, and the shearband boundaries are inclined in the direction of zero extension, as discussed by Roscoe (1970). Again, the solution depends on proper consideration

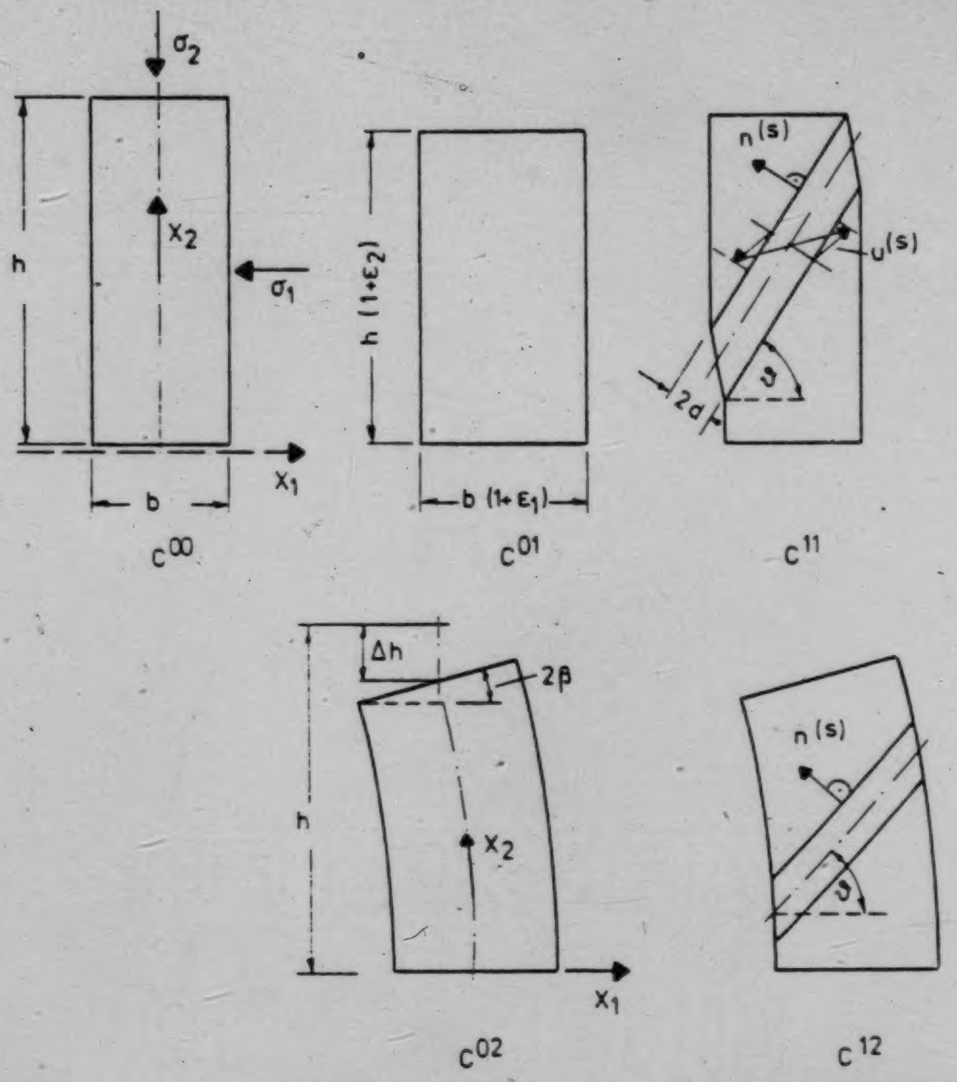
σ2
x2
σ1
h
x1
b
C00
h (1+ε2)
b (1+ε1)
C01
n(s)
u(s)
2α
ϑ
C11
Δh
2β
h
x2
x1
C02
n(s)
ϑ
C12

$C^{00} \rightarrow C^{01} \rightarrow C^{11}$ Irrotational Compression
$C^{00} \rightarrow C^{02} \rightarrow C^{12}$ Uniform Bending plus Compression

FIGURE 2.10 LOCALIZATION MODES FOR BIAXIAL TESTS ON SAND (after Vardoulakis et. al. 1978)

of geometric nonlinearities which include rotations.

The theoretical findings were tested using a specially developed biaxial apparatus. Allowing for experimental error, measurements confirmed that shearzone initiation occurred when peak strength was obtained, and that shearzone orientation and strain conditions agreed well with theoretical predictions for both modes. Shearzone thicknesses varied between 3mm and 5mm, or about 10 times the mean grain diameter (see Section 2.1). Shearband shear strains required to complete the postpeak weakening process were 60% to 100%. Finally, it was observed in these tests that the residual strength depended upon the postpeak weakening characteristics, and that in the initially dense samples significant dilatancy still existed in the residual condition. This is a contradiction of terms from the microstructural viewpoint, and suggests that the observed residual strength was more likely to be an effect of limitations of the testing equipment. Furthermore, the residual state in the shearzone should be independent of the initial grain fabric. It can be concluded that the study of Vardoulakis *et.al.* is pertinent to inception of shearzone response, but is not adequate to fully explain postpeak weakening behaviour. However, the different shearband modes discovered for different deformation conditions are a useful reminder that *postpeak shearzone behaviour is as much a response to deformation conditions as it is to material characteristics.*

2.4 MODELLING SHEARZONES AND PROGRESSIVE FAILURE

A number of aspects of previous investigations have to be examined before modelling progressive failure or postpeak shearzone behaviour, and these include:

1. General concepts of material behaviour, and means for expressing these in engineering terms;
2. Models which recognize strain weakening, but not necessarily localized shearbands;
3. Models which recognize localized shearbands, but not necessarily adequate constitutive behaviour;
4. Attempts to apply any or all of the above aspects to geotechnical problems.

General Concepts of Material Behaviour:

On the basis of elastic stress solutions for embankments, Bishop (1967) showed that shear stresses were maximized along the middle portion of failure surfaces, whereas mobilized friction angles were maximized at the toe and head of the slope. He pointed out that the index of brittleness,

$$I_B = \frac{\tau_P - \tau_R}{\tau_R}$$

was an inadequate description of the likelihood for progressive failure to develop. He further listed four *time effects* which he considered would influence progressive failure. These were: swelling due to pore pressure adjustment and changes in groundwater conditions; weathering; delayed release of strain energy in rebound; and the existence or otherwise of a time-dependent component of peak strength.

Barton (1971) described an interesting consequence of designing rock slopes to account for progressive failure. He attributed weakening to the weathering of overstressed joints and opening of tension cracks. Designing a portion of the slope on the basis of residual strength lead to reduced face heights with respect to design based on intact strength. However, the conditions which lead to the consideration of progressive failure do not exist when a slope is designed to account for progressive failure. The slope design process is therefore not a straightforward matter unless accurate and reliable deformation analyses can be made, and given uncertainties as to rock mass fabric at depth, the analyses cannot be realistic anyway.

Lo (1972) addressed the questions of suitable experimental techniques for measuring strain weakening, and suitable means for applying laboratory test data to field problems. He found that it was possible to characterize the postpeak weakening observed in laboratory tests using a hyperbolic model developed after Kondner (1963). In order to measure the extent of postpeak weakening in the field, he found it necessary to use parameters which were not sensitive to sample size or shearzone thickness. A postpeak shear modulus was identified and the ratio of this to the intact (initial loading) shear modulus was found to be very small for overall triaxial test strains greater than 6%. Instantaneous strength drops from peak to residual were therefore considered reasonable, and contours of shear stress in a model slope associated with postpeak weakening could thus be found without difficulty. By using a logarithmic time law describing the decay of strength at failure with time, he was able to plot the growth of a failure zone in the slope with time. This is shown schematically on Figure 2.11.

While Lo's approach is interesting, it can be criticized on many points, and the degree of generalization involved precludes application in design. For example, no account was taken of the geometric constraints on shearzone location or orientation, and it was assumed implicitly that time-dependent strength parameters measured in laboratory tests were directly applicable in the field. The most useful contribution is probably the insistence on careful postpeak strength and deformation testing. "Progressive failure", by Lo's methodology, is more correctly "delayed failure", and a more reasoned approach in this respect has been described by Skempton (1970) and Morgenstern (1979).

Models of Strain Weakening:

The requirements of acceptable constitutive models for strain weakening have been outlined by Gates (1972), Nayak

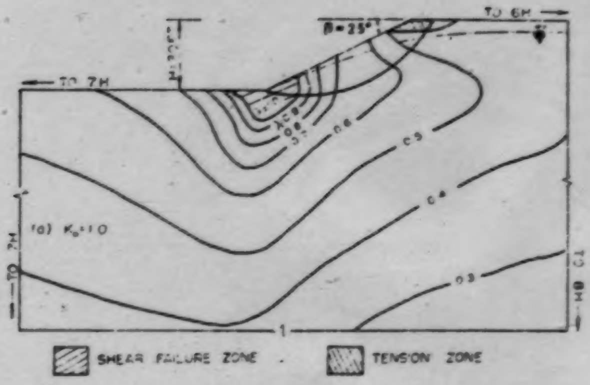
TO 6H
β=25°
TO 7H
H=30 FT
λ=1.0
0.9
0.8
0.7
0.6
0.5
0.4
0.3
(a) K₀=1.0
TO 7H
TO 8H
SHEAR FAILURE ZONE
TENSION ZONE

(a) Ko = 1.0

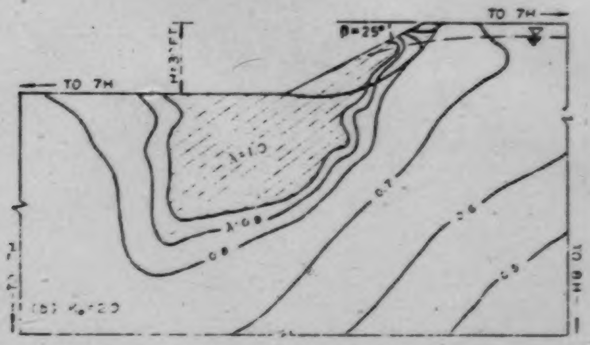
TO 7H
β=25°
H=30 FT
TO 7H
λ=1.0
λ=0.9
0.8
0.7
0.6
0.5
(b) K₀=2.0
TO 8H

(b) Ko = 2.0

Zones where Residual Strength ($\lambda = 1.0$) operates, computed using a strain weakening algorithm which did not consider localized yielding.

Strength at failure was considered to decay as a function of time. Therefore, contours associated with lower values of λ than 1.0 are associated with longer-term failure. Decreasing values of λ thus represent failure zones over longer time periods.

FIGURE 2.11 TIME-DEPENDENT PROGRESSIVE FAILURE IN A SLOPE (after Lo, 1972, and Lo and Lee, 1973)

and Zienkiewicz (1972), Hoeg (1972), Desai (1974) and Sture (1976). Most of these procedures were designed specifically for implementation in finite element analysis of field problems. As a continuation of Lo's earlier work, Lo and Lee (1973) presented finite element analyses of strain weakening which used a stress redistribution procedure for postpeak response. No consideration was given to the geometrical constraints of weakening, and the results were again combined with a model for strength/time-decay to predict the times to failure of some slopes discussed in the progressive failure literature. Hoeg (1972) predicted the behaviour of footings on strain-softening clay, but used a model appropriate to undrained yielding and also did not consider geometrical constraints. Sture (1976) was able to reproduce laboratory tests on coal using nonlinear elastic stress transfer procedures, but only for cases where no localized shear deformations developed. A similar approach (Pariseau, 1979) successfully reproduced laboratory test behaviour. None of these analyses considered shearband modes. Had they done so, the results would have been unsatisfactory because of the lack of account for yielding processes and dilatancy in shearzones.

Sture (1976) observed a variety of fracturing patterns during postpeak testing of coal. Although his finite element analysis did not examine the geometrical constraints of the fractures, Sture and Ko (1978) studied the stability of the machine-specimen system and derived conditions for strain weakening as a localization process. They proved conclusively that the shearband mode could *not* be modelled as an overall homogeneous deformation. In order to carry out an effective finite element analysis, the actual size and orientation of the shearband would have to be discretized.

More recent analysts have developed strain weakening models with due account for the shearbands in which such yielding occurs. Bazant (1976) referred to this problem, and Bazant and Cedolin (1979) reported on progress in calculating the propagation of blunt "crack-bands" in strain-weakening concrete. This obviated the need for special crack-band elements, but the computational details were quite complex. Such procedures, while satisfactory for Mode I crack extension, are much more difficult in Mode II or mixed Mode I/Mode II conditions which exist in geotechnical problems.

An analysis of progressive failure in rock slopes (Kawamoto and Takeda, 1979) is interesting because of the treatment of failed elements. Triangular elements which attained the failure condition were substructured internally to include the subsequent effects of a shearband of appropriate orientation, and this is shown in Figure 2.12. Unfortunately, the constitutive models employed did not account for realistic strain weakening. Cramer *et.al.* (1979) analysed direct shear tests on rock joints, using appropriate shearband elements but strain weakening models which did not realistically match strength-loss and

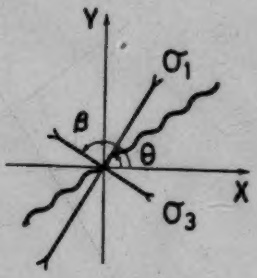
Y
σ_1
β
θ
X
σ_3

Shear "Fracture"

$$\frac{\sigma_1-\sigma_3}{2} \geq \frac{\sigma_1+\sigma_3}{2}\sin\phi + C\cos\phi$$

$$\theta = \beta + \frac{\phi}{2} - \frac{3\pi}{4}$$

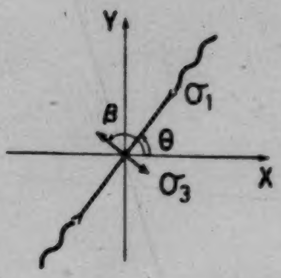
Y
σ_1
β
θ
σ_3
X

Tensile Fracture

$$\sigma_3 \leq \sigma_t$$

$$\theta = \beta - \frac{\pi}{2}$$

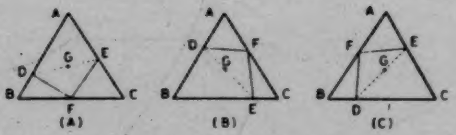
A
G
E
D
B
F
C
(A)
A
D
F
G
B
E
C
(B)
A
F
E
G
B
D
C
(C)

Fracture is assumed to pass through Centroid G of C.S.T.

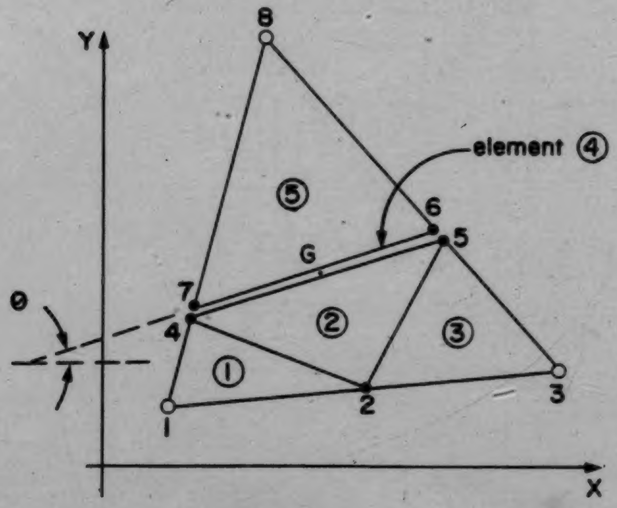
Y
8
element ④
⑤
6
5
G
7
θ
4
②
③
①
2
3
1
X

Elements ①②③, and ⑤ are C.S.T.'s.

Element ④ has orthotropic properties to reflect nature of fracture.

Stiffness for assembly is calculated by condensing internal nodes 2,4,5,6,7.

Substructure of Fractued C.S.T.

FIGURE 2.12 SUBSTRUCTURING TECHNIQUE FOR FAILURE MODELLING (after Kawamoto and Takeda, 1979)

dilatancy characteristics. In a most interesting application, Stuart (1979) demonstrated how strain energy released from surrounding elastic material could cause unstable slip along a fault plane, well after most of the fault had already commenced weakening in a stable slip fashion. Stuart's problem is shown schematically in Figure 2.13, and the antiplane shear mode represents a substantial and successfully economic deviation from standard two- or three-dimensional finite element methods.

In summary, there has been a logical development with time of procedures for generalized deformation analysis of strain weakening in shearbands. Little serious attention has been devoted to the matching of models with physical material behaviour, as even without this step the analytical requirements are very demanding. Indications from all of the analyses reviewed are that no general, practically feasible analytical techniques have been developed to date. The flexibility and power of finite element procedures has, however, been conclusively demonstrated.

Models of Shearband Behaviour:

Some of the analyses referred to above did include specific consideration of shearband geometry. Alternative solution techniques, collectively termed Singular Integral Equation or Boundary Integral Methods, have been developed to analyse field problems in terms of known conditions along discontinuities (for example, ground surface, shearzones,

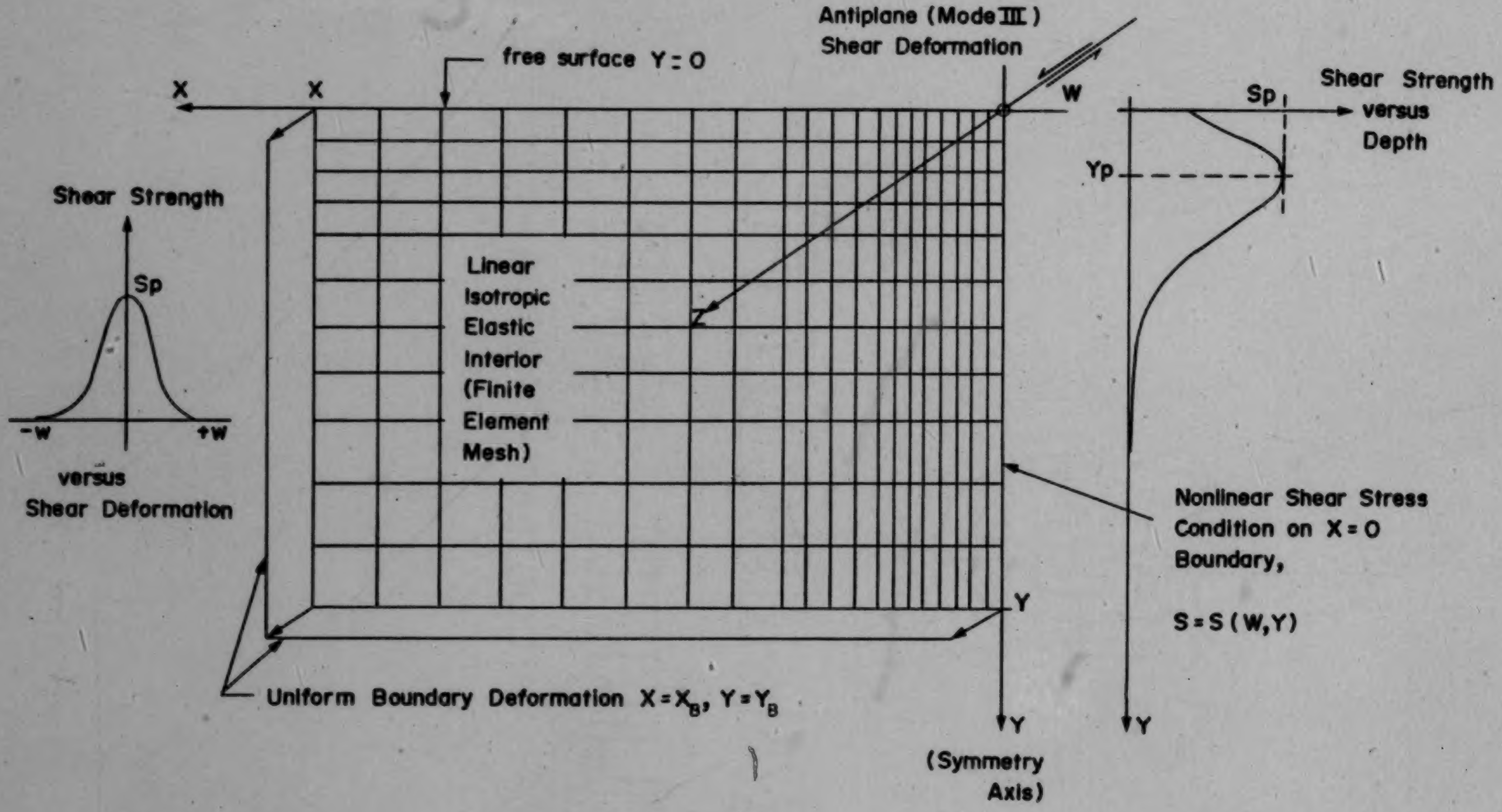
Antiplane (Mode III) Shear Deformation
free surface Y = 0
X
X
W
Shear Strength versus Depth
Sp
Yp
Shear Strength
Sp
-W
+W
versus Shear Deformation
Linear Isotropic Elastic Interior (Finite Element Mesh)
Nonlinear Shear Stress Condition on X = 0 Boundary,
S = S (W,Y)
Y
Uniform Boundary Deformation X = X_B, Y = Y_B
Y
(Symmetry Axis)
Y

FIGURE 2.13 SCHEMATIC VIEW OF ANTIPLANE SHEAR MODEL OF FAULTING (after Stuart, 1979)

tunnel faces, and so on). The material away from such surfaces is assumed to be elastic, and the solution is constructed from influence functions for loads and displacements at points on the surfaces. The techniques are quite economical since only the surfaces need to be treated, as distinct from the entire region of analysis required by the finite element method, and are indicated in Figure 2.14. Crouch (1976) presented details of such a method (which he referred to as the Displacement Discontinuity Method), including the principal influence functions used. Extra nonlinearities, such as the constitutive relationship enforced along the fault in Figure 2.14, can readily be incorporated with the possibility only of convergence difficulties as in any other numerical technique.

Similar influence-function techniques were developed by Rice and Cleary (1976) for modelling coupled stress-diffusion of saturated porous media, but the processes modelled in this case required substantially more difficult solution techniques. They successfully applied the method to the inception of hydraulic fracture around a cylindrical borehole, and were able to explore the relationships between wall-rock strength and permeability, stress state, and frac-fluid viscosity. In an extension of this work, Cleary (1976) developed a procedure for modelling shearbands in strain-weakening materials using the influence functions for arrays of dislocations and a concept of shearband weakening based on the earlier work of Palmer and

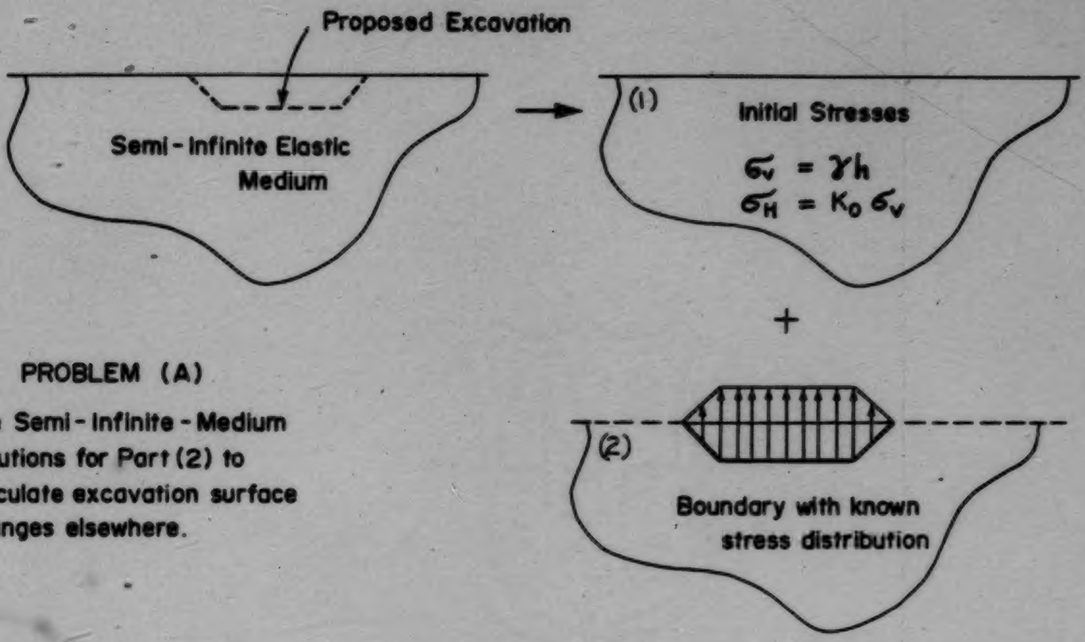
Proposed Excavation
Semi-Infinite Elastic Medium
(1)
Initial Stresses
$\sigma_v = \gamma h$
$\sigma_H = K_0 \sigma_v$
+
(2)
Boundary with known stress distribution

PROBLEM (A)

Use Semi-Infinite-Medium Solutions for Part (2) to calculate excavation surface changes elsewhere.

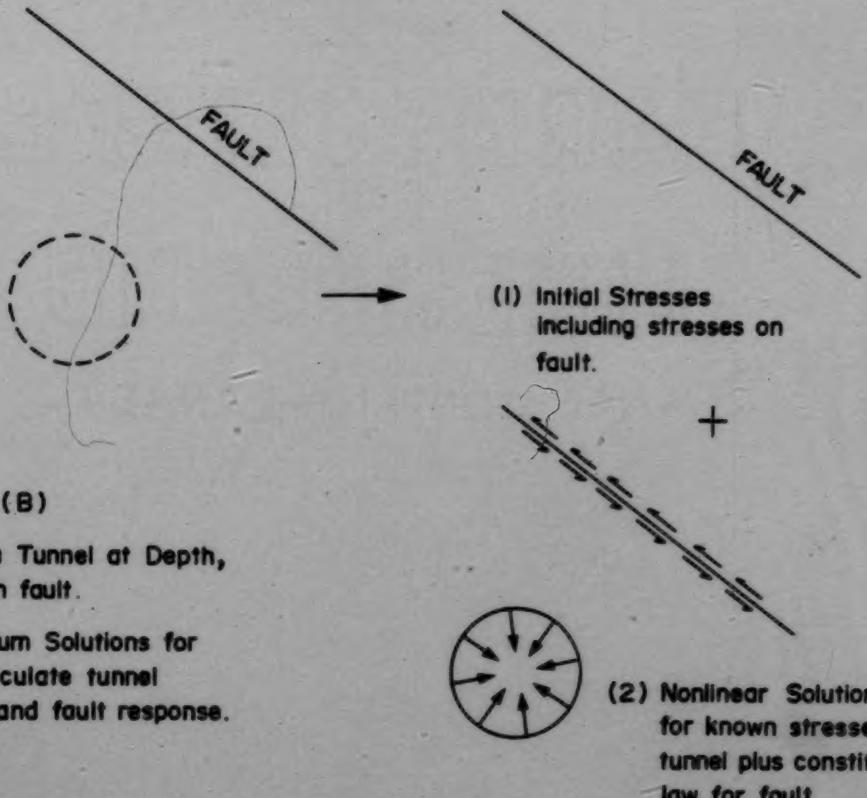
FAULT
FAULT
(1) Initial Stresses including stresses on fault.
+
(2) Nonlinear Solution for known stresses on tunnel plus constitutive law for fault.

PROBLEM (B)

Construction of a Tunnel at Depth, adjacent to known fault.

Use Infinite-Medium Solutions for Part (2) to a calculate tunnel wall movements and fault response.

FIGURE 2.14 EXAMPLE APPLICATIONS OF BOUNDARY INTEGRAL METHODS

Rice (1973). Unfortunately, considerable difficulties were experienced in obtaining numerical solutions for the distributions of dislocations.

Cleary and Bathe (1979) discussed some of the difficulties which arise when trying to adapt classical finite element techniques and associated elastoplastic constitutive laws to shearband problems. Representation of the inception and propagation of shearbands is a difficult task, but a potentially valuable marriage of finite element and boundary integral techniques was suggested which may (after further development) prove quite practical in future. The basic finite element mesh shown in Figure 2.15 is analysed until shearband inception conditions are identified. A hybrid element, equivalent to a substructure superelement (Aamodt and Bergan, 1975) then replaces the yielding element. Embedded in the hybrid are the influence functions for an appropriately oriented shearband, expressed in terms of the element nodal parameters only. This approach requires considerable development to rationalize the criteria for orientation, length, and propagation conditions for shearbands, and also presents difficult nonlinearities. Potentially, it does have the power to make shearband inception solutions feasible.

As a first step in this direction, Dong (1980) obtained some solutions for shearband development during flow of granular material in a hopper. Nodal relative displacement constraints and suitable constitutive laws were enforced

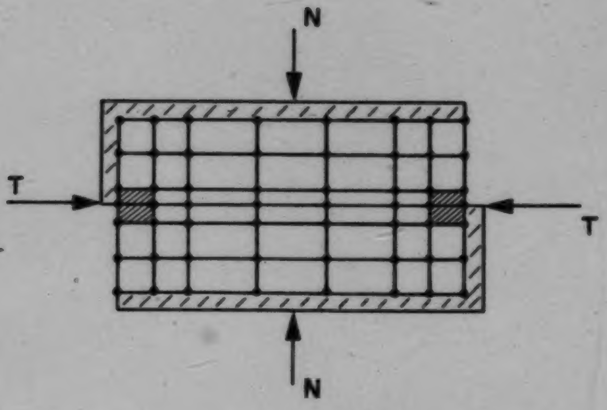

Analysis of Direct Shear Test

Finite Element Mesh for Soil

Where criterion for localized shearing is met in elements of the end-zone (shaded), specialized hybrid elements are introduced.

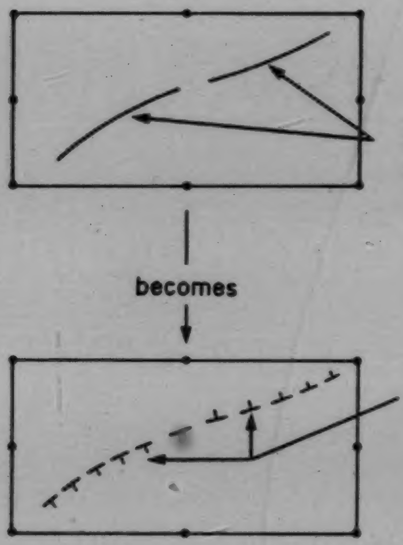

Standard
Q 48
Element

Localization conditions computed at stress sampling points

becomes

Hybrid
Q 48
Element

Standard shape functions replaced by influence functions derived from dislocation distribution along shearband

Hybrid Q 48 element stiffness and stress-strain response still formulated in terms of nodal displacements

FIGURE 2.15 HYBRID ELEMENT SCHEME FOR SHEARBAND DEVELOPMENT (after Cleary and Bathe, 1979)

along the shearband trajectory. The procedure required expensive iterative solutions using the ADINA program, with many hand-calculated user interactions with the machine calculations. Although obviously not a practical shearband analysis tool, this work represents a commendable step in exploring the numerical options available to the analyst.

Applications to Engineering Problems:

Many analyses have been published with only scant regard for the difficult and exacting criteria for representing shearband yielding and strain weakening, and it is not intended to review this literature here. The immediate impact of strain weakening behaviour is in progressive failure problems, particularly with regard to slope stability, and this is now reviewed briefly.

Muller and Malina (1968) obtained shear stress distributions along a planar slip surface, in pursuance of the Bjerrum model for progressive failure. These solutions were developed numerically. Similar one-dimensional models with published analytical solutions are discussed in more detail in Section 3.1, and have been applied to the case history of a slope cut in overconsolidated clay in Chapter 6.

Progressive failure of an example slope, using softened and residual parameters, was discussed by Bishop (1971). In addition to the factors he described in 1967, the influence of prepeak stress-strain characteristics under *appropriate* stress paths, and the initial state of stress in the slope were emphasized. Obviously, the geometry and scale of the slope become important in this light. Limit equilibrium stability analysis cannot adequately account for stress-change effects; and Bishop's conclusions remained largely qualitative.

As discussed above, Lo and Lee (1973) undertook postpeak weakening stress analysis of slopes, which were then coupled to a time-decaying strength law and limit equilibrium analysis in order to predict times to failure. The considerable simplifications of this approach are appealing, but they ignore the vital influence of geological controls on inception and propagation of shearzones, and the subsequent geometrical constraints on shearbands in analysis.

Further limit equilibrium analyses were undertaken by Law and Lumb (1978). A brittle postpeak strength drop was assumed and, in order to prepare stability charts, the classical concept of the Factor of Safety in limit analysis was overlooked in favour of a more convenient definition. This example is included here as a case where insufficient attention has been paid to the nature of the problem at the outset. The result has been a work which could easily be misinterpreted and incorrectly applied by uninformed readers.

One case history of a slope failure (Gudehus and Wichter, 1977) has been found which presents many interesting points. The material was a marl, highly structured and almost lithified. Slope failure appears to have been initiated by excavations in the lower slope and toe area. Investigations revealed an ideal example of a readily-familiar wedge mechanism, usually associated with such materials (Figure 2.16). This has been described by Trollope (1973) in relation to progressive failure development along sequential surfaces. Large-scale laboratory testing failed to reveal any postpeak weakening although discrete shearzones were observed. The analysis was not taken to its full conclusions since, at the time of publication, details were incomplete.

This example is curious and the data presented, to the writer, are inconsistent. Because such large samples were tested (30cm diameter sample in a triaxial cell), a stage loading technique was employed to define the peak strength envelope from as few samples as possible. In stage loading, each test is stopped when peak strength is obtained. The authors mentioned that they were *unable to prevent shearzone development* . Shearzones could be expected to form at or close to peak strength and the probable reason for not finding postpeak weakening was that testing was not carried over into postpeak straining. If this failure was a first-time slide, considerable deformation would probably be required to achieve the postpeak strength drop (if it existed) in the field. This case history raises the kinds of questions to which this thesis is now addressed.

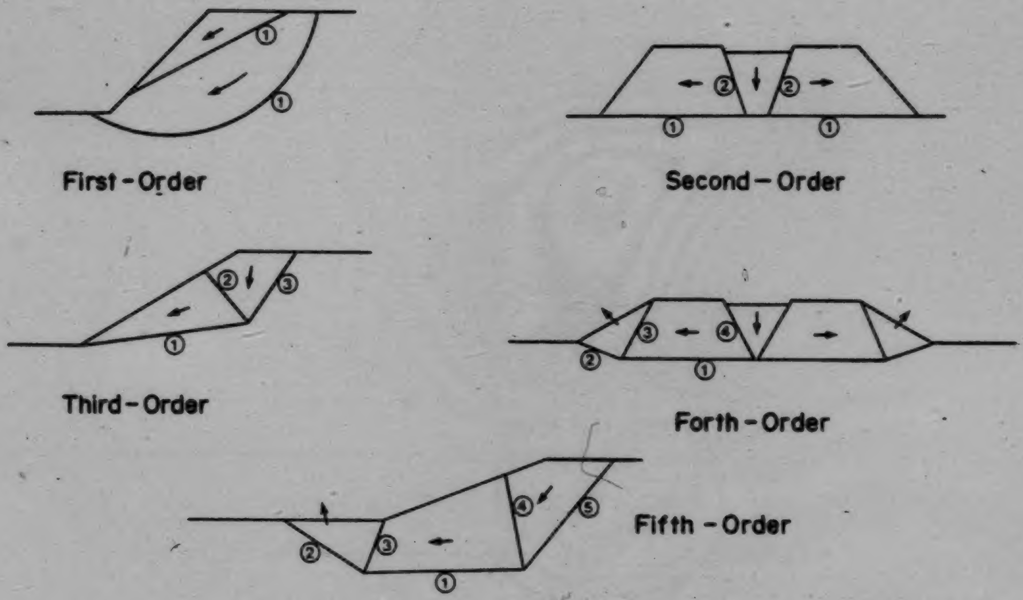
①
①
First-Order
②
②
①
①
Second-Order
②
③
①
Third-Order
③
④
②
①
Forth-Order
④
⑤
②
③
①
Fifth-Order

SEQUENTIAL MECHANISMS (after Trollope, 1973)

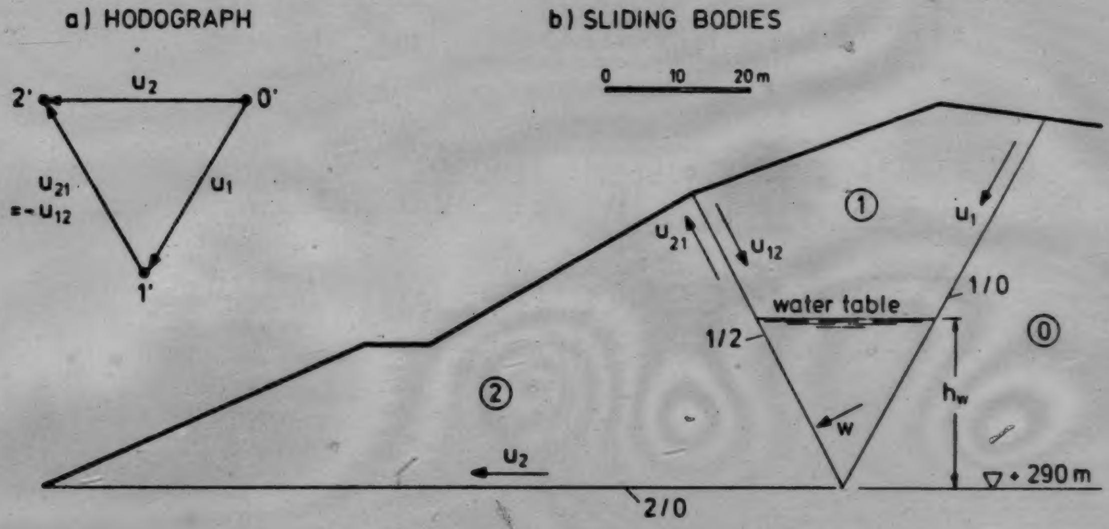
a) HODOGRAPH

b) SLIDING BODIES
2'
u_2
0'
u_{21}
$=-u_{12}$
u_1
1'
0
10
20 m
①
u_1
u_{21}
u_{12}
1/0
water table
1/2
⓪
②
h_w
w
u_2
▽ + 290 m
2/0

OBSERVED SLOPE FAILURE MECHANISM

FIGURE 2.16 WEDGE-TYPE SLOPE FAILURE MECHANISM (after Gudehus and Wichter, 1977)

2.5 SUMMARY OF THE MECHANISTIC VIEWPOINT

Physical and analytical aspects of postpeak shearing and localized shearzone development have been discussed. In considering progressive failure, it is difficult to avoid becoming concerned with time-dependent failure processes as well. The development and application of shearband models incorporating postpeak strength weakening is the goal of this research. From the general review of Chapter 1, and details presented in this chapter, the following points can be clearly identified in attempts to achieve the research goals:

1. Shearzones are physical phenomena for which certain natural controls can often be identified.

2. Complexity of geometry, difficulties in measurement of parameters, and questions of scale all indicate that numerical simulation of shearband behaviour must be a principal part of future research.

3. The numerical approach faces great computational difficulties because of the need to realistically represent geometry, shearband initiation and propagation, and highly nonlinear material behaviour.

4. Interpretation of numerical analysis is just as much an art as any other field of interpretation in geotechnical engineering. Only through careful assessment of case histories of performance can the value of models be realized.

5. A large research effort has already been expended on the problems discussed in this thesis. Some efforts have probably been misguided. Because of the wide range of factors which need to be incorporated, it is very easy to focus on one aspect to the detriment of other important aspects.

6. To the writer, *practical* numerical analysis is a major goal. This is not intended to negate the many areas of "impractical" research efforts which are to be drawn upon in this thesis. From the lack of quantitative studies of progressive failure it is obvious that, at this time, it may be possible to bring analysis closer to reality.

The Concept of Controls:

Inception and propagation of shearzones are two areas where the current state of research has not been developed to a stage of ready practical implementation. Fortunately, geological processes in the materials most susceptible to progressive failure greatly simplify these problems. Natural materials are inherently anisotropic, and shear-induced microstructures are equally so. A sound understanding of depositional and post-depositional geological processes provides the following *controls* on shearband development.

1. Slope failures are, inevitably, problems of unloading and in particular, lateral unloading. Stiffnesses are invariably higher parallel to bedding and hence, very small deformations are required to cause complete unloading

or to induce shear yielding along bedding surfaces.

2. Because of natural and induced fabric anisotropy, the postpeak microstructural processes develop with less deformation along bedding surfaces. This has been noted many times in laboratory tests.

3. Fissure opening and development associated with unloading allows more exposure of the weakening material to weathering agents, enhancing time dependent failure processes.

4. In summary, bedded deposits can be subjected to a variety of post depositional processes which enhance shearband development along bedding surfaces. To complete a failure mechanism, much larger deformations, probably more diffuse in occurrence, have to occur across bedding. Bedding thus controls the development of failure. It is a relatively straightforward matter to associate shearbands with bedding and to treat them by appropriate material response as failure develops.

As discussed by Morgenstern (1977 and 1979), overconsolidation and unloading processes combine to make almost inevitable the development of localized shear yielding in clay shales. To the writer's knowledge, no study has ever been undertaken to determine the relationship between small-scale, apparently discontinuous slickensiding on local bedding surfaces and the long-term available strength of a mass movement which develops along these surfaces. There is a lack of field evidence in a suitably

8

unambiguous form, confirming a cohesive strength component. However, it can be assumed that the natural and stress-induced controls of shearband orientation are bedding surfaces foremost, and other natural discontinuities secondly. Until research into localization is considerably more advanced, the modelling of uncontrolled shearband yielding and strain weakening is a goal for future endeavours.

3. ANALYTICAL MODELS

A mechanistic approach to shearzone behaviour and progressive failure problems has been outlined in the first two chapters of this thesis. This chapter describes analytical models developed to evaluate the mechanistic approach.

First, existing one-dimensional studies of progressive shearzone failure are discussed. A simple generalization of one-dimensional behaviour is then described. The advantages and limitations of these simple studies are discussed, and they are applied to a case history of progressive failure of a clay shale slope in Chapter 6.

Second, more generalized constitutive models amenable to two-dimensional deformation analysis using finite element techniques are described. Both elastic and elastoplastic models are described. Applications to case histories follow in Chapters 6 and 7.

A brief review of the mechanistic approach to shearzone behaviour, and the models developed to study such behaviour, concludes this chapter. The finite element analytical procedures are presented in more detail in Chapter 4, and the behaviour of the constitutive models is discussed in Chapter 5.

3.1 ONE-DIMENSIONAL ANALYTICAL MODELS

In continuation of the work of Skempton (1964) and Bjerrum (1967), several researchers have developed simple analytical models for idealized progressive failure of a simple excavation. Figure 3.1 illustrates the one-dimensional behaviour typically modelled. Strength along the shearzone is defined by peak and residual envelopes with some simple means for describing the post-peak strength transition. In comparison to more realistic slope behaviour, typical approximations neglect the effects of two-dimensional deformations associated with the stress changes along the shearzone and oversimplify constitutive response of the shearzone itself. Also, effects of pore fluid response or drainage are not usually discussed.

Christian and Whitman (1969) approached this problem by developing the differential equation for displacement along the band from equilibrium of an infinitesmal element. A finite pre-yield elastic stiffness and instantaneous strength drop from peak to residual were incorporated into their model. Various slope angles were studied by modifying the governing strength parameters to account for the normal and tangential components of gravity loads on the shearband. Factors of safety for peak and residual strengths were used as parameters to express the condition of the slope. A factor of safety for first yield was developed from peak strength by incorporation of the pre-peak deformation parameters. Results of their analysis are given on Figure

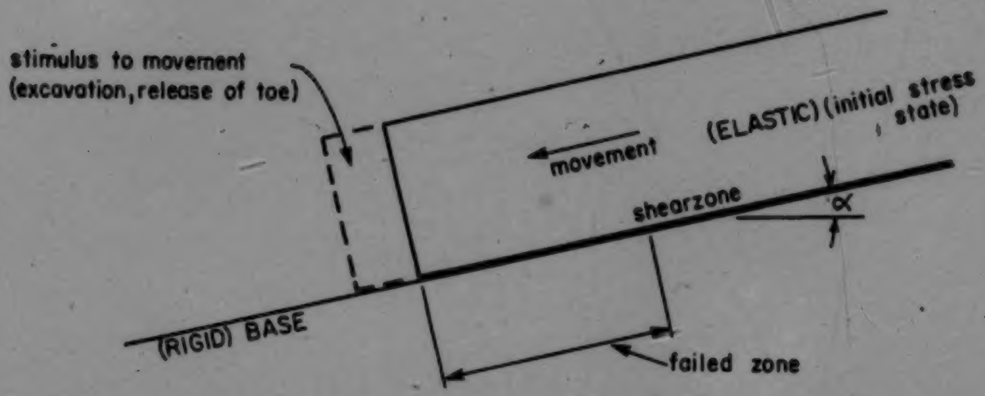
stimulus to movement
(excavation, release of toe)
movement
(ELASTIC) (initial stress state)
shearzone
α
(RIGID) BASE
failed zone

Typical Shearzone Response:

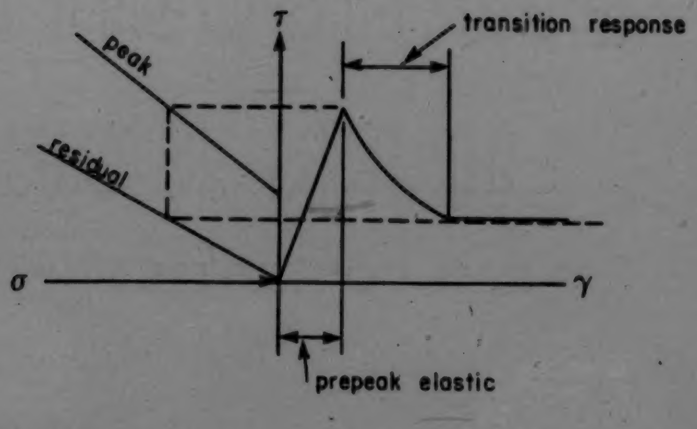
τ
peak
residual
transition response
σ
γ
prepeak elastic

FIGURE 3.1 TYPICAL ONE-DIMENSIONAL RESPONSE MODEL FOR ANALYSIS OF PROGRESSIVE FAILURE OF A SLOPE.

3.2, where the model is described as the CW model for subsequent usage in this thesis. Three classes of response: no yielding, some yielding, and failure, are depicted on this figure. The CW model demonstrates the interaction of strength and deformation parameters with initial stress conditions, and provides the means for simple assessment of these interactions in other problems.

The J-integral developed for fracture mechanics (Rice, 1968) can be interpreted as the energy required for unit extension of a propagating fracture. Its usage has become almost universal for Mode I fracture analysis, as a material measure of fracture toughness. Palmer and Rice (1973) considered the simple slope problem as a Mode II fracture. By allowing for the energy absorbed by residual frictional resistance, they developed solutions for propagation of the shearzone in terms of strength and deformation parameters. The assumptions for their work included having a very small end-region (the peak-residual transition region) in terms of overall shearband length. However, the post-peak transition was incorporate characteristic material parameter to represent the strength loss with accumulating slip. Furthermore, the "driving force" of elastic energy release into the slipping band was explicitly defined. The principal terms of the Palmer and Rice model (henceforth called the PR model in this thesis) are shown in Figure 3.3. Scale effects associated with the assumptions of their model were examined for London Clay. Because of the material characteristic

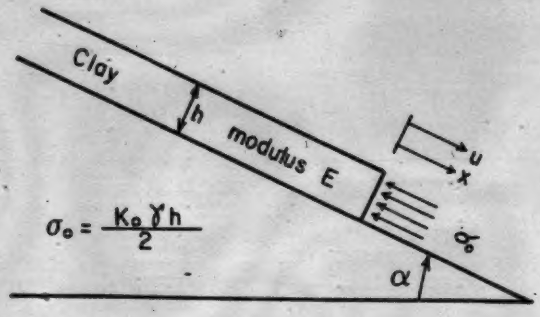
Clay
h
modulus E
u
x
σ_o
α
$\sigma_o = \frac{K_o \gamma h}{2}$

Basic Geometry of the CW Model

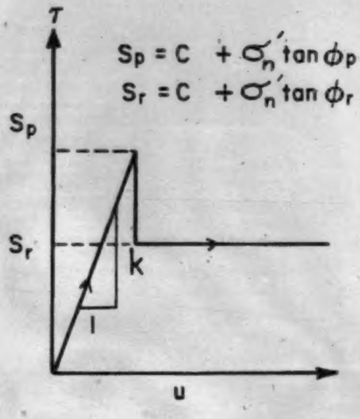
τ
$S_p = C + \sigma_n' \tan\phi_p$
$S_r = C + \sigma_n' \tan\phi_r$
S_p
S_r
k
1
u

Stress-displacement relation for a given level of effective normal stress.

$$FS_p = \frac{C_p + \gamma h \cos\alpha \tan\phi_p}{\gamma h \sin\alpha}$$

$$FS_r = \frac{C_r + \gamma h \cos\alpha \tan\phi_r}{\gamma h \sin\alpha}$$

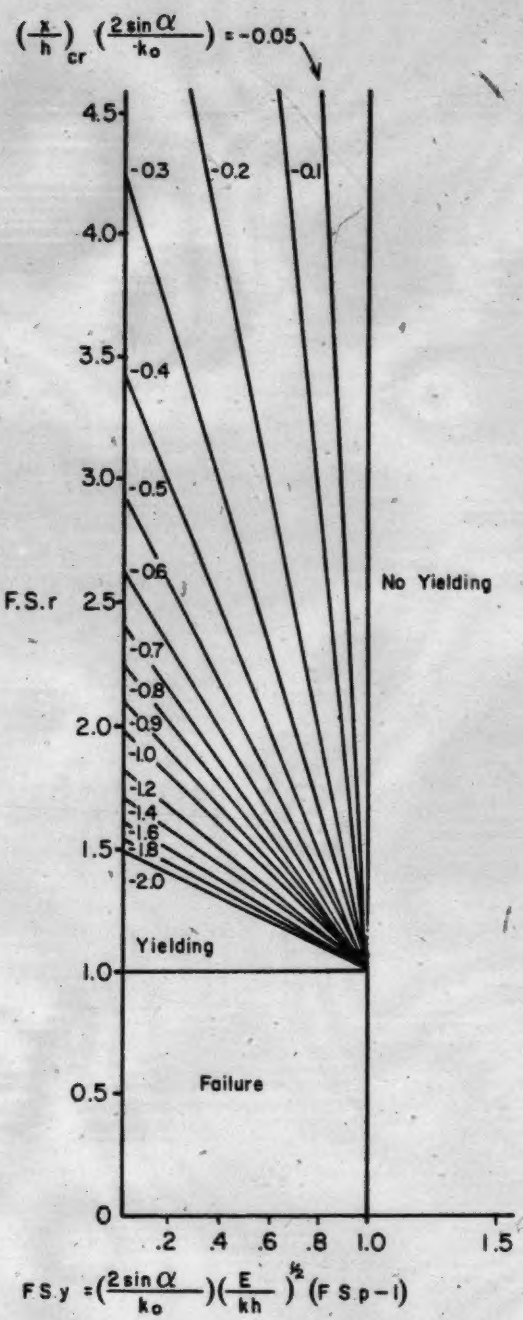

Procedure (1) Calculate FS , FS and identify $\left[\frac{x}{h}\right]_{cr} \left[\frac{2\sin\alpha}{k_o}\right]$

(2) Evaluate extent of yielded zone x_{cr} from (1) and α, k_o

FIGURE 3.2 BASIC TERMINOLOGY AND RESULTS OF THE CW MODEL (after Christian and Whitman, 1969)

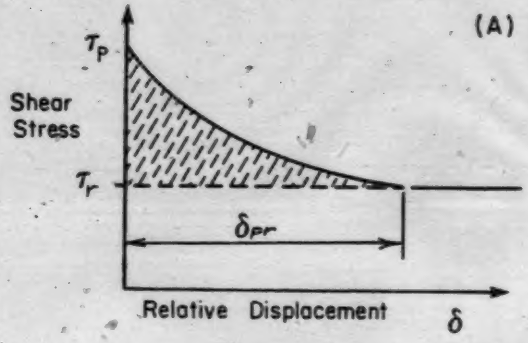

(A) Assumed Shearband Stress-Slip relationship. Material characteristic displacement is:

$$\bar{\delta} = \frac{\int [\tau - \tau_r]\, d\delta}{[\tau_p - \tau_r]}$$

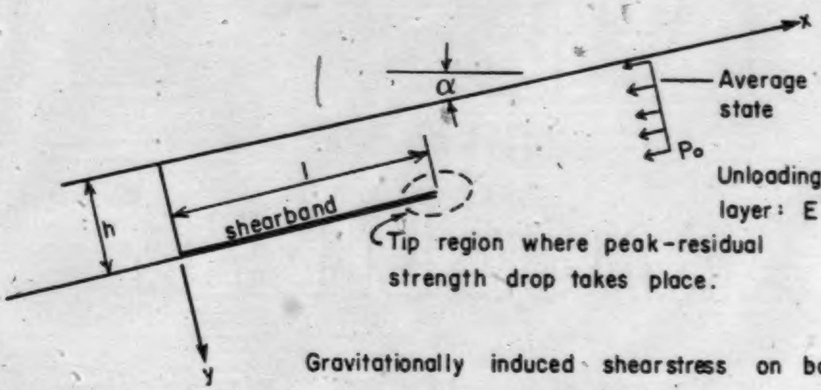

Average virgin stress state

Unloading modulus in layer: $E' = \frac{\Delta \delta x}{\Delta \epsilon_x}$

Tip region where peak-residual strength drop takes place.

Gravitationally induced shearstress on band is

$$\tau_g = \gamma h \sin \alpha$$

Further assumptions (a) long, flat slope with insignificantly small tip region well away from end.

(b) shearband parallel to slope surface.

(B) Propagation Criterion for simple slope is

$$\frac{(\tau_g - \tau_r)\, l/h + p_o}{(\tau_p - \tau_r)} = \sqrt{\frac{2E'\bar{\delta}}{(\tau_p - \tau_r)h}}$$

FIGURE 3.3 CHARACTERISTICS OF PR MODEL
(after Palmer and Rice, 1973)

length, the size of model slope required for studying shearband propagation using their model would preclude laboratory-scale testing.

Palmer and Rice also examined the effects of porewater diffusion in response to stress changes, pointing out the necessity of correctly interpreting the deformation models to be used. Guidance as to the size of their "end-region" for typical material properties was also provided.

Both the CW and PR models were examined by Chowdury (1978), who made several simple and practical extensions to the earlier work. A finite slope was considered, the effects of an arbitrary-sized "end-region" evaluated, and a solution similar to the PR solution was developed for a shearzone not parallel to the slope surface. Chowdury also showed that the approximation of a small "end-region" in the PR model made a significant difference when applied to simple stability problems.

Simple models such as the CW or PR models are most valuable for assessing the significance of the various parameters interacting in a progressive failure problem. The strength parameters can be assessed with some confidence. The effects of pore fluid drainage are not so easily assessed, particularly for field problems. The deformation parameters and initial stress conditions are particularly difficult to assess in practical problems, and one or more assumed values are normally required. There seems little virtue in Chowdury's work in this light, since the extra details involve extra assumptions about unknown quantities. However, one valuable extension to the CW model would allow the effect of a finite "end region" to be evaluated, and this is discussed below.

The CW model provides a displacement solution for the material above the shearband overriding a rigid lower zone. The PR model, on the other hand, provides a solution in terms of relative slip motion across the shearzone. These two models are not directly comparable, although the PR model gives identical results when the material is perfectly brittle (as it is in the CW model). Chowdury discussed this but did not pursue it. Since the present research is concerned primarily with the energetics and mechanics of the post-peak transition, the extension of the CW model to a less brittle transition is now examined.

Post-peak transition of the CW model:

Figure 3.4 shows the configuration and material idealization for which the CW model is extended (hereinafter, the CWX model). Only the case of a horizontal shearband is discussed here, but the extension to a general slope could be accomplished in the manner of the original CW model. The extension was undertaken with the primary purpose of studying the effect of the additional energy expended, shown by the cross-hatching on the stress-displacement curve of Figure 3.4. Also, to facilitate more direct comparison of the CW and PR models, the CWX model is re-expressed in terms

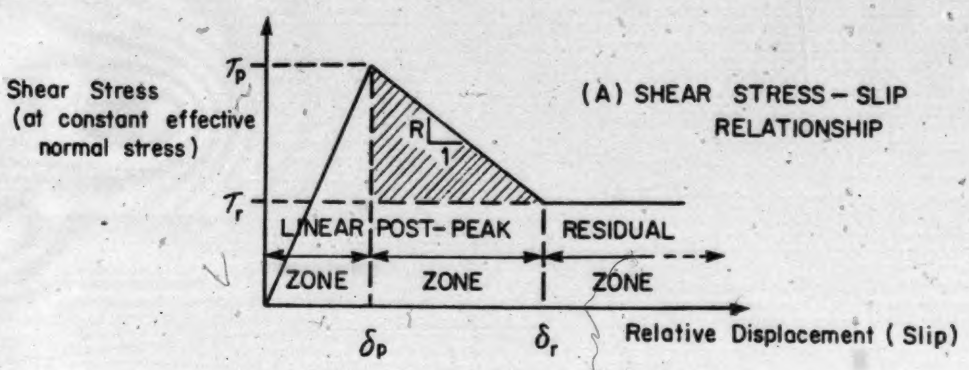

(A) SHEAR STRESS – SLIP RELATIONSHIP

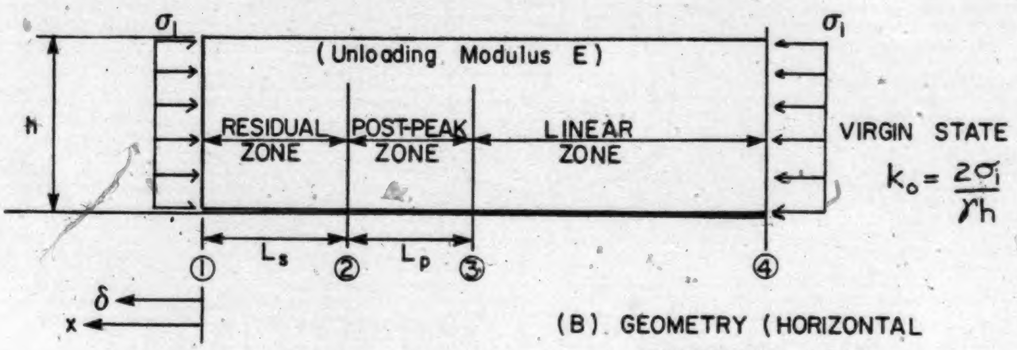
σ_1
σ_1
(Unloading Modulus E)
h
RESIDUAL ZONE
POST-PEAK ZONE
LINEAR ZONE
VIRGIN STATE
$k_o = \frac{2\sigma_1}{\gamma h}$
L_s
L_p
①
②
③
④
δ
x

(B) GEOMETRY (HORIZONTAL SHEARBAND ONLY)

(C) RESULTS $$L_s = \frac{h}{\tau_r}(\sigma_2 - \sigma_1)$$

where $$\sigma_2 = \sigma_1 - \sqrt{\frac{E}{h}} \cdot \sqrt{\tau_p \delta_p + (\tau_p + \tau_r)(\delta_r - \delta_p)}$$

$$L_p = \sqrt{\frac{Eh}{R}} \left[\sin^{-1}\left(\frac{\delta_a - \delta_p}{d}\right) - \sin^{-1}\left(\frac{\delta_a - \delta_r}{d}\right) \right]$$

where $$\delta_a = \left(\frac{\tau_p}{R} + \delta_p\right)$$

and $$d = \sqrt{\frac{\tau_p}{R}\left(\frac{\tau_p}{R} + \delta_p\right)}$$

$$\delta_1 = \delta_r + \frac{h}{E}\left(\frac{\sigma_2 - \sigma_1}{\tau_r}\right)\left[\sigma_1 - \left(\frac{\sigma_1 + \sigma_2}{2}\right)\right]$$

FIGURE 3.4 CONFIGURATION, TERMINOLOGY AND RESULTS FOR CWX MODEL OF ONE-DIMENSIONAL PROGRESSIVE FAILURE

of the relative shearband slip. Also, for convenience and clarity, the three zones of deformation (pre-peak, post-peak transition, residual) are treated separately and completely in the CWX model. Details of the derivation are given in Appendix A. The CWX model is applied to the Saxon Clay Pit slope problem in Chapter 6.

3.2 NONLINEAR ELASTIC CONSTITUTIVE MODELLING

Most earth materials possess quite different strength and deformation characteristics parallel and transverse to bedding or foliation. The clay shales of the North American Great Plains are extreme examples: their montmorillonite-rich seams form potential shearzones of low strength, yet the overall transverse strength may be high. To some extent, such extremes of behaviour may be modelled using piecewise elastic theory.

A transverse-isotropic (sometimes misnamed orthotropic) elastic material requires five independent parameters for complete specification of behaviour (Poulos and Davis, 1974). Consider the transverse-isotropic material shown in Figure 3.5. Properties are isotropic within the horizontal plane but are anisotropic in all other planes. Material parameters necessary to fully describe behaviour are:

Ev = Young's modulus for V-direction,
n = Eh/Ev, ratio of Young's moduli for H and V directions,

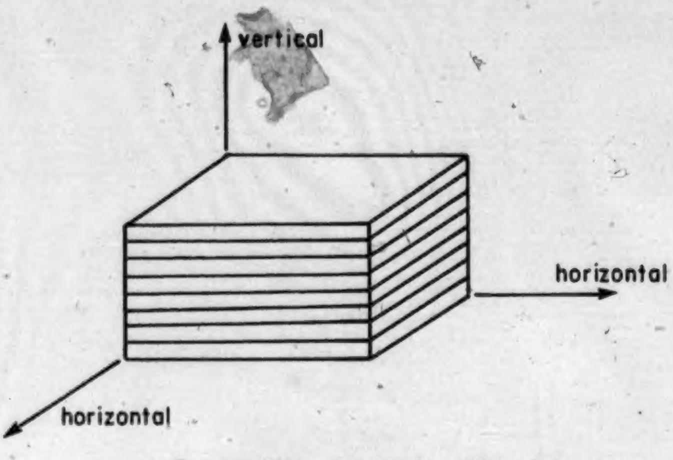
vertical
horizontal
horizontal

Transverse – Isotropic Material

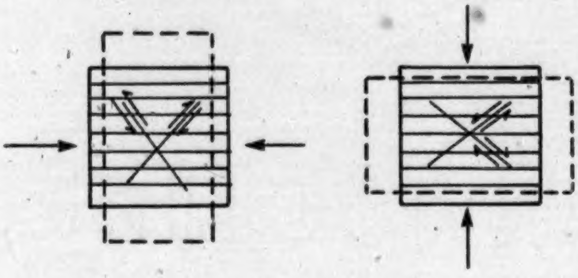

V – H Plane Behavior
(Cross – Bedding Shear)

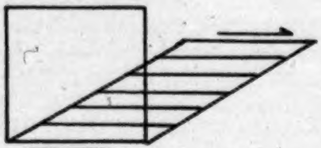

H – H or Bedding – Plane Shear

FIGURE 3.5 TRANSVERSE – ISOTROPIC MATERIAL

ν_{vh} = Poisson's ratio for strain in V direction associated with strain in H direction,

ν_{hh} = Poisson's ratio for strain in one H direction associated with strain in the other H direction,

G_v = Modulus for bedding-plane shear.

Because the Gv modulus can be specified independently, it is possible to simulate the differences in strength mobilization for transverse and bedding-plane shearing. Orthotropic or isotropic transverse behaviour can be specified whilst retaining a low Gv modulus in order to restrict mobilization of bedding-plane shearing. Therefore, a strength limit for bedding-plane shearing can be set by adjustment of the Gv modulus. If necessary, iterative calculations may be made with automatic reduction of the Gv modulus in order to maintain bedding-plane strength limits.

The transverse elastic moduli may be allowed to vary depending upon the mobilized cross-bedding shear stresses. A simple, widely employed, piecewise nonlinear elastic formulation was published by Duncan and Chang (1970), based on a hyperbolic approximation to a normal triaxial test stress-strain curve originally proposed by Kondner (1963). This enabled reasonable account to be taken of nonlinear response up to peak strength, but cannot realistically be extended to include post-peak weakening behaviour. Figure 3.6 indicates the form of stress-strain response possible.

Practical computational advantages are possible with such a model, and its application to a problem of embankment

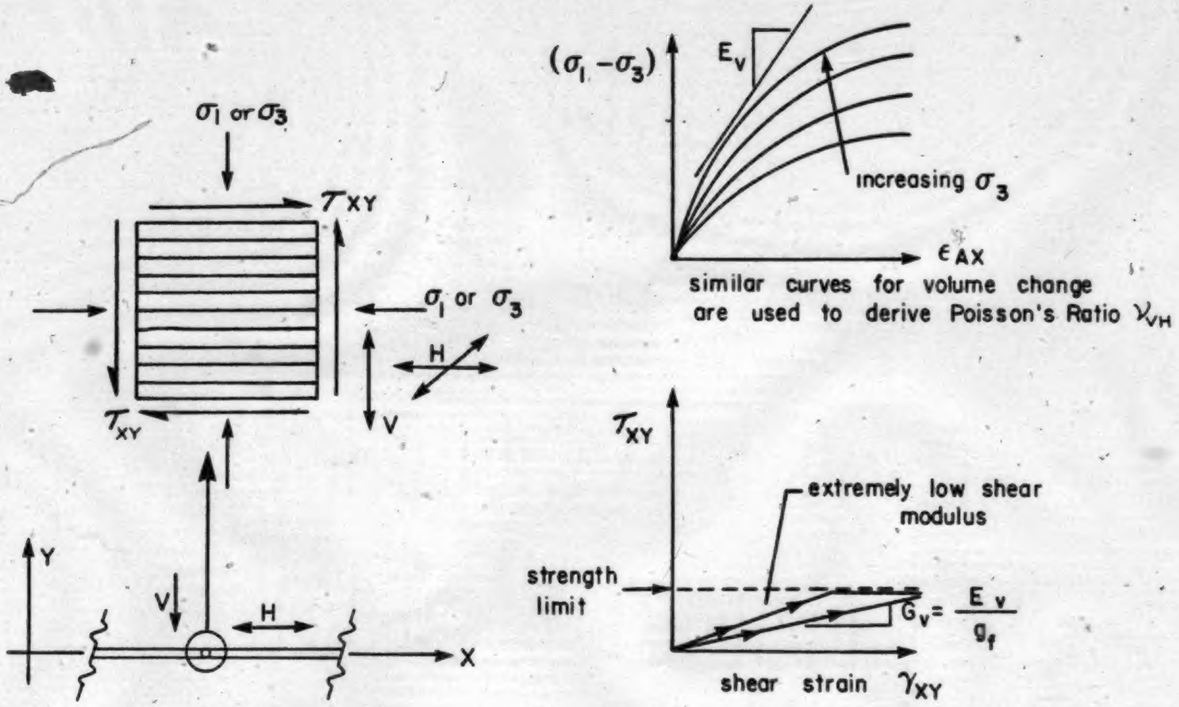
σ_1 or σ_3
τ_{XY}
σ_1 or σ_3
H
V
τ_{XY}
Y
V
H
X
$(\sigma_1-\sigma_3)$
E_V
increasing σ_3
ϵ_{AX}
τ_{XY}
extremely low shear modulus
strength limit
$G_V = \frac{E_V}{g_f}$
shear strain γ_{XY}

similar curves for volume change are used to derive Poisson's Ratio ν_{VH}

NOTES: 1. Ev and ν_{VH} may be specified using the Hyperbolic Nonlinear Elastic Model, or by directly specifying K and G.

2. g_f, which relates the independent modulus Gv to Ev, may be fixed or allowed to vary in an iterative nonlinear procedure.

3. E_H = n Ev, n must be 1.0 if the hyperbolic formulation is used for Ev.

FIGURE 3.6 SCHEMATIC SHEARBAND MODEL BEHAVIOUR SHOWING HYPERBOLIC NONLINEAR ELASTIC PLUS SPECIAL WEAKENED AND SOFTENED SHEARBAND SHEAR MODE.

spreading over weak foundation shearzones is described in Chapter 7.

Details of the nonlinear elastic shearband model are described elsewhere (Simmons, 1980b). While the model has general application, its use would normally be restricted to thin elements, in order to simulate shearzone response. Suitable finite element procedures are discussed in Chapter 4.

3.3 ELASTOPLASTIC CONSTITUTIVE MODELLING

The terms *elastic* and *plastic* have always been used in describing soil behaviour. *Elastic* deformations are recoverable while *plastic* deformations are not.*Elastic behaviour* can be readily understood whilst *plastic behaviour* is a general term which is often not sufficient to describe clearly the processes intended. Hill (1950) established a framework for describing the mechanics of irrecoverable, path-dependent deformation for *perfectly plastic* materials, that is, materials which yielded without plastic volume change, without dependence on confining stress, and without strengthening or weakening. The terms *yield surface* and *plastic potential*, which Hill standardized, are now widely used in theories of incremental plasticity for soils or rocks undergoing irrecoverable deformations involving volume change and frictional behaviour.

In modelling post-peak weakening, it is necessary to be careful about the use of the terms elastic and plastic. Elastic unloading releases strain energy which may be absorbed in plastic work or liberated in a purely elastic process. *Elastoplastic* is the correct term for simultaneous existence of the two processes, while *elastic-plastic* can and has been used to describe two separate phases of behaviour. Most soil plasticity theories are elastoplastic in form, in the sense of allowing simultaneous existence of elastic and plastic components of response.

Many different elastoplastic constitutive models have been described in the geomechanics literature. Most readers will be familiar with elastic theory and terms, and in particular be familiar with the limitations of elastic theory for practical purposes. Yet how many readers are prepared to deal with the the bewildering array of elastoplastic constitutive models now available? Little attempt is made in this thesis to review the available literature: it is extensive and can be studied at great length. The Cambridge University approach (Roscoe and Burland, 1968; Atkinson and Bransby, 1978) has dealt successfully in overview terms with the mechanics of normally consolidated clays. The models proposed by Lade and Duncan (1975) and subsequently elaborated upon by Evgin and Eisenstein (1980) have contributed much to the study of sand behaviour. Neither approach has yet been widely accepted as an engineering tool, although the Cambridge model probably comes closest in that regard (Evgin, 1981; Dang and Magnan, 1977).

No matter which elastoplastic formulation is adopted, the complexity of the mathematical details usually tends to confuse the reader. A simple Mohr-Coulomb material, as illustrated in Figure 3.7, is reviewed below. This is an elastoplastic model which can readily be adapted to more complex behaviour. Some of the terms and concepts of this model are described at length in an attempt to clarify the principles involved.

Yield Functions and Flow Rules:

The *yield function* is a concept common to most plasticity theories. It is a mathematical formulation in terms of stresses and material strength parameters which defines a current stress state of stress where yielding occurs. Negative values of the function imply no yielding, and positive values define stress states which the material cannot attain without incremental elastoplastic response. A value of the yield function can be assigned to any point of a body. Mathematically, the function may be visualized as a surface in suitable stress-space within which only elastic behaviour occurs. The most important properties of a yield function are that it be mathematically continuous and differentiable (with provision for dealing with vertices of the surface), because its primary purpose is to define permissible stress increments when yielding occurs.

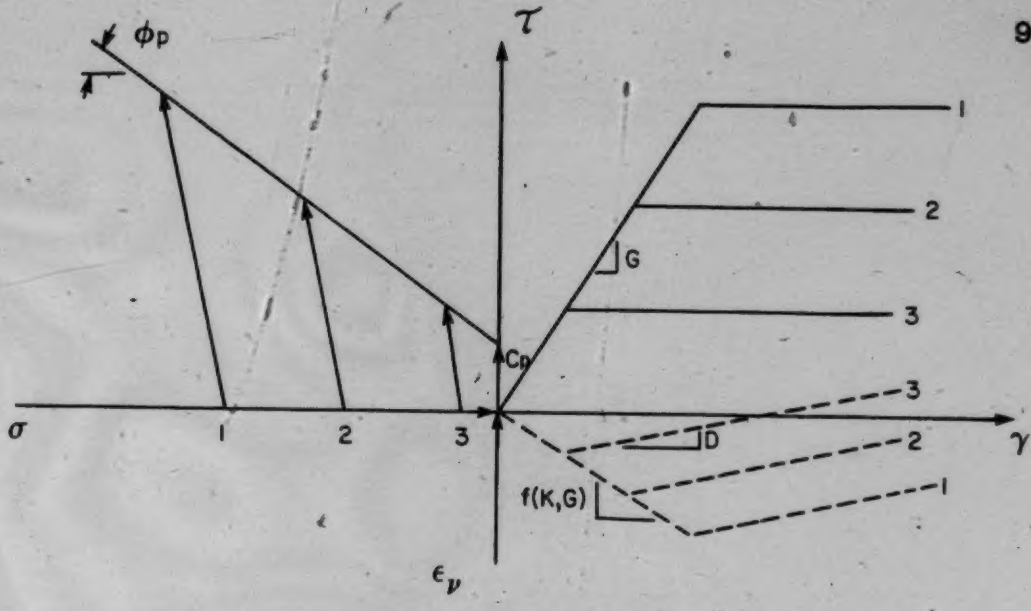
φp
τ
1
2
G
3
Cp
3
σ
1
2
3
D
2
γ
f(K,G)
1
ε_ν

(A) Material Properties : C_p , ϕ_p , D , (elastic K,G)

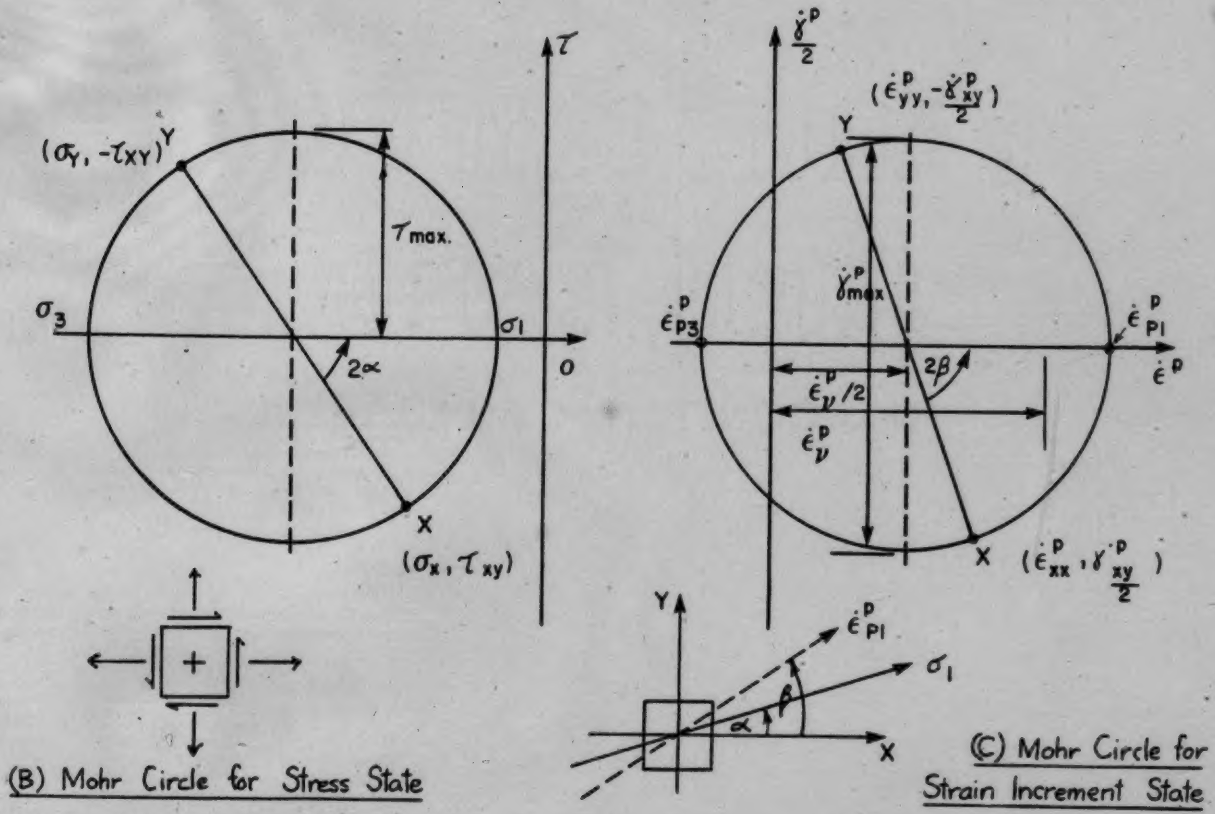
τ
(σ_Y, -τ_XY) Y
τ_max.
σ_3
σ_1
2α
O
X
(σ_x, τ_xy)
+
γ̇^p/2
(ε̇^p_yy, -γ̇^p_xy/2)
Y
γ̇^p_max
ε̇_P3^p
ε̇_P1^p
2β
ε̇^p
ε̇_ν^p/2
ε̇_ν^p
X
(ε̇^p_xx, γ̇^p_xy/2)
Y
ε̇_P1^p
σ_1
α
β
X

(B) Mohr Circle for Stress State

(C) Mohr Circle for Strain Increment State

FIGURE 3.7 SCHEMATIC CONSTANT-RATE-OF-DILATION MATERIAL AND EXPLANATORY MOHR CIRCLES.

The material parameters which describe the yield function may be variables of stress state or strain state. It is only important that their variation be defined so that as yielding occurs the associated changes in the yield surface can be computed.

Soil behaviour is dominated by stress-path or strain-path dependency, therefore yield surface changes are important constituents of most elastoplastic models. Historically, the variation of these parameters has been termed "hardening" or "softening", so the terms *hardening law* or *softening law* refer to expressions for strength-gain or strength-loss during yielding. Mathematically, *hardening* is associated with expansion of the yield surface, and vice versa for *softening*. Criteria can be established mathematically concerning the stability and uniqueness of the hardening or softening processes (Drucker and Prager, 1952).

The deformation theory of plasticity has been found inappropriate for application to soil mechanics because of the incremental path-dependency of soils, whereas the incremental flow theory has become the mainstay of soil plasticity. It is necessary to predict, at a given yielding stress state, the relationship between the components of plastic strain associated with an increment of plastic flow. The means for predicting these strain increment components is called the *flow rule*. In classical metal plasticity (Hill, 1950) the flow rule was obtained mathematically by differentiation of an expression called the *plastic potential*. The plastic potential provides a convenient means for keeping account of the flow rule, and is no more than a mathematical convenience.

In combination, the yield function, flow rule, and hardening law provide a self-contained means of predicting plastic strains associated with known stress changes during yielding, or vice versa. The mathematical formulation is more complex than for nonlinear elasticity because a far more complex process is to be described. When frictional soil behaviour was formulated by Drucker and Prager (1952), care was taken to preserve the requirements for material stability and solution uniqueness. (Equivalent requirements in elasticity place bounds on allowable combinations of material parameters). Mathematically, the stability and uniqueness requirements took the form of restrictions on the plastic potential. If this was identical in form to the yield function (ie, with the yield function) the criteria were met almost unconditionally. The criteria could not be fully met for *nonassociated* flow rules, but as pointed out by Prevost (1974) and Prevost and Hoeg (1975) this does not mean that nonassociated flow rules are unacceptable in soil mechanics. Davis (1969) described simple and effective associated and nonassociated plasticity theories which have subsequently been widely used by researchers at the University of Sydney. The Mohr-Coulomb material described below is an alternative formulation of the Davis model. A

Davis-type model will be discussed in detail below.

Separability of Strain Components:

It is reasonable intellectually (and convenient mathematically) to assume that an increment of yielding strain involves components of elastic and plastic behaviour,

$$\dot{\underset{\sim}{\epsilon}} = \dot{\underset{\sim}{\epsilon}}^{E} + \dot{\underset{\sim}{\epsilon}}^{P} \qquad \text{... Equation (3.1)}$$

where $\dot{\underset{\sim}{\epsilon}}$ is a vector of strain increment components

E,P superscripts denote elastic and plastic components respectively

This fundamental relationship cannot generally be evaluated experimentally without assuming isotropy or otherwise of material behaviour.

Mohr-Coulomb Nonassociated Elastoplasticity:

This simple and effective elastoplastic tool consists of material which has a fixed yield function and constant plastic dilatancy rate. A linear Mohr-Coulomb strength relationship is used as a strength criterion. The dilatancy rate, or ratio of increments of plastic volumetric strain and plastic shear strain, is a material constant which may assume any reasonable value. Over a restricted range of strains (of the order of 5%) this characterization agrees with experimental observation. The means of expressing the dilatancy rate may vary. Davis (1969) used a dilatancy angle which, when equal to the friction angle, leads to identical mathematical forms for the yield function and plastic potential (associated flow rule). An alternative approach is introduced here and will, it is hoped, clarify the derivation of the elastoplastic model.

Figure 3.7A shows schematically the intended material model behaviour. This model will henceforth be termed the Constant-Rate-of-Dilation Mohr-Coulomb model, or CRD for short. Also shown on the figure are Mohr circles of stresses and strain increments. The strain increment circle uses the engineering notation for shear strains and thus ignores the possible effects of rotational motion (de Josselin de Jong, 1959).

The *yield function* is

$$f = \tau - c_P - \sigma \tan \phi_P \qquad \text{... Equation (3.2)}$$

Expressed in terms of global XY axis components, this becomes

$$f = f(\sigma_X, \sigma_Y, \tau_{XY}, c_P, \phi_P) \qquad \text{... Equation (3.3)}$$

The yield function must remain equal to zero for sustained yielding, this occurs when

$$\frac{\partial f}{\partial \sigma_x}\dot{\sigma}_x + \frac{\partial f}{\partial \sigma_y}\dot{\sigma}_y + \frac{\partial f}{\partial \tau_{xy}}\dot{\tau}_{xy} + \frac{\partial f}{\partial c_p}\dot{c}_p + \frac{\partial f}{\partial \phi_p}\dot{\phi}_p = 0 \qquad \text{... Equation (3.4)}$$

(The dot notation refers to a small incremental quantity, not to differentiation with respect to time). For the CRD model, the strength parameters are constants. Summarizing equation 3.4,

$$\underset{\sim}{b}^T \dot{\underset{\sim}{\sigma}} = S \qquad \text{... Equation (3.5)}$$

where $\underset{\sim}{b}^T = \left\langle \frac{\partial f}{\partial \sigma_x} \; \frac{\partial f}{\partial \sigma_y} \; \frac{\partial f}{\partial \tau_{xy}} \right\rangle$

$$\dot{\underset{\sim}{\sigma}} = \begin{Bmatrix} \dot{\sigma}_x \\ \dot{\sigma}_y \\ \dot{\tau}_{xy} \end{Bmatrix}$$

and $S = -\frac{\partial f}{\partial c_p}\dot{c}_p - \frac{\partial f}{\partial \phi_p}\dot{\phi}_p$

$= 0$ for the CRD model.

The *flow rule* has two parts. Firstly, referring to Figure 3.7C, the dilatancy rate is a constant and is expressed as

$$D = \frac{\dot{\epsilon}_v^p}{\dot{\gamma}_{max}^p} \qquad \text{... Equation (3.6)}$$

which is a natural physical property of the Mohr circle. Secondly, it is *assumed* that the principal stress axes and principal strain increment axes coincide in space so that angles α and β are identical.

From the Mohr Circle of Strain Rates (Figure 3.7C),

$$\left.\begin{aligned} \dot{\epsilon}^{p}_{xx} &= \frac{\dot{\gamma}^{p}_{max}}{2}(D + \cos 2\alpha) \\ \dot{\epsilon}^{p}_{yy} &= \frac{\dot{\gamma}^{p}_{max}}{2}(D - \cos 2\alpha) \\ \dot{\gamma}^{p}_{xy} &= -\frac{\dot{\gamma}^{p}_{max}}{2} \sin 2\alpha \end{aligned}\right\} \quad \ldots \text{ Equation (3.7)}$$

From the Mohr Circle of Stress (Figure 3.7B),

$$\cos 2\alpha = \frac{\sigma_x - \sigma_y}{2\tau_{max}}$$

$$\sin 2\alpha = \frac{-\tau_{xy}}{\tau_{max}}$$

and hence

$$\left.\begin{aligned} \begin{Bmatrix} \dot{\epsilon}^{p}_{xx} \\ \dot{\epsilon}^{p}_{yy} \\ \dot{\gamma}^{p}_{xy} \end{Bmatrix} &= \frac{\dot{\gamma}^{p}_{max}}{4\tau_{max}} \begin{Bmatrix} 2D\tau_{max} + \sigma_x - \sigma_y \\ 2D\tau_{max} - \sigma_x + \sigma_y \\ 4\tau_{xy} \end{Bmatrix} \\ \text{or,} \quad \underset{\sim}{\dot{\epsilon}}^{p} &= g\,\underset{\sim}{a} \end{aligned}\right\} \quad \ldots \text{ Equation (3.8)}$$

Using equation 3.1,

$$\dot{\underset{\sim}{\epsilon}} = \dot{\underset{\sim}{\epsilon}}^{E} + \dot{\underset{\sim}{\epsilon}}^{P}$$

$$[D]\dot{\underset{\sim}{\epsilon}} = [D]\dot{\underset{\sim}{\epsilon}}^{E} + [D]\dot{\underset{\sim}{\epsilon}}^{P}$$

where $[D]$ is the elasticity matrix $\dot{\underset{\sim}{\sigma}} = [D]\dot{\underset{\sim}{\epsilon}}^{E}$

Therefore,

$$[D]\dot{\underset{\sim}{\epsilon}} = \dot{\underset{\sim}{\sigma}} + g[D]\underset{\sim}{a}$$

Premultiplying by $\underset{\sim}{b}^{T}$ gives

$$\underset{\sim}{b}^{T}[D]\dot{\underset{\sim}{\epsilon}} = \underset{\sim}{b}^{T}\dot{\underset{\sim}{\sigma}} + g\,\underset{\sim}{b}^{T}[D]\underset{\sim}{a}$$

In finite element calculations the total strain increment (or a trial value of it) is always known, and g has to be evaluated, so inserting equation 3.5 gives

$$g = \frac{\underset{\sim}{b}^{T}[D]\dot{\underset{\sim}{\epsilon}} - S}{\underset{\sim}{b}^{T}[D]\underset{\sim}{a}} \qquad \text{... Equation (3.9)}$$

All of the quantities of the R.H.S. of equation 3.9 are known for the current stress state and given total strain increment. Having obtained g, equation 3.8 can be used to evaluate the plastic strain increment and thus

$$\dot{\underset{\sim}{\sigma}} = [D]\,(\dot{\underset{\sim}{\epsilon}} - \dot{\underset{\sim}{\epsilon}}^{p}) \qquad \text{... Equation (3.10)}$$

The significance of the parameter g is clear. It must have a positive value and cannot be less than zero (Davis and Booker, 1974) because it is a measure of the rate of plastic work. It is also possible to describe the effect of hardening or softening via the parameter S. For the CRD material S is zero (no hardening or softening), but in more general applications,

$$\underset{\sim}{b}^{T}[D]\dot{\underset{\sim}{\epsilon}} - S > 0 \qquad \text{... Equation (3.11)}$$

which may be described as a stability criterion for realistic yielding.

The mathematical details of the CRD model are given in Appendix B, and some examples of the application of the model to bearing-capacity problems are given in Chapter 5.

Effect of Dilation Rate:

The dilatancy rate is an important material characteristic, both in physical modelling of behaviour and in terms of numerical behaviour of elastoplastic formulations. As the dilatancy rate increases, so the volume of yielding material is forced to expand to a greater extent and elastic stress changes are likely to be greater. It can generally be stated that lower dilatancy rates lead to more rapid numerical convergence.

3.4 ROWE'S STRESS-DILATANCY MODEL

In previous sections the microstructural link between strength and dilatancy was discussed. The reasons for adapting Rowe's Stress-Dilatancy theory for an elastoplastic model include:

1. experimental justification of a microstructural mechanism of yielding;
2. a theoretical basis in terms of internal energetics of the yielding system; and
3. a simplicity which permits easy application.

Rowe's (1962) introduction of the Stress-Dilatancy relationship was based upon observation of idealized particulate material (uniform-sized ballotini) using possibly inadequate testing equipment (inadequate provision for reducing end-restraint to ensure uniform deformations). Attempts to apply the theory to natural sand necessitated the replacement of a material frictional constant μ with a curve-fitting parameter ϕ_f that varied with the strain history of the material. At large strains ϕ_f approached a material constant ϕ_{cv} at which no further dilatancy took place. It was argued that a unique microstructural condition developed during constant-volume yielding and that this corresponded in principle with Taylor's (1948) concept of critical void ratio.

Subsequently, a great deal of research effort has focussed on the elaboration of the Stress-Dilatancy theory. Rowe (1963, 1969) and Rowe *et.al.* (1964) endeavoured to explain the reasons for strength differences under different test configurations such as triaxial compression, triaxial extension, plane strain, and direct shear. This effort neither clarified the value of the theory substantially nor contributed much to its utilization in engineering practice. The three reasons for adopting the theory in this work are now discussed and it is hoped that such discussion will establish the value of the concepts of the theory.

Experimental Justification:

The Stress-Dilatancy theory leads to a relationship for plane strain of the form

$$R = D.K \qquad \text{... Equation (3.12)}$$

where $R = \frac{\sigma_3'}{\sigma_1'}$, principal stress ratio,

$D = \frac{\dot{\epsilon}_1}{\dot{\epsilon}_3}$, inverse principal strain increment ratio,

K = a frictional parameter which at constant-volume yielding becomes Kcv.

A tension-positive convention is adopted for all mechanical quantities, and Figure 3.8 illustrates the quantities used. Implicit in Equation 3.12 is the coaxiality of principal stresses and principal strain increments. A fundamental assumption in establishing this relationship is the ratio of work increments of a stress system, therefore the extension to non-coaxiality can be made if the work increments are formed from coaxial components.

The quantities D and R may easily be measured in a triaxial or plane strain apparatus, assuming that homogeneous deformations occur. The experimental parameter K is the slope of a plot of R versus D. This may be found for any number of tests reported in the literature. Rowe (1972) discussed such experimental evidence at length, and concluded that ϕ_f is a curve-fitting parameter lying within the bounds of μ (interparticle friction) and ϕ_{cv}. Figure 3.9 shows the variation of ϕ_f throughout a triaxial test. However, in plane strain ϕ_f was shown to be essentially constant at the value of ϕ_{cv}. This can be explained in terms of the more restrictive kinematic conditions of the plane strain test. (Cornforth, 1964).

Rowe (1972) showed that a Stress-Dilatancy relationship could be found for a variety of strain conditions, provided that ϕ_f was allowed to vary somewhat during straining. For example, Figure 3.9 shows an R-D plot for a conventional triaxial compression test. The value of ϕ_{cv} was attained only following extensive grain slippage and remoulding of the material.

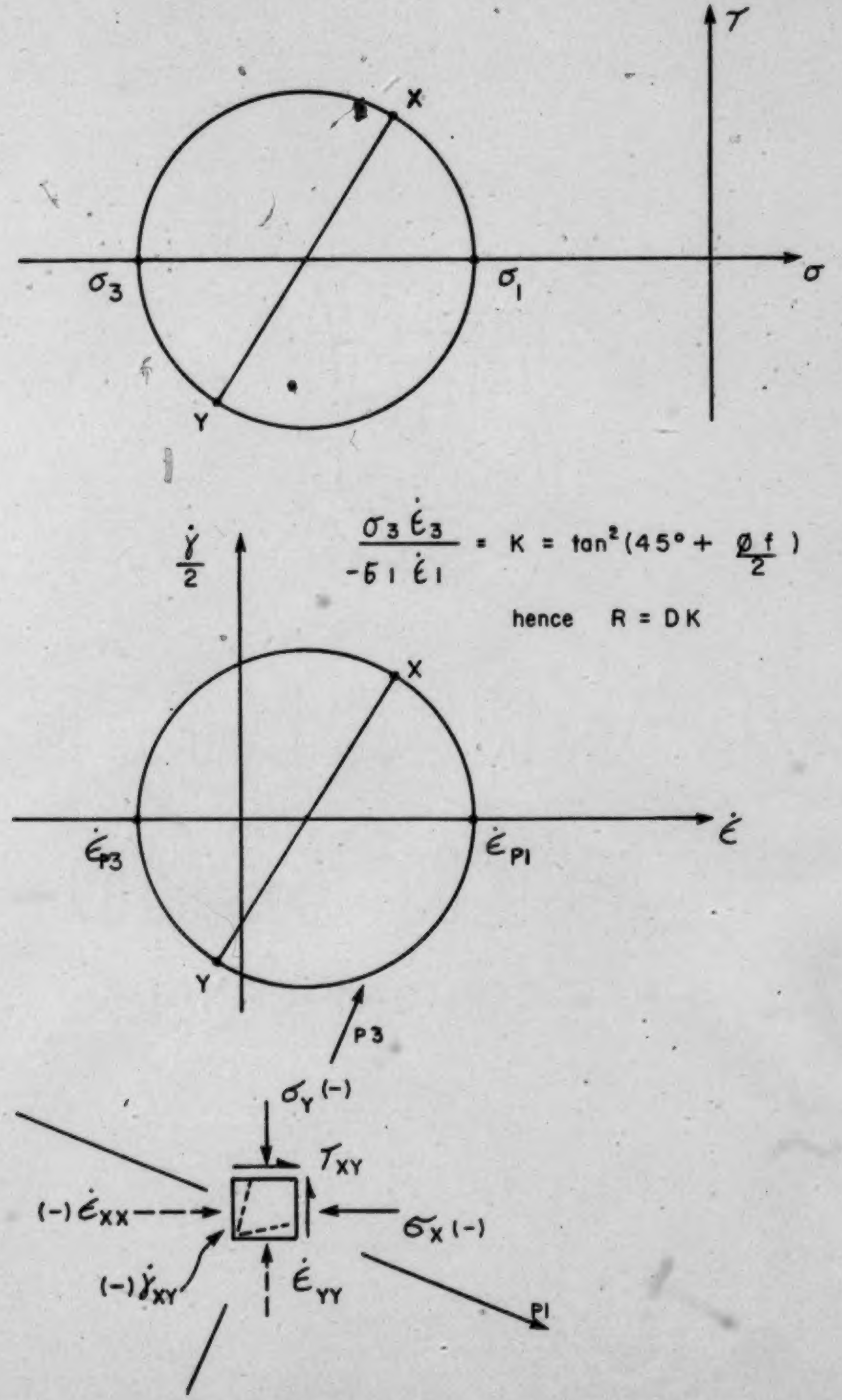

τ
X
σ_3
σ_1
σ
Y
$\frac{\dot{\gamma}}{2}$
X
$\dot{\varepsilon}_{P3}$
$\dot{\varepsilon}_{P1}$
$\dot{\varepsilon}$
Y
P3
σ_Y (-)
τ_{XY}
(-) $\dot{\varepsilon}_{XX}$
σ_X (-)
(-) $\dot{\gamma}_{XY}$
$\dot{\varepsilon}_{YY}$
P1

$$\frac{\sigma_3 \dot{\varepsilon}_3}{-\sigma_1 \dot{\varepsilon}_1} = K = \tan^2(45° + \frac{\phi f}{2})$$

hence $R = DK$

FIGURE 3.8 PRINCIPAL STRESS AND STRAIN INCREMENTS AND STRESS-DILATANCY RELATIONSHIP

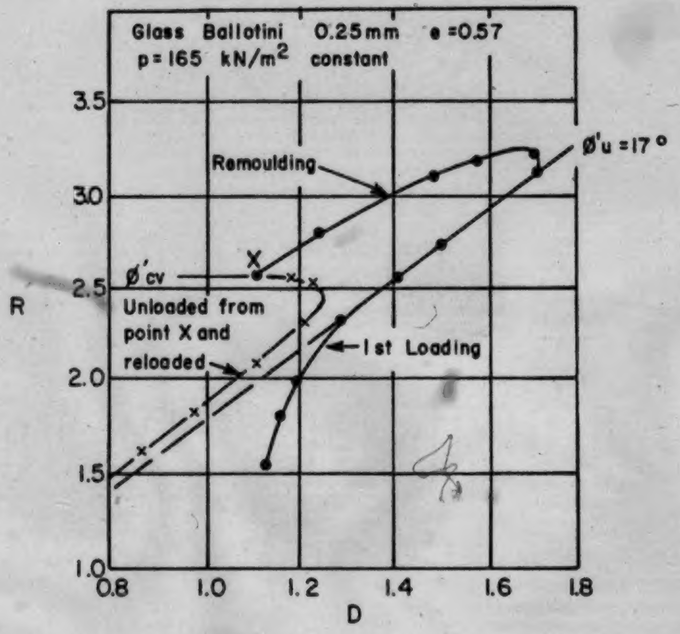

FIGURE 3.9 R-D PLOT FOR TYPICAL TRIAXIAL TEST (after ROWE, 1972)

Because the kinematic conditions of the plane strain test are more restrictive, much smaller overall deformations should be required to generate substantial remoulding. This test would therefore be a better means of investigating the influence of intergranular fabric characteristics on the development of the R-D relationship. Such features as anisotropy due to preferred grain orientation were studied in this manner by Oda *et.al.* (1978). Markedly different strength envelopes were obtained for different preferred grain orientations with respect to the principal stress axes. The R-D plots for some of their tests are shown in Figure 3.10. While the prepeak R-D paths vary in response to intergranular processes, the post-peak paths converge to a unique value of K. This suggests that grain slippage and reorientation and consequent fabric expansion created a unique microstructural response as the constant volume state was approached. The observations of Morgenstern and Tchalenko (1967 a,b) should be recalled at this point. They observed the development of a microfabric during direct shear of reconsolidated kaolin, that the shearzone of the sample developed into particle-like domains of clay material, and that an essentially unique structural arrangement of these domains developed as the constant volume condition was approached.

It can be concluded that variation of ϕ_f during shearing reflects internal energetics during evolution of the fabric to a constant volume condition. In plane strain,

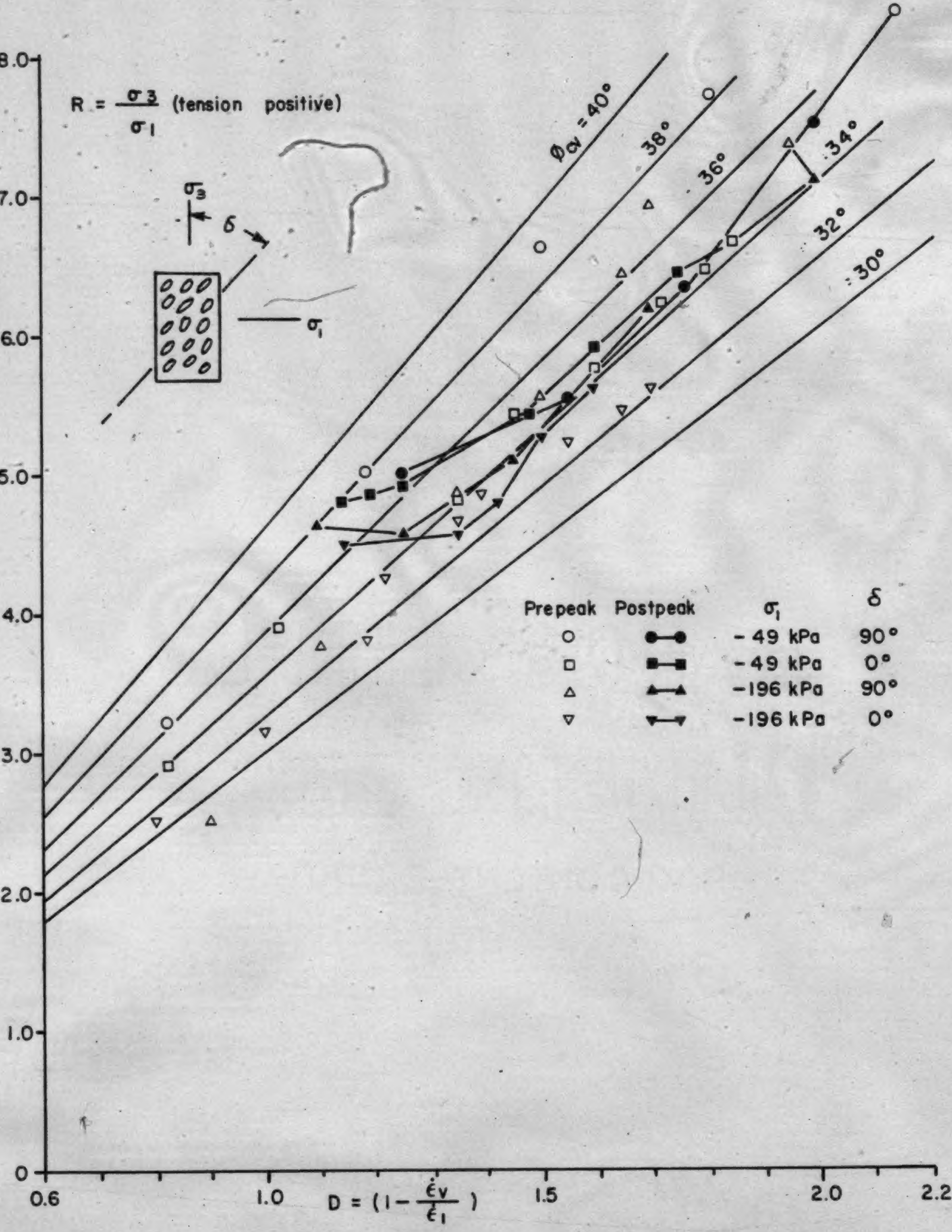

FIGURE 3.10 R – D PLOTS FOR PLANE STRAIN RESPONSE OF VARIOUS INITIAL SAND FABRICS (ODA et. al., 1978)

the value of ϕ_f is essentially constant in the post-peak regime. This last conclusion has great significance for modelling post-peak behaviour in plane strain.

The structure of shearzones was clarified by Skempton (1966) and a fine example of a large-scale fault-zone was discussed by Tchalenko and Ambrayseys (1970). The common features of shearzones ranging from microscale (direct shear tests) to macroscale (regional faults) were summarized by Tchalenko (1970). As a first approximation, it would seem that equivalent fabric processes should be governed by equivalent physical relationships. It can then be concluded that experiment and observation confirm the general applicability of the Stress-Dilatancy relationship to post-peak yielding of shearzones of any scale.

Theoretical Basis:

Rowe's original argument was that intergranular (or in its extended context here, intrafabric) motion consists primarily of irrecoverable slip at grain contacts. Slippage is controlled by interparticle friction, but the incremental work done by the slip between two adjacent surfaces cannot be generalized to the aggregate slippage of an irregular particulate assemblage without considering its volumetric behaviour. The virtual work relationship for simple frictional sliding reduces to a force equation. The equivalent virtual work relationship for the stress tensor of the aggregate, on the other hand, requires equating components of stress and strain tensors. Rowe chose, perhaps unfortunately, to explain his theory in terms of the ratio of input to output work and this was not a satisfactory physical basis for most of his contemporaries. However, Horne (1965) went to some trouble to explain that Rowe's concept was based upon a suitable frictional equilibrium model. De Josselin de Jong (1976) demonstrated by means of a frictional sliding model identical to Rowe's that the Stress-Dilatancy relationship was in fact a correct expression for the equilibrium of a dilatant aggregate.

Experimental observation of sand fabrics sheared in triaxial tests lead Oda (1972b) to an alternative derivation of the Stress-Dilatancy relationship based solely on mechanisms of intergranular contact and slip. More remarkably, Oda demonstrated firstly by theory and then by experiment that two phases of intergranular frictional mobilization can take place. Initially, deviatoric stress changes give rise to significant changes in the orientation of intergranular contact areas without noticeable rearrangement of the grains themselves. The pre-peak phase of shearing constitutes rearrangement of interparticle forces to sustain deviatoric stress. Progressively, further deformation requires interparticle slip which occurs by remoulding of the grain fabric, or by particle crushing and cleavage, or both.

Theoretical bases thus exist for the Stress-Dilatancy relationship as an expression of equilibrium of a frictional system. Oda's experimental work is also valuable as a clarification of the pre-peak and post-peak shearing processes in a granular aggregate. From an entirely theoretical point of view, Horne (1965) studied assemblies of uniform spheres, which enabled bounds to be placed on the value of ϕ_f , fully in accordance with experimental observation.

It is worthwhile to describe briefly other, parallel studies of granular aggregates undertaken over the same period as Rowe's work. Rennie (1959) considered the equilibrium mechanics of an assembly of ideal particles and developed bounds for the stress systems which could result. Further elaboration was undertaken by Parkin (1964), and Trollope (1968) formalized this work as an engineering stress distribution theory which he called Clastic Mechanics. Unfortunately, this work was not amenable to generalized numerical analysis and could not be used to predict magnitudes of deformations. Recently, a numerical elaboration was provided by Trollope and Burman (1980), but it still remains difficult to select material parameters from test data in order to carry out practical engineering analysis using discrete particle concepts.

Simplicity of Concepts:

A body of literature has been developed either in support of or in opposition to Rowe's work, but from a practical viewpoint these developments do not substantially affect the significance of the original concepts. Rowe proposed a remarkably simple, approximate relationship and verified it using test data which would probably be considered inadequate by modern standards. For the purposes of this research, Rowe's relationship is attractive for its simplicity and its implicit recognition of the internal microstructural processes controlling post-peak yielding. The details of faithfulness to real material behaviour can temporarily be set aside until the significance of post-peak weakening and dilatancy have been evaluated with the simple model.

Accepting the simple and approximate nature of the model, its adaptation to elastoplastic numerical analysis must be clarified. Considerable research effort has been spent on this aspect of Stress-Dilatancy, rather fruitlessly because of some fundamental misconceptions. Adaptation of the model will next be clarified.

Adaptation to Elastoplastic Theory:

The twin concepts of the *yield surface* and the *plastic potential* were adapted to soil mechanics from classical plasticity theory. Drucker and Prager (1952) established that frictional yielding had to be accompanied by an associated flow rule in order to guarantee stability and uniqueness on theoretical grounds. Critical State soil mechanics was established using similar concepts to Drucker and Prager's work.

The Stress-Dilatancy theory was naturally regarded as a flow rule because it linked components of incremental strain to the current stress state. In this research, the microstructural control of yielding has been emphasized, and *it is more reasonable to regard the Stress-Dilatancy relationship as a yield function controlled by the instantaneous strain rates*. By integrating the strain rates, the instantaneous volumetric strain establishes the current void ratio. Alternatively, the current void ratio establishes the available strain rate ratio, and, as noted by Taylor (1948), the instantaneous yield function. *It is therefore reasonable to establish a flow rule whereby current strain rate increments are a function of current void ratio.*

One further piece of information is required: these strain rates must be linked physically to the current stress state. Roscoe *et.al.* (1967) showed clearly that principal plastic strain increment axes tend to be coaxial with current principal stress axes, although Drescher and de Josselin de Jong (1972) and Drescher (1976) presented data which support a restricted amount of non-coaxiality. While there may be phases of transition from the more elastic pre-peak processes to fully developed plastic post-peak behaviour, *let the flow rule be completed by assuming the unconditional coaxiality of principal strain increment axes and principal stress axes.*

If the coaxiality assumption is not made, further information is required to specify the directional relationship between the current stress axes and current strain increment axes. An axial deviation parameter might be introduced, but theoretical and experimental justification would need to be sought.

De Josselin de Jong (1959) considered the critical void ratio (constant-volume) frictional yielding of sand, and established that there could be a restricted range of non-coaxiality of the quantities adopted above. His research was most elegant, and on theoretical grounds deserves to be extended to dilatant yielding. Thornton (1979) examined the flow rules available for various idealized packings of spheres and did describe bounds on the "undefiniteness" described by de Josselin de Jong. There is a large literature on such theoretical models, and there have been many fine experimental research efforts aimed at clarifying flow rules. Arthur *et.al.* (1977) portrayed the development of yielding in terms of hardening and softening (densification and dilation) but did not appear to come any closer to evaluating the importance of various elements of response which they identified.

The purpose of the Stress-Dilatancy model is to evaluate the role of microstructural dilatancy in overall stress-strain response. Such a model is limited to the shearband (that is, *internal*). The evolution of discrete shearzones and non-uniform straining has been examined as a bifurcation problem by Vardoulakis *et.al.* (1978) and the parameters used in their work are necessarily those governing response at the boundaries of the shearband (that is, *external*). With clarification of the importance of internal versus external characterizations of shearband response as an aim of this thesis, the finer points of plasticity theory and observed soil behaviour will not be discussed further. It remains to evaluate critically a model which incorporates, in as simple a fashion as possible, a reasonable representation of dilatancy. The mathematical development of elastoplastic Stress-Dilatancy is described in detail in Appendix C. Henceforth, the Stress-Dilatancy model will be referred to as the SD model.

3.5 A POST-PEAK PLASTICITY MODEL

Real physical and numerical limitations to the adoption of the Stress-Dilatancy model caused consideration to be given to a simplified post-peak model. It can be argued that non-uniform yielding may affect and control stress-strain response of a material element of any scale. The post-peak plasticity model was designed to be a simple continuum model reflecting the internal, perhaps non-uniform, yielding processes affecting such an element. By this means, a large-scale continuum element could behave as if affected by an internal, stress dilatant shearzone (or shearzones) of arbitrary size and orientation. As a simple example, plane strain testing of dense sand generally shows a transition from peak to residual behaviour over a few percent (axial) strain. Application of the Stress Dilatancy model typically requires a total shear strain of at least 100% to accomplish the peak-residual transition. Localized within the test sample there must be a shearzone which is straining at a much higher rate than the sample average.

The post-peak plasticity model was formulated in the simplest possible terms. Linear Mohr-Coulomb strength envelopes were assumed for peak and residual conditions,.

A schematic illustration of the model is given in Figure 3.11. The accumulated plastic shear strain was chosen as an indicator of available strength (Stroud, 1971) and to measure the peak-residual transition. The *derivable strength index*, which may be a nonlinear function of accumulated plastic shear strain, is used to interpolate strength and dilatancy characteristics between peak and residual conditions.

The elastoplastic form of the model is similar to the CRD model, with extra terms to take account of the change in strength associated with an increment of plastic shear strain. Mathematical development is described in detail in Appendix D, and the post peak plasticity model will henceforth be denoted by the abbreviation PPP.

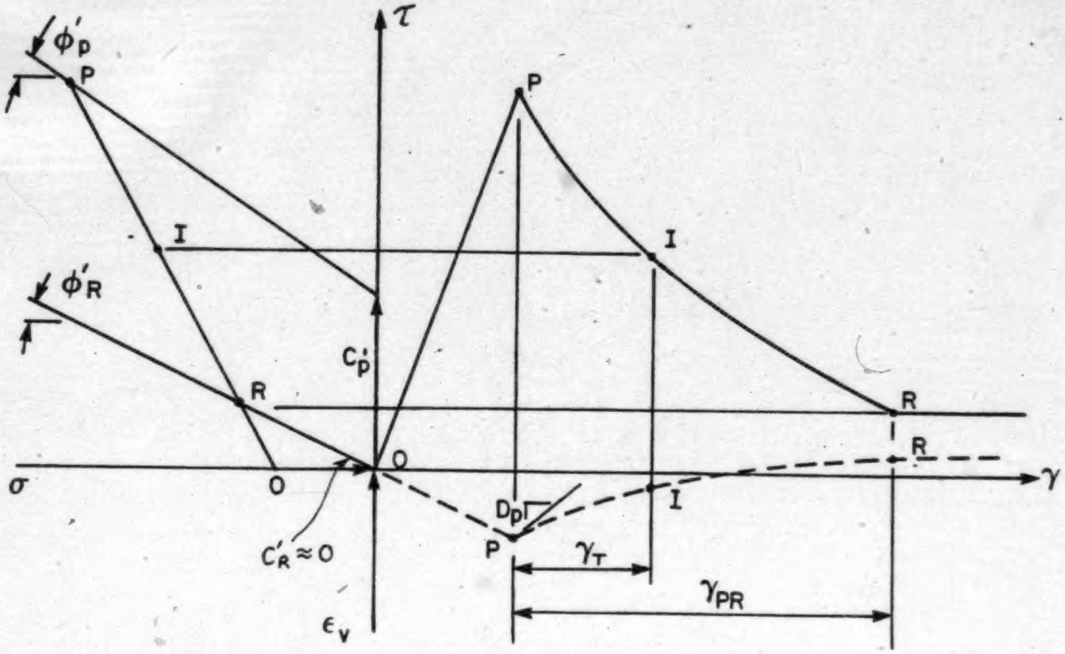
τ
ϕ'_P
P
P
I
I
ϕ'_R
C'_P
R
R
R
σ
O
O
D_P
I
γ
$C'_R \approx 0$
P
γ_T
γ_{PR}
ϵ_v

Pre-Peak Behavior : Isotropic Elastic

Post-Peak Behavior : $\dot{\epsilon} = \dot{\epsilon}^E + \dot{\epsilon}^P$

$\dot{\epsilon}^E$ = isotropic elastic portion of strain

$\dot{\epsilon}^P$ = plastic portion of strain

At an intermediate post-peak point, I,

Accumulated plastic shear strain $= \sum \dot{\gamma}^P{}_P = \gamma^P_T$

Derivable strength index DSI $= (1 - \frac{\gamma^P_T}{\gamma^P_{PR}})^{DSIX}$

$= 0$ if $\gamma^P_T \geq \gamma^P_{PR}$

Instantaneous strength $C'_I = DSI \cdot C'_P$

$\phi_I = \phi_R + DSI\,(\phi'_P - \phi'_R)$

Instantaneous dilatancy rate $D_I = \frac{\dot{\epsilon}^P_v}{\dot{\gamma}^P_{max.}} = DSI \cdot D_P$

Instantaneous tensile strength $t_I = DSI \cdot t_P$

Material Parameters K, G, C'_P, ϕ'_P, ϕ'_R, γ^P_{PR}, DSIX, D_P, t_P

FIGURE 3.11 SCHEMATIC POST-PEAK PLASTIC MODEL

3.6 REVIEW OF ANALYTICAL CONCEPTS

This chapter has been devoted to the development of analytical models for pursuing the behaviour of post-peak weakening. In particular, known micromechanical attributes of localized shearzones were chosen for modelling. This research poses the difficult problem of balancing exessively theoretical developments against sufficiently complex models of material response.

To start with, simple one-dimensional models for progressive shearzone failure were reviewed and an extension made to one analysis to account for the peak to residual strength transition. A two-dimensional, nonlinear, transverse-isotropic elastic constitutive model was then developed as an analytical tool for practical analysis of shearbands using finite element techniques. Together, these elasticity-based models provide means for obtaining stress-deformation solutions to shearband problems of known geometry and with known controls over shearband behaviour.

A review of elastoplastic theory, as adopted for this research, was given as a basis for establishing more rigorous constitutive models for shearzone mechanics. As an illustration, the familiar CRD model was derived. Models specifically capable of modelling post-peak weakening and associated internal dilation were then developed. The SD model is theoretically more rigorous. However, the geometric uncertanties associated with shearzone evolution and the practical computational problems associated with modelling such geometry necessitated development of a simpler and more phenomenological model, the PPP model.

The simple one-dimensional analytical models stand alone. They may be adapted readily to superficial analysis of shearzone problems of resticted geometry. In order to solve more general problems, the more powerful and realistic nonlinear elastic or elastoplastic models are required. This demands the development of suitable computational procedures, which for the complex geometrical and stress conditions of shearband problems require powerful, state-of-the-art finite element analytical techniques.

The computational models and the analytical technique cannot be considered separately. To a large extent the selection of the analytical techniques must follow the practical dictates of material models.

4. FINITE ELEMENT ANALYTICAL TECHNIQUE

A major portion of this research work involved development of computer programs for analysing localized deformations. It was important at the outset to define design criteria in order to utilize state-of-the-art numerical techniques, but so that development work could be concentrated where it was most necessary.

This chapter describes the development of computer programs for finite element analysis of localization problems. Design criteria and computational aspects are discussed. Alternative, readily available programs are reviewed. Two parallel developments, with elastoplastic and nonlinear elastic capabilities respectively, are outlined.

Verification of the accuracy and capabilities of the adopted finite elements is provided using a classical problem of linear elastic fracture mechanics.

4.1 REVIEW OF DESIGN CRITERIA

The critical elements of design, identified as a consequence of nonhomogeneous yielding, are:

1. localized, nonhomogeneous deformations,
2. high deformation gradients,
3. stress concentrations,
4. strength limits in shear,

5. strength limits in tension.

Localized Deformations:

The development of discrete shearzones as a consequence of post-peak weakening was discussed in Chapter 2. The finite element used to model this behaviour must not distort homogeneous deformation fields during elastic pre-peak straining, yet it must be capable of reasonably representing localized deformation when post-peak yielding commences. The distortion-free criterion requires geometrical behaviour independent of the orientation and shape of the element. This is not necessarily the case with the simple and popular Constant Strain Triangle (CST), and therefore cannot be the case with quadrilaterals composed of CST's (Yamamoto and Tokuda, 1971; Desai and Abel, 1972; Bathe and Wilson, 1976). Furthermore, stress equilibrium can only be approximated along inter-element boundaries. Clearly, elements should be able to represent variations of stresses in order to meet this equilibrium criterion as well as possible without demanding excessive mesh refinement (Cook, 1974). A higher-order general purpose element is required to meet such objectives.

Research is presently being conducted into self-adaptation of finite elements (automatic internal subdivision using non-nodal degrees of freedom) for solving fracture mechanics problems (Peano *et.al.* 1978, 1979; Peano and Riccioni, 1979) but this does not appear to have reached the stage where confident application can be made to localization problems. Figure 4.1 shows CST and multi-CST elements, higher-order isoparametric elements, and illustrates the self-adaptive technique. It was decided to examine higher-order isoparametric elements more closely.

High Deformation Gradients:

In Chapter 2, deformation compatability across a shearzone boundary was discussed, and it became apparent that very high local deformation gradients could be expected. The finite element model of a shearzone is a thin continuum or, in the limit, a displacement discontinuity.

In the case of a thin continuum element, displacement compatability between elements is assured. However, strain discontinuities between elements are permitted and stress equilibrium along the boundaries is approximated. Higher order (that is, quadratic order or higher) isoparametric elements allow more accurate representation of stress equilibrium in regions of high deformation gradient, and thus are suitable candidates for appropriate representation of shearband deformation fields.

Displacement-discontinuity elements were first utilized for modelling jointed rock (Goodman *et.al.* 1968) and have been extended to include dilatancy and nonlinear response to both normal and shear stresses (Goodman and Dubois, 1972). The behaviour of these elements is reduced to the

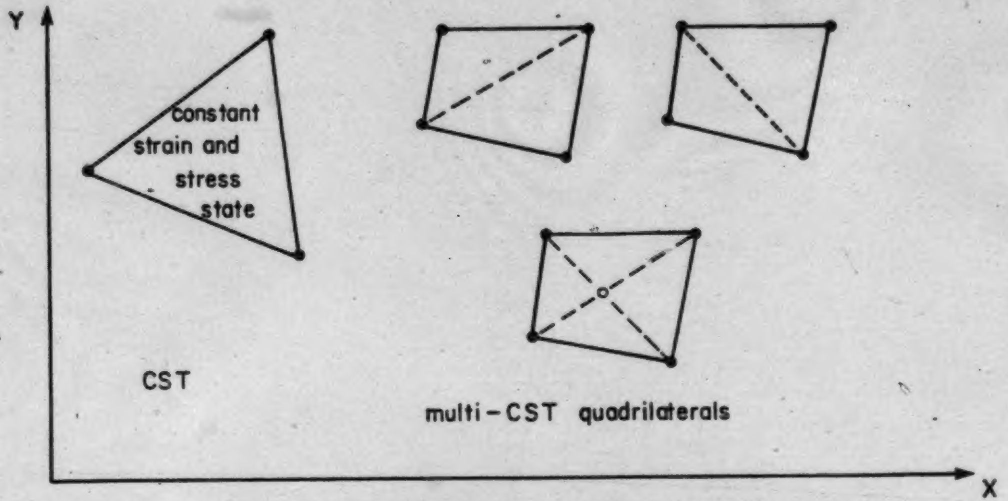
Y
constant
strain and
stress
state
CST
multi-CST quadrilaterals
X

(element performance depends upon orientation with respect to X-Y axes)

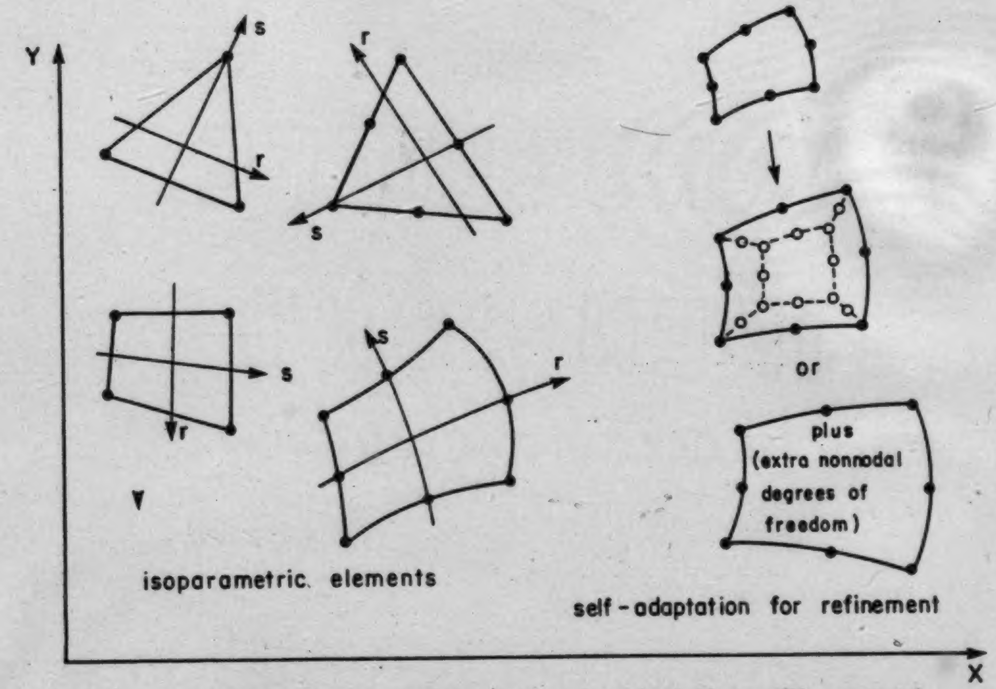
Y
s
r
r
s
s
r
s
r
or
plus
(extra nonnodal
degrees of
freedom)
isoparametric elements
self-adaptation for refinement
X

(element performance independent of orientation with respect to X-Y axes)

FIGURE 4.1 EXAMPLES OF FINITE ELEMENTS AVAILABLE FOR LOCALIZATION RESEARCH

relationship between stresses on the boundary and the relative displacements along and across the boundary. The element itself thus represents an *interface* between other materials.

Many variations of the basic interface formulation have been proposed (Ghaboussi *et.al.* 1973; Zienkiewicz *et.al.* 1970). Rowe and Davis (1977) used a similar element interface to introduce rupture lines into the analysis of bearing capacity problems, and the study of pile/rock-socket interaction has been addressed using the same approach (Rowe and Pells, 1980).

The thin continuum element creates constitutive problems only if large-displacement or large-strain formulations are required to accurately represent the high shearzone strains or strain gradients. On the other hand, there are unresolved, scale-dependent constitutive problems associated with the interface element. Ladanyi and Archambault (1970) and Barton (1975) described the nonlinear strength of rock joints with reference to the physical mechanisms involved. However, the determination of an appropriate scale for representative measurement of surface-roughness (Bruce,1978; Tse, 1979) remains open to debate. It is necessary to make semi-arbitrary assumptions of stiffness parameter values when applying the interface approach to shearzone problems, and these assumptions will change somewhat with the scale of the problem being analysed (shear-box shearband versus regional faulting, to cite extreme examples). Furthermore, no elucidation of the microstructural constitutive response within the shearband is possible using the interface approach.

An interface element was developed as part of this research. It is illustrated in Figure 4.2, the midside nodes being necessary for boundary compatability with adjoining higher-order continuum elements.

At the stage when constitutive response was being evaluated, the difficulties of accounting for scale-dependent interface response were recognized and the alternative of a thin continuum element was finally adopted. Figure 4.2 also shows the adopted shearzone continuum element. Studies (Pande and Sharma, 1979) have indicated that this element should perform reliably for very high aspect ratios (b/h=1000). High aspect ratios (b/h up to 6000) were used in the studies described in Chapters 6 and 7.

Stress Concentrations:

Stress concentrations at loaded or unloaded boundary intersections pose mathematical difficulties for analysis using elastic theory. Recognition of the singularities that develop in mathematical expressions for the stress concentrations lead to the development of alternative means for representing such phenomena. For real materials, the problem is experimental in nature: determination of a parameter which describes the effect of a stress

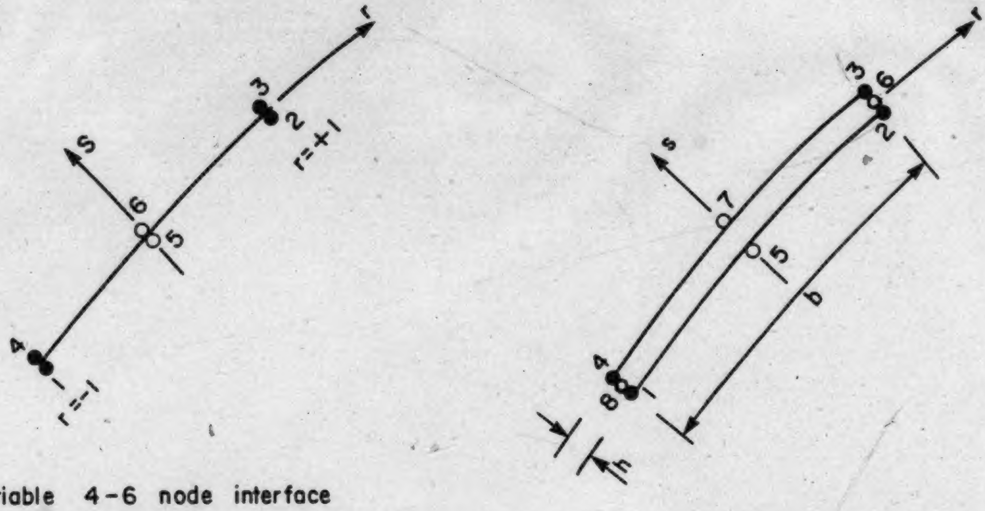
r
s
3
2
r=+1
6
5
4
1
r=-1
r
3
6
2
s
7
5
b
4
8
1
h

Variable 4-6 node interface element (node pairs share same coordinates)

Variable 4-8 node, thin continuum element (aspect ratio h/b > 10)

FIGURE 4.2 ELEMENTS FOR REPRESENTING SHEARBAND STRAIN GRADIENTS.

concentration for a particular load and geometry. The analogy in material strength theory is a stress concentration or stress intensity factor, which must be determined mathematically or by numerical analysis.

The key concept of progressive failure invokes development of shear stress concentrations which exceed the material strength. In order to study such behaviour numerically, finite elements must be capable of resolving the spatial extent of stress concentrations. In principle this can always be done with increased mesh detail. However, the spatial extent of a required level of detail cannot always be predetermined and, in any event, excessive refinement extracts a cost penalty. Higher order elements, particularly those of the isoparametric family, can represent stress variations effectively without excessive refinement (Cook, 1974). In particular, a special distortion of the eight node quadrilateral (Q48) element, as shown in Figure 4.3, allows accurate representation of the singularity at a Mode I crack tip. (Barsoum, 1976 and 1977).

For the foregoing reasons, the Q48 element was adopted as the basic tool for the numerical analysis described in this thesis. The computer programs using this element were developed using the concepts of Cook (1974) and Bathe and Wilson (1976), and are described separately (Simmons, 1980a,b). The reasons for this development, rather than adaptation from available program listings, are discussed in Section 4.2 below. The Q48 element has become a basic tool

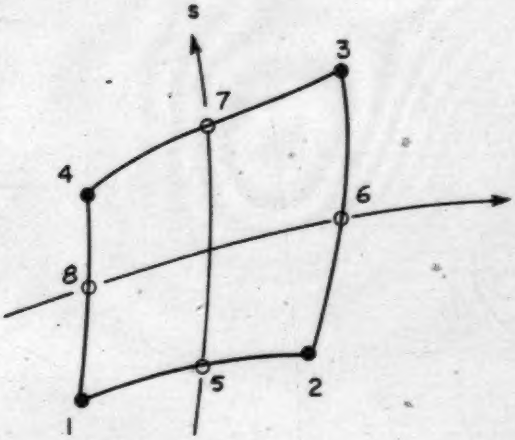

Basic Q48 element
Nodes 1-4 mandatory
Nodes 5-8 optional

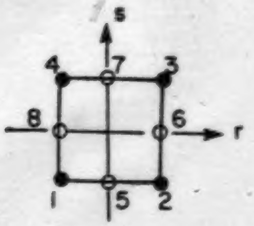
s
4
7
3
8
6
r
1
5
2

Mapping form of Q48 element

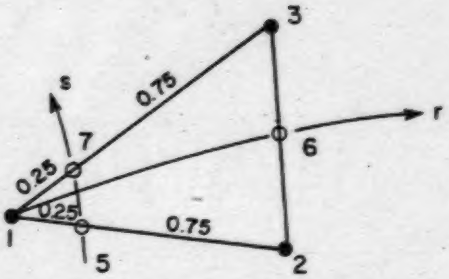
3
s
0.75
r
7
6
0.25
0.25
0.75
1
5
2

Special Distortion, gives rise to $\frac{1}{r^{1/2}}$ strain singularity at node 1.
(Similar stress singularity if linear elastic)
– after Barsoum (1976)

FIGURE 4.3 HIGHER ORDER ISOPARAMETRIC FINITE ELEMENTS

of finite element research in solid mechanics since it effectively combines accuracy and economy. Unfortunately, a detailed evaluation of its reliability for Mode II or mixed Mode I/Mode II stress concentrations has yet to be published.

The stress and strain singularities may take different functional forms depending on the nature of loading and the geometry of the crack or notch (Tada *et.al.* 1973; Tracey and Cook,1977). Best-known is the inverse-square-root-of-distance singularity at a perfectly elastic crack tip, which can be modelled using a special distortion of the Q48 element as noted above. Generally, to incorporate a known singularity into a numerical solution such as a finite element scheme requires the embedment of special shape function terms into the formulation of designated crack-tip elements. This in turn requires specialized coding and an anticipation of the correct singularity form, disadvantages in general applications. Also, the form of the singularity may change: for instance frictionless yielding at an initially elastic crack tip changes the Mode I singularity to an inverse-distance relationship. This would be very difficult to incorporate into a specialized crack-tip element. Wherever possible, it would thus seem that finer element subdivision, good mesh design, and general-purpose elements such as the Q48 element are the best means of generalizing numerical analysis of stress concentrations.

Strength Limits in Shear:

In most geotechnical problems there will be some region where the material shear stresses approach their strength limit. If the strength limits are not respected, the analysis may have little practical relevance unless the yielded zone is insignificant with respect to the overall structure. When material approaches a shear strength limit, the deformations become predominantly irrecoverable.

Strength limits and plastic deformations should therefore be accounted for in analysis. Clough and Woodward (1967) attempted to do this by adopting very low shear moduli in those elements where strength was exceeded, in an otherwise piecewise linear elastic analysis. Soon afterwards, Duncan and Chang (1970) introduced the hyperbolic nonlinear piecewise elastic model based upon earlier work by Kondner (1963). This model adopts tangent moduli based upon a hyperbolic approximation to work-strengthening triaxial compression stress-strain curves. It has become quite popular on account of its convenience, being based on standard testing techniques. Similar work by Krishnayya (1973) represented triaxial test data in a more direct manner. More recently, Elwi and Murray (1979) described a nonlinear piecewise orthotropic elastic model which was applied to strain-weakening response of concrete, but which could equally well be used for rock.

Many elastoplastic models have been inspired by earlier rigid-plastic models developed for limit equilibrium analysis (Drucker and Prager, 1952; Davis, 1969) but others have been developed as completely as possible from observed soil behaviour in simple laboratory tests (Roscoe and Burland, 1968; Lade and Duncan, 1975; Evgin and Eisenstein, 1980). It is not possible to review the literature on this subject here as such an undertaking would be immense given the published material now available. However, it is worth mentioning some approaches which have been taken for the representation of strain weakening.

Goodman *et.al.* (1968) modelled the post-peak yielding of rock with a simple nonlinear secant modulus approach. More realistic nonlinear elastic models were used by Lo and Lee (1973) and Sture (1976) for studying progressive failure, although no account was taken of the geometric limitations of shearband formation in these studies. Sture and Ko (1978) demonstrated that stable strain-weakening could only occur in a continuous medium if heterogeneous mechanisms (shearbands) were introduced into the medium. Analyses by Hoeg (1973) and Prevost and Hoeg (1975) demonstrated the more powerful potential of the elastoplastic approach, but created controversy because the original stability and uniqueness postulates of Drucker and Prager were violated. Concerns over the significance of these postulates, and the debate on implications of non-uniqueness, continue to this day (Cleary *et.al.* 1979; Dong, 1980). A study of the literature could easily leave the impression that a model displaying suitable mathematical properties (associated flow rules) may be more acceptable than a model which can more reasonably reproduce soil or rock behaviour.

In practical terms there are many ways of representing soil shear strength and irrecoverable deformations. For practical problem solving, a simple Mohr-Coulomb representation of strength in combination with the hyperbolic model appears to represent the current state of the art. For research purposes, the fundamentally greater significance of the elastoplastic models is attractive.

Tensile Strength:

Soils and jointed rock masses are characteristically weak in tension. Analyses in which significant tensile stresses develop are simply invalid except as crude indicators of tensile rupture location. Zienkiewicz *et.al.* (1968) introduced an iterative relaxation procedure to remove excessive tension. While the concept of the technique is sound and forms the basis for most elastoplastic computational schemes, there is a fundamental lack of uniqueness in techniques for applying a tensile yield criterion in this form. Experience has shown also that numerical tension-removal procedures have poor convergence characteristics in practice. An alternative means of dealing with tensile yield in elastoplastic analysis was developed. Both schemes were implemented where appropriate in computer programs written for this research.

4.2 COMPUTATIONAL ASPECTS

The only feasible means of modelling highly nonlinear material behaviour are:

1. piecewise loading using extremely small increments and constantly updated stiffness; or
2. piecewise loading using a few well-chosen increments, suitable approximate stiffnesses, and some iterative procedure which restores computed behaviour to that specified by the material laws.

The first method generally is uneconomical in practice, and numerical inaccuracies or instabilities are difficult to control. The second method usually can be adopted economically provided that sound and consistent numerical techniques are used. Only this second method will be discussed.

Irrecoverable (or plastic) deformations dominate nonlinear soil or rock response under load. Consider the simple example of Figure 4.4, where ideal stress-strain behaviour is to be approximated using two fundamentally different material models. The piecewise nonlinear elastic model can follow the portion of the stress curve where the tangent stiffness is positive and the tangent volume change rate is negative (compressive loading). However, a direct numerical solution cannot in general be achieved for the dilatant volume change curve nor for the strain-weakening stress curve. In practice, the achievable numerical solution may or may not be adequate for the purposes for which the

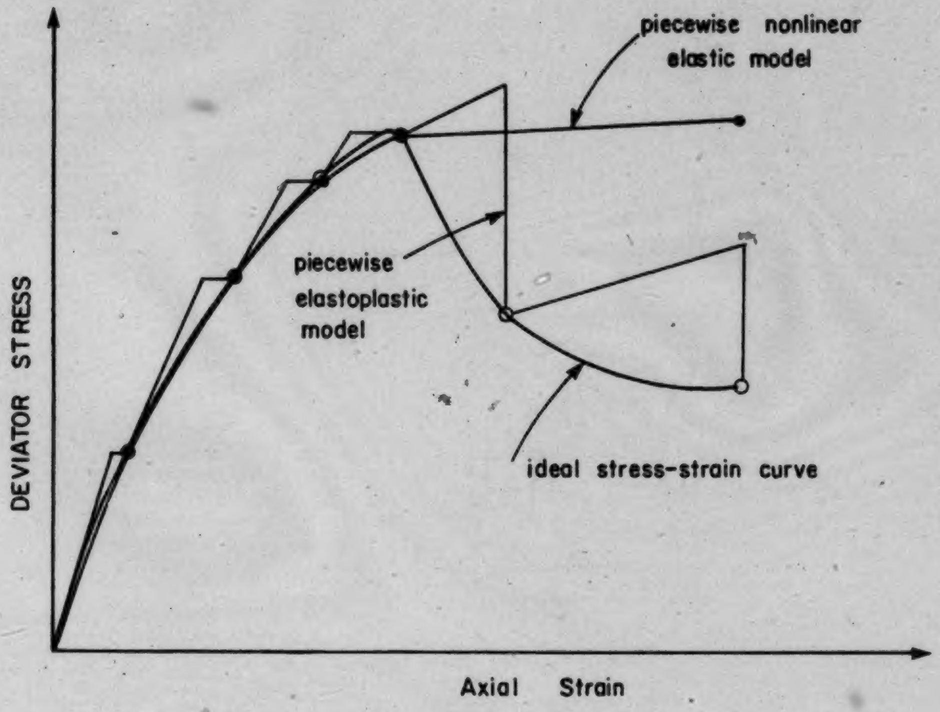
piecewise nonlinear elastic model
piecewise elastoplastic model
ideal stress-strain curve
DEVIATOR STRESS
Axial Strain

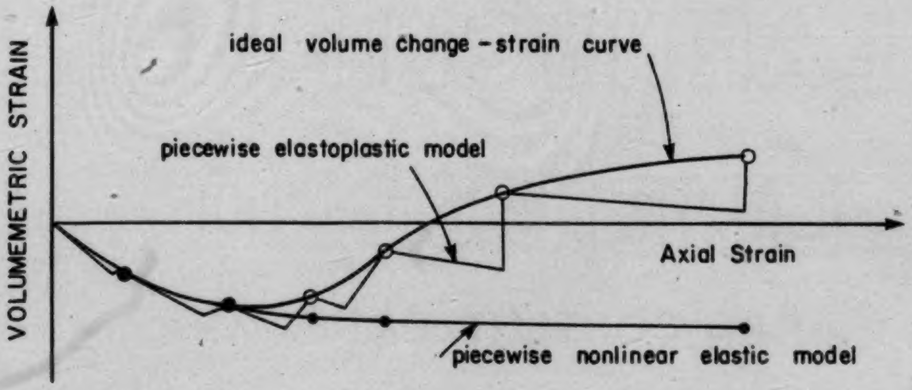
ideal volume change - strain curve
piecewise elastoplastic model
VOLUMEMETRIC STRAIN
Axial Strain
piecewise nonlinear elastic model

FIGURE 4.4 CAPABILITIES OF NONLINEAR ELASTIC AND ELASTOPLASTIC MODELS.

analysis was undertaken. The elastoplastic model is in principle capable of using some trial stiffness and then formulating a correcting adjustment to maintain agreement with specified behaviour. The nonlinear elastic (NLE) model produces its results by direct calculation while the elastoplastic (EP) model requires an iterative calculation sequence. Computationally, the NLE model is more efficient but less capable than the EP model. Therefore, some iterative process could in principle be built into the NLE model to achieve more reasonable results for computational effort equivalent to the EP model.

Whether or not the NLE or EP model is most suitable for a given problem will depend very much on the nature of the problem. If prepeak behaviour only is invoked, or if the materials do not strain-weaken, obviously the NLE model has economic advantages. If prepeak behaviour only is invoked but a significant volume of the material dilates, the misfit of computed strains becomes important since to correct these strains imposes significant volumetric expansion on the mass. The solution to any field problem requires equilibrium *and* compatability of deformations. The displacement formulation of the usual finite element procedure enforces compatability and approximates equilibrium. It becomes increasingly important to enforce the compatability of *correct* deformations, as dilatant zone behaviour increasingly dominates that of the mass. Since most deformation problems are undertaken because of uncertainties about the size and role of nonlinear material zones, the EP model has the best potential for geometrical as well as numerical accuracy. Corrections to the NLE model to more closely mimic true material response can be made, but there is no fundamental significance to either the processes invoked or the methods used, and therefore no guarantee as to how well the correction process will perform under given conditions. The path dependent nature of nonlinear response has been recognized for a long time, and piecewise EP calculations would thus seem to have inherent advantages over NLE calculations in any event. It is concluded (for this research) that the NLE approach is an appropriate tool for yielding which does not involve post-peak weakening and dilatancy, but that the EP approach must be adopted if post-peak microstructural processes are to be accounted for. In both models, a careful piecewise loading approach is required particularly if there are changes in directions of loads. The question of identifying the volume within which such processes operate is an entirely separate problem. In this section the NLE and EP model computational approaches, within a displacement formulated finite element scheme, are now described.

Nonlinear Elastic Model:

In principle, the strain and stress increments for each stage of loading follow the secant moduli for the material at the start of the increment. It is not generally possible to predict what the secants are, but the tangent moduli can be evaluated readily. For typical nonlinear loading, shown in Figure 4.5, the use of tangent moduli will not always accurately predict the material response. In practice, the load step is analysed iteratively, with some intermediate tangent moduli, in order to approximate the secant behaviour. The average stress approach (Kulhawy and Duncan, 1970) has been found to work well in practice. Within such an iterative process other adjustments may be made to the moduli. For example, tensile yield can be recognized and direction-dependent, orthotropic elasticity used to weaken the tensile zone in the appropriate direction (Sandhu, 1973). Shear yielding can also be accounted for. Mohr-Couloumb yielding was treated by Clough and Woodward (1967) by appropriate reduction of the shear modulus in an isotropic elastic formulation. The transverse-isotropic formulation, which allows one shear modulus to be adjusted independently of all other strain components, was successfully used to simulate the response of a weak shearband and this is described in Chapter 7. A schematic flow diagram for an increment of a nonlinear elastic analysis is shown on Figure 4.5.

Elastoplastic Model:

There are many means for formulating elastoplastic response. For displacement-method finite elements, results at any computational stage are correct for deformations but

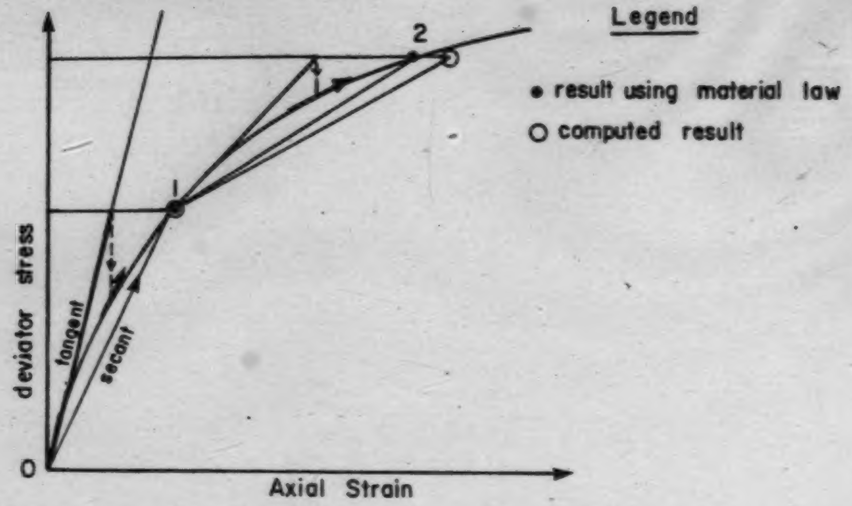
Legend
• result using material law
○ computed result
2
1
deviator stress
tangent
secant
0
Axial Strain

Schematic Nonlinear Elastic Computational Scheme

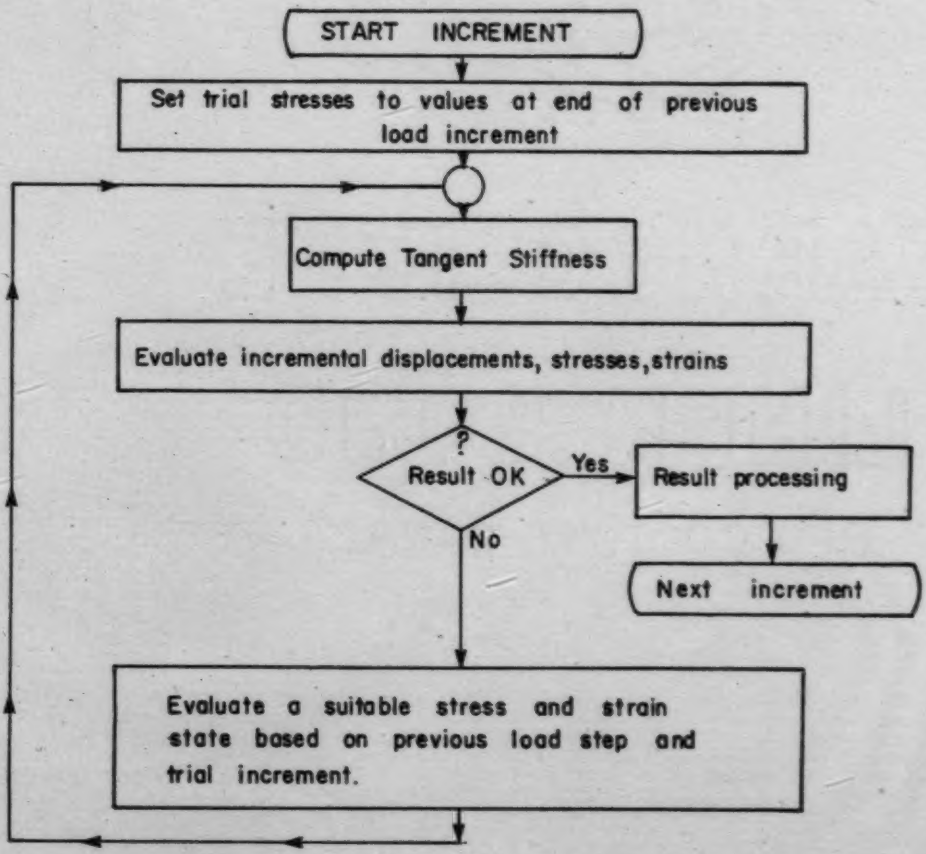
START INCREMENT
Set trial stresses to values at end of previous load increment
Compute Tangent Stiffness
Evaluate incremental displacements, stresses, strains
?
Result OK
Yes
No
Result processing
Next increment
Evaluate a suitable stress and strain state based on previous load step and trial increment.

FIGURE 4.5 NONLINEAR ELASTIC COMPUTATIONAL PROCEDURE

incorrect for stresses unless the true secant moduli has been used. The elastoplastic formulation should thus be a means of correctly predicting stress response for a given strain increment. Use of the term elastoplastic implies that strain response consists of elastic and plastic components. A number of formulations are available (Desai and Abel, 1972; Desai and Christian, 1977) and for illustrative purposes an initial stress method will be described here. Figure 4.6 shows a typical incremental elastoplastic load step. The unload/reload elastic stiffness is an appropriate modulus choice since if the load step results in a stress state within the yield surface, a reasonable response has been guaranteed. Application of the load causes a first trial elastic strain as given by the chosen moduli. The corresponding trial stresses do not coincide with the material's elastoplastic response. Out-of-balance forces equivalent to the stress discrepancy can be computed. The displacements necessary to release the stress discrepancy can then be found and added to the previous trial displacements. This process is repeated until a converged solution is obtained (an equilibrium stress state *with* completely compatable elastoplastic strains). The likelihood of divergence of the solution, implying possible structural instability, has of course to be anticipated. This process is shown schematically on Figure 4.6.

It should be noted that many documented elastoplastic computer programs do not fully consider the equilibrium

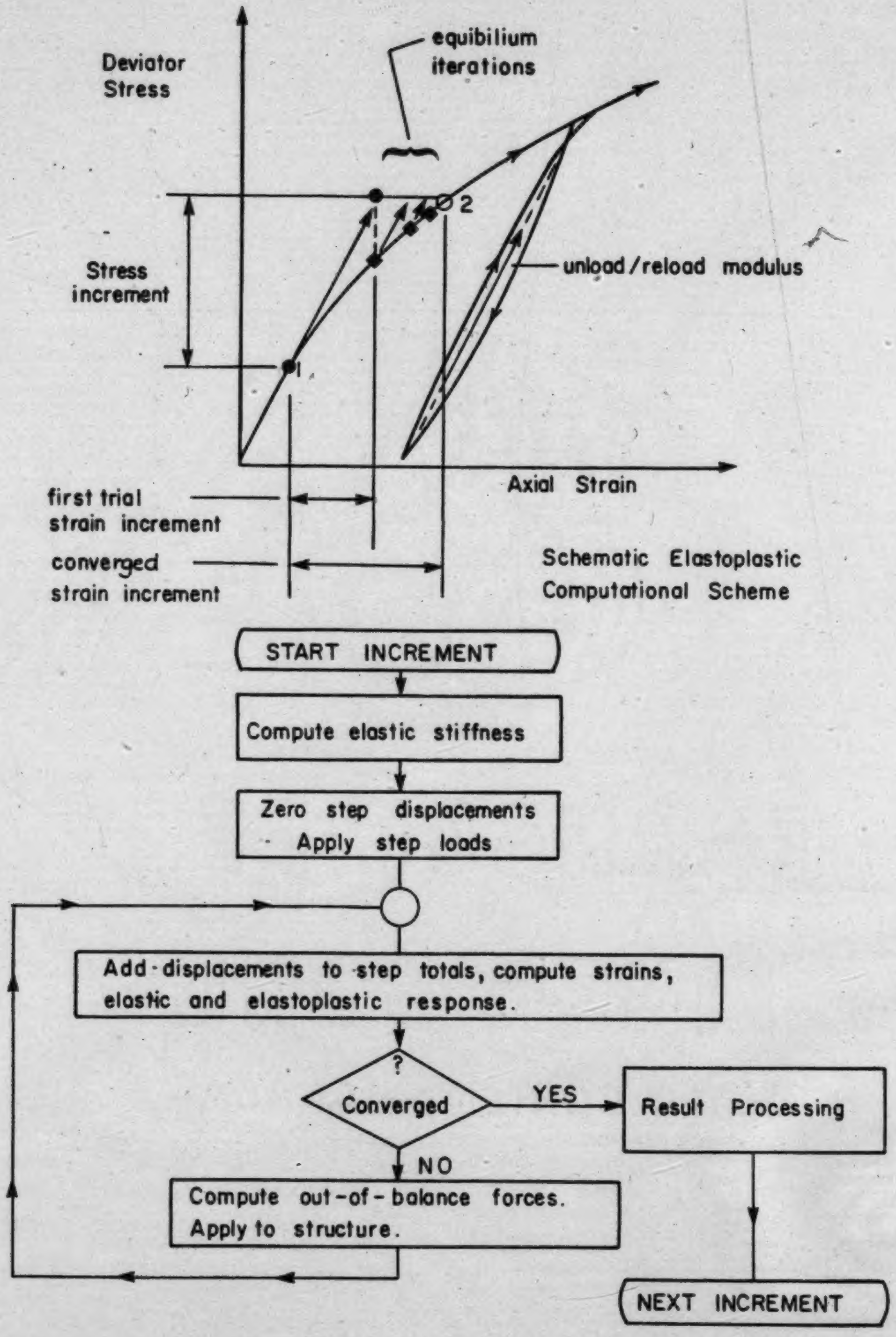
equibilium
iterations
Deviator
Stress
2
Stress
increment
unload/reload modulus
1
Axial Strain
first trial
strain increment
converged
strain increment
Schematic Elastoplastic
Computational Scheme
START INCREMENT
Compute elastic stiffness
Zero step displacements
- Apply step loads
Add displacements to step totals, compute strains,
elastic and elastoplastic response.
?
Converged
YES
Result Processing
NO
Compute out-of-balance forces.
Apply to structure.
NEXT INCREMENT

FIGURE 4.6 ELASTOPLASTIC COMPUTATIONAL PROCEDURE

iterations referred to above. This was found to be the case with three programs examined (Wong, 1978; Sandhu, 1973; Christian *et.al.* , 1977). Only two analytical schemes (Nayak and Zienkiewicz, 1972; Bathe, 1978) were known to the writer to deal correctly with equilibrium iteration. For this reason, a primary concern of computer program development for this research was the proper treatment of elastoplastic convergence. The next sections of this thesis document some available computer programs, and indicate the subsequent program designs undertaken.

4.3 COMPUTER PROGRAM CHOICES

There is an immense gulf between conceptual development and successful implementation of numerical techniques. Usually, research is undertaken to explore ideas well in advance of practical serviceablility. Hence even the present-day wealth of program material and instant accessibility through modern telecommunications are no guarantee that an alternative to the basic re-writing of computer programs can be found by the researcher. Often, there is a lack of knowledge or experience upon which to base a choice between writing a program, modifying an existing program, or finding and proving suitable a publicly available program.

There is a mystical quality to large complex computer programs which clouds their true character. Linear elastic finite element analysis can be performed reliably by probably hundreds of programs. Every departure into nonlinear behaviour carries not merely a cost penalty but the many undefinable uncertainties of approximation and assumption. There is no such phenomenon in existence as a nonlinear finite element program which can be successfully and reliably used without continued support by and consultation with its originators. The claims often made for program capabilities are without doubt based on author's perceptions of the correctness of the principles proposed. Nonlinear analysis is far more complex than it is often taken to be, and author's perceptions are not always fully substantiated by user's experience. This is not to condemn nonlinear analysts or their programs, but to point out that it is naive and possibly dangerous to believe anything about nonlinear computer programs which cannot be independently tried and proven by the unaided user. It was, after all, on this basis that linear analyses became acceptable. One is therefore tempted to conclude that any development of new nonlinear techniques requires a new computer program.

At the outset of this research the envisaged geometric and material modelling problems made the development of a new program seem unavoidable. A brief review is given below of the alternatives available when this decision was made. Alternative facilities within the computing system at the University and commercially available outside the University were examined.

Program Facilities Available at the University of Alberta:

Programs readily available through the Civil Engineering facilities at the time when this thesis was prepared include a group from Ohio State University (designated OSU here, and described by Sandhu, 1973), FENA2D and FENA3D (Krishnayya, 1973) and NONSAP (Bathe *et.al.* 1974)

Attempts to use the OSU programs were fruitless. Only CST-type elements were available, nonlinear procedures were neither adequately described nor properly coded, and special coding (for solving only the problems introduced in the manual overview) was widespread. Some coding was obscure enough that it was not possible to determine how the material nonlinearities (for instance) could be modified for current research purposes.

The FENA programs are adequately coded and documented but would require extensive modifications to upgrade the elements and incorporate different material models. The OSU programs were quickly abandoned and it was felt that comparable energies would be absorbed either in modifying FENA or in writing a program from first principles. NONSAP has never been a successful nonlinear analysis tool and is now somewhat outdated (independent personal communications, K.-J. Bathe and D.W. Murray).

Long after original program development was embarked upon, Elwi (1981) developed the FEPARCS program for post-peak behaviour of concrete shells. With minor modifications to the material model (Elwi and Murray, 1979) this program is potentially suitable for rock mechanics research, but it cannot be used beyond the limitations of nonlinear elasticity.

It was concluded that there would be little difference in the efforts required either to completely develop a new program or to adapt an available program. Therefore, computer programs were written specifically for elastoplastic and for nonlinear elastic analysis. An attempt was made to make various sections of these programs as modular as possible. Ideally, a master management program system would have been developed, allowing complete modularity of material models, elements, and solution algorithms. Commercial programs of this nature exist, and have great advantages when further modifications are required.

Program Facilities Available Commercially:

The University of Alberta computer system allows direct incorporation of internal computing costs within an overall operating budget. It is therefore difficult to justify spending "real" dollars on using programs on outside systems, let alone afford the cost of developing programs on these systems at commercial rates. However, some of the programs available on outside systems have attractive capabilities which are worthy of review here.

Nonlinear and drained or undrained response of oilsand is simulated by the NEAT program (Thurber Consultants

Limited, 1979). An updated version, OILSTRESS (Byrne and Grigg, 1980), is installed on a computing system at the University of British Columbia which is nearly identical to that at the University of Alberta. OILSTRESS has a procedure for incorporating dilatant weakening. Neither of these programs were available when this research was undertaken, and they do not incorporate the higher order elements thought necessary in any event.

A popular commercial nonlinear finite element program is MARC (MARC Analysis Research Corporation, 1973). MARC was written specifically to achieve either nonlinear elastic or elastoplastic response, using many different families of elements and a restricted number of material models and solution algorithms. Only Drucker-Prager associated plasticity is available for frictional materials, and there is no facility for specifying other material models. MARC is expensive and is generally used on a month-by-month lease basis. Widespread usage for fracture mechanics analysis and design of metal structures has been reported (J. Swanson, ANSYS program author, personal communication) but the program is in a state of restricted support at present (P. Patillo, Amoco Petroleum Company, personal communication). It has been adapted and somewhat modified for geomechanics research (Geertsma, 1976) but apparently large expenses were incurred with rather unsatisfying results.

Enlarged versions of NONSAP are available on most commercial systems. There is no immediately available guide as to the usage pattern for the program but it is unlikely to be significantly improved over the version at the University of Alberta.

Large capacity, readily available finite element and generalized structural analysis packages include MSC/NASTRAN, STARDYNE, GT STRUDL, SAPIV and ANSYS. Features available with these programs include enhanced pre- and post-processing, choice of solution algorithms, large element libraries, selection of material models, and large-strain or large-displacement formulations. The most important factor to be evaluated when choosing among such program systems is the level of support offered by the computer service organization being dealt with.

ANSYS, available through most service companies, is the only commercial system currently undergoing intensive research and development (R. Zirin, General Electric Company, personal communication 1979). SAP IV is satisfactory for linear elastic problems but lacks significant nonlinear capacity. STARDYNE is a widely used system which can perform economical static and dynamic analyses, but it lacks support in nonlinear material model options. MSC/NASTRAN is probably the largest and most diversified of all systems in its capabilities, but there is no documented experience with the MSC (MacNeal Schwendler Corporation) material model enhancements to properly evaluate capabilities in geotechnical plasticity. GTSTRUDL is an extremely efficient program to use and includes geometric nonlinear analysis, but has no material models suitable to geomechanics.

ANSYS has gained an excellent reputation amongst practicing engineers for its ease of use, interactive sophistication, and nonlinear capabilities. However, it does not yet support frictional plasticity and because of its highly proprietary nature is unlikely to be enhanced for geomechanics applications until sufficient demands arise from its market. The originator of ANSYS, John Swanson, recommended MARC as a tool for frictional plasticity as recently as August 1979 (personal communication).

A users group based at Massachusetts Institute of Technology has recently marketed ADINA/ADINAT. These programs (structural analysis and thermal analysis respectively) are deliberately modular in design, specifically embrace satisfactory iteration methods for nonlinear analysis (Bathe, 1978) and represent state-of-the-art development in these areas. ADINA has limited commercial support but has been widely adopted by research groups. There is documented experience of its application to a shearband problem (Dong, 1980). Costs for this application were high (by university research standards at any rate) and it does not possess non-associated frictional plasticity. A material model for concrete is available and other material models can be "plugged-in".

It was decided that a specialized program should be developed to incorporate the geometric and material demands identified at the outset of the research program. Later, two parallel programs were developed to deal specifically with nonlinear elasticity and elastoplasticity. Much benefit was gained from communications from and discussions with Klaus-Jurgen Bathe and many features of ADINA were adopted.

4.4 REVIEW OF PROGRAM DESIGN

This section describes the various aspects of the finite element programs developed for this research.

Isoparametric Q48 elements were used, and appropriate boundary conditions and loading schemes were developed. Equilibrium equations were solved by direct gaussian elimination and backsubstitution. Stress sampling and averaging was carried out in a manner consistent with the isoparametric formulation, and similar techniques for stress initialization were developed. These features are common to both the nonlinear elastic program (NLCP) and the elastoplastic program (ESB) and are described in more detail below.

Constitutive models as described in Chapter 3 were incorporated into the programs, and appropriate nonlinear algorithms for each class of material behaviour were developed.

Element Design:

The basic continuum element is a variable 4 to 8 node isoparametric quadrilateral (Q48) described by Bathe and Wilson (1976). The optional midside nodes permit economy in areas of low strain gradient and also provide the quarter-point distortion enabling the crack-tip strain singularities of linear elastic fracture mechanics to be represented, as noted in Section 4.1. A matching 4 or 6 node interface element, in an isoparametric formulation but based upon the work of Goodman *et.al.* (1968), was also developed. When the midside nodes are included, the Q48 elements may have curved boundaries. Experience (R. Zirin, General Electric Company, personal communication) has shown that under certain configurations these elements do not perform very well (Figure 4.7). When used to check various problems of classical elasticity, the elements performed remarkably well: comparative accuracy of the Q48 element was generally much better than that achieved using an equivalent number of nodes but simpler elements.

A classical problem of linear elastic fracture mechanics was used to test the capabilities of the continuum element, and the results are discussed in Section 4.6.

The interface element has so far been developed only as an elastic tool, since the constitutive requirements for its nonlinear response were not investigated in this thesis. It performed in a similarly excellent manner to the Q48 element when tested on elastic problems.

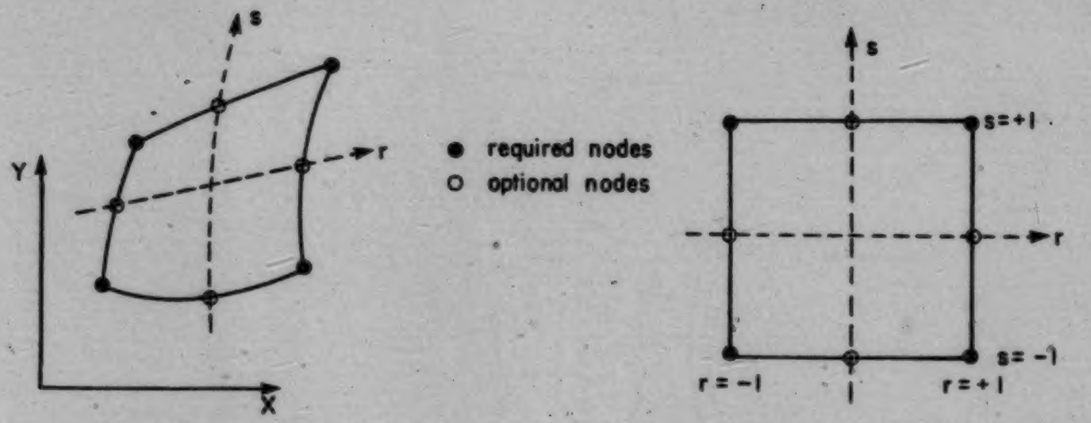
s
r
Y
X
● required nodes
○ optional nodes
s
s=+1
r
s= -1
r = -1
r = +1

Physical configuration

Natural r, s coordinate mapping

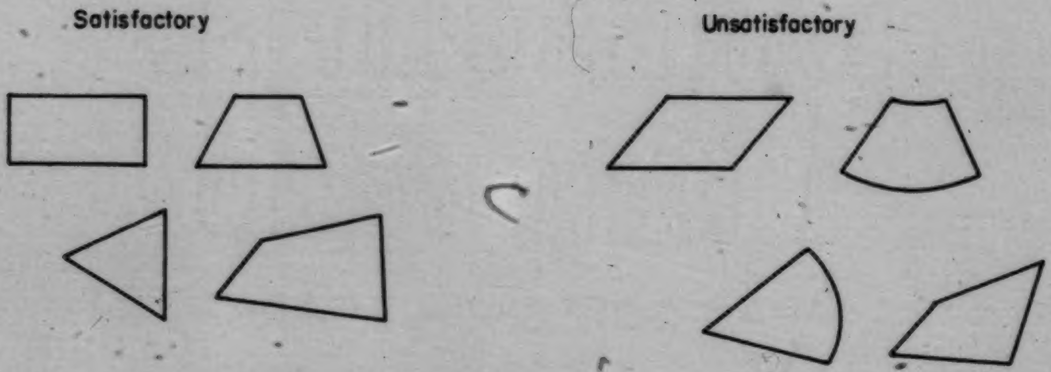
Satisfactory
Unsatisfactory

Without midside nodes, sides must be linear.

FIGURE 4.7 Q48 ELEMENT CONFIGURATIONS

Boundary and Loading Conditions:

Both NLCP and ESB allow nodal constraint to be specified in either of the global coordinate directions. It would be a simple undertaking to extend capabilities to include inclined roller supports but this was not undertaken for this thesis.

Both NLCP and ESB allow bodyforces to be generated from global bodyforce densities (such as self-weight). Otherwise, global force components may be specified at nodes.

There is no facility for accepting distributed forces directly, but an auxiliary program (WEBT) can generate the required global force components at nodes for arbitrary surface traction distributions. This was not incorporated as an automatic feature of NLCP and ESB: the correct work-equivalent forces along a quadratic element edge (that is, having a midside node) do not coincide directly with the statically equivalent forces for any given traction distribution. They may, however, be easily computed using WEBT, but such automatic features were not priorities for the research program.

Equation Solving:

Nonlinear problems are solved by a succession of linear approximations. In nonlinear elasticity, the equilibrium equations are formed from the incremental forces, displacements, and incremental tangent elastic moduli. Purely elastic stiffness equations are most efficiently solved by direct Gaussian elimination and backsubstitution (Meyer, 1973 and 1975) and the main questions concern the method of manipulating equations and loads. If core usage had been an important limiting factor, some form of out-of-core solver would have to have been developed, particularly since the Q48 elements dramatically increase the bandwidth of the equations. Core usage was not an issue, so the entire symmetric bandwidth was stored.

For elastoplastic analysis the tangent elastoplastic stiffness leads to nonsymmetric stiffness equations, which have to be fully recalculated at every equilibrium iteration. It is often more economical to use a constant initial stiffness (for example, the elastic unload/reload stiffness) and not have to perform so much stiffness recalculation. However, more equilibrium iterations are required with this constant-stiffness approach and the relative economy of one or the other stiffness approach varies from problem to problem.

The constant-stiffness approach was adopted. It performed quite well except for conditions near structural collapse, or at first-yield in strain-weakening problems. The option of one or the other stiffness approach would be valuable if further program development occurs.

Thought was given also to using the Gauss-Seidel iterative procedure for solving the equilibrium iteration steps. This proved to be less economical than standard Gaussian Elimination and Backsubstitution, and so was not adopted.

Stress Sampling and Averaging:

The design of the Q48 finite element is based on provision of a suitable displacement field. The derivatives of the displacements (strains) can vary greatly within these elements. The Gauss points of an element are defined by natural geometry (Figure 4.8), and the isoparametric element stiffness coefficients are obtained by numerically integrating stiffness functions by sampling the functions at these Gauss points. It has been shown (Hinton *et.al.* 1975; Barlow, 1976) that the second-order (or 2x2) Gauss points are positions within the element at which the strains sampled provide a least-squares best fit to the element strain field. Therefore, it is customary to sample the strains and stresses at the 2x2 Gauss points and then fit a suitable smoothing function to obtain suitable stresses at other element locations. Averaged nodal stresses are then calculated from the smoothed stress values of all elements contributing to the node in question.

Initial stress fields are most easily specified at the nodal points. The smoothing process may be inverted in order to interpolate suitable initial stress values at the Gauss points.

A question arose with the use of these smoothing functions. It is easy to specify a distribution of boundary tractions which satisfies (for example) a gravitational

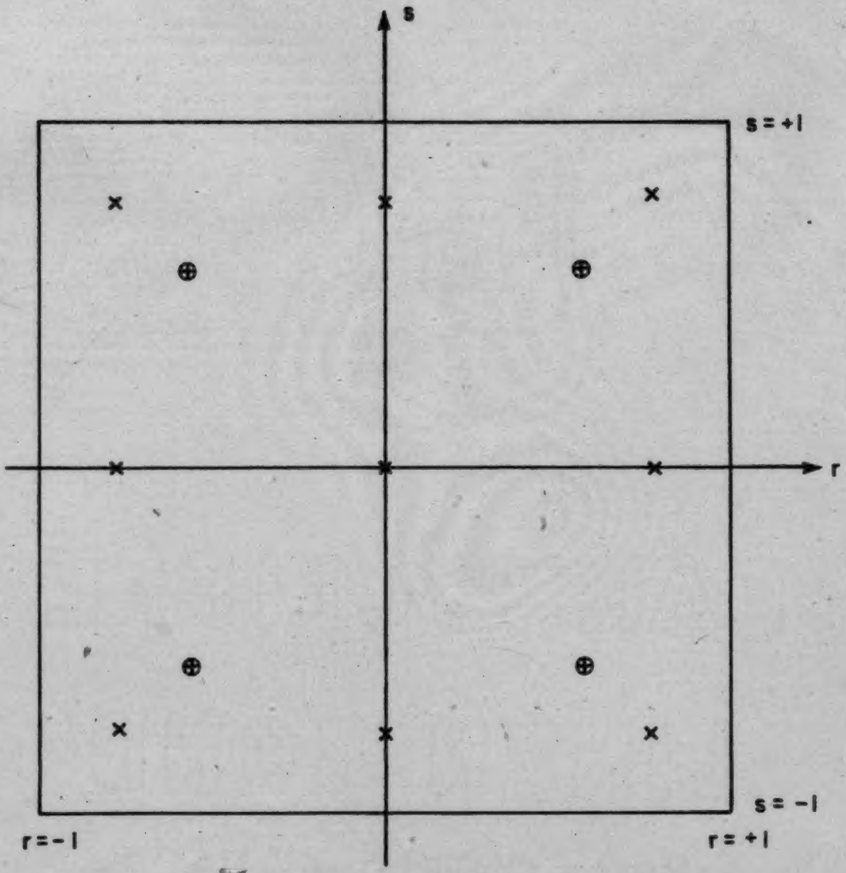

⊕ 2×2 Gauss points (second order) $r, s = \pm 0.577350269$

× 3×3 Gauss points (third order) $r,s = \begin{cases} \pm 0.774596669 \\ 0.0 \end{cases}$

FIGURE 4.8 ISOPARAMETRIC ELEMENT GAUSS POINTS

stress field. The assumed form of the interpolating function leads to Gauss point stresses which reflect correctly the gravity stress field, but mathematically the equivalent forces at the element nodes do not agree with the statically equivalent forces one might calculate as a check. The effect of these minor but irritating paradoxes was not fully explored and possibly deserves more attention, but did not lead to any errors in subsequent calculations.

Nonlinear Elasticity Algorithm:

Figure 4.5 shows the operation of a nonlinear elastic program. The initializing procedure used in NLCP to evaluate moduli selects correct tangent values, or default initial tangent values, for starting the increment. Stress increments are calculated using these moduli, and the resultant overall stresses form the basis of the next trial. This leads (in theory) to moduli softer than required. However, displacement finite element formulations lead to over-stiff structural discretization, so the weaker modulus to some degree compensates for discretization error.

The average stress approach of Kulhawy and Duncan (1970) is probably a more stable process than that used in NLCP, but only minor modifications would be required to NLCP to implement the average stress approach.

Elastoplastic Algorithm:

Figure 4.6 shows a typical elastoplastic computational procedure, with a constant stiffness iterative solution technique. Central to plasticity theory is the concept that one or more yield surfaces in stress space separate the region within which deformation is elastic from that which defines elastoplasticity. For any stress sampling point it is necessary to know whether or not a strain increment starts from a condition of elastoplasticity and whether or not trial elastic stresses computed during an incremental cycle result in an elastoplastic state. It is a misleading simplification to visualize stress points and stress increment vectors in the manner of Figure 4.9, but the following concepts are well illustrated in this manner.

Mathematically, the yield surface is conveniently described as the locus of zero values of some yield function "f". The initial stress point, "a" on Figure 4.9A, must lie within (elastic) or on (elastoplastic) the current yield surface. Application of a trial stress increment may result in a positive, zero, or negative value of the trial resultant "b". Elastoplastic response occurs only when "f" becomes positive at "b". (In more general terms than shown on this figure, the yield surface will change as a function of the plastic work achieved in yielding and of the change in stress state).

Bearing in mind that a trial strain increment was applied, the correct elastoplastic response has to be computed. The proportion "ab′" of the trial strain increment

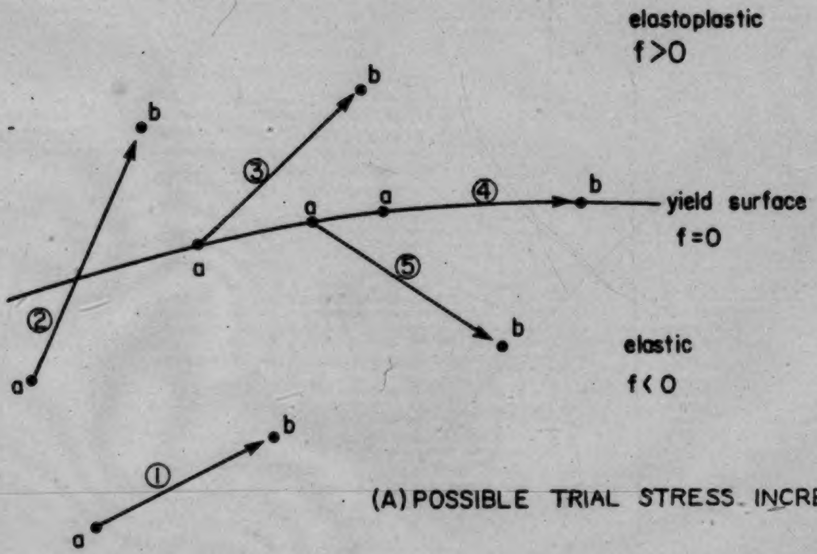
elastoplastic
f>0
b
b
③
a
a
a
④
b
yield surface
f=0
②
a
⑤
b
elastic
f<0
b
①
a

(A) POSSIBLE TRIAL STRESS INCREMENTS

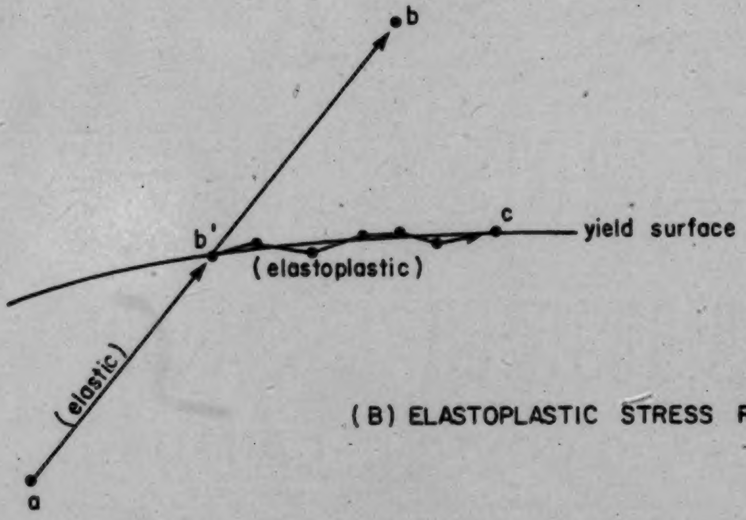
b
c
b'
yield surface
(elastoplastic)
(elastic)
a

(B) ELASTOPLASTIC STRESS RESPONSE

FIGURE 4.9 SIMPLIFIED ELASTOPLASTIC RESPONSE

which is elastic can be computed from the stress states "a" and "b". The remainder "b′c" is elastoplastic and the elastic and plastic portions can be computed from the constitutive laws. In order to maintain numerical accuracy, a subincremental approach is used in applying the laws, as shown in Figure 4.9B. Generalized subincremental procedures are discussed more fully by Bushnell (1977).

Numerically, there have to be many controls on the process. Exact zero is a difficult quantity computationally, therefore a tolerance is necessary on the "f" values which constitute the yield surface. The number of subincrements is important, there being complex tradeoffs between economy, accuracy, and stability. The stress difference "bc" at each sampling point leads to compatible strain states which do not exist in stress equilibrium with the specified loading conditions. Successive application of the resulting out-of-balance forces has to be carefully controlled. In the ESB program, tolerance levels are placed on the comparative out-of-balance force and incremental work magnitudes (Simmons, 1980a).

Constitutive Models:

The common ancestor of all models is linear isotropic elasticity, used in incremental form. Two programs were developed, NLCP for nonlinear elasticity and ESB for elastoplasticity. The constitutive models incorporated into these programs are described in Chapter 3 and in Appendices

B,C, and D.

In summary, the hyperbolic nonlinear isotropic and transversely-isotropic shearband models were employed in the NLCP program. This program was developed as a tool for practical analysis and its application to a practical problem is described in Chapter 7. The various elastoplastic models: CRD, SD, and PPP; were incorporated into the ESB program primarily for research purposes. In Chapter 5 the application of the ESB program to simple test problems is described, while Chapter 6 explains the analysis of a case history which may have involved progressive failure.

Before embarking on the discussion of such highly nonlinear problems, it is first necessary to establish the accuracy capabilities of the Q48 element by comparison with closed-form solutions to an appropriate linear problem. A crack problem of linear elastic fracture mechanics was chosen; this allows examination of the desired attributes for resolving stress concentrations.

4.5 TEST PROBLEM: ACCURACY OF THE Q48 ELEMENT

A classical problem of linear elastic fracture mechanics is the stress intensity factor KI for a Mode I double-edge cracked plate. This problem was used by Ingraffea (1977) for similar checking purposes. Geometry and loading conditions are shown in Figure 4.10, and are identical to those given by Ingraffea.

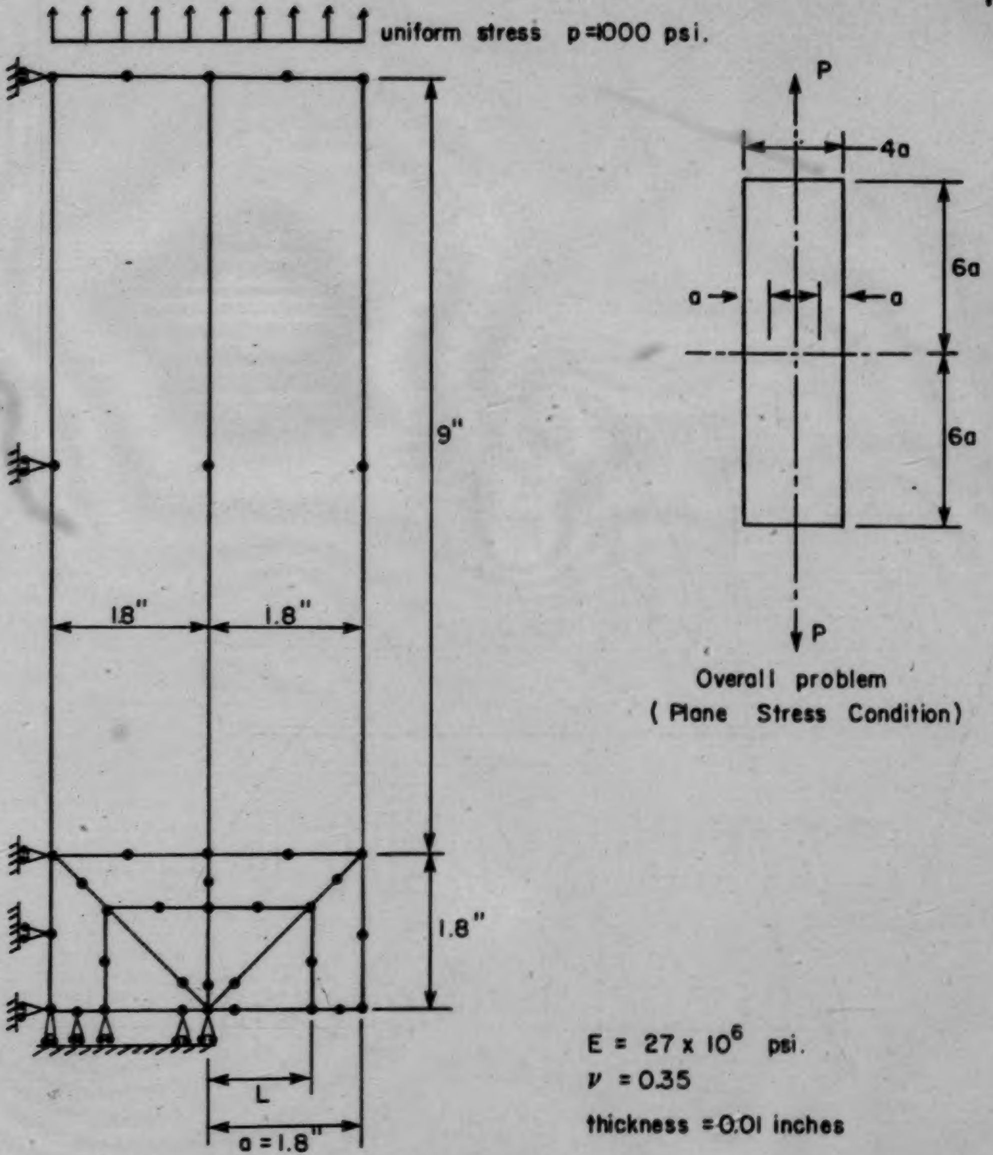
uniform stress p=1000 psi.
9"
1.8"
1.8"
1.8"
L
a = 1.8"
P
4a
6a
a
a
6a
P

E = 27 x 10^6 psi.
ν = 0.35
thickness = 0.01 inches

Element Idealization

Overall problem
(Plane Stress Condition)

Statement of Problem : Calculate Mode I stress intensity factor for various L/a ratios to establish optimum discretization for a limited number of nodal points.

FIGURE 4.10 DOUBLE-EDGE-CRACKED PLATE PROBLEM
(after Ingraffea, 1977)

The stress intensity factor KI is a scaling factor which, for a given loading and geometry, describes the strength of the singular stress and strain fields near the crack tip. The closed-form solution for KI for the double-edge-cracked plate problem is known. What is of interest here is the derivation of KI from a numerical solution to the problem. Figure 4.11 indicates the form of the stress and strain solutions to the problem. The displacements of the finite element solution provide a simple means for back-calculating KI. Since the singular field is influential only near the singularity source, employment of a finite element imposes a fixed scale on the approximating singular field of the shape functions. The determination of an appropriate element size for most accurate solution of the problem is thus the primary aim of this exercise. It is a most important exercise in the guidance it provides for mesh design for other problems.

With the Q48 element, two independent estimates of KI may be made (Barsoum, 1977; Shih *et.al.* 1976). These are the "C.O.D." (Crack Opening Displacement) and "Shih" estimates indicated in Figure 4.11. Results of a series of calculations are shown in Figure 4.12, which also gives Ingraffea's results. Ingraffea used only the Shih estimation while this study uses both estimates. It can be seen that Ingraffea's results were successfully reproduced.

The comparison between the two estimates is interesting. In both cases the minimum error was obtained

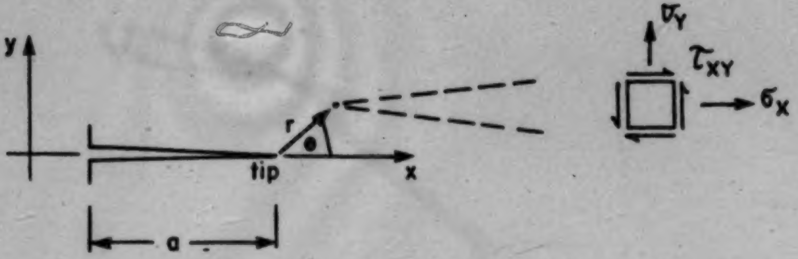

$$\left.\begin{aligned}
\sigma_X &= \frac{K_I}{\sqrt{2\pi r}}\cos\frac{\theta}{2}\left(1-\sin\frac{\theta}{2}\sin\frac{3\theta}{2}\right) \;\ldots\ldots\ \text{H.O.T.}\\
\sigma_Y &= \frac{K_I}{\sqrt{2\pi r}}\cos\frac{\theta}{2}\left(1+\sin\frac{\theta}{2}\sin\frac{3\theta}{2}\right) + \ldots\ldots\ \text{H.O.T.}\\
\tau_{XY} &= \frac{K_I}{\sqrt{2\pi r}}\sin\frac{\theta}{2}\cos\frac{\theta}{2}\cos\frac{3\theta}{2} + \ldots\ldots\ \text{H.O.T.}\\
\text{and}\quad u &= \frac{K_I}{G}\sqrt{\frac{r}{2\pi}}\cos\frac{\theta}{2}\left(\frac{1-\nu}{1+\nu}+\sin^2\frac{\theta}{2}\right) + \ldots\ldots\ \text{H.O.T.}\\
v &= \frac{K_I}{G}\sqrt{\frac{r}{2\pi}}\sin\frac{\theta}{2}\left(\frac{2}{1+\nu}-\cos^2\frac{\theta}{2}\right) + \ldots\ldots\ \text{H.O.T.}
\end{aligned}\right\}\ \frac{r}{a} \ll 1.0 \qquad \text{—— (i)}$$

where $K_I = p\sqrt{\pi a}$ for the double-edge-cracked plate of Fig. 4.10

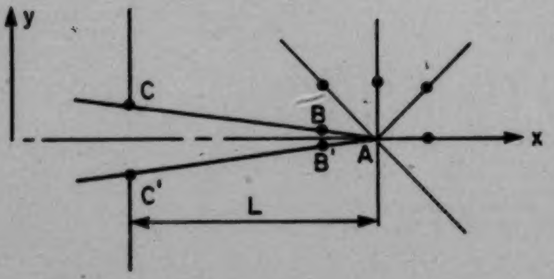

When applied to the crack-tip element, the shape functions for the side ABC (AB'C' is symmetrical) yield (for θ = 180°)

$$v = \left[(4v_B - v_C)\sqrt{\frac{x}{L}} + (-4v_B + 2v_C)\frac{x}{L}\right] \text{-(ii)}$$

Let the f.e. approximation to K_I be K_I^*

Using eq.(i) and ignoring H.O.T. $K_I^* = \sqrt{\frac{2\pi}{L}}\,\frac{G(1+\nu)}{4}(v_C - v_{C'})$

ie. $K_I^* = \sqrt{\frac{2\pi}{L}}\,\frac{G(1+\nu)}{2}v_C$ (C.O.D. estimate)

Using eq.(ii) $K_I^* = \sqrt{\frac{2\pi}{L}}\,\frac{G(1+\nu)}{2}(4v_B - v_C)$ (Shih et. al. estimate)

Theorectical value of $K_I = 2.74\ p$

FIGURE 4.11 CLOSED-FORM NEAR-FIELD ELASTIC SOLUTION FOR DOUBLE-EDGE-CRACKED PLATE PROBLEM

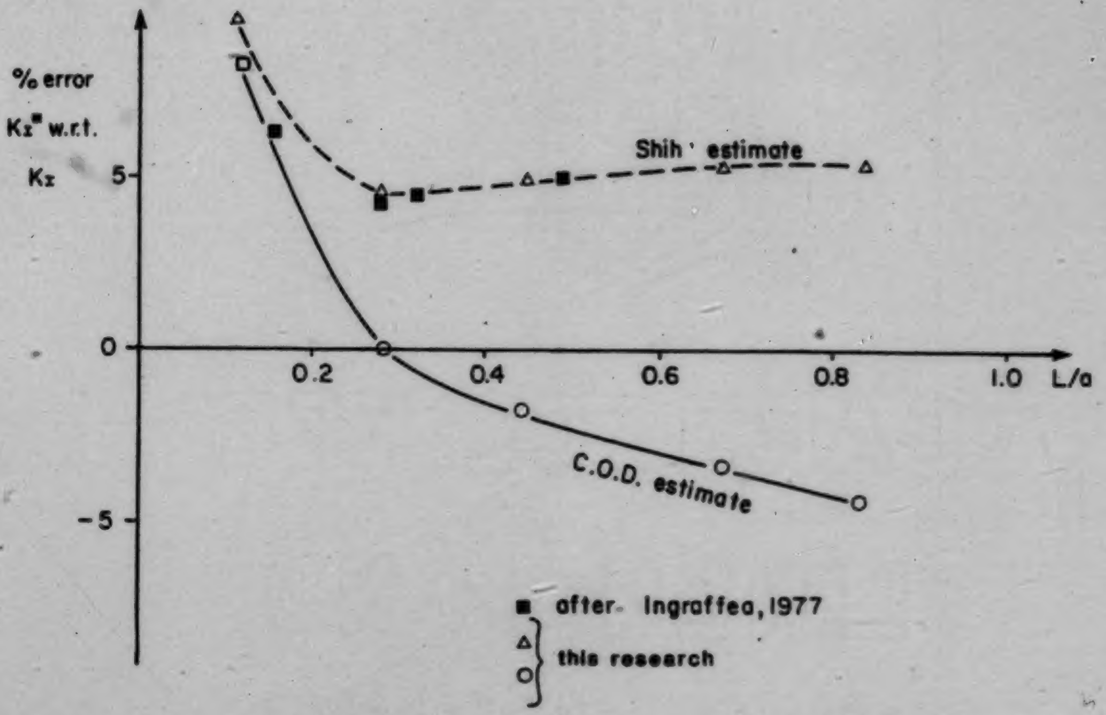

Conclusions: 1. The Shih estimate is insensitive to element size once a given minimun size is exceeded. It fully takes advantage of the Q48 element.

2. The C.O.D. estimate is more precise for a given element size, but is sensitive to the discretization. It does not fully take advantage of the Q48 element.

FIGURE 4.12 RESULTS OF PLATE PROBLEM

for L/a approximately equal to 0.28, and in both cases smaller L/a ratios indicate a lack of stiffness of the mesh. The Shih method, which makes full use of the quadratic element, is insensitive at higher L/a ratios, while the C.O.D. estimate becomes too stiff. (Both the "Shih" and "C.O.D." estimates are defined in Figure 4.11).

It can be concluded that the Q48 element is a potentially very accurate element for resolving stress concentration effects, although the stress results will not display the same order of accuracy as the displacements. By making full use of the higher order mode, the effect of stress concentrations is not critically dependent on the size of element used to study the problem. Such size effects have concerned other researchers (Bazant and Cedolin, 1979).

5. BEHAVIOUR OF COMPUTATIONAL MODELS

There are two basic aspects to the development of a constitutive model for numerical analysis. Firstly, the physical concepts and necessary approximations have to be established. Secondly, numerical techniques for implementing the model have to be developed.

Simple material test configurations are used to evaluate parameters for the model, and as a matter of self-consistency the model must be capable of reasonably reproducing such test behaviour. By this means, the physical concepts and approximations are established.

Numerical techniques must be tested against proven solutions. For linear elasticity this process is quite straightforward since a wide selection of problems having closed-form solutions exists (for example, Poulos and Davis, 1974). For elastoplastic problems the range of closed-form solutions is far more restrictive, but the same procedure may be followed.

In this chapter, development of the various computational models is presented. Sections 5.1 to 5.3 discuss the constitutive behaviour aspect of the verification process, by deriving parameters from test data and simulating the test. The particular example chosen (the plane strain compression test) is shown to be dominated by nonuniform post-peak yielding, and an unresolved numerical impasse was reached. In Section 5.4, two bearing capacity problems are compared successfully with established solutions. Conclusions concerning the present stage of computational model development are made.

5.1 DERIVATION OF MODEL PARAMETERS

Cornforth (1964) conducted plane strain compression tests on Brasted Sand (a river sand) over a range of densities. The influence of strain conditions was discussed by comparison with triaxial compression and plane strain extension tests on the same material. Other sources of plane strain test data are available (for example, Oda *et.al.* 1978) but Cornforth's presentation concentrates on the measurement of strength parameters, dilatancy rates, and development of ultimate strength assuming homogeneous deformation. Cornforth also described clearly the nonhomogeneous behaviour he encountered, so his tests are particularly useful for the purposes of this discussion.

Constant - Volume Friction Angle:

Cornforth presented full stress-strain details for two plane strain tests. One involved constant lateral stress, axial compression while the other involved constant axial stress, lateral extension. Since lateral deformations were stress-controlled, no post-peak data were available for the latter test. The R-D relationships for these tests are shown on Figure 5.1 and indicate similar pre-peak characteristics. The single post-peak characteristic is consistent with a constant-volume friction angle of 32°. Other plots of Cornforth's show peak strength as a function of initial porosity and are also consistent with a constant-volume friction angle of 32°.

In Cornforth's plane strain apparatus, the post-peak geometrical evolution of the samples could not be observed. After completing a test the failure zone was examined and found to be always looser than elsewhere in the specimens. The overall volume changes were always larger in comparable triaxial tests than in plane strain. It was concluded that there is less kinematic freedom in the plane strain configuration, leading to a much more restricted zone of post-peak weakening. Following these arguments, the overall sample strain required to reach ultimate conditions is less in plane strain tests and the overall volumetric expansion correspondingly lower.

Assuming consistency in sample preparation, the evolution of a dilating zone in Cornforth's tests was simulated using the relationship between R and D at peak strength for a number of samples of different initial densities. Figure 5.2 shows the resulting R-D plot for both plane strain and triaxial tests. It may be concluded (after Rowe, 1972) that the constant-volume friction angle for plane strain is between 32° and 33°. For triaxial tests, the value of ϕ_f at peak strength (28.7°) lies between the

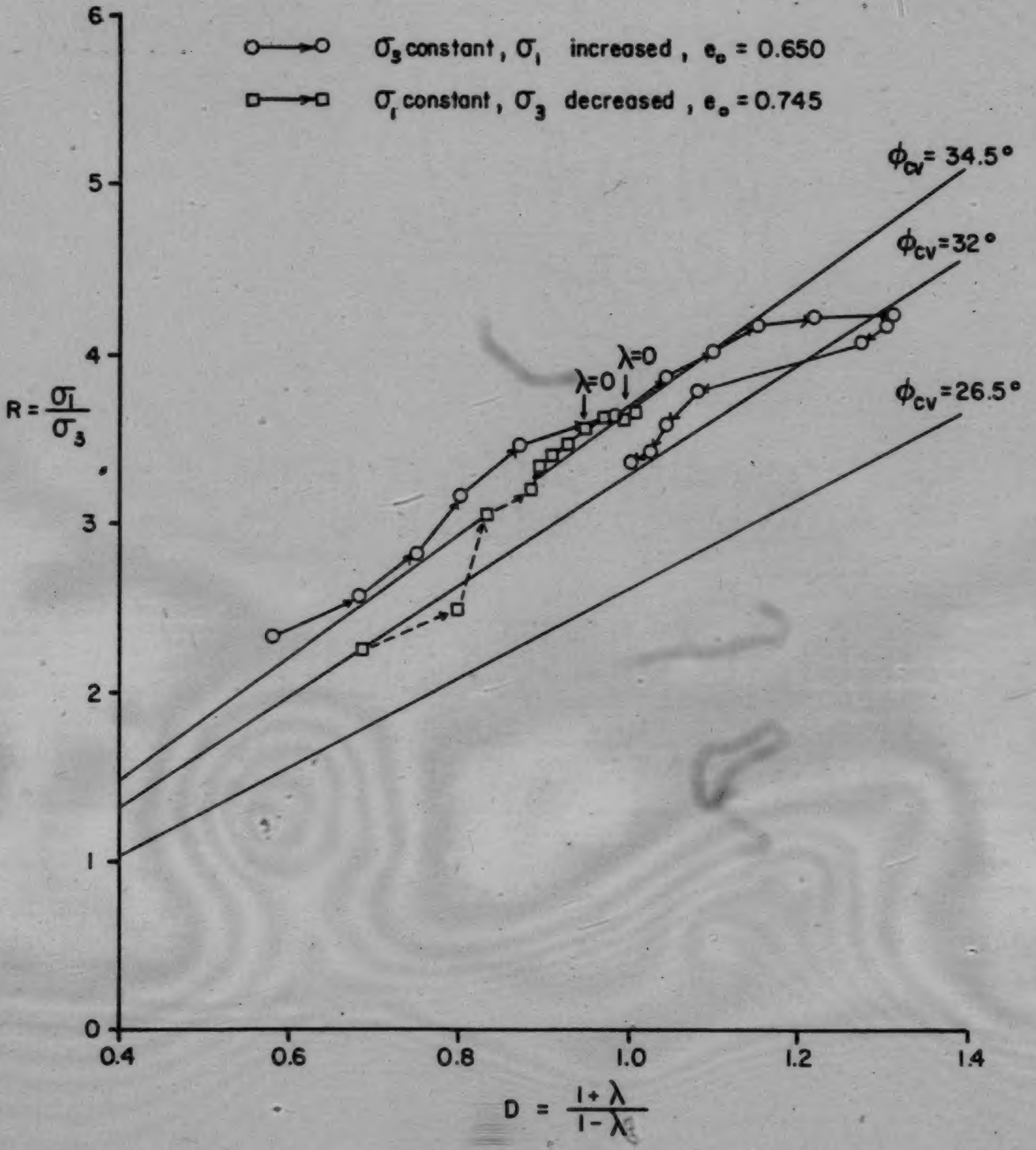

FIGURE 5.1 STRESS-DILATANCY PLOTS, SELECTED PLANE-STRAIN TESTS, BRASTED SAND (after Cornforth, 1964)

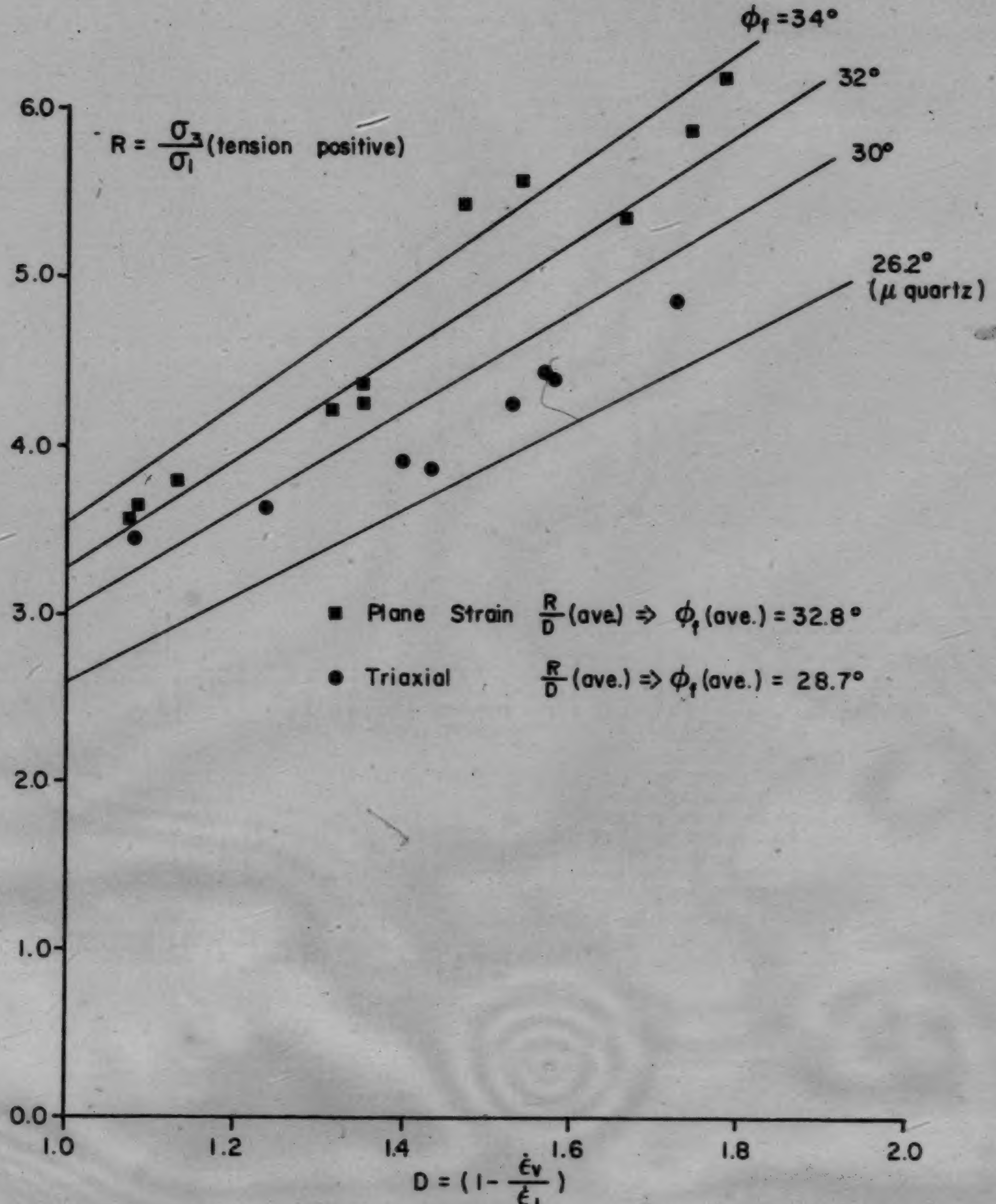

FIGURE 5.2 PLOTS FROM PLANE STRAIN AND TRIAXIAL TESTS AT PEAK STRENGTH, CONVENTIONAL STRESS PATHS.

mineralogical friction angle of quartz (26.2°) and the constant volume friction angle.

Ultimate strengths measured by Cornforth indicate friction angles of 32.3° and 33° for plane strain and triaxial tests respectively. Since these conditions appear to correspond to zero volume change, these values should closely approximate the constant-volume friction angle.

In summary, all evidence suggests that the operational constant-volume friction angle lies between 32° and 33°.

Variation of Dilatancy Rate with Void Ratio:

Cornforth established maximum and minimum void ratios of 0.792 and 0.475 respectively. Assuming no stress-dependency of these values over the stress ranges of interest here, these values may be adopted as limits of a functional representation of dilatancy rate with void ratio. Figure 5.3 shows Cornforth's peak dilatancy rate expressed in terms of the parameter λ. Peak conditions are assumed to represent homogeneous deformation and a series of peak values at different initial densities are assumed to simulate the evolution of λ with changing void ratio. A suitable curve-fitting function is shown in Figure 5.3.

Variation of Dilatancy Rate with Confining Stress:

There is assumed to be no variation of λ with mean compressive stress in Cornforth's tests. Any convenient functional parameters may therefore be selected. Values

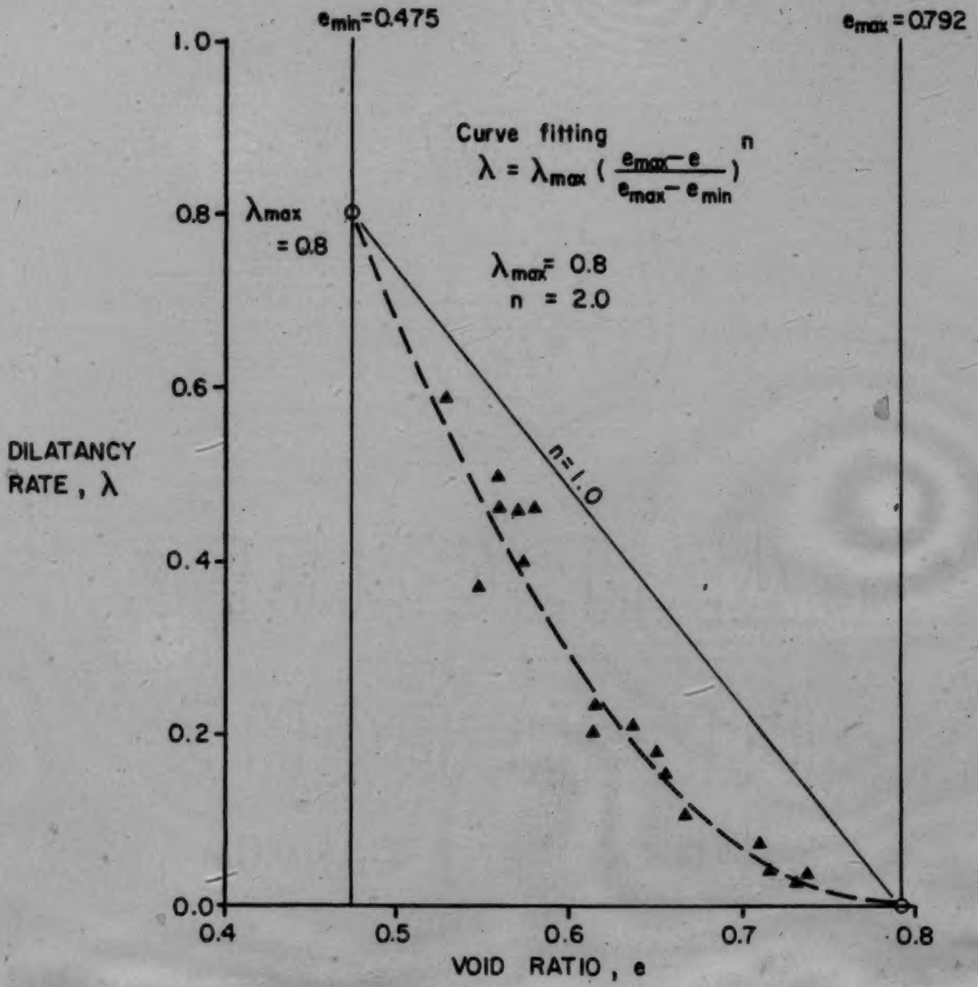

FIGURE 5.3 EMPIRICAL CURVE-FITTING OF DILATANCY RATE AS A FUNCTION OF VOID RATIO, VOLUME CHANGE DATA, BRASTED SAND

consistent with a convenient relationship are shown in Figure 5.4. In other circumstances some variation might be expected, For example the test data of Oda *et.al.* (1978) presented in Figure 3.4C are consistent with smaller instantaneous friction angles at higher confining stresses.

Consistency Amongst Adopted Parameters:

The parameters derived above are consistent with Stress-Dilatant homogeneous deformation at peak strength. Using the dilatancy data it should be possible to predict the measured values of peak strength or vice versa. Figure 5.5 compares predicted and measured peak strengths and demonstrates a lack of consistency which becomes more pronounced with increased density.

On theoretical grounds (Horne, 1965) the dilatancy rates measured by Cornforth are very high. Also, conditions at peak strength are more complex than the Stress-Dilatancy relationship might indicate. Finally, the exact procedure by which Cornforth arrived at his dilatancy data is not clearly established, and elastic components of strain have not been fully accounted for (Rowe, 1972). It is best for the purposes of this work to accept that the measured dilatancy rate is an excellent indicator of material processes, but to find a more acceptable dilatancy rate consistent with measured strengths.

The measured friction angles can be used to back-calculate values of dilatancy rate which fit the

Relationship between dilatancy rate and stress regime,

$$\lambda_{max} = \lambda_{max} \left(\frac{P - P_{cv}}{P_o - P_{cv}} \right)^m$$

For no stress - dependency, assume

P_o = -10 kPa.
P_{cv} = -10000 kPa.
m = 0.0
λ_{maxo} = 0.8

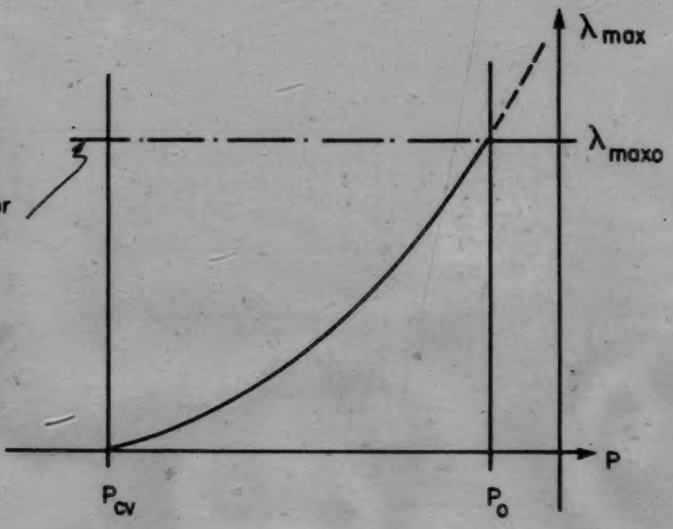

form of function for m = 0.0 , adopted for Comforth's data.

FIGURE 5.4 ASSUMPTION OF NO VARIATION IN DILATANCY RATE WITH STRESS REGIME

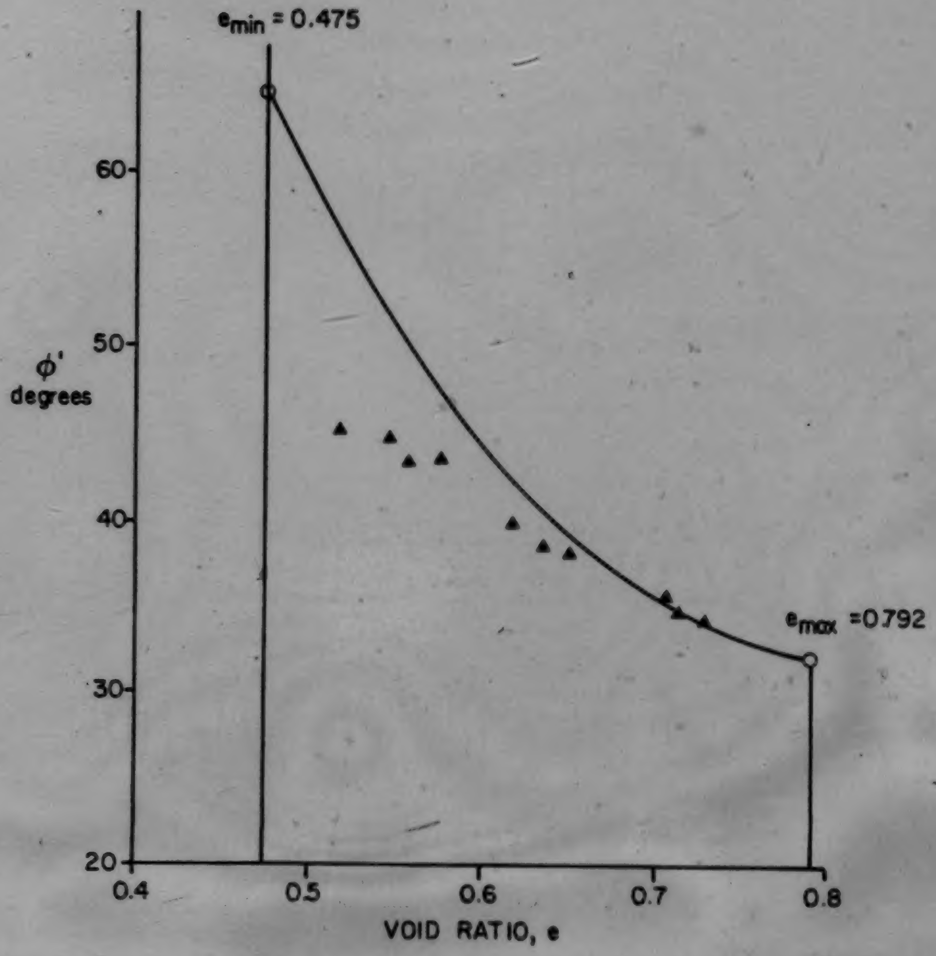

FIGURE 5.5 COMPARISON OF ϕ PREDICTED FROM VOLUME CHANGE DATA WITH ϕ MEASURED: PLANE STRAIN TESTS, BRASTED SAND

Stress-Dilatancy relationship. This is shown in Figure 5.6 The maximum dilatancy rate is then consistent with Horne's theoretical considerations, and the data of Figure 5.6 will be adapted for the studies which follow.

Elastic Parameters:

Elastic parameters to fit the pre-peak part of the models will vary both with density, confining stress, and stress path. Cornforth did not include sufficient data to make a study of variations with confining pressure worthwhile, and this aspect is ignored here. The variation with density can be assessed from Cornforth's data as shown in Figure 5.7. The Young's modulus must be calculated from the Plane Strain modulus using an appropriate operational value of Poisson's ratio. Figure 5.8 shows detail of a plane strain test and indicates that the operational value of Poisson's ratio is almost 0.5 at maximum density. These values were used to calculate the Young's moduli shown in Figure 5.7.

Alternative estimates of Poisson's ratio may be made by assuming that isotropic elasticity governs stress response in the zero-strain direction of Cornforth's tests. From Figure 5.8, this zero-strain Poisson's ratio assumes values of 0.30 to 0.33, and such values are typical of operational Poisson's ratios in the very small strain regime much prior to peak strength.

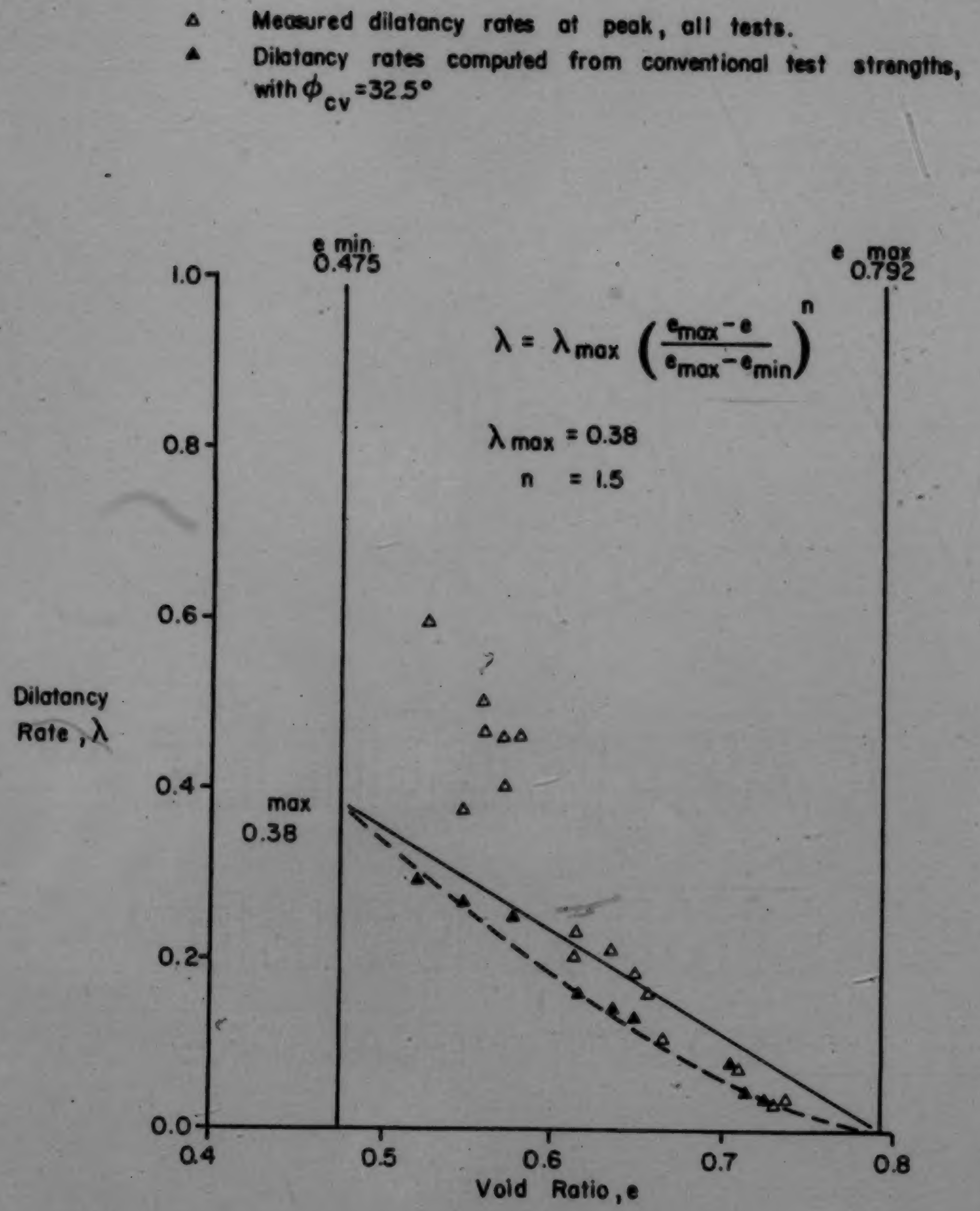

FIGURE 5.6 DILATANCY RATES CONSISTENT WITH MEASURED STRENGTHS IN PLANE STRAIN TESTS.

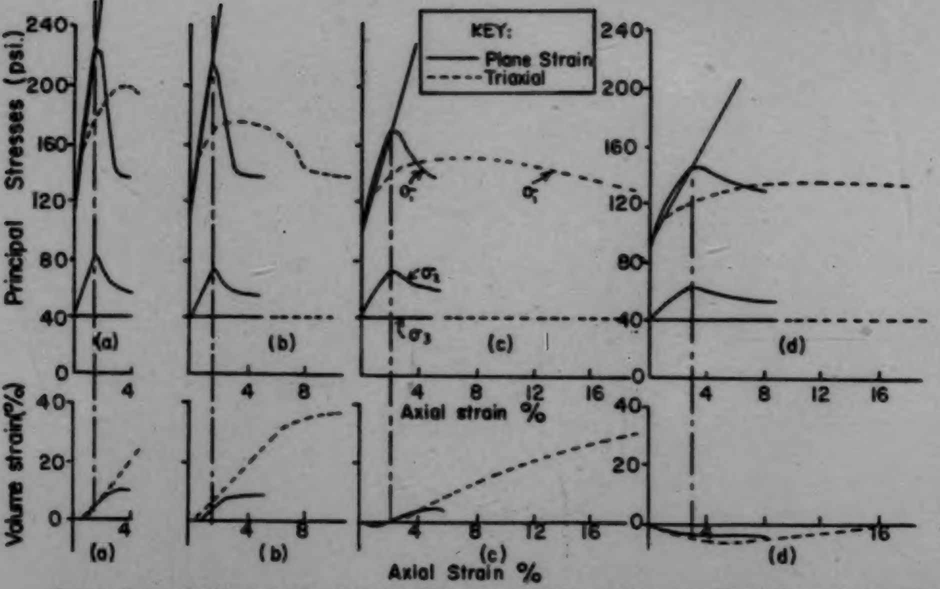

Comparison of plane strain and triaxial compression tests at different sand densities a) Dense, relative porosity 80% ; b) Medium-Dense, relative porosity 65%; c) Loose-Medium, relative porosity 40%; d) Loose, relative porosity 15%.

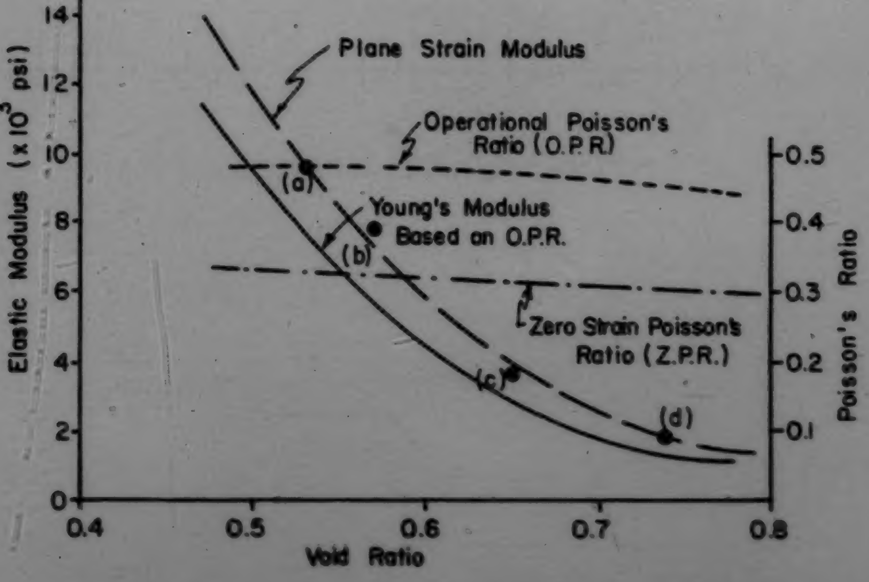

FIGURE 5.7 CONVENTIONAL PLANE STRAIN TESTS: VARIATION OF PREPEAK ELASTIC MODULUS WITH VOID RATIO, BRASTED SAND, (after Cornforth, 1964)

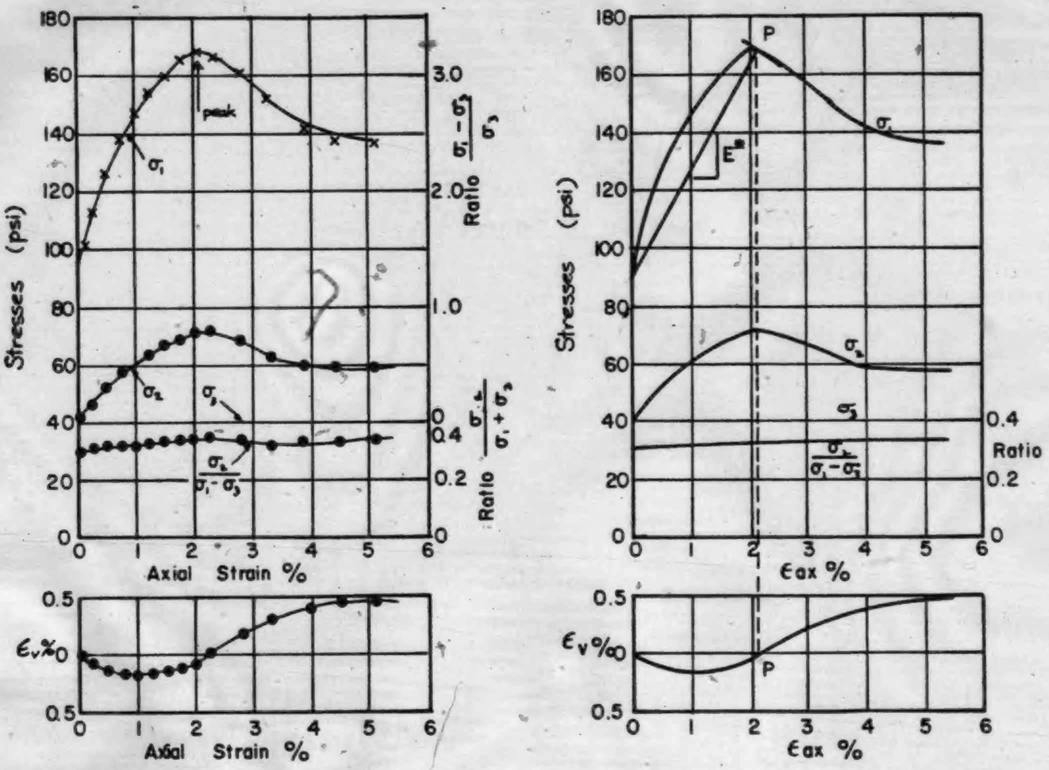

Plane strain test. Cell pressure constant, axial stress increased (medium dense specimen, initial porosity 34.9%)

$$\nu^*_{peak} = \left[\frac{\epsilon_{ax}-\epsilon_v}{\epsilon_{ax}}\right]_{peak} \qquad \nu = \frac{\nu^*}{1+\nu^*} \qquad E^* = \left[\frac{\Delta\sigma_{ax}}{\Delta\epsilon_{ax}}\right]_{peak}$$

$$=0.96 \qquad =0.490 \qquad = 3500 \text{ p.s.i.}$$

$$E = E^*(1-\nu^2) \qquad \nu_{zs} = \frac{\sigma_2}{\sigma_1+\sigma_3}$$

$$= 3500\,(1-0.49\ )$$

$$= 2660 \text{ psi.}$$

FIGURE 5.8 INTERPRETATION OF STRESS DILATANT MODEL FROM PLANE STRAIN TEST DATA.

While two quite different Poisson's ratio values seem to be consistent with different aspects of Cornforth's tests, it is necessary to view all such elastic parameters as convenient curve-fitting data only. It is acknowledged that the mechanics of stress-strain response in the region of peak strength are very complex and it is the role of this research to concentrate on realistic simulation of post-peak response. Therefore, the more computationally convenient zero-strain values of Poisson's ratio were finally adopted as they lead to more stable elastoplastic response. These values were used to reduce the measured Plain Strain moduli to values of Bulk and Shear moduli for computation.

Tensile Strength:

Brasted Sand was reported to be a clean cohensionless material and the appropriate tensile strength cutoff value is zero.

Summary:

The foregoing analysis of Cornforth's data can now be assembled. Two conditions of density were chosen, *dense* and *loose-medium*, having initial void ratios of 0.529 and 0.650 respectively.These correspond to conditions (a) and (c) of Figure 5.7, while condition (c) is shown in greater detail in Figure 5.8.

Selection of the SD parameters was quite straightforward. The CRD parameters had to be chosen with account taken of the elastic pre-peak deformations, in order to match the peak SD conditions as well as possible. The PPP parameters are an extension of the CRD model, with account for the observed strain required to obtain ultimate conditions. All parameters are shown in Table 5.1.

5.2 SIMPLE PLANE STRAIN TEST SIMULATION

A sample having the same dimensions as Cornforth's test configuration is shown in Figure 5.9. Homogeneous deformation is assumed, so that a single element can be used in the analyses. Conventional deformation-controlled axial compression was applied using a variable number of displacement increments.

Using both the Stress-Dilatancy (SD) and Constant-Rate-of-Dilation (CRD) Mohr-Coulomb models, axial strain to a total of 16% was simulated. The results are shown on Figures 5.10 and 5.11 for the dense and loose-medium samples respectively. Naturally, the CRD model did not record any strength change. It can be seen that the assumption of homogeneous deformation in the test was not correct because only about half of the strength drop from peak to residual was accomplished by the SD model. The sand must have weakened in a (thin) shearzone where the local dilatancy rate and accumulated volumetric strain were much higher.

TABLE 5.1 PARAMETERS FOR SD, CRD, PPP ANALYSES BASED UPON DATA FROM CORNFORTH (1964)

MODEL	CONDITION	UNITS	DENSE	LOOSE-MEDIUM
ALL	Bulk modulus K	psi	8445	2841
	Shear modulus G	psi	3238	1199
	(Poisson's ratio, ν)	-	(0.330)	(0.315)
	tenst	psi	0.0	0.0
SD	ϕ cv	degrees	32.5	32.5
	e max	-	0.792	0.792
	e min	-	0.475	0.475
	e_o (initial)	-	0.529	0.650
	n	-	1.5	1.5
	λ maxo	-	0.38	0.38
	p_o	psi	-10	-10
	p_{cv}	psi	-10000	-10000
	m	-	0.0	0.0
CRD PPP	e peak (approx)	-	0.5168	0.6385
	c' peak	psi	0.0	0.0
	ϕ' peak	degrees	46.467	38.959
	D	-	0.30743	0.13813
PPP	ϕ' residual	degrees	32.5	32.5
	γ_{PR}	-	0.043	0.063
	D_P	-	0.30233	0.11111
	* DSIX	-	1.0	1.0

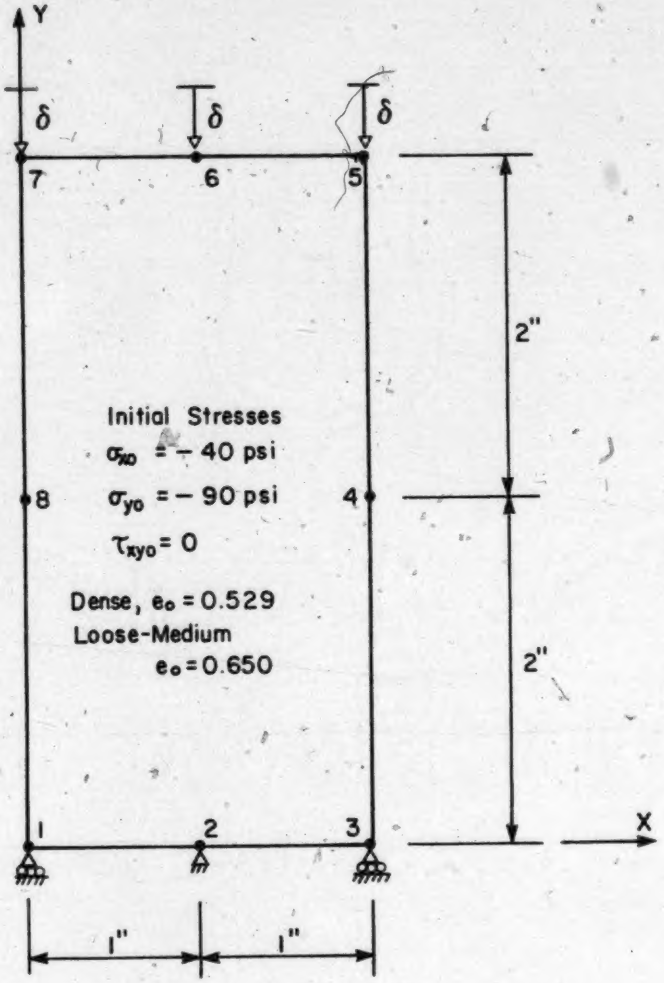
Y
δ
δ
δ
7
6
5
2"
Initial Stresses
$\sigma_{xo} = -40$ psi
8
$\sigma_{yo} = -90$ psi
4
$\tau_{xyo} = 0$
Dense, $e_o = 0.529$
Loose-Medium
$e_o = 0.650$
2"
1
2
3
X
1"
1"

FIGURE 5.9 SIMPLE PLANE STRAIN TEST SIMULATION

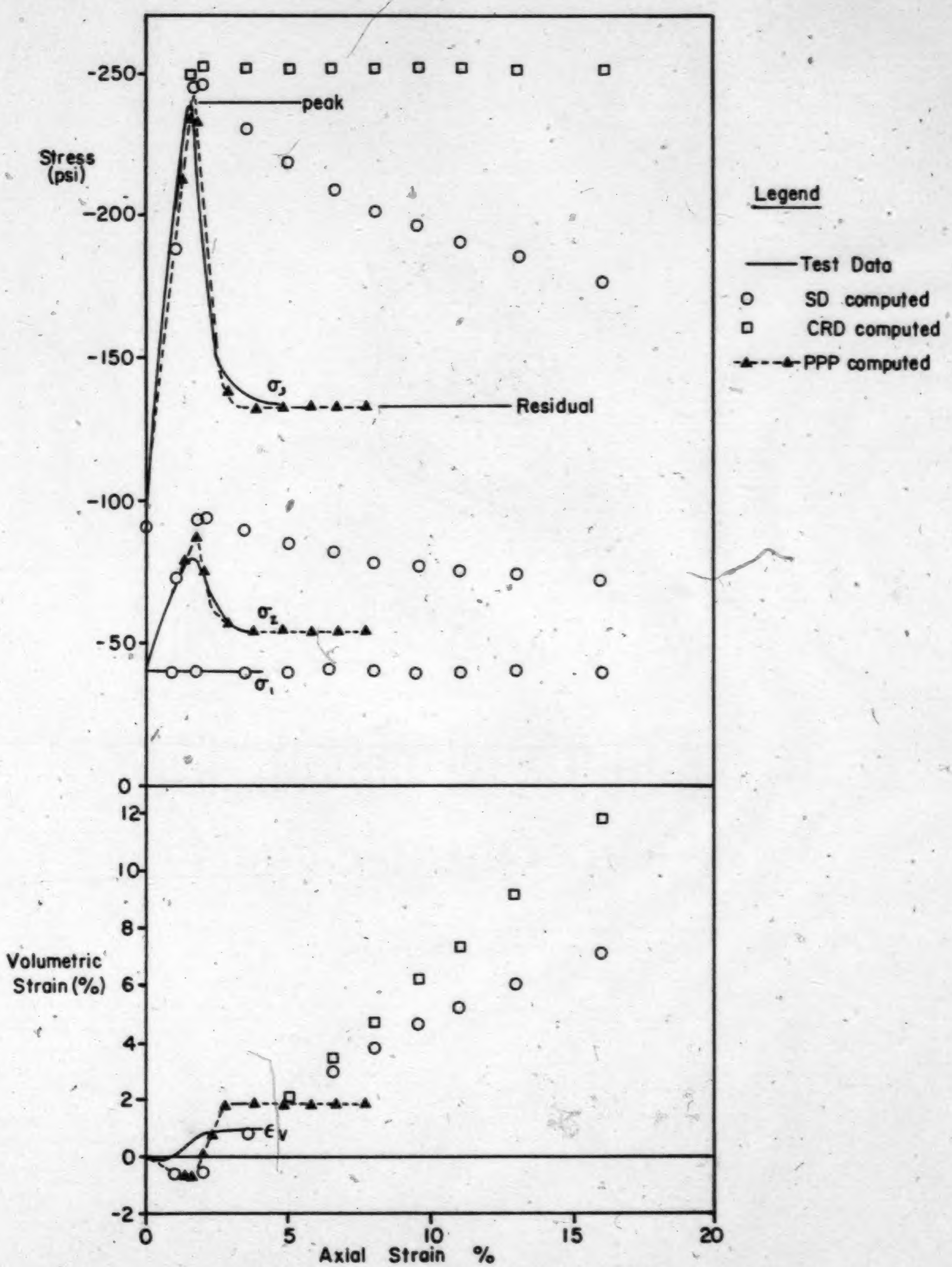

FIGURE 5.10 SIMULATED PLANE STRAIN TEST:
DENSE SAND, e_o =0.529 (after Cornforth, 1964)

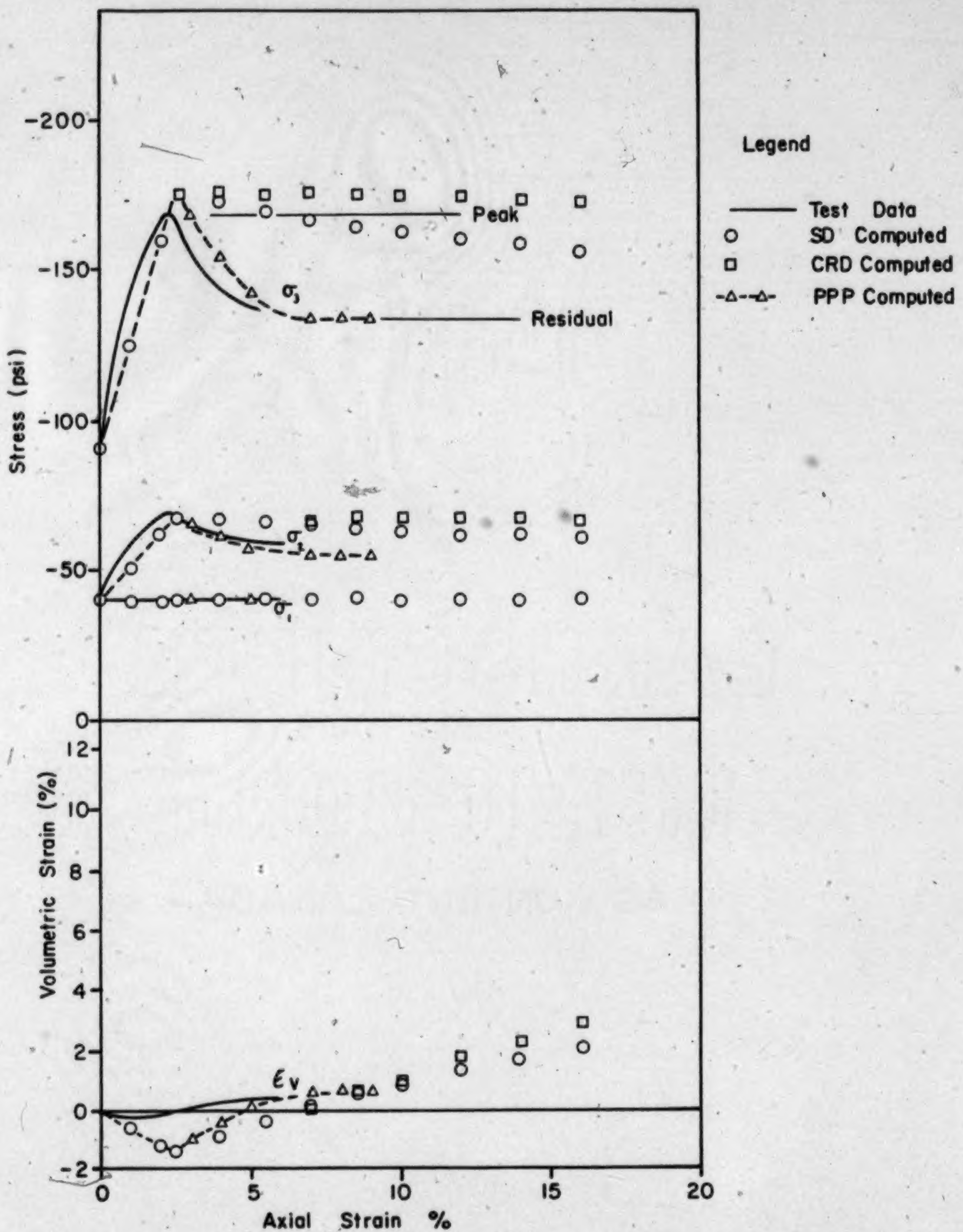

FIGURE 5.11 SIMULATED PLANE STRAIN TEST
LOOSE-MEDIUM SAND, $e_o = 0.650$
(after Cornforth, 1964)

There is a modest discrepancy between the computed SD peak strength and that obtained from the test, which can be ascribed either to computational approximation or to localized progressive failure in the test sample. A detailed pursuit of the reasons for the discrepancy was not undertaken.

The PPP model was applied to the problem in the following manner. The peak strength was chosen equal to that predicted by the SD data. The residual strength was chosen equal to the constant-volume friction angle. The dilatancy rate from peak to residual was based on approximation to the test data while the plastic shear strain required for post-peak weakening was based on the shape of the test stress-strain curve. The results of the PPP simulation show excellent agreement with test data except that the dilatancy rates in both dense and loose-medium samples were clearly overestimated. This was due to the fact that all of the test-sample dilatancy was assumed to be plastic, whereas a significant portion of it is in fact elastic expansion accompanying the drop in deviatoric stress. The dilatancy rate parameter is an independent variable and so closer agreement with the volumetric strain data could have been pursued in a straightforward fashion.

The void ratio changes computed during these tests are shown in Figure 5.12. The limitations of the CRD model are immediately evident. Firstly, no physical material can continue to dilate indefinitely. Secondly, the post-peak

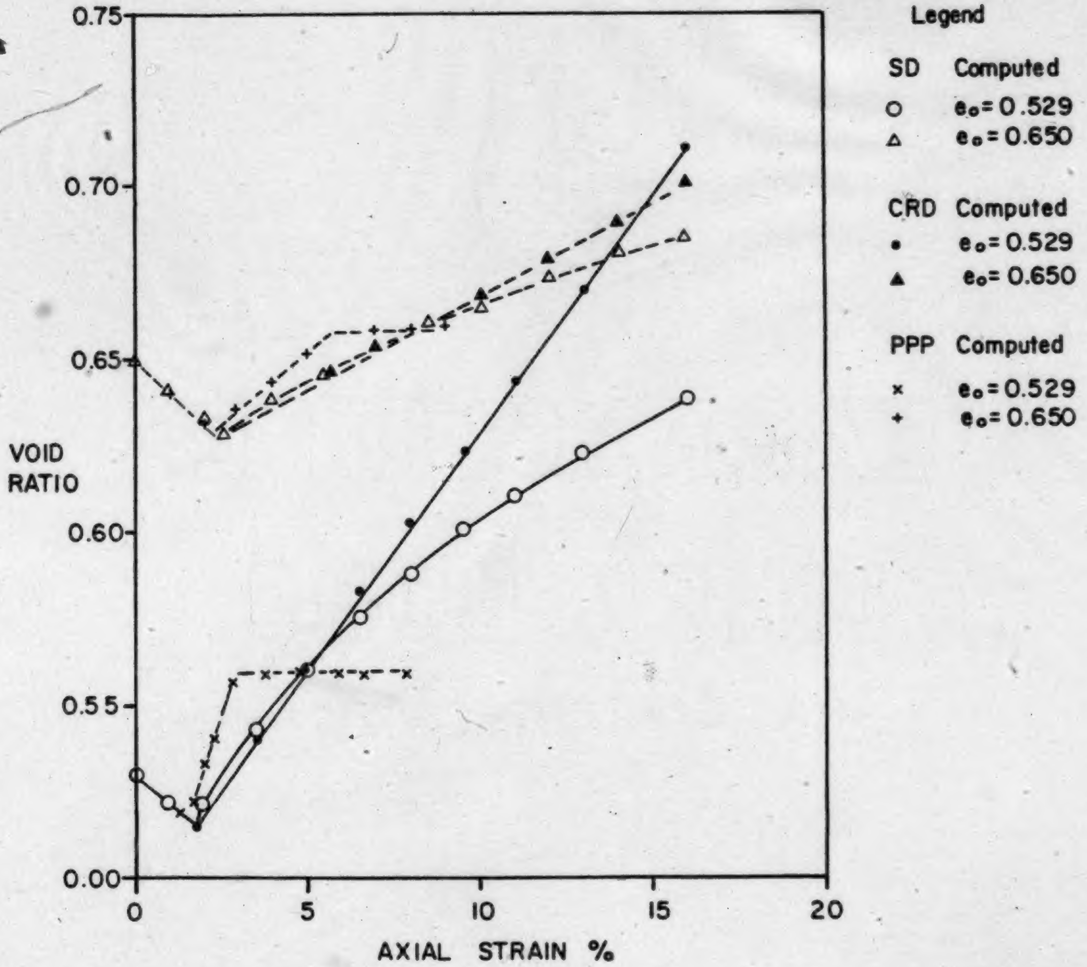

FIGURE 5.12 VOID RATIO CHANGES DURING SIMULATED PLANE STRAIN TESTS.

strength is not influenced by the evolving dilatancy, and by approximately 15% axial strain the void ratios for two materials of different strengths are equal. Obviously the most realistic application of the CRD model is to analysis of problems where shearzones already exist close to or at residual strength.

There is an apparent paradox in the dilatancy rates implied by Figure 5.12, caused by the interaction of elastic and plastic strain components. For either the dense or loose-medium case, the dilatancy rates chosen as material parameters are essentially the same for all three models (Table 5.1). The dilatancy rates shown in Figure 5.12 include both elastic and plastic volume change. The greater the rate of stress change, the greater the associated elastic strain changes. Therefore, the overall SD dilatancy rate is a little higher than for the CRD model at first yield, but becomes smaller as the effects of lower density influence the material's plastic dilatancy rate. The PPP model dilates very strongly, indicating that the elastic and plastic volume changes are of approximately equal magnitude. It is necessary to recall that the material dilatancy rate parameter affects only plastic components of strain.

The SD model shows a satisfactory trend of dilatant weakening. However, it should only be used within the actual shearzone and must therefore be associated with a reasonable shearband element configuration. On the other hand, the PPP model provides a convenient phenomenological tool for representing the effects of nonhomogeneous deformation within a larger volume which can be treated as homogeneous.

Having established the pattern of response of the models, attempts were made to analyse a plane strain test configuration into which a shearband was introduced. Insurmountable numerical difficulties were eventually encountered, but the aims and results will now be discussed.

5.3 BEHAVIOUR OF A NONHOMOGENEOUS TEST

Figure 5.13 shows a simple plane strain test. The size of the "specimen" is different from that used for the homogeneous tests (Figure 5.9), in order to study a wide variety of shearband orientations and thicknesses. The configuration of elements imposes a severe numerical test because the shearband element (number 2) is known to be of a shape which is very unfavourable to reliable numerical performance.

Figure 5.14 shows the stress sampling points (2 x 2 Gaussian quadrature points) for this problem. Stresses calculated at these points formed the basis for all elastoplastic computations.

Material parameters for all tests were those shown in Table 5.1. A series of different tests were planned, as follows:

1. Elements 1,2,3 elastic, to test for uniformity of response under uniform conditions;

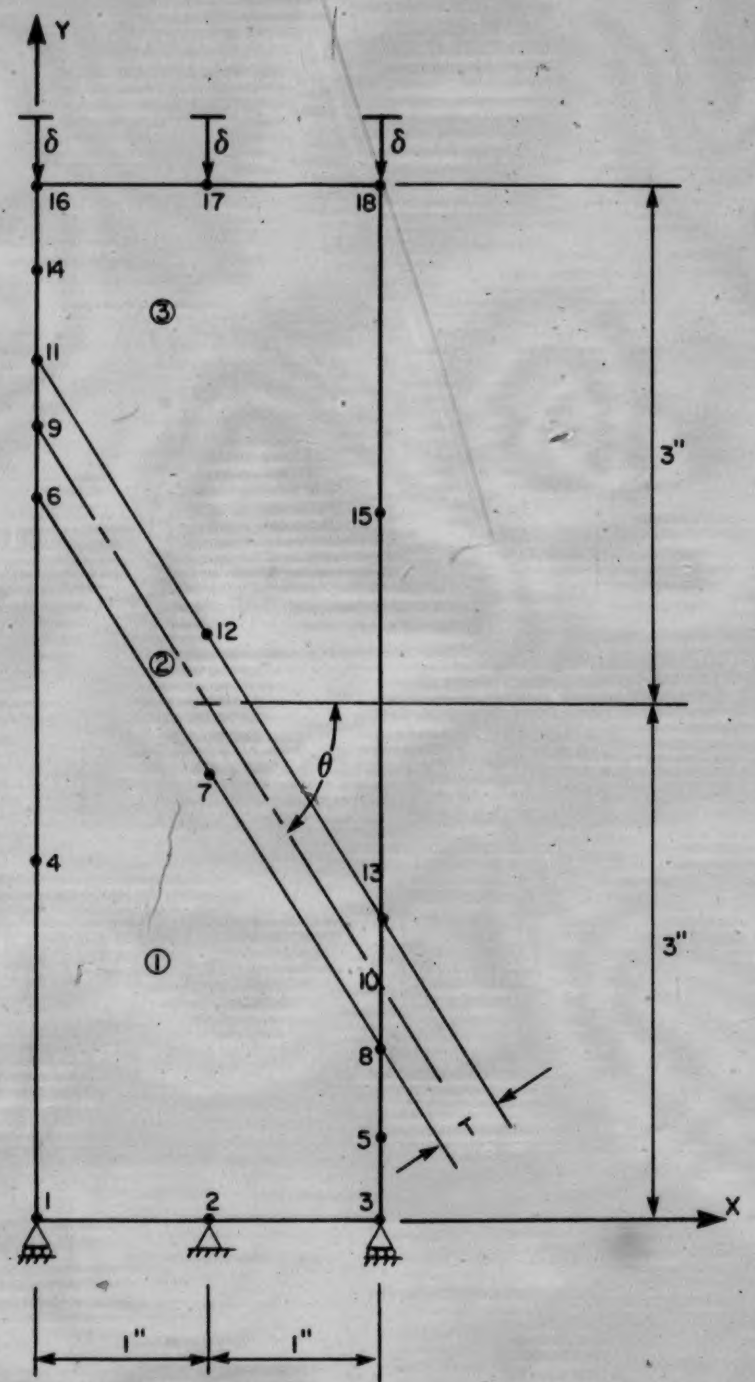
Y
δ
δ
δ
16
17
18
14
③
11
9
6
15
12
②
7
θ
4
13
①
10
8
5
T
1
2
3
X
3"
3"
1"
1"

Initial Stresses
$\sigma_{xo} = -40$ psi
$\sigma_{yo} = -90$ psi
$\tau_{xyo} = 0$

Dense, $e_o = 0.529$
Loose - Medium
$e_o = 0.650$

Shearband
T, θ variable

FIGURE 5.13 SIMPLE PLANE STRAIN TEST, VARIABLE ATTITUDE OF SHEARBAND

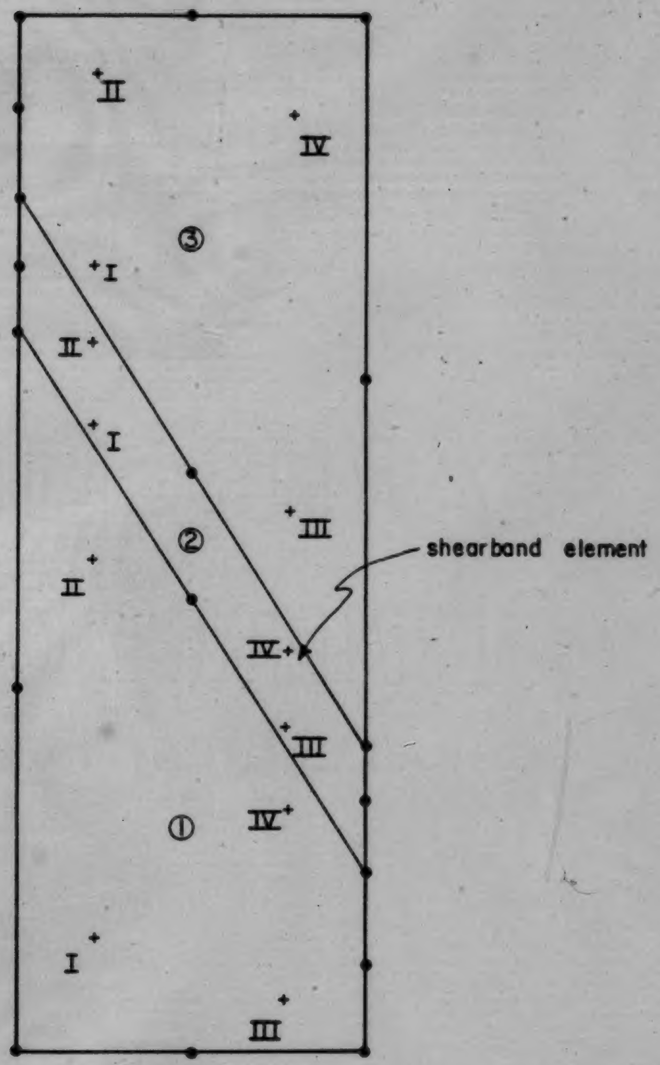
II
IV
③
I
II
I
III
②
II
shearband element
IV
III
①
IV
I
III

FIGURE 5.14 STRESS SAMPLING POINTS FOR SHEARBAND TEST PROBLEM

2. Elements 1,2,3 elastoplastic, again to test for uniformity of response for uniform CRD, SD, and PPP conditions;
3. Elements 1 and 3 elastic, element 2 elastoplastic to explore the relationship between overall sample response and response of the shearzone;
4. Repeats of series 3 with different geometrical configurations of the shearband.

The first two series were successfully carried out. Using double precision computation, uniform behaviour was noted to 9-figure accuracy and response was identical to that described in Section 5.2. Samples were tested to 16% axial strain without any numerical difficulties whatsoever, despite the nonuniform element shapes and Gauss point locations.

It was not possible to obtain any results for Series 3 and 4, because the elastoplastic algorithm would not converge. A number of numerical control parameters are employed in the algorithm and sensitivity analysis revealed that none of these parameters had any significant effect on the convergence process. Examination of the stress and strain behaviour indicated that nonuniform stress distributions were being computed when each iteration of the yield algorithm was performed. Stress concentrations developed at Gauss points II and III of elements 1 and 3 respectively. Stresses at Gauss points I and IV, II and III respectively of the shearband element (number 2) were identical but oscillated about the correct solution from iteration to iteration. Characteristics of this process are shown schematically in Figure 5.15.

The oscillatory behaviour of the yielding iterations occurred regardless of the elastoplastic model employed, although it was naturally more exaggerated in the post-peak weakening models (SD and PPP). The mechanism believed to be responsible for this behaviour is as follows. The onset of yielding effectively created a model whose stiffness is highly nonuniform, whereas the equilibrium iterations were performed using a uniform incremental stiffness. Stress concentrations developed as a consequence of the effectively nonuniform stiffness, and the equilibrium-correction algorithm, sensing this, overcorrected the response behaviour. Couching the behaviour in different terms, the computational procedure did not specifically account for the details of equilibrium across the shearband (Vardoulakis *et.al.* 1978; Pariseau, 1979) and was not capable of resolving the lack of local equilibrium computed with the three-element model.

Typical details of the lack of convergence are also shown in Figure 5.15. Two measures are employed for checking convergence. One is a measure of the out-of-balance force magnitude at each iteration, expressed as a ratio of the out-of-balance force magnitude at the first iteration. The second is a measure of the incremental work at each iteration, expressed as a ratio of the incremental work

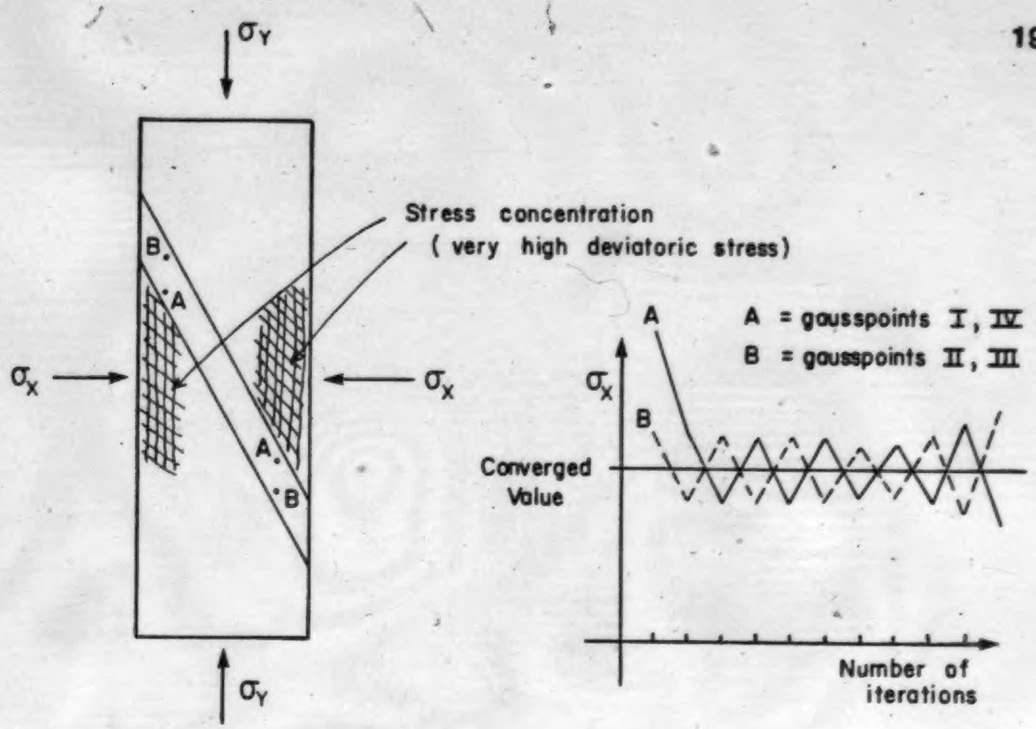
σ_Y
Stress concentration
(very high deviatoric stress)
B
A
σ_X
σ_X
A
B
σ_Y
A
A = gausspoints I, IV
B = gausspoints II, III
σ_X
B
Converged Value
V
Number of iterations

Characteristics of Stress Oscillations in Shearband Element during Equilibrium Iterations for an Elastoplastic Load Step

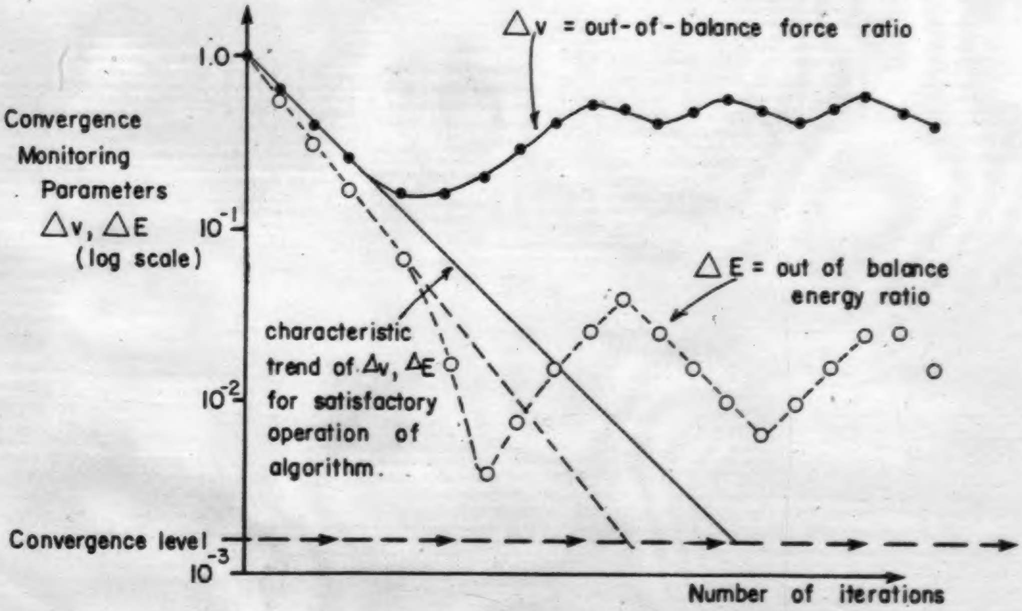

FIGURE 5.15 LACK OF CONVERGE OF ELASTOPLASTIC ALGORITHM FOR SHEARBAND ANALYSES.

performed during the first equilibrium iteration. For uniform yielding, each of these values plots as a straight line on a semi-logarithmic scale versus number of cycles. Deviation from an essentially straight line indicates a breakdown of the convergence process, and development of the oscillatory stress state.

A number of possible remedies could have been pursued but were not. Perhaps the best potential means for improving convergence would have been adoption of a tangent elastoplastic stiffness rather than the constant elastic stiffness algorithm. Smaller load increments and less stringent performance tolerances had little or no effect. It was decided to attempt a shearband stress averaging procedure, whereby the computed stresses at Gauss points I and III, II and IV were averaged at each step.

Shearband Stress Averaging:

This procedure averages the stress results across the top and bottom of the shearband element and assigns the average stress values to the Gauss point pairs II-IV and I-III respectively. By this means it was hoped to avoid the stress oscillation and subsequent out-of-balance force cycling experienced above.

Initial numerical experiments were carried out using the CRD model, and the stress averaging procedure was found to allow satisfactory convergence to occur. Figure 5.16 shows the convergence characteristics for a set of experiments. Cases A and B show the advantage of the averaging procedure, while Case C shows that convergence could be obtained using an accelerator. Note that a very large number of cycles were required to obtain satisfactory convergence (to about 0.1% in terms of stress state). Figure 5.17 shows the deformed shape of the test as deformation proceeded.

Further experiments were conducted using the CRD model. Firstly, the centre-top of the specimen was prevented from translating. This problem did not converge: it is a severe test on the constitutive formulation since it demands intense strain increment gradients in the shearzone and should really be handled by further mesh refinement. Convergence characteristics are shown in Figure 5.16 by Case D. Secondly, stress averaging was carried out for all elements of the mesh: more uniform convergence was achieved as shown by Case E in Figure 5.16, but the deformed shape of the end elements was not satisfactory. It was concluded that Case C represented the most effective result using the CRD model.

The relationship between the elastoplastic behaviour of the composite model and the overall (external) behaviour of the sample (ie, the behaviour which could be deduced from measurement of external dimensions of the sample) was next examined. For the configuration analysed (T=0.5 inches, =60°) the plastic dilatancy rate in the shearzone was specified as 0.30233 (Table 5.1) whereas the overall

CASE A LE/CRD/LE $\Omega = 1.0$ no shearband stress averaging, top translating.
B LE/CRD/LE $\Omega = 1.0$ with shearband stress averaging, top translating.
C LE/CRD/LE $\Omega = 1.4$, otherwise as for B.
D as for C, but top constrained against translating.
E as for C, stress averaging in all elements.
(Ω is acceleration factor for solution algorithm.)

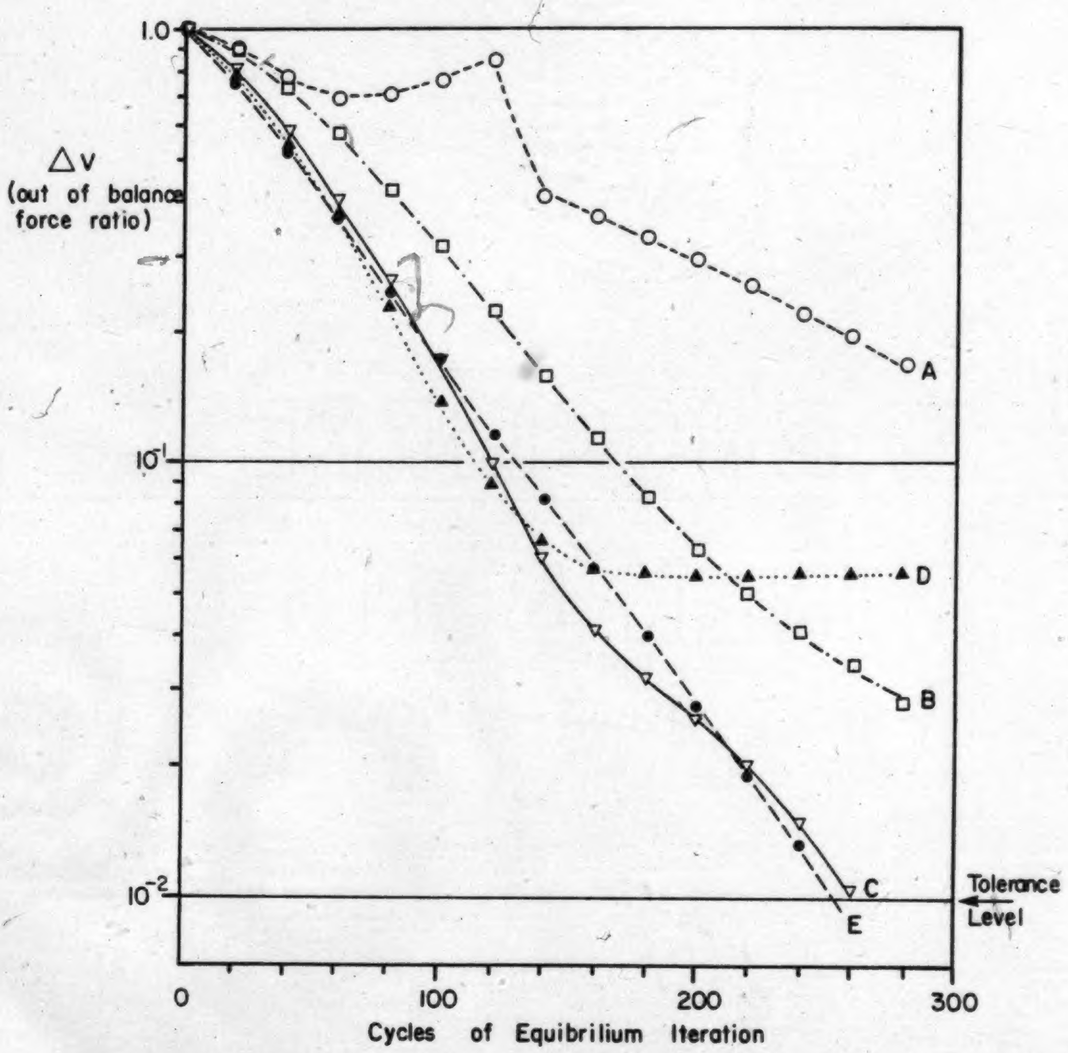

FIGURE 5.16 CONVERGENCE CHARACTERISTICS FOR 3-ELEMENT SIMULATION OF PLANE STRAIN TEST. FIRST ELASTOPLASTIC LOAD INCREMENT SHOWN, AND EFFECTS OF ACCELERATOR AND SHEARBAND STRESS AVERAGING COMPARED.

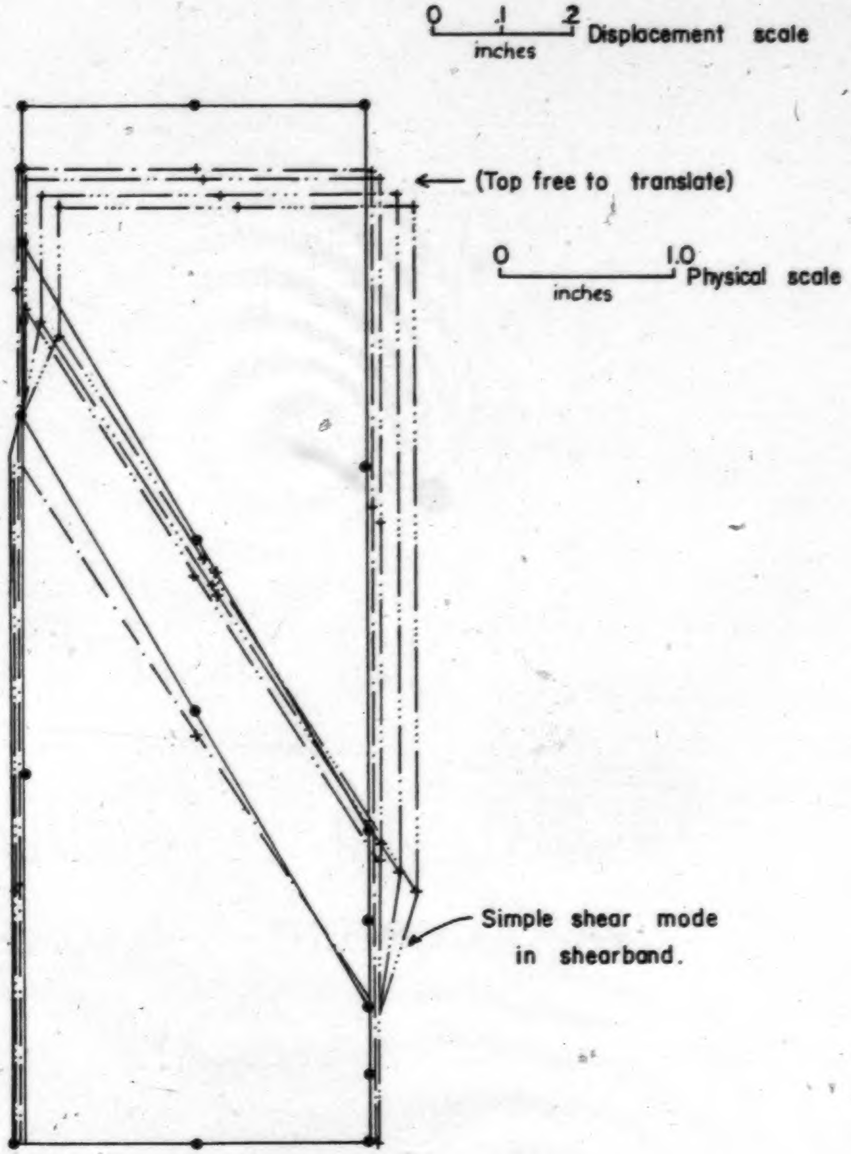
0
.1
.2
inches
Displacement scale
(Top free to translate)
0
1.0
inches
Physical scale
Simple shear mode
in shearband.

FIGURE 5.17 DEFORMATIONS OF 3-ELEMENT SIMULATION OF PLANE STRAIN TEST. FOUR CONVERGED STEPS OF CRD MODEL RESPONSE, WITH SHEARBAND STRESS AVERAGING, SHOWN.

elastoplastic dilatancy rate was measured as 0.3019. This near-coincidence seems fortuitous, but no detailed investigation was undertaken to check whether other factors may have dictated this result. It would be interesting to pursue this point via a small parametric study. This was not carried out because the CRD model was not seen as an important aspect of this part of the research.

Attempts to implement the SD model failed due to numerical difficulties within the shearband. During the elastoplastic calculations, trial elastic stress increments tended to result in small, temporary tensile states which prevented satisfactory performance of the SD model. It is suggested that some reformulation of the SD model, or perhaps some relaxation of the numerical tolerances, could have helped achieve convergence. The matter was not pursued at this stage because quite a far-reaching test program would be necessary, and the matter would be best left for another investigation.

The PPP model produced similar behaviour to that of the SD model. Convergence was not achieved. Stress oscillations in the outer (elastic) elements indicated that very small displacement increments would be necessary, yet attempts to do this still resulted in very poor partial convergence followed by divergence as tensile yielding occurred.

Conclusions from the nonhomogeneous test:

Numerical difficulties were encountered. Reasonable, converged solutions were obtained only with the CRD model. The post-peak weakening models would require more sophisticated solution techniques, or more elaborate and specialized loading specifications.

The problems encountered with the nonhomogeneous test are hardly surprising. To research the behaviour of the computational technique and the various consititutive models would be an end in itself, worthy of much time and effort. Thought was given to using the NLE model within the shearband. This could be done without much trouble, but the value of the exercise was judged questionable for the following reasons. Firstly, the hyperbolic stress strain curve would give no information on post-peak behaviour since it specifically deals with pre-peak behaviour. Secondly, numerical illconditioning could be expected as peak strength was approached. Thirdly, the incremental elastic shearband model, while readily allowing the shearband slip mode to develop, would not contribute any specifically valuable insights into the influence (controlling or otherwise) of the various parameters describing the process. This could be handled just as adequately with a 2-rigid-block model with the Mohr-Coulomb criterion governing interface slip. The NLE shearband slip mode is viewed more as a convenient computational procedure, when examining overall structural response,. than as an established model of material behaviour.

The only question worth raising at this point, in relation to this research, is the role of the coaxiality criterion in the plastic flow rule. There is variable evidence (Drescher, 1976; Roscoe *et.al.* 1967; Stroud, 1972) concerning the existence or otherwise of noncoaxiality. Numerical experiments with discrete models (Trollope and Burman, 1980; Thornton, 1979) suggest that de Josselin de Jong's (1959) conclusions regarding a restricted, indefinite range for noncoaxiality are sound. The means by which this mechanism could be incorporated into a numerical procedure are not explored here, but perhaps this matter needs to be examined quite carefully to see whether some clarifications are in order.

Experience with this test configuration reinforces the opinion that post-peak yielding poses delicate numerical problems. The tools presently developed are clearly inadequate and many avenues for further work have been indicated. Clearly the tests are quite severe. However, the following section demonstrates that despite the computational difficulties experienced, the basic numerical procedures are reliable.

5.4 BEARING-CAPACITY PROBLEMS

Section 5.3 described the numerical difficulties encountered when attempts were made to apply the elastoplastic constitutive models to a problem of non-uniform deformation. In order to assess whether these were due to characteristics of the constitutive models or to the numerical solution algorithms, elastoplastic analyses were carried out for problems having established solutions. Only the CRD model could be tested in this way, as the SD and PPP models were developed specifically for this research.

Two problems were considered. Firstly, the ultimate bearing capacity of a flexible strip footing on cohesive, frictionless soil was evaluated. Secondly, the load-deformation behaviour for a flexible strip footing on cohesive, frictional soil was compared with a published numerical solution.

Bearing Capacity of Cohesive, Frictionless Soil:

Figure 5.18 shows the finite element mesh used for predicting the yield and collapse loads for a flexible strip footing on an elastoplastic half-space. The known solutions for this problem are:

first yield: $q = \pi C_u$ ... Equation (5.1)

collapse: $q = (\pi + 2) C_u$ ... Equation (5.2)

The load-deformation behaviour for this problem is shown on Figure 5.19, each point representing the vertical

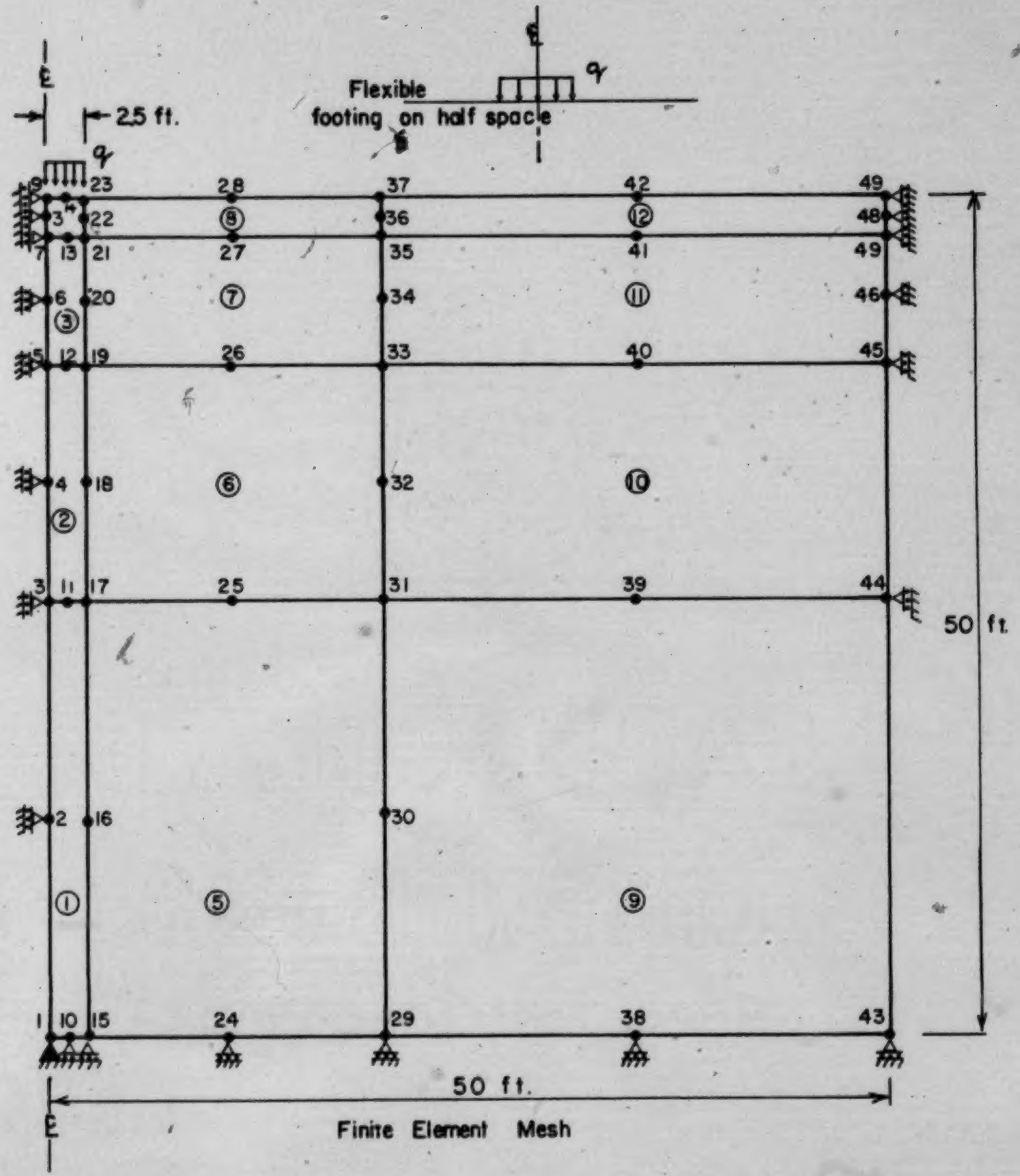
℄
q
Flexible
footing on half space
℄
2.5 ft.
q
9
23
28
37
42
49
8
3
14
22
⑧
36
⑫
48
7
13
21
27
35
41
49
6
20
⑦
34
⑪
46
③
5
12
19
26
33
40
45
4
18
⑥
32
⑩
②
3
11
17
25
31
39
44
50 ft.
2
16
30
①
⑤
⑨
1
10
15
24
29
38
43
50 ft.
℄
Finite Element Mesh

E = 1000 tsf.

ν = 0.25

Cu = 2.5 tsf. ($\phi = 0$)

$$\lambda = \frac{\dot{\epsilon}_v^p}{\dot{\gamma}^p_{max.}} = 0$$

tensile strength = 1.25 tsf.

Theoretical Solution :

First yield $q = \pi \, Cu$

Collapse $q = (\pi + 2) \, Cu$

FIGURE 5.18 BEARING CAPACITY PROBLEM FOR CHECKING AGAINST CLOSED-FORM SOLUTION.

displacement under the centre of the footing as a function of load level. A repeat analysis indicated the onset of yield at the Gauss point shown in Figure 5.20, at a load level within 0.2% of the theoretical value of Equation 5.1. Further analyses, of load levels greater than the collapse value given by Equation 5.2, failed to converge and indicate collapse in accordance with the known solution. Figure 5.20 also shows the Gauss points which were yielding at this load level. Given the coarseness of the mesh and the lack of special techniques for introducing rupture lines at collapse (Rowe and Davis, 1978), these results demonstrate very satisfying performance.

Figure 5.21 indicates convergence behaviour during an elastoplastic load increment for this problem. A straight line plot on a semi-logarithmic scale indicates uniform behaviour. An accelerating parameter can be used in the convergence process, and this figure demonstrates the numerical performance obtained by varying the accelerator. Firstly, curvature indicates the spreading of the yielded zone (more Gauss points yielding). Secondly, the oscillation of the accelerated iterations demonstrates the potential instabilities which may be introduced by this means. Thirdly, a rather large acceleration factor does not lead to a corresponding reduction in the iterations required for convergence. In fact, the convergence rate becomes a little slower for the highly accelerated iterations. Figure 5.21 is important because it demonstrates proper functioning of the

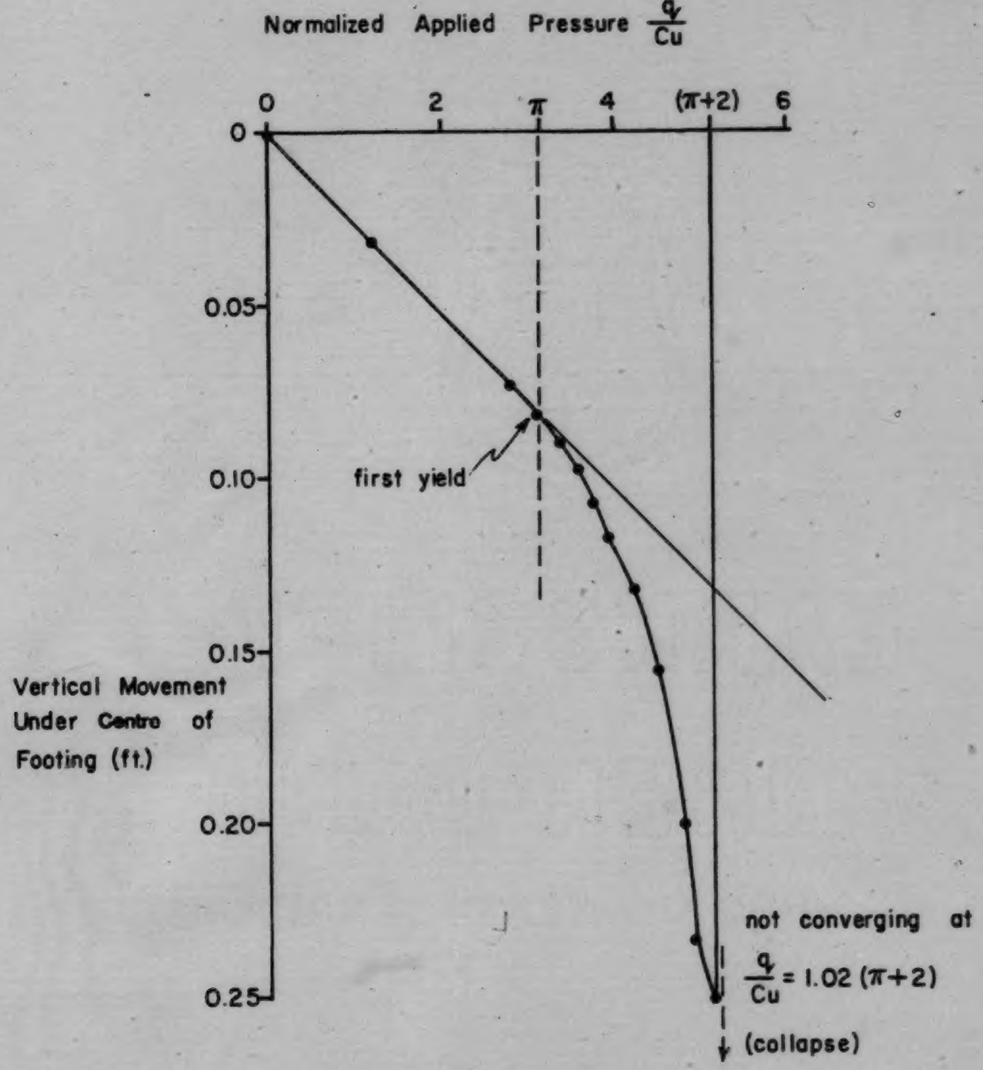

FIGURE 5.19 LOAD-DEFORMATION BEHAVIOUR SHOWING FIRST-YIELD AND COLLAPSE LOADS FOR FOOTING ON COHESIVE SOIL.

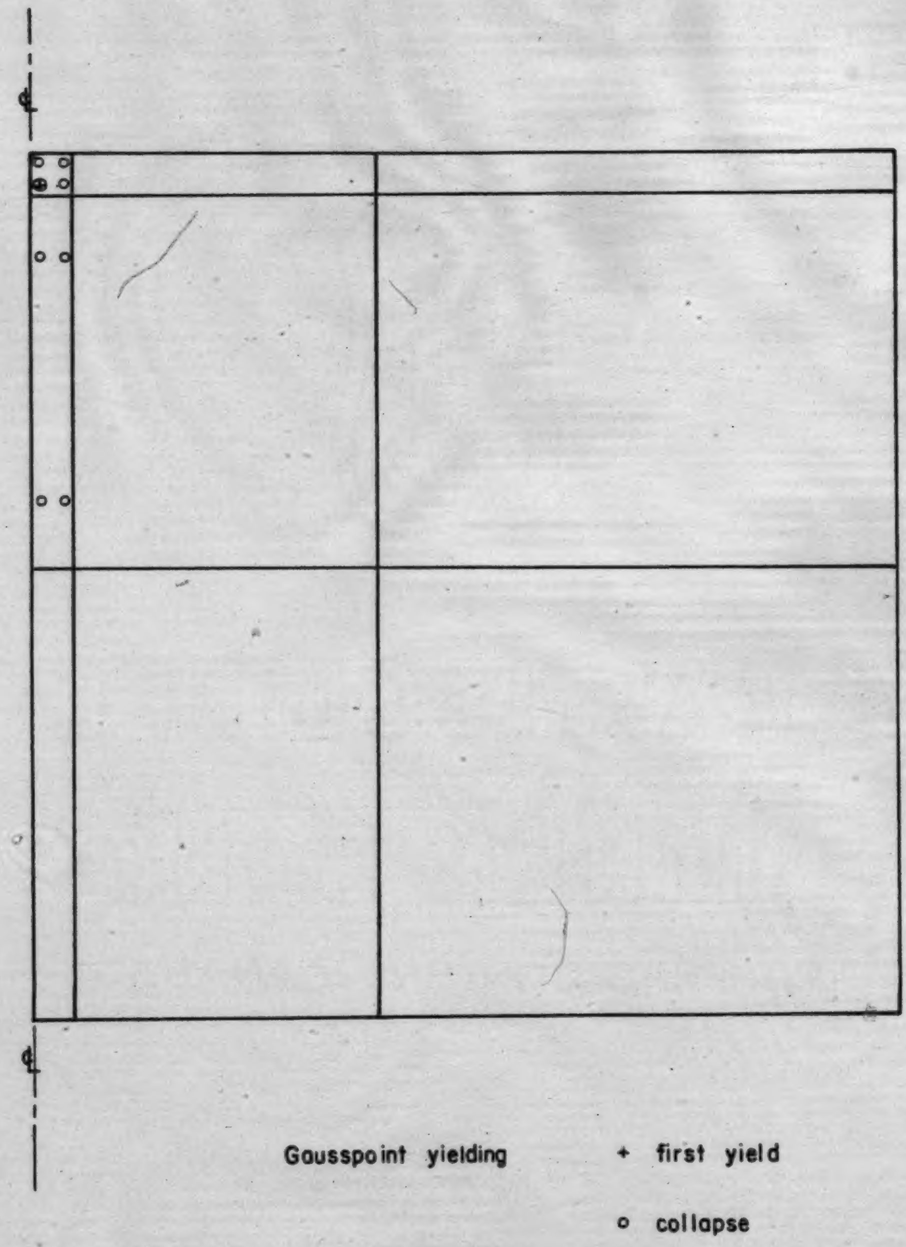
℄
℄
Gausspoint yielding
+ first yield
o collapse

FIGURE 5.20 FOOTING ON COHESIVE SOIL: YIELD ZONES FOR FIRST YIELD AND COLLAPSE.

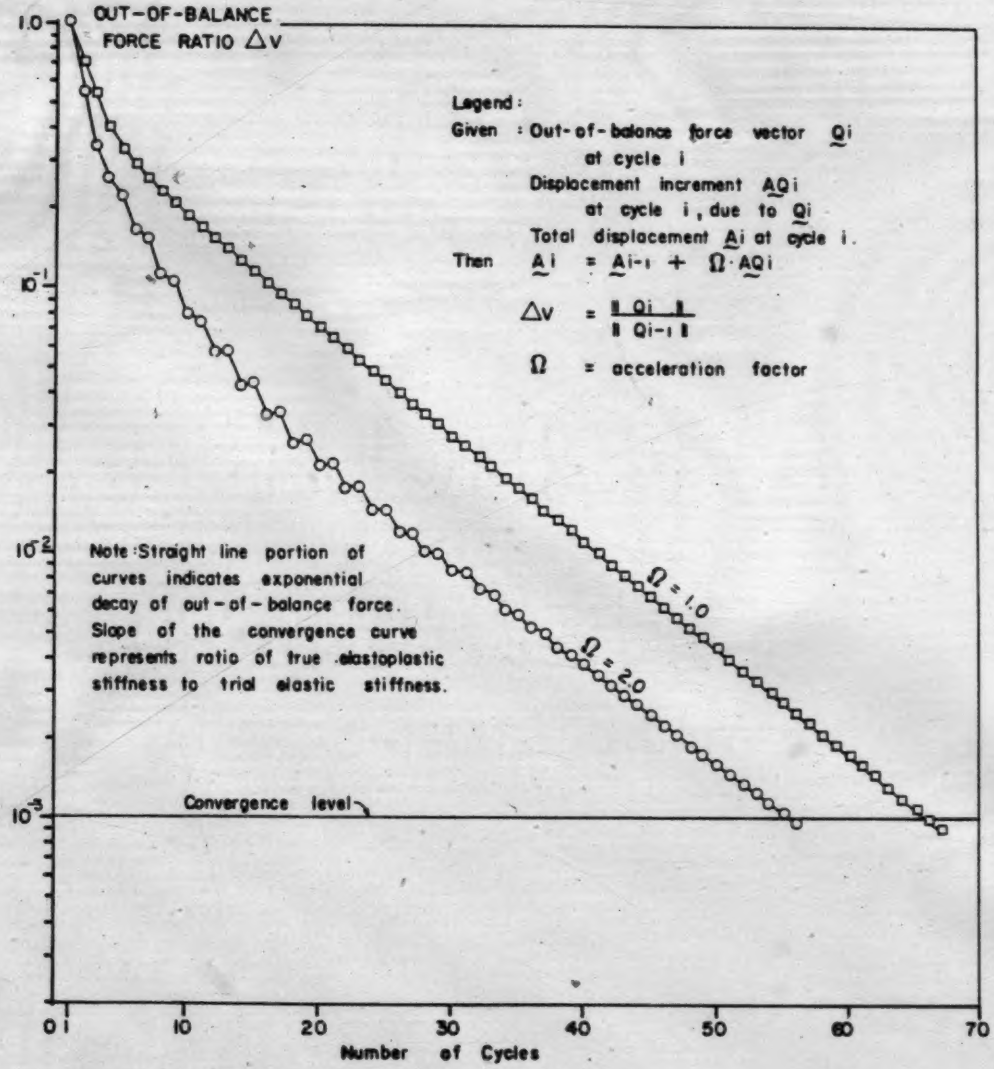

FIGURE 5.21 CONVERGENCE CHARACTERISTICS FOR BEARING CAPACITY PROBLEM, SHOWING INFLUENCE OF ACCELERATION FACTOR FOR A PARTICULAR LOAD STEP.

elastoplastic algorithm. Details of the convergence plot, of course, will vary from problem to problem. For a particular problem, convergence will also vary somewhat with different mesh details.

Load-Deformation Behaviour of Cohesive, Frictional Soil:

Hoeg *et.al.* (1968) published an analysis of bearing capacity of a strip load on an elastoplastic soil which utilized a finite difference solution procedure. They examined effects due to load level, boundary roughness, Poissons ratio, and location of lateral boundaries. Subsequently Zienkiewicz *et.al.* (1975) examined associated and nonassociated visco-elastoplasticity and included a load-deformation result for a flexible strip footing on a cohesive, frictional soil. The boundaries of the deforming mass were chosen to be the same as those used in the original work (Hoeg *et.al.* 1968).

A similar geometry was adopted by Christian *et.al.* (1977) who analysed cohesive, frictional soil with variable dilatancy rates. Their work provides quite a detailed discussion of various incremental plasticity laws, but description of their computational technique suggests that a rather unsatisfactory procedure for equilibrium iteration had been used.

It was decided to repeat the analyses of Zienkiewicz *et.al.* (1975), although this was for a non-dilatant (nonassociated) material. There was a reasonable assurance that the same basic elastoplastic model had been used and that, therefore, the results should compare closely with analyses using programs developed for this research. Figure 5.22 shows details of the mesh and gives relevant material data. Figure 5.23 shows a comparison of the present study with that of Zienkiewicz *et.al.* (1975), and the agreement is remarkably good. Also shown on this figure are indications of the iterative effort required at each stage of the analyses. Gauss points which were yielding at collapse are shown in Figure 5.24 in comparison with the earlier study.

Convergence data for the writer's program ESB, used for this analysis, are shown in Figure 5.25. The characteristics are somewhat curved, indicating the spreading of yielding during iterative solution of a load step. Small discontinuities in the gradients of these curves represent some elastic unloading associated with spreading of the elastoplastic zone. The convergence rate diminishes noticeably as the collapse load is approached.

Discussion of Bearing Capacity Analyses:

The results of these two test problems demonstrate unequivocably the accuracy and capabilities of the computer program ESB written for this research. Considerable time could have been spent in parametric studies of the problems, particularly in order to obtain a feel for the effect of the plastic dilatancy rate on the load-deformation behaviour.

Material Properties $E = 30000$ psi

$\nu = 0.30$

$c = 10$ psi

$\phi = 20°$

nonassociated flow rule $D = \frac{\dot{\epsilon}^p_v}{\dot{\gamma}^p_{max}} = 0$

(tensile strength of 20 psi used)

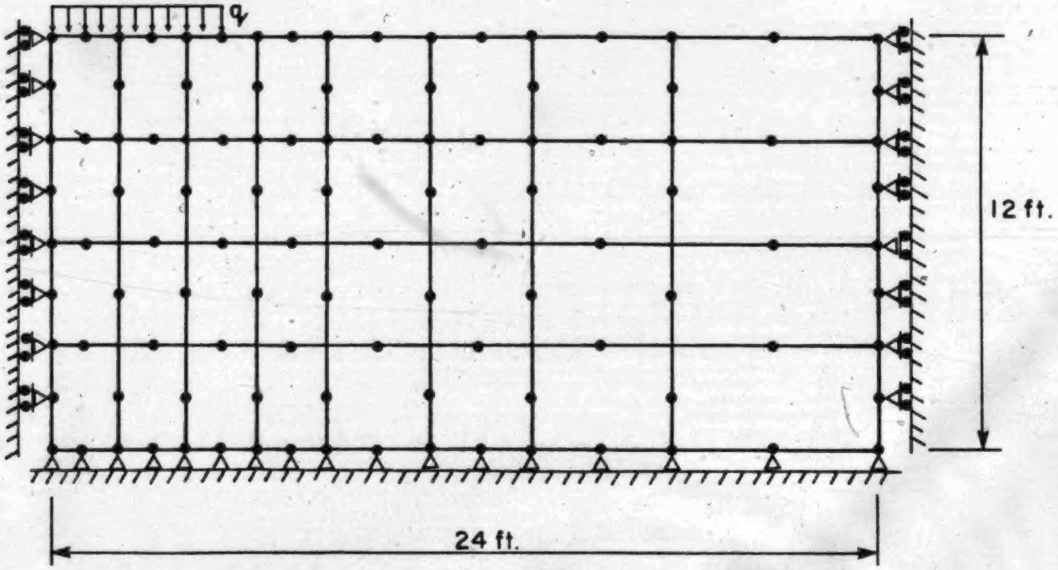

FIGURE 5.22 BEARING CAPACITY PROBLEM FOR LOAD-DEFORMATION RESPONSE OF FRICTIONAL SOIL. (after Zienkiewicz et. al, 1975)

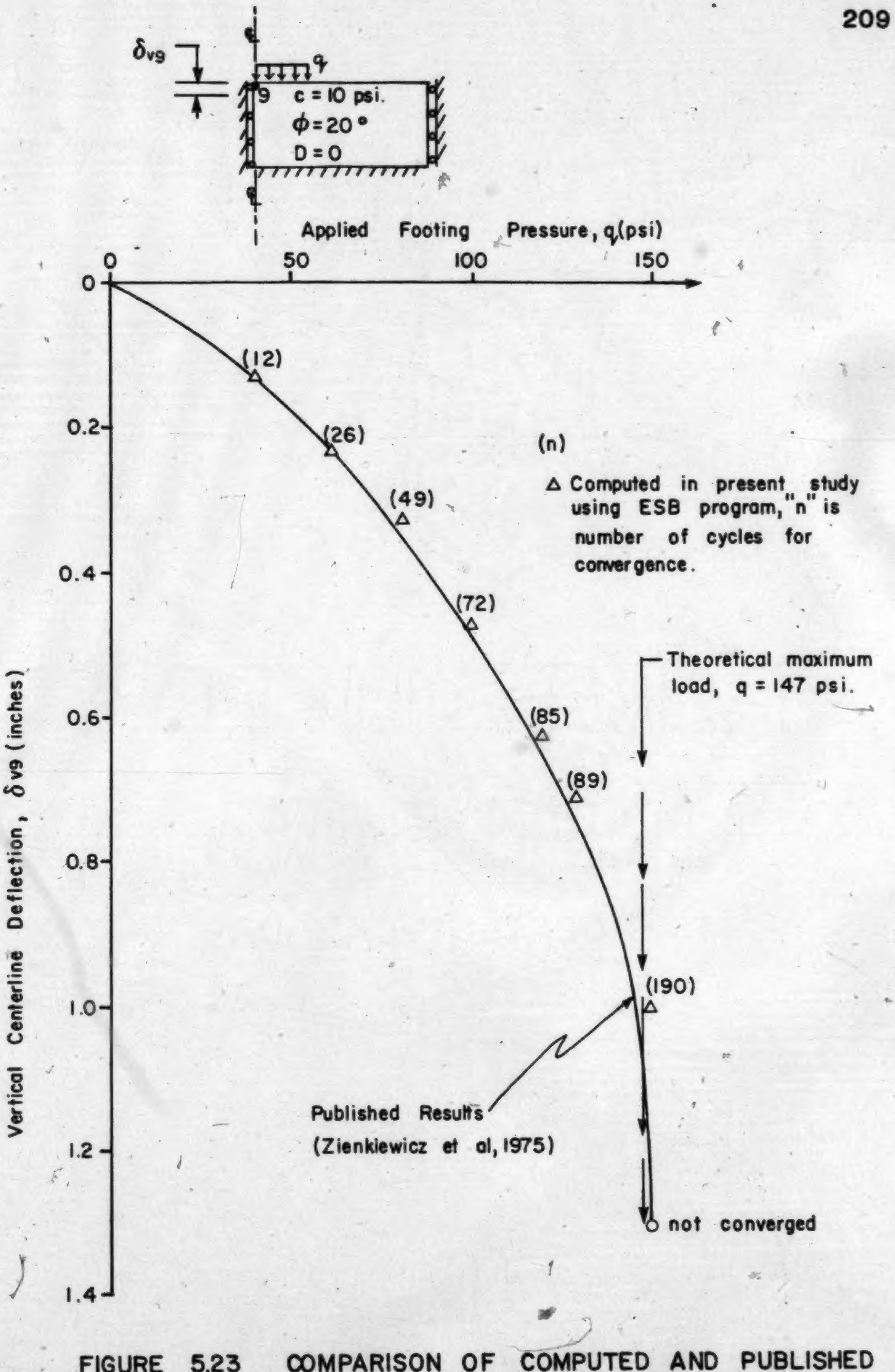

FIGURE 5.23 COMPARISON OF COMPUTED AND PUBLISHED LOAD-DEFORMATION RESPONSE OF FRICTIONAL SOIL.

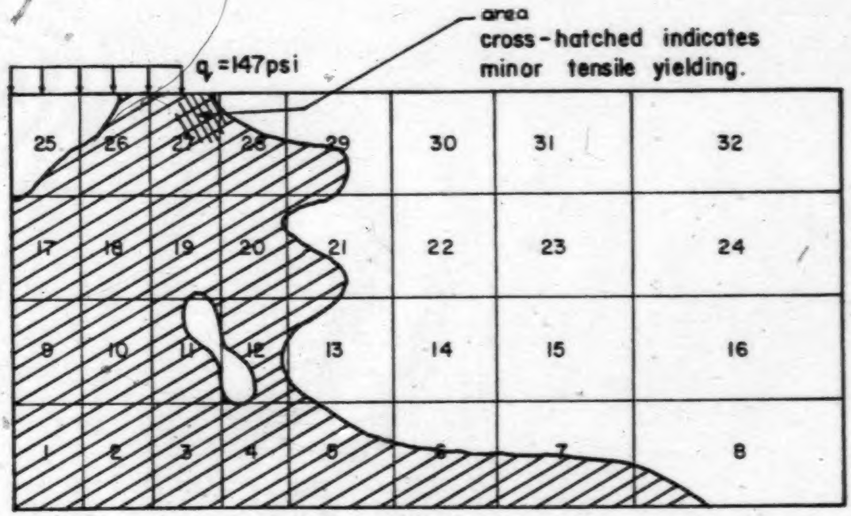
area
cross-hatched indicates
minor tensile yielding.
q = 147psi
25
26
27
28
29
30
31
32
17
18
19
20
21
22
23
24
9
10
11
12
13
14
15
16
1
2
3
4
5
6
7
8

Computed yielding zones at collapse ESB program, CRD model, (Simmons, 1980a)

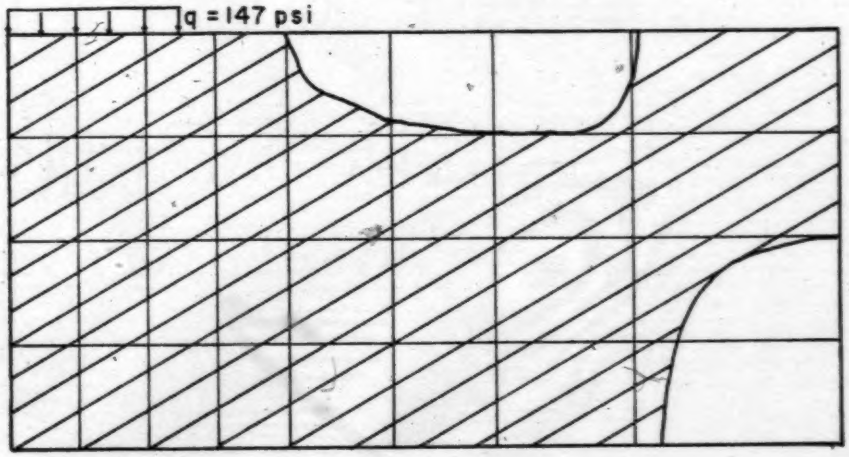

Published yielding zones at collapse (Zienkiewicz et. al., 1975)

FIGURE 5.24 COMPARISON OF YIELDING ZONES AT COLLAPSE: COMPUTED FOR THIS STUDY VERSUS PUBLISHED DATA.

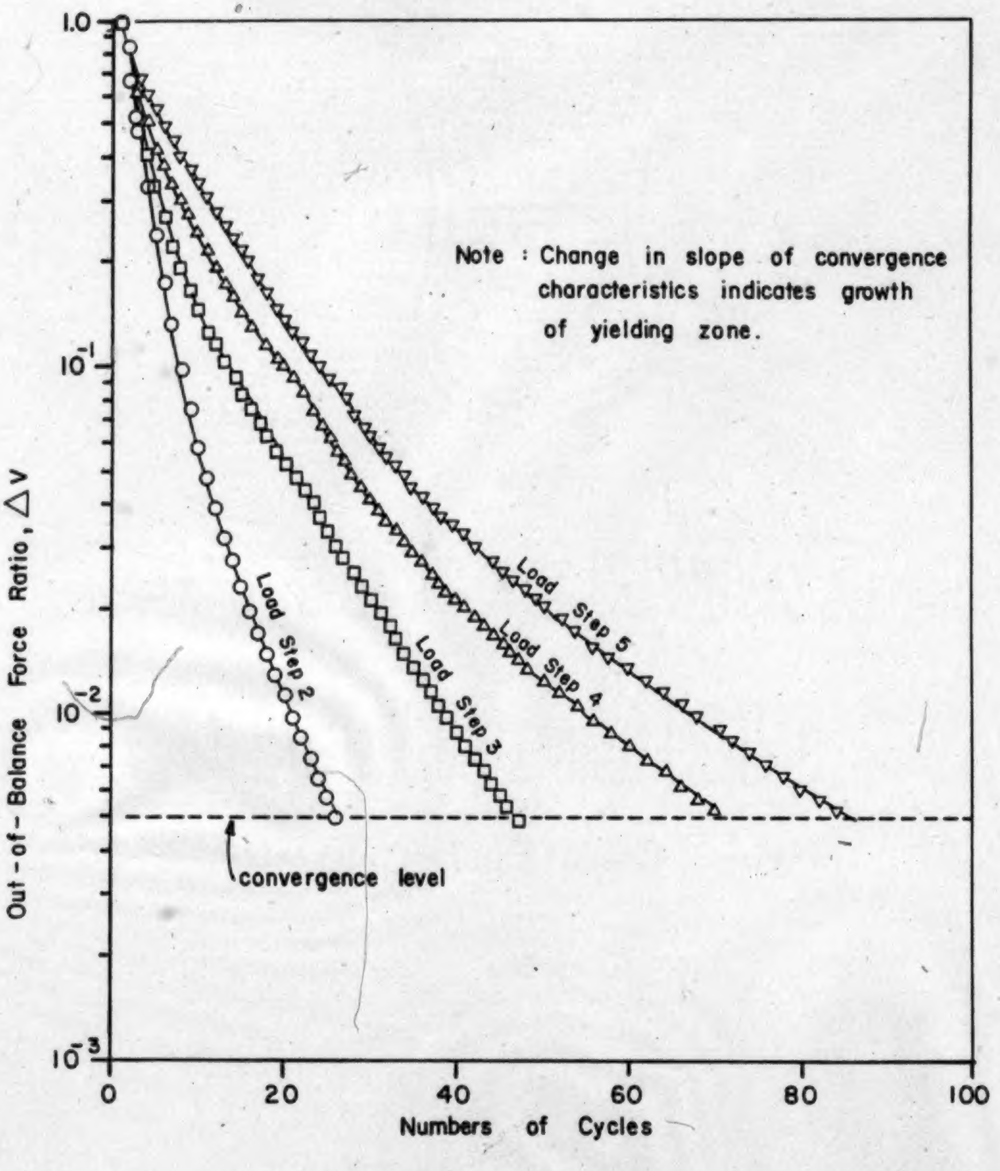

FIGURE 5.25 CONVERGENCE CHARACTERISTICS FOR LOAD-DEFORMATION PROBLEM, FOR FOUR ELASTO-PLASTIC LOAD STEPS.

For the study of yield and collapse loads, a remarkably coarse mesh was used. The only numerical problem associated with this analysis was the development of some tension zones underneath the footing. The material model has a tension strength cutoff procedure, but a small tensile strength was employed so as to avoid influencing the behaviour too much. Use of a more refined mesh would have permitted sufficient deformational freedom so as not to generate any tension at all.

As far as is understood, the Zienkiewicz *et.al.* (1975) study used a time-stepping algorithm for visco-elastoplasticity. This would be similar to the writer's work only in its requirements for equilibrium iteration, but the numerical results still indicate surprisingly good correlations between two independently-developed procedures.

5.5 CONCLUSIONS CONCERNING COMPUTATIONAL MODELS

The analyses described in this chapter raise as many questions as they answer. There is insufficient literature describing experience with numerical analysis, particularly in describing numerical difficulties, and it is hoped that in future authors will be less hesitant in describing these difficulties. There is a desperate need to de-mystify the subject of elastoplastic finite element analysis, in order to encourage its acceptance as a tool for research and for practical problem solving.

The success of the ESB program in reproducing established elastoplastic behaviour implies that its basic program design is satisfactory. Quite possibly, more sophisticated procedures will be required to overcome some of the numerical difficulties encountered. It is clear that the nonhomogeneous deformation problem is an intrinscially difficult one, to the point where it might best be pursued by other means at present.

To this point, a class of physical problems involving localized deformations has been described, and some means by which these problems may be explored by numerical experimentation have been developed. Chapters 6 and 7 describe application of the elastoplastic and nonlinear elastic shearband models to two well-documented case histories: the so-called progressive failure of a slope cut in overconsolidated clay, and the construction and operation of an embankment dam on a clay shale foundation.

6. SHEARBAND PROPAGATION IN THE SAXON CLAY PIT WALL

Progressive failure, as discussed in Chapter 2, involves the interaction of three principal elements:

1. strain-weakening strength parameters;
2. deformation parameters;
3. ground stress state.

Because there are many parameters to be considered, it is unlikely that a unique set can be found as a solution for a progressive failure problem. More likely, a few sets of parameters may all satisfy the conditions of the problem. This lack of uniqueness must be expected, and unfortunately it makes difficult the task of transferring experience from one site to another. The limitations of the one-dimensional progressive failure models (Chapter 3) are related to deformations, because an adequate appreciation of the deformation field surrounding the failure cannot be obtained. The lack of uniqueness mentioned above could in many cases be resolved if the surrounding deformation field was better understood.

The response of the Saxon Clay Pit wall to full-face excavation was carefully monitored by Burland *et.al*. 1977. Details of the deformation field lead to the hypothesis of true progressive failure, causing propagation of a shearzone behind the toe of the wall. Only one-dimensional models were available for analysing this hypothesis, and so the operational strength controls in the field remain somewhat indeterminate.

This case-history provided much of the impetus for development of the analytical approach of this thesis. At the time of writing, certain analytical techniques still had not been developed to the stage of routine application to problems of the Saxon Clay Pit type.

The case history is reviewed in this Chapter. Application of the one-dimensional progressive failure models is described in order to define a limited range of parameters for detailed deformation analysis. The most significant question, whether or not true progressive failure did occur, is answered by the presentation of deformation analyses which assumed the negative argument to begin with.

6.1 REVIEW OF FIELD BEHAVIOUR

The Saxon Clay Pit is operated by the London Brick Company at Whittlesey near Peterborough, England. Overconsolidated clay shale is mined in a 25 metres high face at a slope of 72° by a mobile continuous-face planer. The section of the pit wall described by Burland *et.al.* 1977 is about 200 metres long. The planer moved parallel to the wall, removing 10m to 15m from the face, and completing a full traverse of the face in 3 to 6 months. Figure 6.1 is a plan view of the studied pit wall, showing successive faces of excavation. When the study commenced, the face had advanced approximately 650 metres. The field measurements terminated when the planer was moved to another location.

Geological Conditions:

Figure 6.2 is a cross section of the working face, and also shows a geological profile. Between 3 and 6 metres of surficial deposits, collectively termed "callow", overlie the mineable clay shale. The callow consists of peat, sandy gravel, and completely weathered clay shale, and was periodically stripped for some distance away from the pit wall.

The clay shale consists of 8 to 10 metres of Middle Oxford Clay overlying 17 metres of Lower Oxford Clay. The Middle Oxford Clay is moderately weathered at the top, with frequent oxidized fissures, and a homogeneous mass appearance. Lower down, it becomes less fissured and weathered and more blocky in appearance. It is summarized as a grey-green, calcareous plastic clay. The Lower Oxford Clay consists of two lithological types: dark brown-grey highly bituminous strongly laminated shale and interbeds of paler green-grey blocky clay.

Underlying strata are 3.2 metres of green-grey dense clayey silt and fine sand, locally cemented for the top 0.6 metres, termed the Kellaways Sand (and "Rock"); 2.1 metres of dark blue-grey plastic Kellaways Clay; 2.5 metres of massive biolithic limestone; and then alternating clays,

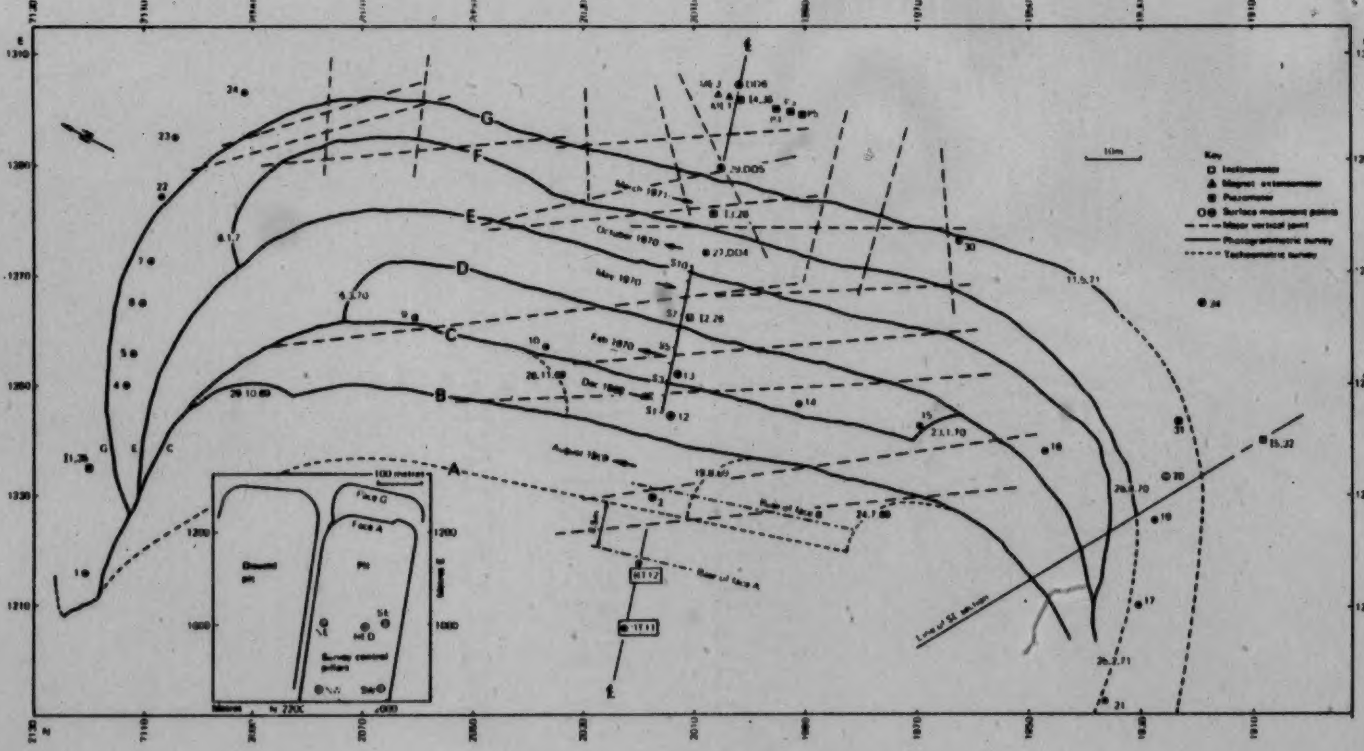
Key
Inclinometer
Magnet extensometer
Piezometer
Surface movement points
Major vertical joint
Photogrammetric survey
Tacheometric survey
10m
A
B
C
D
E
F
G
March 1971
October 1970
May 1970
Feb 1970
Dec 1969
August 1969
11.5.71
26.2.71
Line of S1 section
100 metres
Face G
Face A
Pit
Survey control pillars

FIGURE 6.1 PLAN VIEW OF EXCAVATION FACE, SAXON CLAY PIT
(after Burland et. al. 1977)

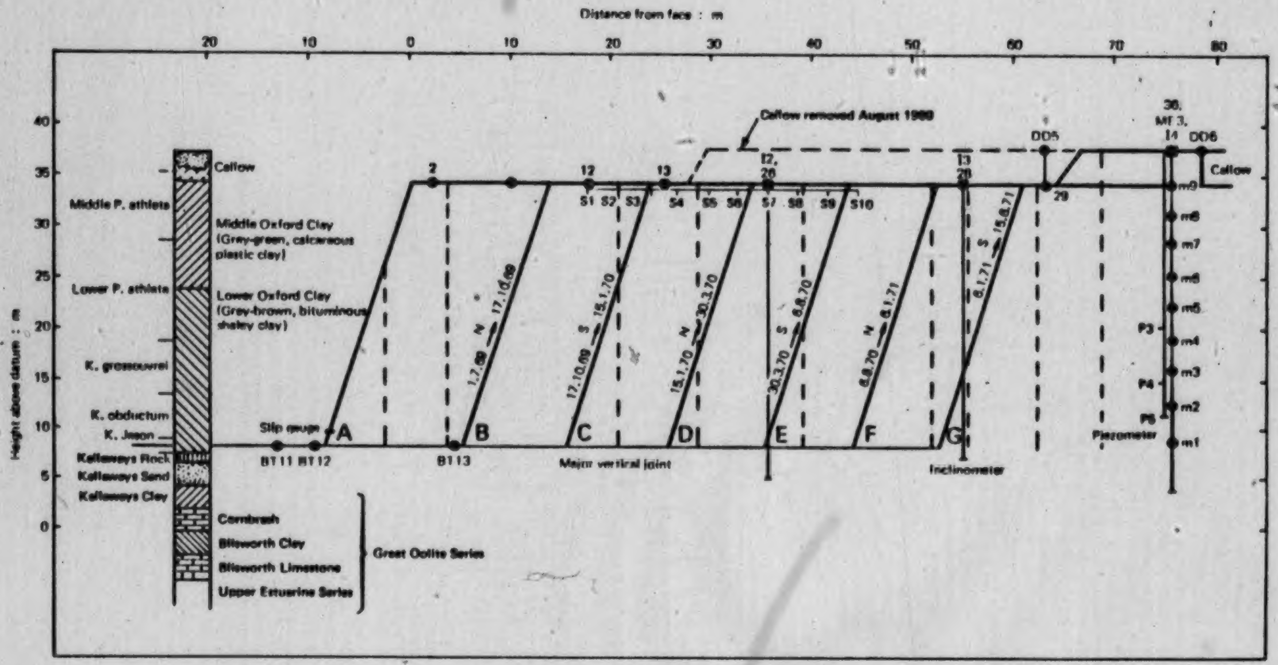
Distance from face : m
20
10
0
10
20
30
40
50
60
70
80
Height above datum : m
40
35
30
25
20
15
10
5
0
Callow
Middle P. athleta
Middle Oxford Clay (Grey-green, calcareous plastic clay)
Lower P. athleta
Lower Oxford Clay (Grey-brown, bituminous shaley clay)
K. grossouvrei
K. obductum
K. Jason
Kellaways Rock
Kellaways Sand
Kellaways Clay
Cornbrash
Blisworth Clay
Blisworth Limestone
Upper Estuarine Series
Great Oolite Series
Slip gauge
BT11 BT12
BT13
Major vertical joint
Callow removed August 1980
2
12
13
12,
26
13
20
DD5
29
36,
MT 3,
14
DD6
Callow
S1 S2 S3 S4 S5 S6 S7 S8 S9 S10
A
B
C
D
E
F
G
1.7.69
N
17.10.69
17.10.69
S
15.1.70
15.1.70
N
30.3.70
30.3.70
S
6.8.70
6.8.70
N
6.1.71
6.1.71
S
15.6.71
Inclinometer
Piezometer
P3
P4
P5
m1
m2
m3
m4
m5
m6
m7
m8
m9

FIGURE 6.2 GEOLOGY AND EXCAVATION CROSS-SECTION
(after Burland et. al. 1977)

limestones and sands in a thick sequence. The minimum estimated depth of burial of the Oxford Clay is about 330 metres.

Oxford Clay Fabric: There are two sets of major joints, of 100 metres or more lateral extent, forming near-parallel 5 to 20 metre spacings. One set is approximately parallel and the other approximately perpendicular to the face, as indicated in Figure 6.1. These joints appear to die out upwards in the middle Oxford Clay. The smaller-scale fissure fabric is typical of an overconsolidated clay: a blocky fissure fabric ranging from 10 to 300 millimeters in spacing is displayed.

Geotechnical Properties:

The unit weight was approximately constant, and averaged 19.9 kNm^{-3}. Average liquid and plastic limits were 55% and 24% respectively, denoting highly plastic clay and clay shale. The average calcium carbonate content was 10% to 20%, which is high and which probably caused local cementing. Summary properties are shown on Figure 6.3. With depth, moisture contents plot consistently below the plastic limits, implying that brittle behaviour could be expected.

Laboratory undrained shear strength values range from 50 kPa to more than 1200 kPa with depth. The strengths were found to be strongly anisotropic, typically having a ratio of 1.7 between horizontally and vertically oriented specimens. The ratio Eu/Cu shows no net increase with depth

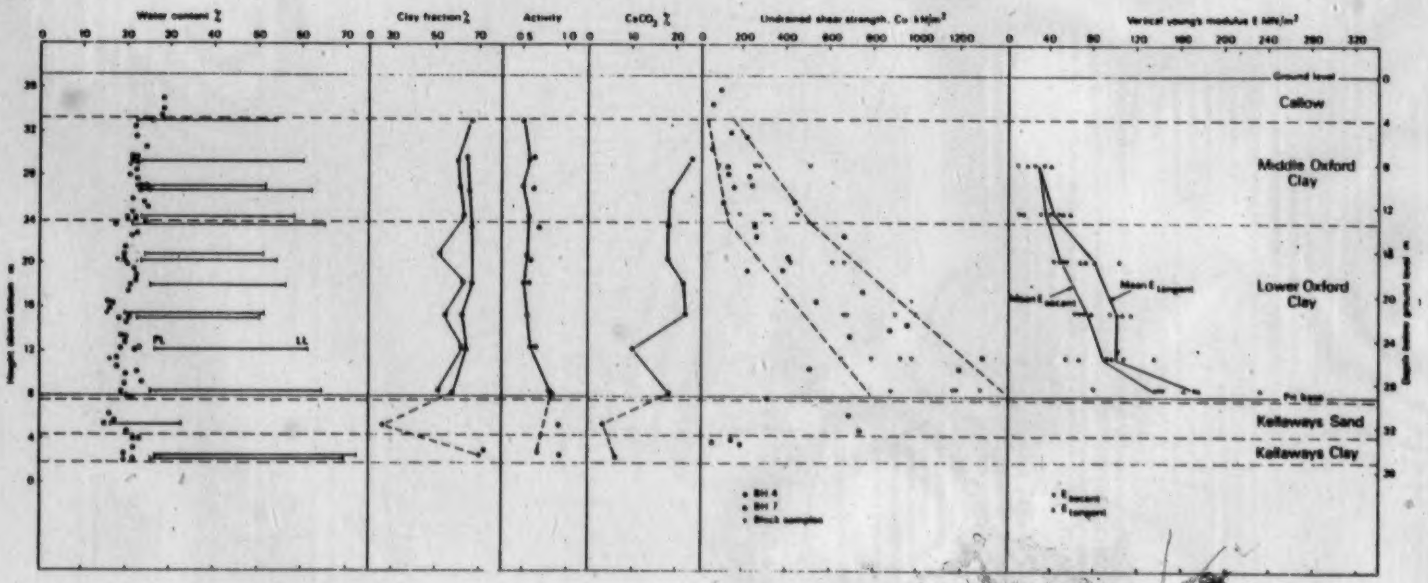

FIGURE 6.3 SUMMARY GEOTECHNICAL PROPERTIES (after Burland et. al. 1977)

and averages about 100. The ratio Eh/Ev is approximately 2.

Peak strength parameters from triaxial tests are scattered, but not in a consistent manner: average values are c'_P =80 kPa, ϕ'_P =28°. Direct shear tests parallel to bedding gave peak parameters c'_{PD} =172 kPa, ϕ'_{PD} =27.5° and residual parameters c'_{RD} =3.5 kPa, ϕ'_{RD} =13°. Figure 6.4 illustrates that typical shear stress/displacement curves were very sharp and strengths dropped to near residual after only 3 to 4 millimeters of shearing displacement.

Sampling of the Kellaways beds proved difficult and testing indicated substantial disturbance. Therefore, little reliable data was available for these materials.

Instrumentation:

A variety of instrumentation and measurement techniques were employed, to measure ground movement and groundwater pressure.

Piezometers: Casagrande-type standpipes were installed. Groundwater pressures dropped as the excavated face approached piezometers. Significantly, the lower piezometers recorded the lowest water levels. This could have been due to pressure drops associated with dilatant shearing in the basal shearzone. However, it may also have been due to downward flow into the more permeable basal Kellaways Sand, which was exposed in drainage ditches in the floor of the pit. Interpretation of the piezometric measurements was difficult because of the highly anisotropic initial fabric,

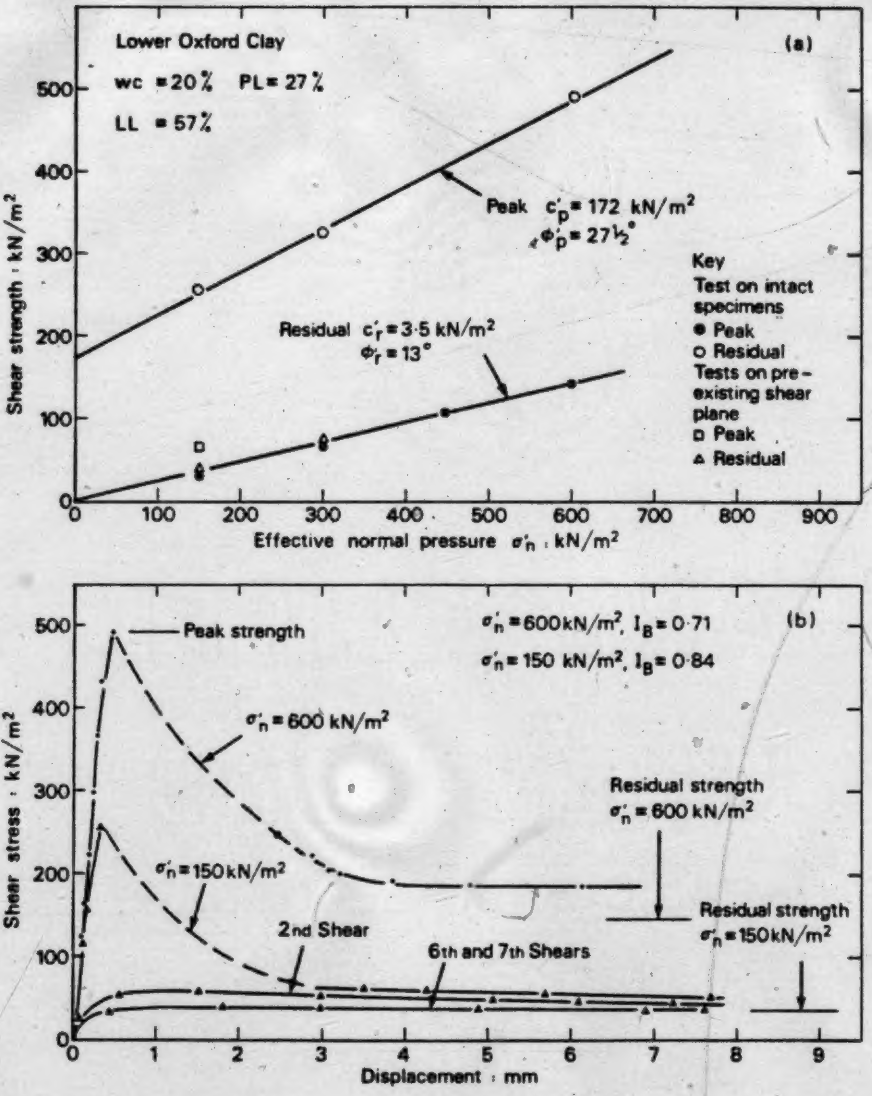

FIGURE 6.4 DIRECT SHEAR TEST SUMMARY DATA
(after Burland _et.al._ 1977)

and subsequent stress relief and drainage.

Precise surveying: This was used to control surface movement points, mapping, and photogrammetry. A grid of surface-movement points was monitored throughout the study. Reference pillars were installed in the base of the pit, and were affected by sudden, uncontrolled basal heaving due to groundwater pressure in the underlying aquifer. Wherever possible, subsequent measurements were corrected for this occurrence.

Photogrammetry: The positions of the face, and of major joints, were recorded by a series of eight photogrammetric surveys.

Horizontal Extensometers: A horizontal multiple point extensometer was installed on the upper surface of the clay behind the wall, to measure surface strains and to indicate the influence of the major joints on the surface displacements.

Inclinometers: Five vertical inclinometers were installed to measure lateral movements with depth. An overall accuracy of less than 10 millimeters in 30 metres was achieved. The surface collars were surveyed using the precise survey grid.

Vertical Extensometers: Following early site experience, it was found necessary to measure the distribution of vertical displacements with depth thoughout the height of the face and to a certain depth below it. Two multipoint magnet extensometers with accuracies better than

1 millimeter were installed.

Observed Horizontal Movements:

The first instruments installed were the horizontal extensometers. Little or no horizontal strain was measured for up to 31 metres from the face, even though significant horizontal displacements were measured. This suggested block movement towards the pit, and some discrete overthrusts were found near the base of the wall, particularly one located 1.6 metres above the base. Micrometer slip gauge measurement points were mounted at eight locations along the overthrust. A typical slip episode (from immediately after passage of the planar until its imminent return) is shown in Figure 6.5. Note that the slip movement accelerated when the planar was close to the gauge location. These early measurements indicated that the ground within a region of 1.0 to 1.5 times the wall height was sliding as a block on a horizontal shearzone formed by a series of bedding planes near the pit base. More instrumentation was then installed to study ground behaviour during propagation of the shearzone.

Horizontal movements with depth, as measured by inclinometers, showed that displacement at the base of the excavation was always at least 70% of surface movement. Some horizontal movement was observed down to 3 metres below pit base level. The inclinometer tubes kinked near pit base level as the face advanced. Examination of a tube, recovered after the planer had passed, showed kinking to have also

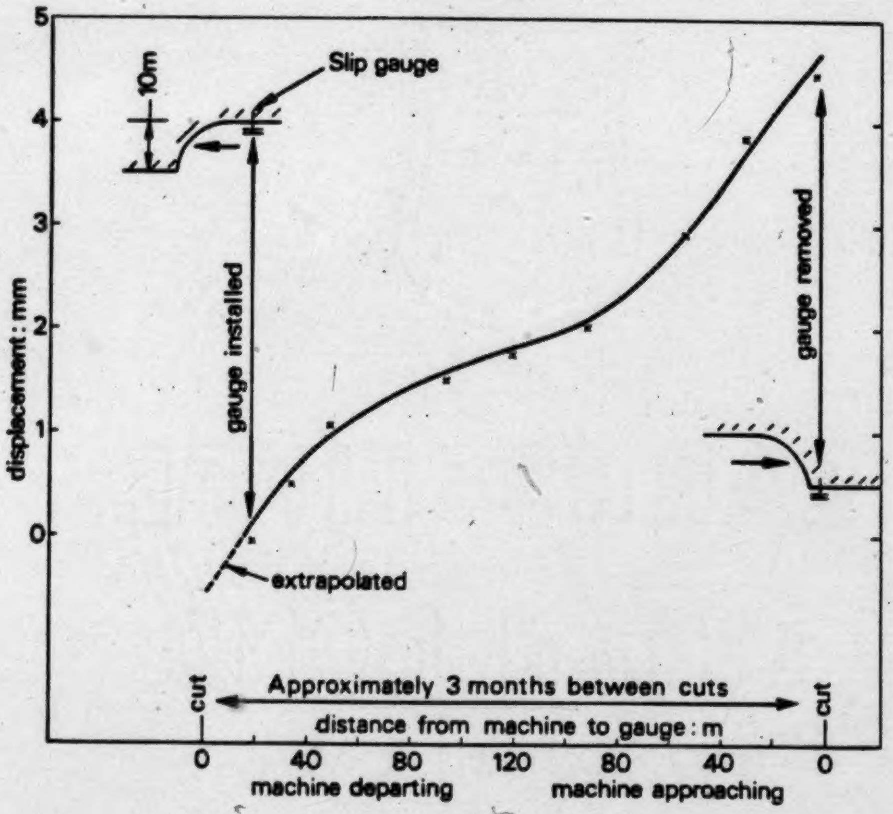

FIGURE 6.5 TYPICAL OVERTHRUST GAUGE MOVEMENTS (after Burland et.al. 1977)

developed just below pit base level. After the planer was moved to a new location significant time-dependent inclinometer movements continued to be observed.

Observed Vertical Movements:

Significant consolidation of the callow was observed to result from the drawdown of the originally perched upper water table.

Time-dependent settlements were observed generally. There appeared to be somewhat of an acceleration of the settlement rate when the planer passed close to a measurement point.

Movements recorded by a vertical extensometer are summarized as a function of time in Figure 6.6. Settlements are seen to decrease with depth until by mid-height of the face they give way to heaving. Thus the entire sliding block underwent increased compression as horizontal movements developed. Base heave amounted to just over 100 millimeters in two years, during which the face was cut back 60 metres.

Overall Displacement Pattern:

Summary surface displacements at points on the top of the moving block are shown in Figure 6.7. Typical displacement trajectories as a function of distance from the face are shown in Figure 6.8. Some influence of the callow was noted from the measurements. When the excavated face passed close to the callow (that is, prior to another cycle

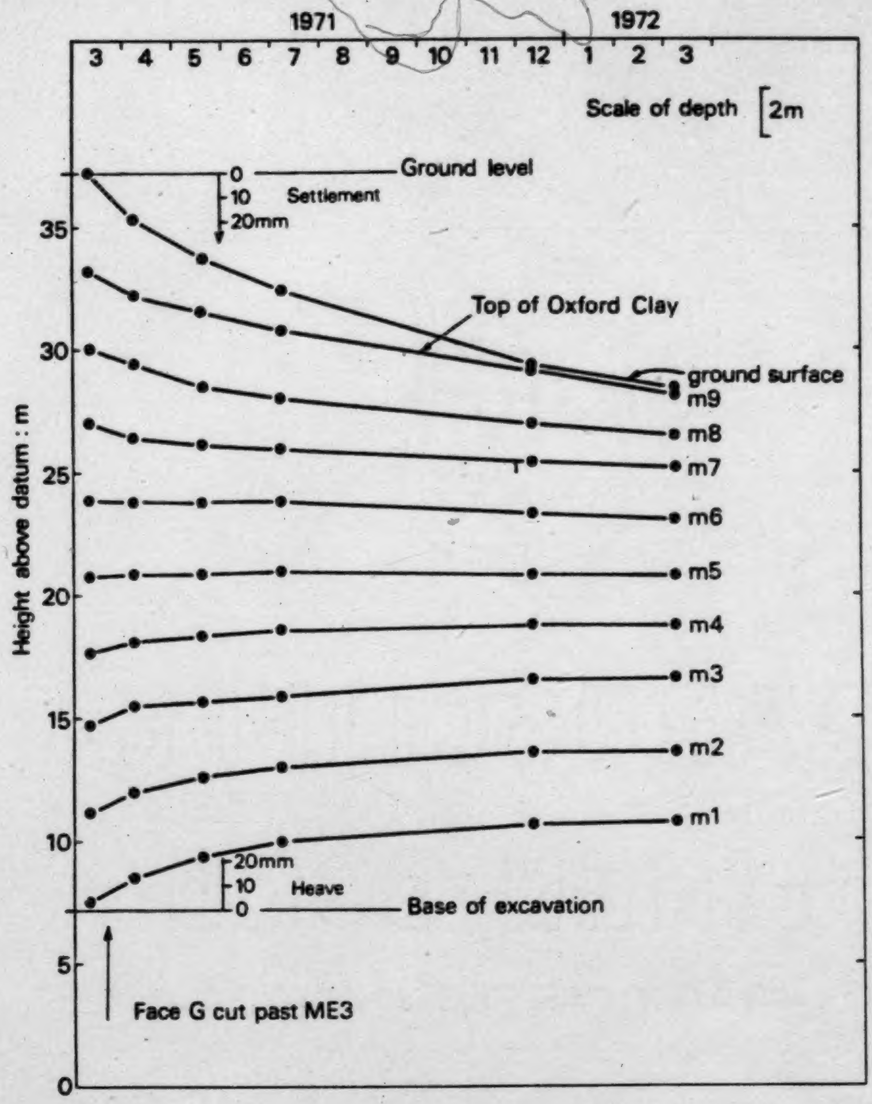

FIGURE 6.6 VERTICAL COMPRESSION PATTERN VARIATION WITH TIME (after Burland et.al. 1977)

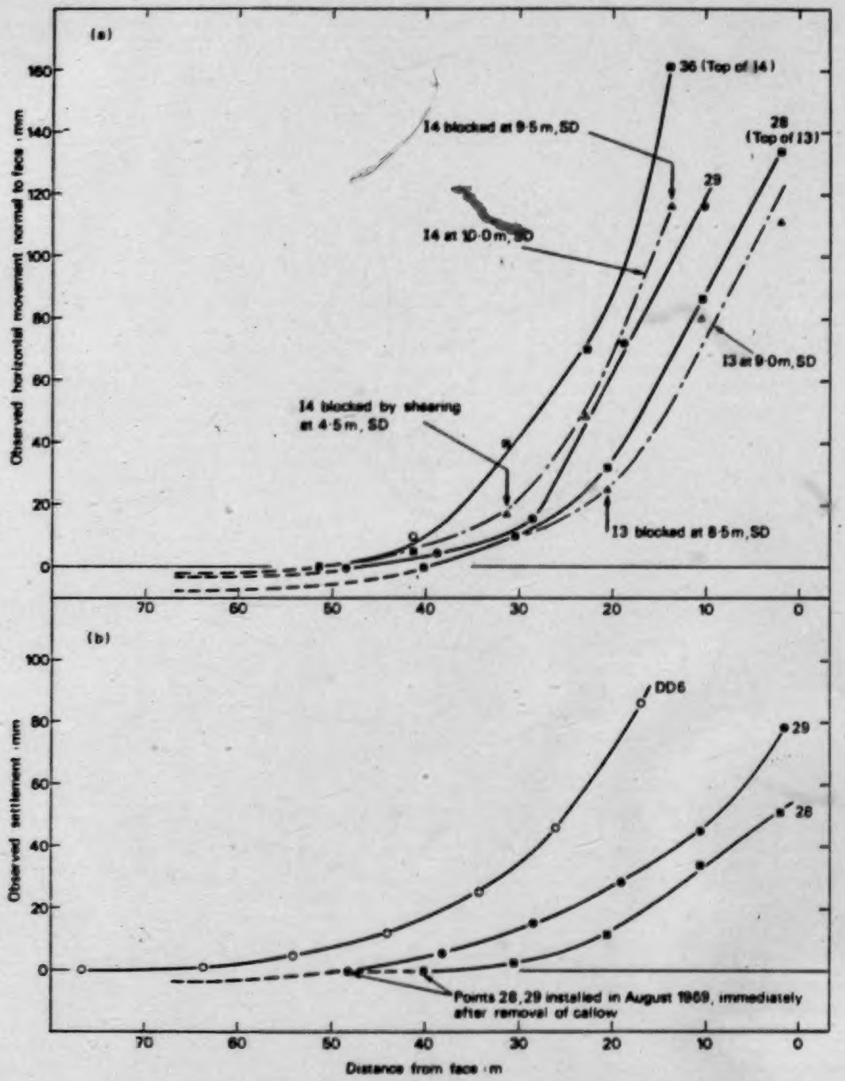

FIGURE 6.7 SUMMARY SURFACE DISPLACEMENTS (after Burland et. al. 1977)

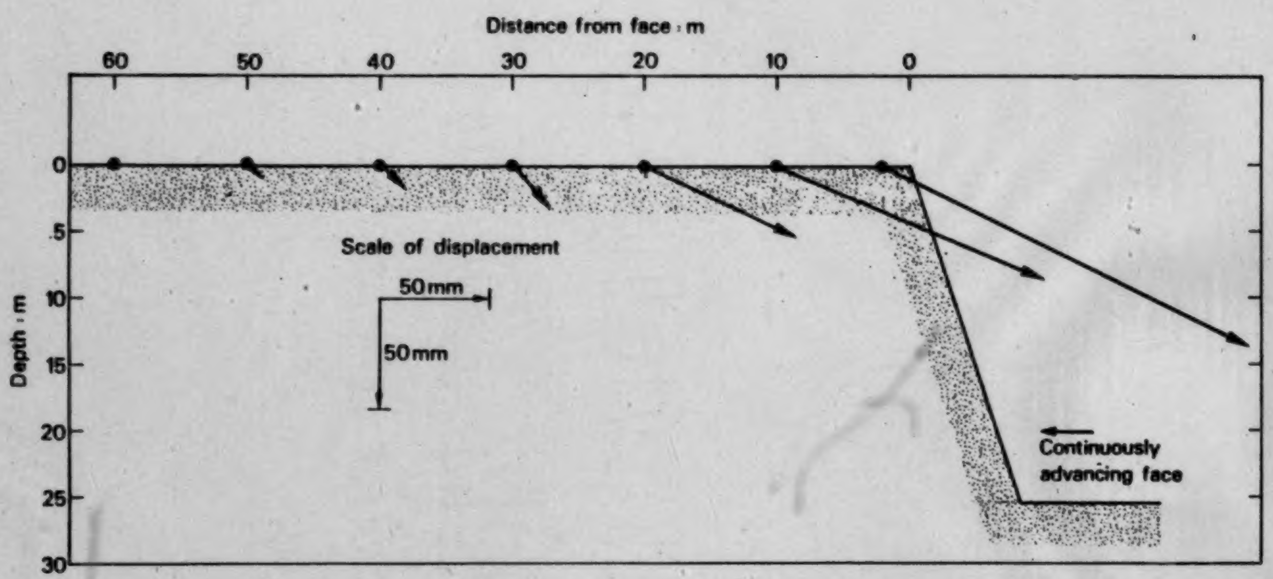
Distance from face : m
60
50
40
30
20
10
0
Depth : m
0
5
10
15
20
25
30
Scale of displacement
50mm
50mm
Continuously advancing face

FIGURE 6.8 INFERRED SURFACE DISPLACEMENT TRAJECTORIES
(after Burland et.al. 1977)

of stripping) extra movement was noted, presumably as a result of the extra wall height.

Inferred Shearzone Propagation:

By understanding the excavation to be a quasi-continuously advancing face, a model for the observed behaviour was developed as shown on Figure 6.9. As the face approached a given surface point, the tensile strain at first increased slowly. A sudden increase in tensile strain, with the face between 20 and 30 metres away, was inferred to mark the *end-region* of the shearzone. Following this, nonextensional block glide occurred.

In conclusion, some stick-slip shearzone movements were also interpreted. Although the overall mechanism of movement was clearly identified, the propagation of the shearzone was inferred to be sensitive to such matters as local variations in strength, drainage conditions, presence of major joints, and rate of face excavation.

6.2 APPLICATION OF ONE-DIMENSIONAL MODELS

A brief review of one-dimensional progressive failure models was presented in Chapter 3. Each of these models was applied to the Saxon Clay Pit problem in order to determine relationships among the three principal elements (described at the beginning of this chapter).

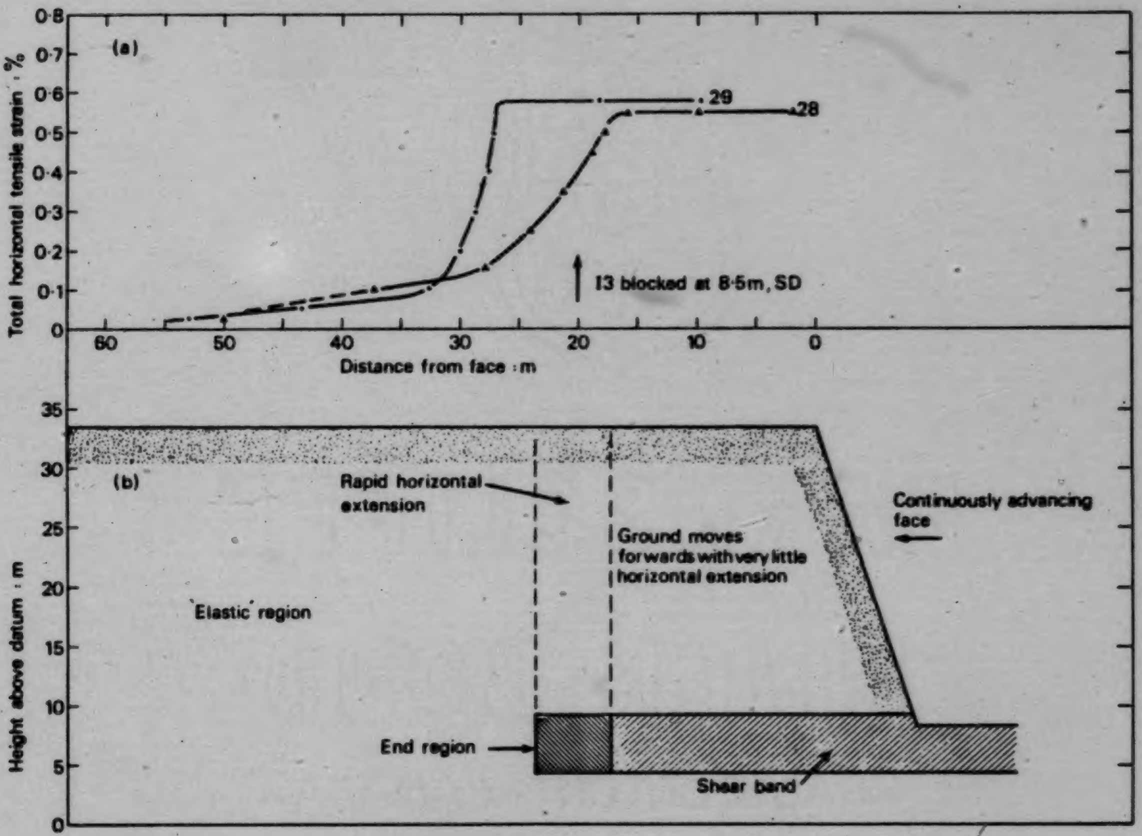

6

FIGURE 6.9 INFERRED SHEARBAND YIELD MECHANISM
(after Burland et. al. 1977)

In order to apply these models, the problem geometry had to be simplified, and appropriate strength and deformation parameters selected. Although a substantial geotechnical testing program was undertaken, there was a shortage of data on which to base refinements to the selection of these parameters.

The relationship between the initial ground stress state, the unloading modulus of the sliding block, and reasonable strength parameters was explored. Comments are made about the advantages and disadvantages of various models, and the applications of more detailed deformation analyses are discussed.

Geometry and Material Parameters:

The actual pit wall stood 27 metres high on a 72° slope, with 3 to 6 metres of overlying callow stripped off for some distance back from the face. An idealized vertical wall 27 metres high, shown in Figure 6.10, was used as a model for all analyses.

Laboratory tests gave vertical Young's moduli averaging about 100 MPa, and the horizontal Young's moduli were generally higher by a factor of two. Consequently, a Young's modulus of 200 MPa was chosen as a standard. However, it is generally recognized that field moduli are substantially higher, and a Young's modulus of 400 MPa was also adopted as a reserve value. The drained direct shear strength parameters (parallel to bedding) noted on Figure 6.4 were

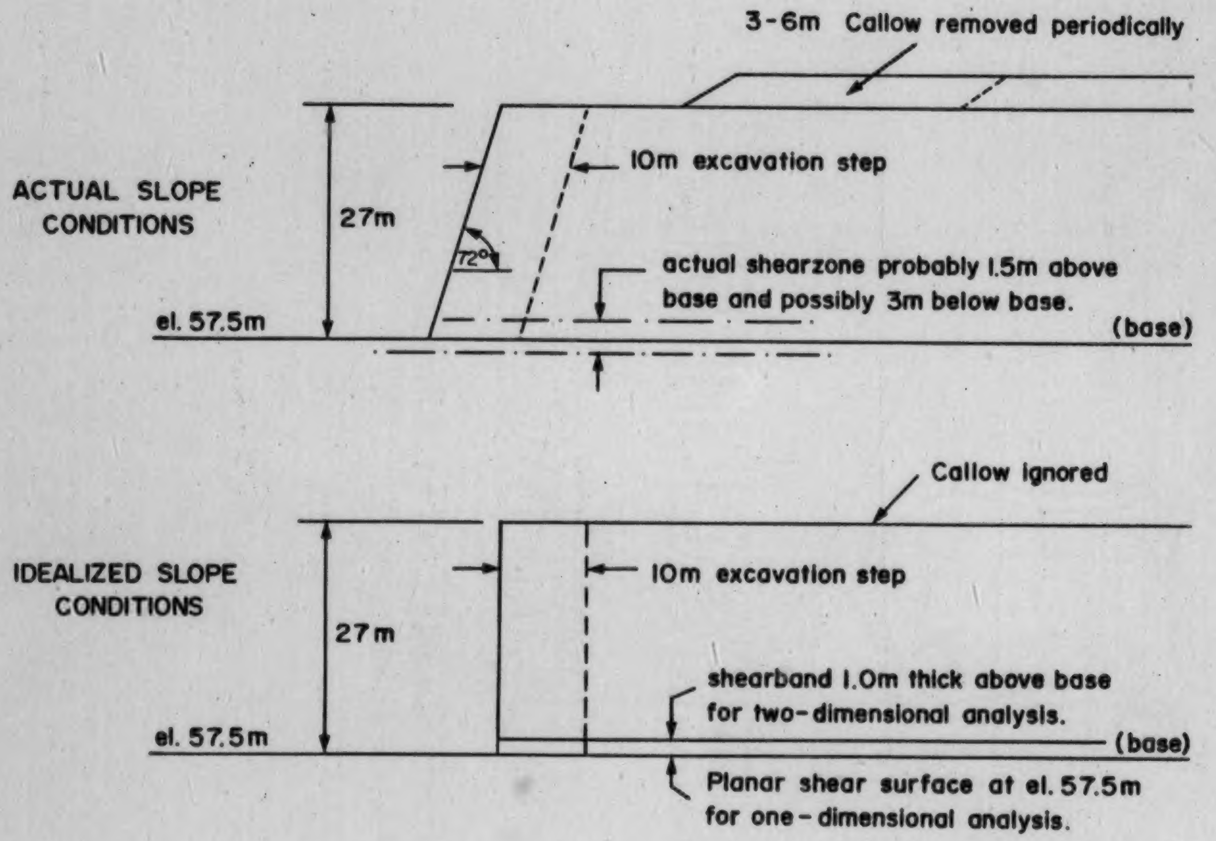
3-6m Callow removed periodically
ACTUAL SLOPE CONDITIONS
27m
10m excavation step
72°
actual shearzone probably 1.5m above base and possibly 3m below base.
el. 57.5m
(base)
Callow ignored
IDEALIZED SLOPE CONDITIONS
27m
10m excavation step
shearband 1.0m thick above base for two-dimensional analysis.
el. 57.5m
(base)
Planar shear surface at el. 57.5m for one-dimensional analysis.

FIGURE 6.10 IDEALIZED SLOPE FOR ANALYSIS

adopted.

As noted earlier, it is difficult to be precise about the operational pore pressures along the sliding surface. Use of the average pore pressure coefficient r_u was decided upon. The average maximum value of this parameter was 0.2, but this does not allow for pressure decreases associated with dilatant shearing in the sliding zone. Calculations were therefore made for a range of r_u between 0.0 and 0.3. An alternate and much more rigorous approach (Cleary, 1976) will be discussed at the conclusion of this chapter.

Application of the PR Model:

The PR model (Palmer and Rice, 1973) relates the work done in lateral elaştic unloading of the sliding block, energy release during the peak-residual transition, and energy absorbed in friction along the shearband. As an approximation, no relative slip occurs along the shearband until peak strength is attained. It is also assumed that the physical *end-region* in which the peak-residual transition occurs is negligible in proportion to the length of shearband where sliding occurs with residual resistance only. A characteristic material length $\bar{\delta}$ obtainable from direct shear tests measures the energy density of the peak-residual transition. For the Saxon Clay Pit tests, an essentially constant value of $\bar{\delta}$ =2.85 mm was measured at the different normal stress levels quoted.

Figure 6.10 also indicates the relationship between the uniform far-field horizontal stress assumed in the model and the standard coefficient of lateral pressure at rest, Ko. The application of the model yields a linear relationship between the value of Ko and L, the shearband length. Results are presented in Figures 6.11 and 6.12 for a range of r_u and for the two assumed values of the Young's modulus. Clearly, as the effective stress on the band decreases, the value of Ko necessary for forming a given band length also decreases. Also, longer band lengths require larger Ko values, for the same effective stress conditions. What is not so obvious is the relationship between Ko and the Young's modulus. All other things being equal, less strain energy density is stored in the stiffer material, and hence a higher Young's modulus requires a higher Ko to form a shearband of a given length.

For a shearband between 20 metres and 30 metres in extent, the PR model predicts Ko values within the range 0.85 to 1.15. In contrast, the suggested Ko range based upon plasticity index and overconsolidation ratio (Brooker and Ireland, 1965) is 1.4 to 1.7. This will be discussed below.

Application of the CW Model:

The CW model (Christian and Whitman, 1969) relates the work done in lateral elastic unloading of the sliding block to energy absorbed in frictional sliding along the band. The loading stiffness for sliding was considered, but a

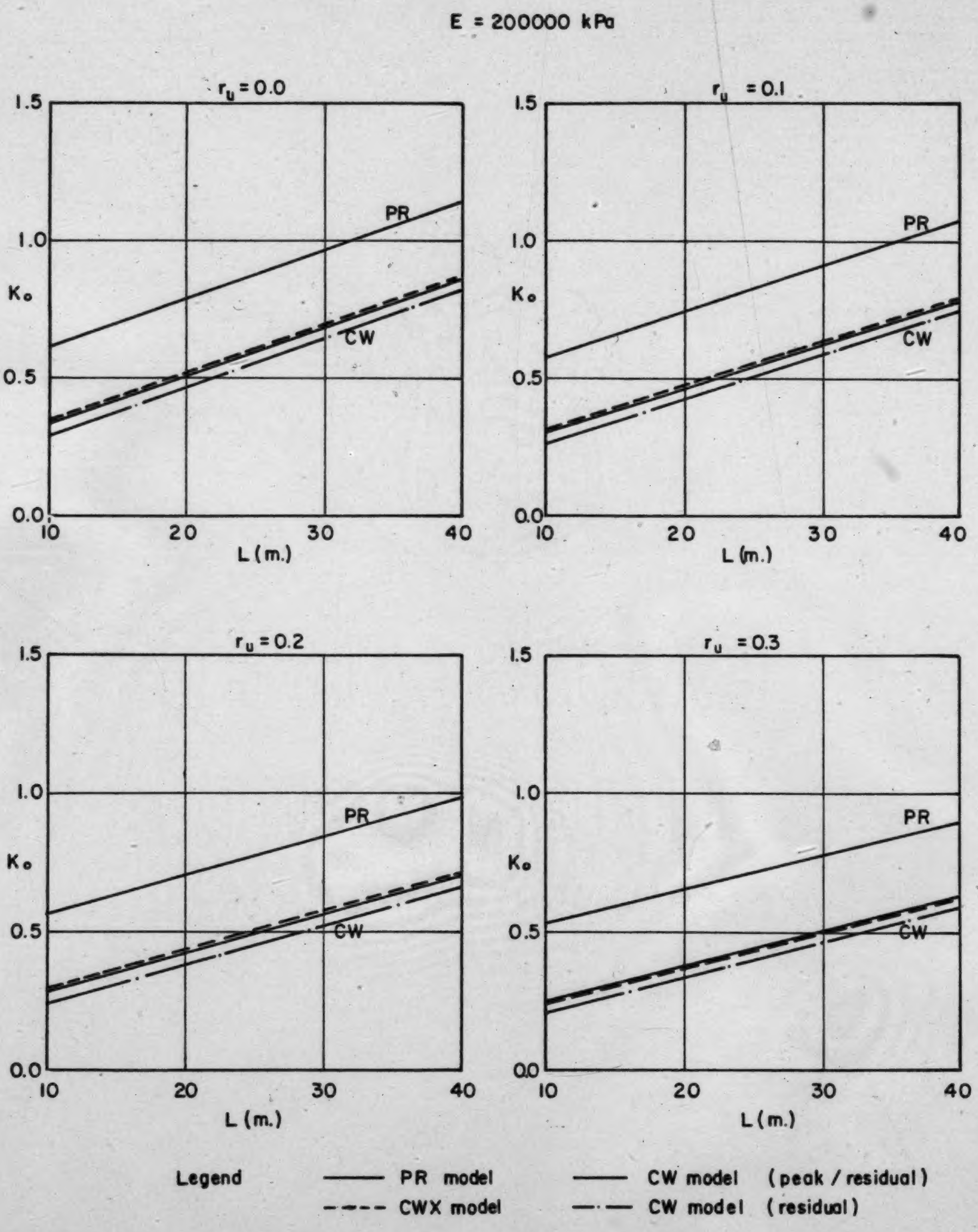

FIGURE 6.11 ONE DIMENSIONAL MODEL PREDICTIONS , E = 200 MPa.

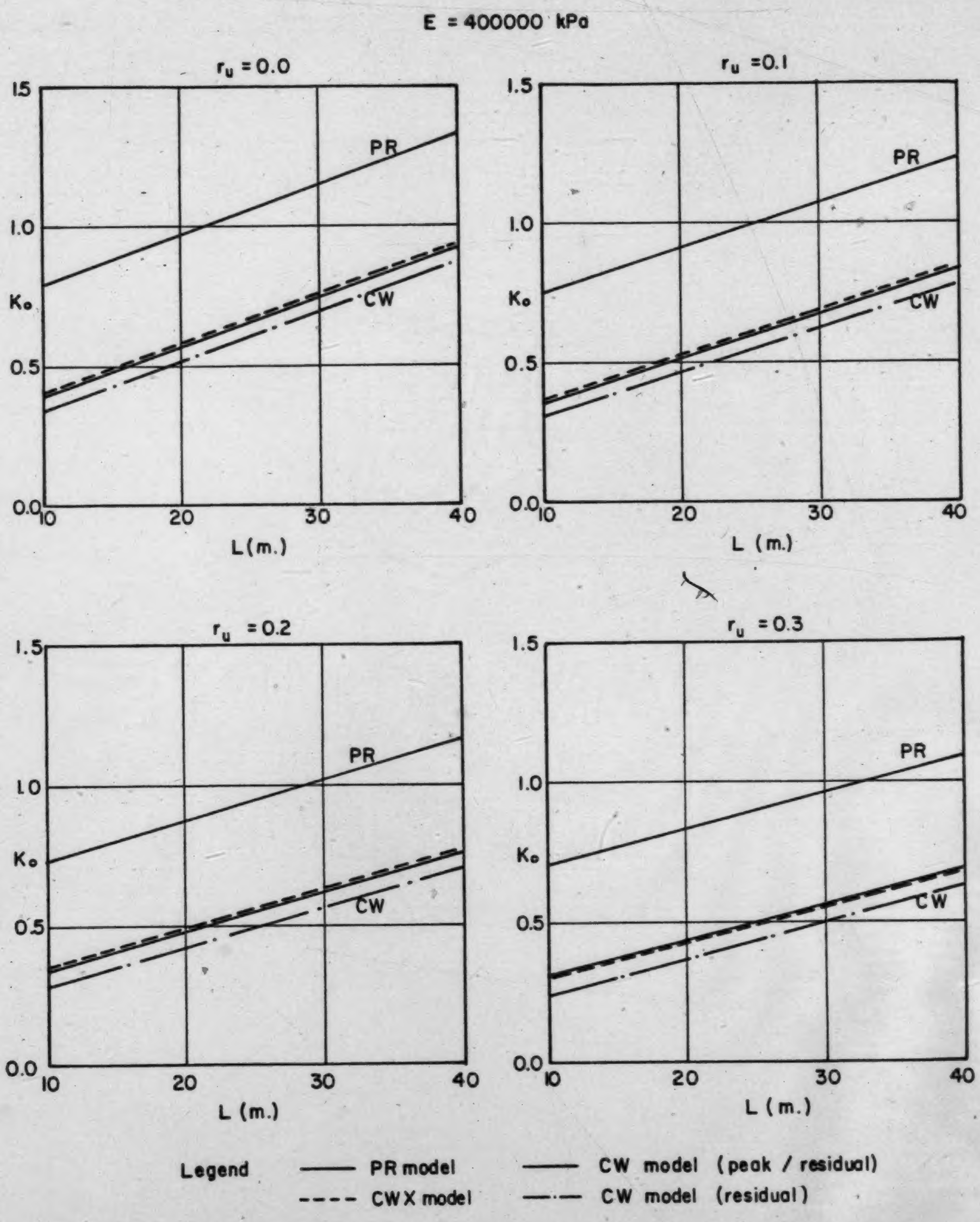

FIGURE 6.12 ONE-DIMENSIONAL MODEL PREDICTIONS, E = 400 MPa.

perfectly brittle drop from peak to residual resistance was assumed. Relative slip along the base zone occurs at all stages of deformation, and the shearband is considered to be that portion where maximum strength has been attained. The model can be applied with equal facility to cases which do not involve strain-weakening.

In order to evaluate the CW model for the Saxon Clay Pit, representative shearband stiffnesses had to be determined for both peak and residual sliding. Referring to the direct shear tests of Figure 6.4, the slip stiffnesses in the direct shear tests were measured as:

(peak) k_P=900 MPa.m^{-1} (average)

(residual) k_R=125 MPa.m^{-1} (for 7th shear)

The model was applied in two forms. Firstly, a full peak-residual transition was assumed with peak stiffness. Secondly, only residual resistance was assumed, with residual stiffness. The CW model also leads to a linear relationship between the values of Ko and L, and these results are also shown on figures 6.11 and 6.12. The same trend of individual results holds, except that the effect of changes in Young's modulus is not so marked.

Of particular note is the close correspondence of the strain-weakening and residual cases. This is a result of the choice of slip stiffness parameters obtained from the direct shear tests: combinations of peak stiffness and strength, and residual stiffness and strength, lead to the same relationship between shearband length (L) and Ko. Clearly, more detailed test information might make it easier to have faith in the use of different strength/stiffness combinations. However, *if these model parameters and calculations are representative of field conditions, it may be concluded that progressive failure did not necessarily occur in the Saxon Clay Pit.*

There is a substantial difference in the predictions of the PR and CW models. The calculated Ko values from the CW model represent a greater divergence from the empirical values presented by Brooker and Ireland (1965). This could be due to differences between laboratory-scale and field-scale shearband slip stiffness (as described by Palmer and Rice, 1973). The shearzone was observed in the field to consist of a number of surfaces of discrete slip, over a thickness of at least 1.6 metres and probably extending below the base of the pit. The previous conclusions regarding progressive failure versus residual slip would only be altered if the field relationship between the slip stiffnesses was different from that observed in laboratory testing.

Application of the CWX Model:

The CWX model is an extended version of the CW model, developed for this research to include finite post-peak stiffness. It is described in Chapter 3 and detailed in Appendix A.

The assumed shearband slip response is indicated in Figure 6.13. The post-peak characteristic of the direct shear tests is highly curved, and some simple and consistent means had to be developed for selection of an appropriate value of the post-peak stiffness R. The shaded area on Figure 6.13B represents the energy density available for post-peak release in the PR model. It was decided to choose R so that the energy density available for post-peak release in the CWX model was the same as that used in the PR model. This is represented by the shaded area on Figure 6.13C. The values of R calculated on this basis ranged from 65.0 kPa to 53.5 kPa as r_u was varied between 0.0 and 0.3. The stress-slip curve of Figure 6.13A is drawn to scale to represent conditions at an r_u value of 0.0.

Results of the CWX model are quite surprising, as the predictions are almost indistinguishable from those of the CW model. (The relationship between Ko and L is almost linear). *It is concluded that the behaviour of the one-dimensional CW models is not sensitive to the details of post-peak response.* On a more detailed level, there will of course be a difference in stress distribution and slip distribution along the shearband. However, it is only the *initial* slip stiffness (be it peak or residual) which significantly affects the interaction with the unloading of the sliding block above the shearband.

Summary:

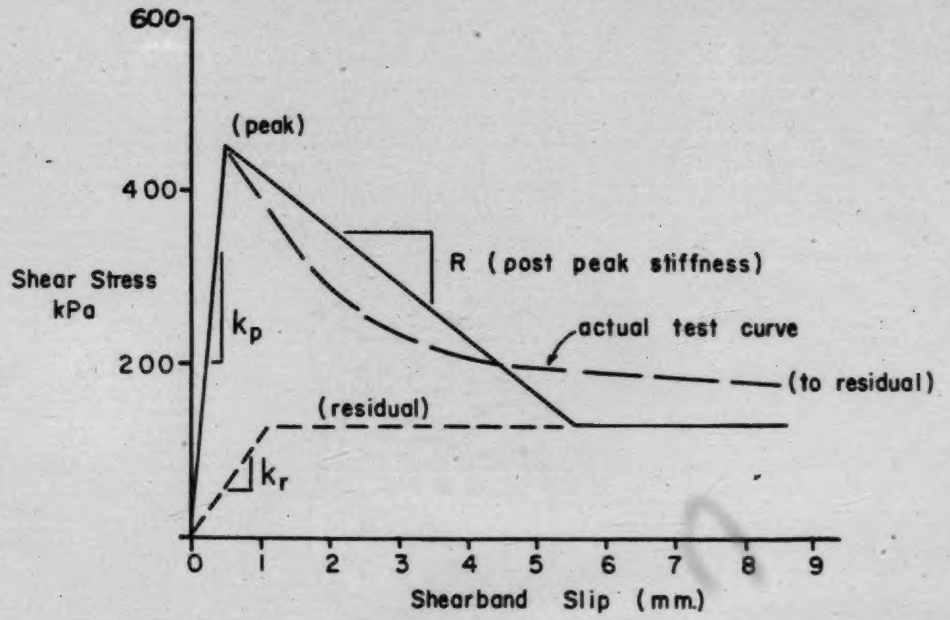

Figure 6.13A CWX Model Stress-Slip Curve.

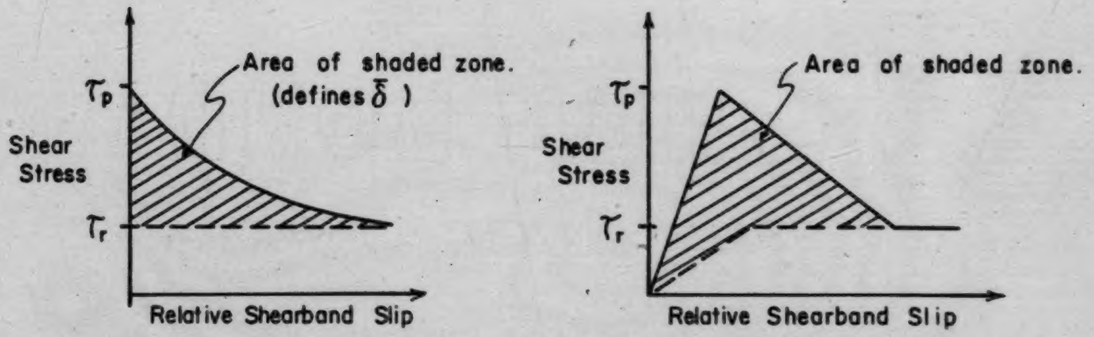
Area of shaded zone.
(defines $\bar{\delta}$)
τ_p
τ_r
Shear
Stress
Relative Shearband Slip
Area of shaded zone.
τ_p
τ_r
Shear
Stress
Relative Shearband Slip

Figure 6.13B PR Model

Figure 6.13C CWX Model

Details of Equivalent Post-Peak Energy Densities

FIGURE 6.13 DERIVATION OF POSTPEAK STIFFNESS FOR CWX MODEL .

Application of the one-dimensional models has helped clarify the interaction between the principal elements of the progressive failure problem. Differences between the PR and CW model predictions can be explained in terms of different assumptions. Parameter differences arising from test data also contribute in this regard.

The lack of contrast between the CW and CWX predictions is surprising and perhaps deserves further attention.

If the direct shear test stiffnesses are representative of field behaviour, then the contrast between peak and residual stiffnesses leads to almost identical CW relationships between Ko and shearband length L. Perhaps, then, progressive failure need not have occurred at Saxon Clay Pit. Only a more detailed deformation analysis could test this hypothesis.

The empirically-obtained values of Ko (Brooker and Ireland, 1965) are much higher than any of the models predicted. Predictions of higher values of Ko could be made under any of the following conditions:

1. Higher operational Young's modulus;
2. Higher slip stiffnesses (CW models);
3. Lower pore pressures (suctions) as a result of dilatant shearband slip.

More attention could perhaps be focussed on these matters at a later date.

6.3 FINITE ELEMENT ANALYSIS PROCEDURES

During the original site investigation, the possibility that only residual strength was mobilized in the field was not precluded. Experience with the one-dimensional models also raised the question of whether or not progressive failure need have occurred in the Saxon Clay Pit. The minimum estimated overconsolidation ratio of 10 for the Oxford Clay deposit at the site suggests that *insitu* preshearing could have developed by flexural slip during stress relief.

Detailed deformation analysis is required to address the question of progressive failure; the one-dimensional models lead to a number of feasible combinations of controlling parameters but the deformation patterns, it may be expected, should yield a unique set of parameters compatible with field deformation measurements. Numerical difficulties were anticipated with the finite element analysis, and it was therefore decided to investigate in detail only the case of residual strength mobilization. For comparison, the case of softened (cohesion intercept set to zero) peak strength mobilization, with no postpeak weakening, was also considered.

A number of non-routine matters had to be considered in designing and carrying out the finite element analysis. These included:

1. overall dimensions of mesh;
2. simulation of excavation procedures;

3. selection of material models and parameters;
4. selection of shearband thickness;
5. mesh detailing in the critically stressed and deforming notch region.

Overall Dimensions of Mesh:

The simplified vertical notch shown in Figure 6.10 was adopted for finite element modelling. With a 27 metres high face, and a shearband with stress concentrations possibly extending 40 metres behind the face, lateral and bottom mesh boundaries had to be chosen to minimise any effects of boundary constraints. Distances from the face to the left (excavated) and right boundaries were chosen as 110 metres and 330 metres respectively. A series of preliminary discretizations were undertaken, since it was critically important to provide sufficient mesh detail while maintaining the greatest possible computational economy. The final design was not made until the simulation of excavation was decided upon and the final shearband thickness determined.

Simulation of Excavation Procedures:

It is standard practice in simulation of excavations to assume an initial Ko stress distribution and then remove excavated material. This is done by physically eliminating the excavated portion, and applying equal and opposite tractions along the excavated boundary to create stress-free surfaces. The situation at the Saxon Clay Pit is more complex because a long history of incremental excavation had been carried out prior to the commencement of the field measurement program. This is illustrated by part (A) of Figure 6.14.

The finite element simulaton of a long sequence of small excavation increments was not feasible. A two-stage scheme was therefore designed, and is illustrated in part (B) of Figure 6.14. Firstly, the bulk of the excavation was achieved by removal of a large amount of material. This created a pit wall isolated from boundary effects, and subjected to an appropriate stress field corresponding to a "history" of small excavation steps. Secondly, a 10 metre section of wall was removed by the usual procedures, in order to study the incremental and final displacement and stress fields resulting from a typical pass of the planer. Selection of these stages had an important influence on mesh discretization close to the wall(s).

Selection of Material Models and Parameters:

It was assumed that a reliably convergent elastoplastic analysis could be carried out only for non-weakening material response, following the experiences outlined in Chapter 5. In practical terms, this implies a pseudo-undrained strength. For residual strength mobilization along a shearband of constant depth below

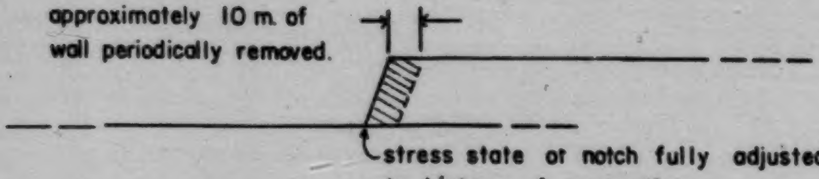

approximately 10 m. of wall periodically removed.

stress state at notch fully adjusted to history of excavation.

(A) FIELD SITUATION

(B) FINITE ELEMENT SIMULATION

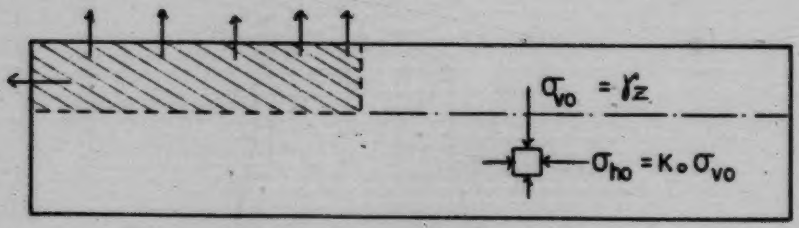

(B1) Firstly, adjust stress state at notch to "history" of excavation.

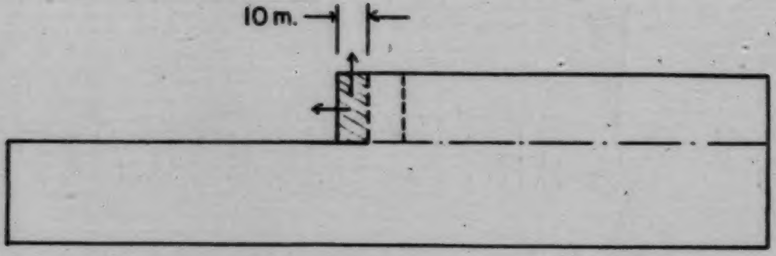

(B2) Secondly, remove 10 m. of material from wall and observe response.

(B3) Remove another 10 m., if desired.

FIGURE 6.14 SIMULATION OF EXCAVATION PROCEDURE.

ground surface, pseudo-undrained strength is realistic if no pore pressure changes occur during shearing. On theoretical grounds (Rice and Rudnicki, 1979) the use of a pseudo-undrained strength equivalent to the ambient shear strength under pre-existing effective stress conditions has been shown to be realistic. Therefore, the CRD elastoplastic model and the transverse-isotropic shearband nonlinear elastic models could be adopted directly for deformation analysis under residual strength conditions. The CRD model was also used for analysis of the softened peak strength case: a pseudo-undrained strength equivalent to the shear strength under ambient effective stresses was chosen and any strength loss due to weakening was assumed to be offset by dilatant pore pressure reductions (Rice and Rudnicki, 1979).

By assuming undrained behaviour, the question of detailed processes near the shearband was partly circumvented. Undrained behaviour over the time-scale of an excavation step is probably a reasonable assumption, except perhaps for local processes in the shearband. This assumption leads to better numerical performance of the nonlinear models, which in turn leads to greater confidence in model predictions. Model predictions could thus be compared to field measurements with a much better cognizance of the similarities and differences involved.

Prior to performing nonlinear analyses, several elastic tests had to be undertaken. The nature and extent of the stress concentrations at the notch had to be established, and an optimum shearband thickness chosen.

The notch was first analysed with uniform isotropic elastic properties, and for this the Young's modulus used in the one-dimensional studies was adopted.

A nonuniform isotropic elastic analysis was also carried out to assess the effect of nonuniform elastic properties on the nature and extent of the stress concentrations at the notch. High modulus contrasts are known to be associated with strain concentrations along interfaces of different materials. Therefore, the shearband and overlying Oxford Clay were assigned elastic stiffnesses three times less than the basal materials. It was expected that this would realistically simulate base stiffness without introducing noticeable material-contrast effects into the results.

Undrained behaviour in principle requires an isotropic Poisson's ratio approaching 0.5. There is considerable experience to suggest that as this limit is approached, numerical instability and inaccuracies may be introduced. A Poisson's ratio of 0.35 was therefore chosen for the uniform elastic analysis to ensure reliable performance. For the nonuniform elastic analysis, a higher Poisson's ratio of 0.4 was selected. The Young's modulus was chosen to be considerably smaller than for the previous case, in order to replicate laboratory measured values. (The insights of the one-dimensional analysis allow the effects of higher modulus values to be assessed).

For subsequent nonlinear elastic analyses, the transverse-isotropic shearband model was assigned initially isotropic elastic parameters. When shearband yield was initiated, the Gv modulus was automatically reduced as required. This prevented any prejudicial assumptions about shearband behaviour from being introduced.

Appropriate undrained shear strengths were assigned to all materials. The values chosen for the shearband reflected residual strength and "softened" peak strength (cohesion set to zero), at an r_u value of 0.0. Again, insights into the effect of varying r_u are possible using the one-dimensional model predictions.

Table 6.1 shows the material parameters used in the finite element analysis.

Selection of Shearband Thickness:

The observed shearzone consisted of a series of discrete sliding surfaces, extending for at least 1.6 metres above the base of the pit. Discrete sliding surfaces possibly also developed in the Kellaways clay down to 3 metres below pit base level, according to some field measurements. The finite element shearband consisted of a single layer of Q48 elements whose lower surface coincided with pit base level. A series of uniform isotropic elastic analyses were undertaken to examine the effects of shearband thickness on behaviour of the stress concentrations. Thicknesses of 0.005, 0.01, 0.1, 1.0, and 2.0 metres were

TABLE 6.1

PARAMETERS FOR ANALYSIS OF SAXON CLAY PIT

MATERIAL	K (MPa)	G (MPa)	C′ (kPa)	ø′	Ten. str. (kPa)	$D=\frac{\dot{E}v^{p}}{\dot{\gamma}^{p}_{max.}}$	Transverse - Isotropic gf
Uniform Elastic Analysis	222.222 (E = 200)	74.074 (v = 0.35)	-	-	-	-	-
Nonuniform Nonlinear Analysis							
Below Shearband	600.0 (E = 360)	128.571 (v = 0.4)	3600.0	0.0	200.0	0.0	n.a.
Above Shearband	200.0 (E = 120)	42.857 (v = 0.4)	1200.0	0.0	50.0	0.0	n.a.
Shearband	200.0	42.857	125.0 (Residual) 275.0 (Softened Peak)	0.0	25.0	0.0	2.80
(Fully Yielded)	20.0	4.2857	a.a.	a.a.	a.a.	a.a.	a.a.

a.a. = as above n.a. = not applicable

tried. For a 10 metres long element near the notch, the element aspect ratio (Chapter 4) varied from 2000 to 5, while for the 60 metres long element at the right boundary of the mesh, aspect ratios of 12000 to 30 resulted.

Behaviour was assessed in terms of the horizontal displacement of the pit wall 5 metres above the base, interpolated from nodal displacements. The average maximum compressive stress for the shearband Gauss points nearest the excavation was also examined. These results are shown in Figure 6.15. It was decided that a shearband 0.01 metre thick, or greater, would be satisfactory, but a final thickness of 1.0 metre was chosen so as to reasonably reflect the field observations. Apart from some sensitivity of the stresses at the shearband tip, the pattern of stress concentration behind the face was essentially constant when the shearband thickness was varied.

Mesh Detailing near Notch:

Figure 6.16 shows a typical detail of an early mesh design. The shearband tip element is an ordinary Q48 type. The first stage of unloading produced severe stress oscillations along the shearband. Even though the average value of these stresses seemed satisfactory, nonlinear analysis (which commences with elastic trials) would not have been possible. The shear stress and normal stress components were out of phase as well, resulting in severe oscillations of mobilized friction angle along the

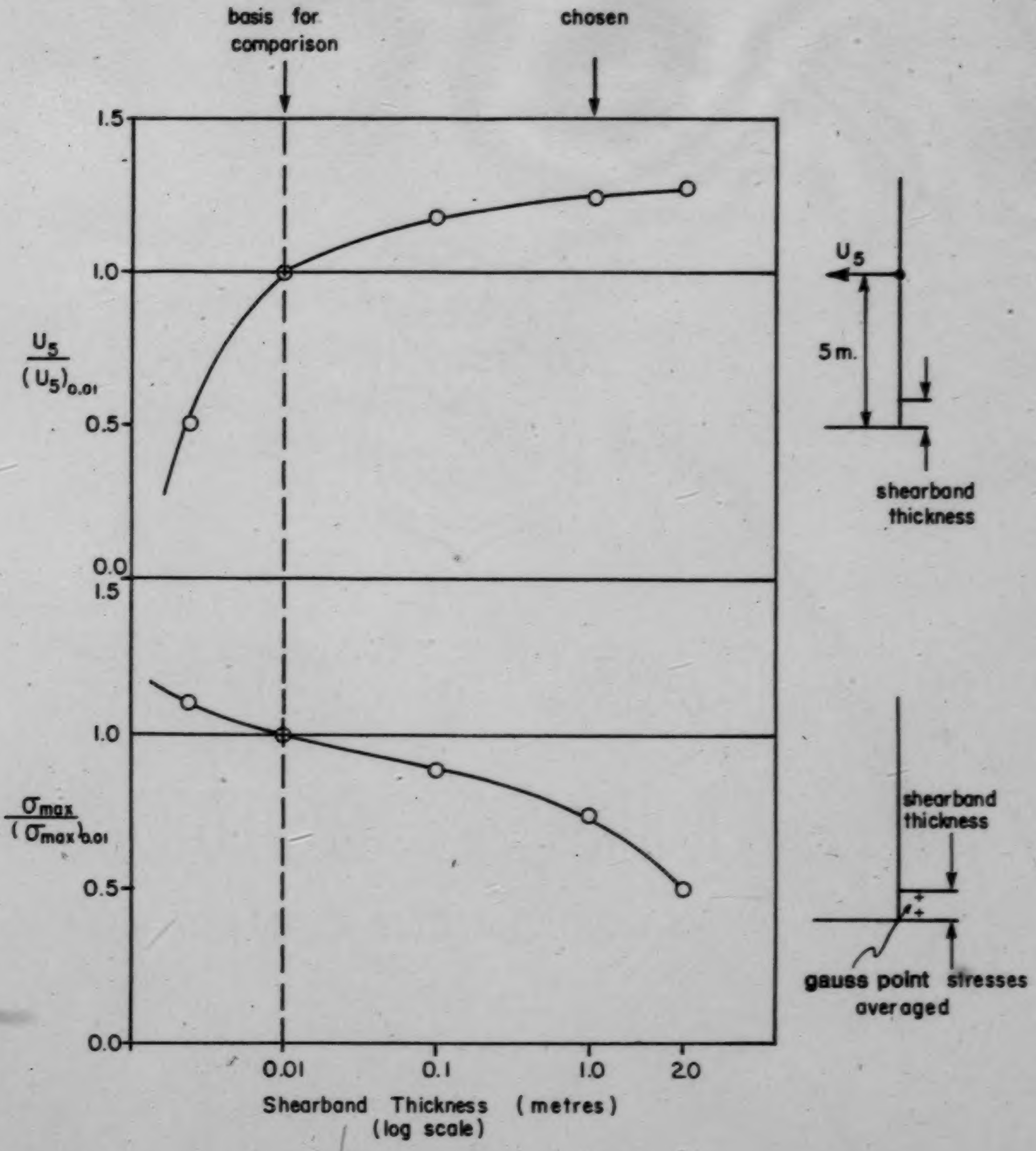

FIGURE 6.15 ASSESSMENT OF OPTIMUM SHEARBAND THICKNESS.

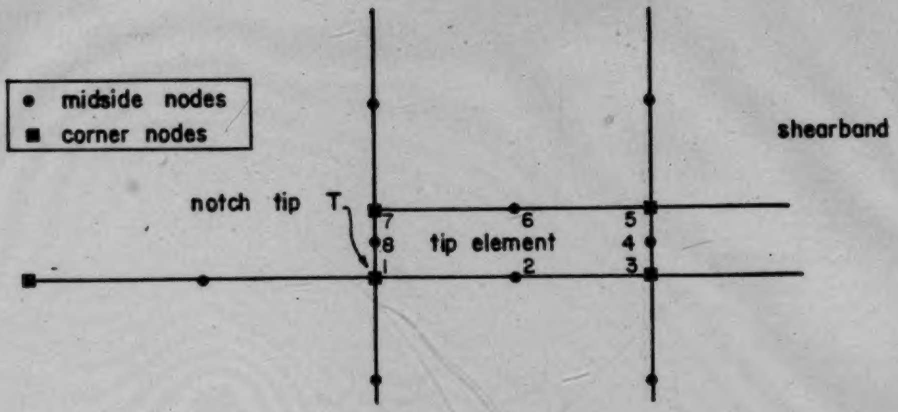
midside nodes
corner nodes
shearband
notch tip T
7
6
5
8
tip element
4
1
2
3

(A) ORIGINAL MESH DESIGN

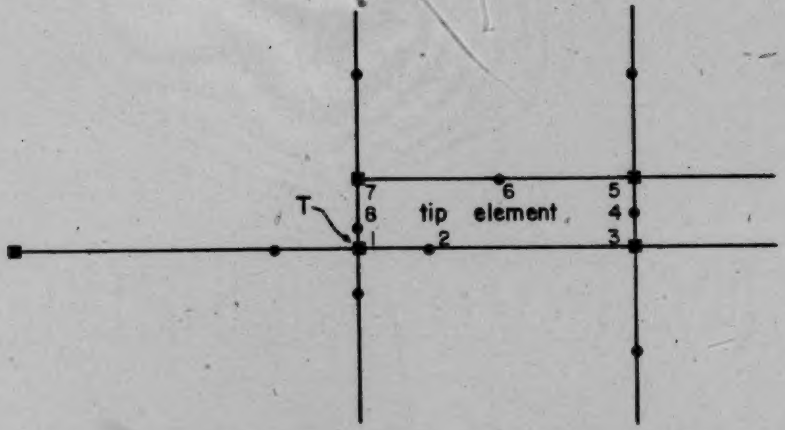
T
7
6
5
8
tip element
4
1
2
3

(B) WITH $r^{-\frac{1}{2}}$ SINGULARITY AT TIP

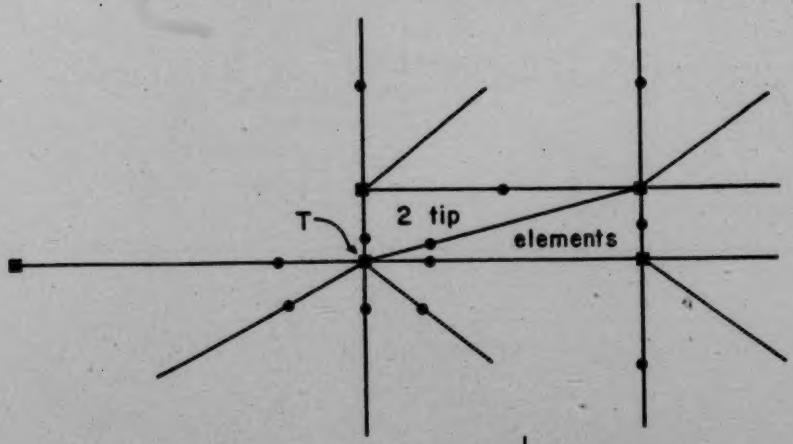
T
2 tip
elements

(C) TRIANGULARIZED $r^{-\frac{1}{2}}$ SINGULARITY AT TIP

FIGURE 6.16 SHEARBAND TIP DETAILING

shearband.

At first it was assumed that these stress oscillations arose from the consequences of trying to fit the functional form of the singularity (unknown, but probably inverse-logarithmic) with the partially complete polynomials of the element shape functions. As an approximation, therefore, the midside nodes adjacent to the tip were moved to the quarter-points to represent the $r^{-\frac{1}{2}}$ singularity of linear elastic fracture mechanics (Barsoum, 1976 and 1977, see also Chapter 5). This is shown in Figure 6.16B. Minor but ineffective smoothing of the oscillations resulted.

It was then assumed that the problem was caused by lack of mesh refinement. A much more detailed mesh was devised, but the only effect on the oscillating stresses was to make the amplitudes of oscillation larger. Figure 6.17 demonstrates the oscillations in normal and shear stresses along the upper Gauss points of the shearband adjacent to the tip.

The oscillations in stresses were definitely related to the element configuration. Upon re-reading of Barsoum (1977), reference was found to a study of rectangular versus triangular representation of the $r^{-\frac{1}{2}}$ singularity, using Q48 elements. Hibbit (1977) demonstrated that the quarter-point node distortion for a rectangular Q48 element leads to an unbounded strain energy density integral, hence the element stiffness becomes unbounded. He noted that in some cases numerical results of reasonable accuracy might be obtained

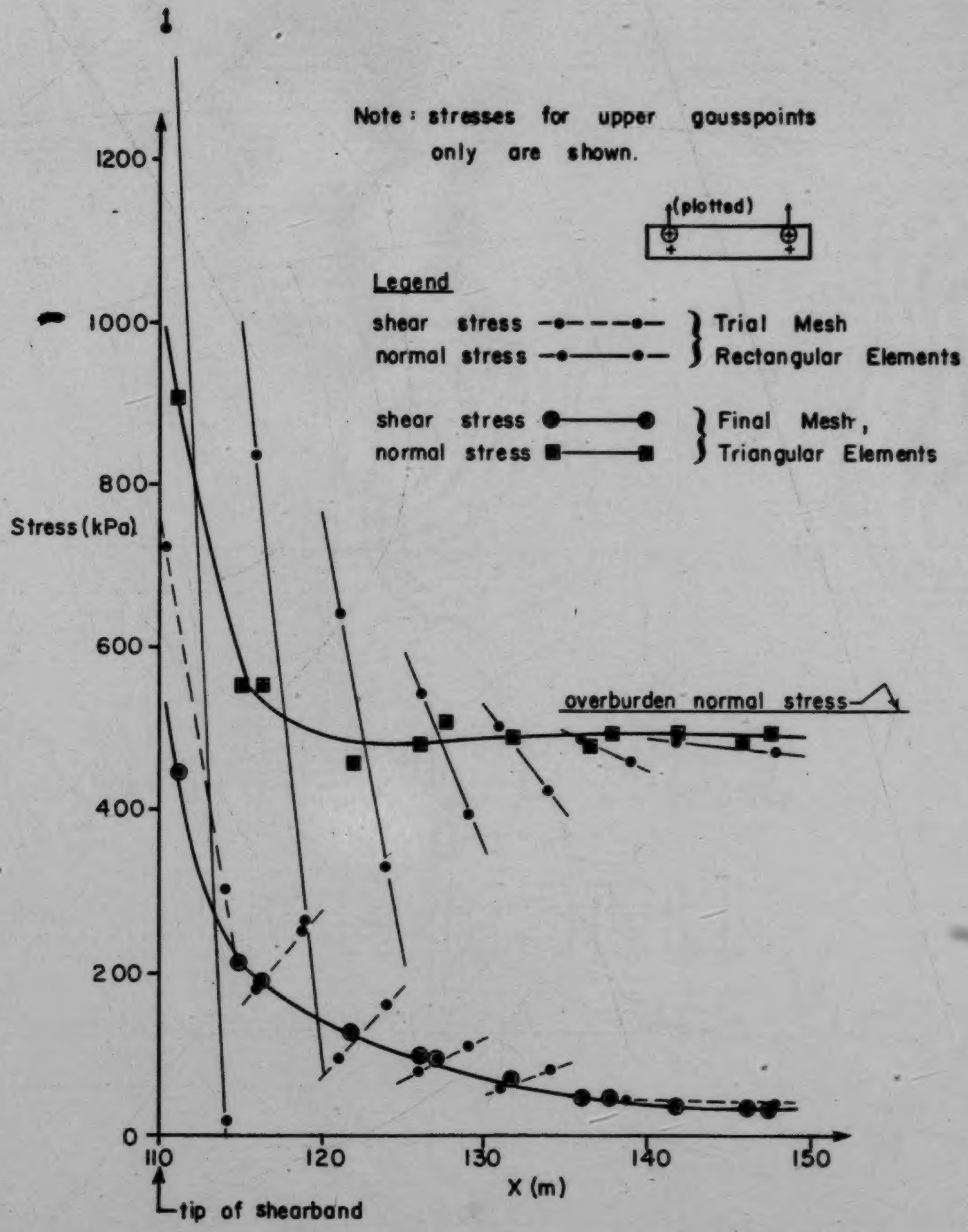

FIGURE 6.17 UNIFORM ELASTIC NOTCH STRESSES

because the singularity in the strain energy field of the element is weak. By collapsing one side of the Q48 element to form a six-node triangle, the strain singularity can be represented *and* the strain energy integral is always bounded.

Remodelling of the mesh in the vicinity of the shearband tip was undertaken, to triangularize the elements where a strain singularity had to be represented. The tip detail is shown in Figure 6.16C. Stress distributions for the uniform isotropic elastic test using this mesh arrangement are also shown on Figure 6.17 and the result is most satisfactory.

Summary:

The final mesh design is shown in Figure 6.18. A total of 233 nodes and 76 elements are represented, while 219 nodes and 70 elements remain after the second-stage excavation of 10 metres of the wall. The elements below pit base level have elastic stiffnesses three times that of the shearband and wall elements.

Elastoplastic analysis using the CRD model was selected, and parameters were chosen to represent undrained behaviour. Nonlinear elastic analysis was restricted to the automatic reduction of the Gv modulus to simulate shearband yielding; the hyperbolic nonlinear elastic models were not invoked because they would only have introduced extra complicating factors into the interpretation of results.

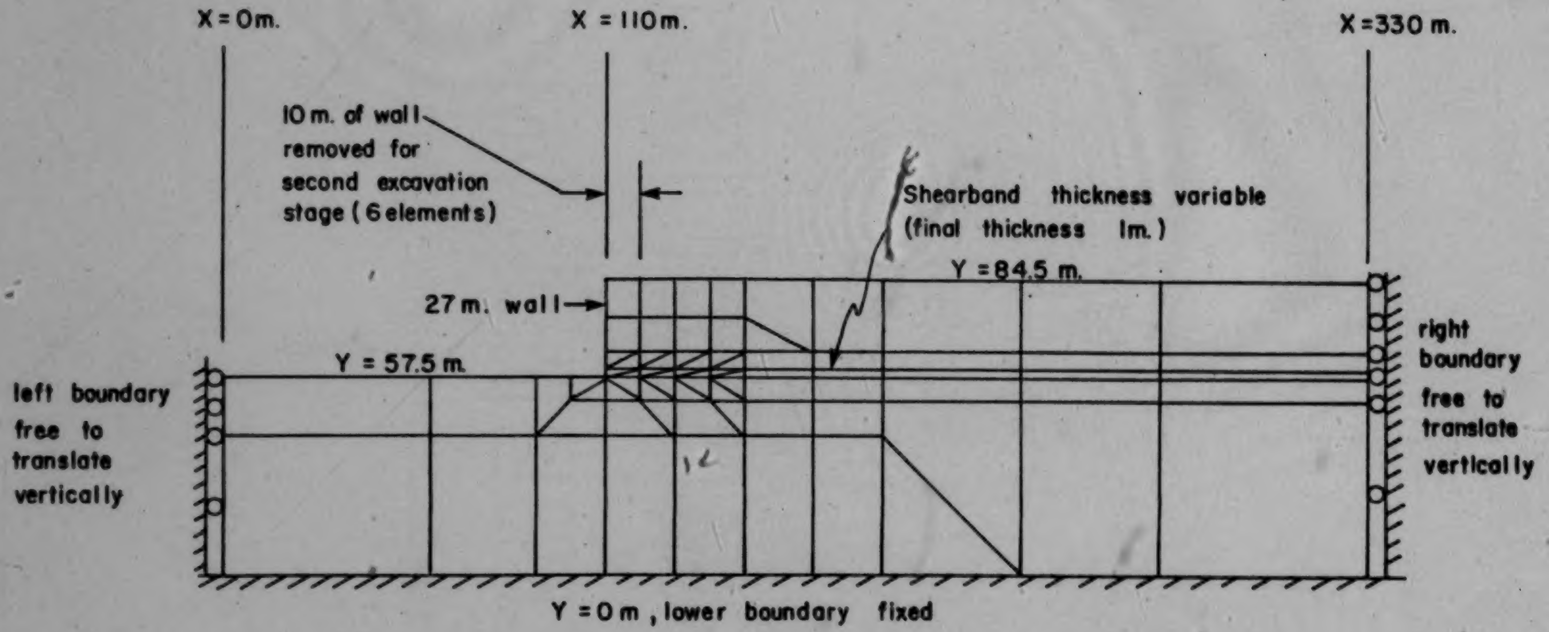
X = 0m.
X = 110m.
X =330 m.
10 m. of wall removed for second excavation stage (6 elements)
Shearband thickness variable (final thickness 1m.)
Y = 84.5 m.
27 m. wall
Y = 57.5 m.
left boundary free to translate vertically
right boundary free to translate vertically
Y = 0 m , lower boundary fixed

FIGURE 6.18 OUTLINE OF FINITE ELEMENT MESH

6.4 SIMULATION OF EXCAVATION BEHAVIOUR

In principle, the objectives of the simulation of excavation behaviour were twofold:

1. Examination of displacement, strain, and stress patterns in order to evaluate the hypothesis that only residual sliding occurred;
2. Generation of a set of relationships among the parameters controlling behaviour, to be presented in a form similar to that shown in Figures 6.11 and 6.12.

The first and most important aspect was to obtain solutions for each of the two excavation stages. This proved to be very costly in terms of computation time and of effort involved in evaluating the results. The elastoplastic analysis, in particular, invoked large computation costs. The nonlinear elastic analysis was much cheaper to perform, as expected, but demanded a great deal of evaluation effort because of the extreme sensitivity of results to variations in the material parameters.

Consequently, no effort was made to generate relationships among the parameters controlling behaviour. This objective is of great interest, but would be most efficiently dealt with after refinements were made to the analytical procedures.

Initial ground stress conditions were assumed to correspond to a Ko value of 1.0. In light of the one-dimensional PR analysis results, this would lead to a shearband between 20 and 30 metres long if r_u = 0.0 and full progressive failure developed. It therefore seemed to be the most convenient starting point.

The various aspects of the excavation simulation, treated in detail below, are:

1. Stage I elastoplastic analysis,
2. Stage II elastoplastic analysis,
3. Stages I and II nonlinear elastic analysis.

Stage I Elastoplastic Analysis:

An initial attempt was made to achieve a converged elastoplastic solution in a single unloading step, but this proved impossible. The geometrical and loading conditions at the notch constitute a very severe test on the numerical behaviour of the elastoplastic algorithm. A series of ten partial unloadings, each constituting one-tenth of the unloading stop forces, was therefore decided upon.

Yielding of the shearband commenced at the first load step, due to the elastic stress concentraton. Once yielding spread across the first shearband element (a "propagation" of 10 metres), the convergence rate slowed down very dramatically. This was caused by the initial elastic stiffness adopted for the equilibrium analysis. In order to improve the convergence rate, reductions had to be made in the elastic stiffness parameters for yielded elements. Under general stress conditions this procedure is not advisable, because it alters the energy balance between the elastic and plastic strain components. However it was suitable in this case because the stress state in fully-yielding elements was essentially constant (constant vertical stress and constant maximum shear stress), hence the elastic component of elastoplastic strain was negligible. Figure 6.19 shows schematically the effects of reducing the elastic stiffness, and shows the resulting improvement in convergence when a reduction to 10% of original stiffness was used.

Of interest at this point is a brief discussion of the computational costs of the elastoplastic model. When the *best* convergence rate was achieved, the elastoplastic solution for one load step typically required 150 CPU seconds on the University's Amdahl 470 V/7. This was for *only* 9 yielding elements and an overall mesh of 76 elements, and the ESB program convergence rates are comparable with the best commercially available programs. The tolerance levels and numerical controls on the yielding process also deserve brief mention here. The tolerance level on the out-of-balance force ratio was set at 0.05. In other words, a 5% force imbalance was considered acceptable. The tolerance level on the yield surface was set at 0.1%. This means that the yield "surface" consisted of "f" values between -0.001 and +0.001. An overcorrection of 15% (overrelaxation factor 1.15) was made in applying the equilibrium iteration forces. Subincrements for computing elastoplastic response were 10 at low levels of yielding,

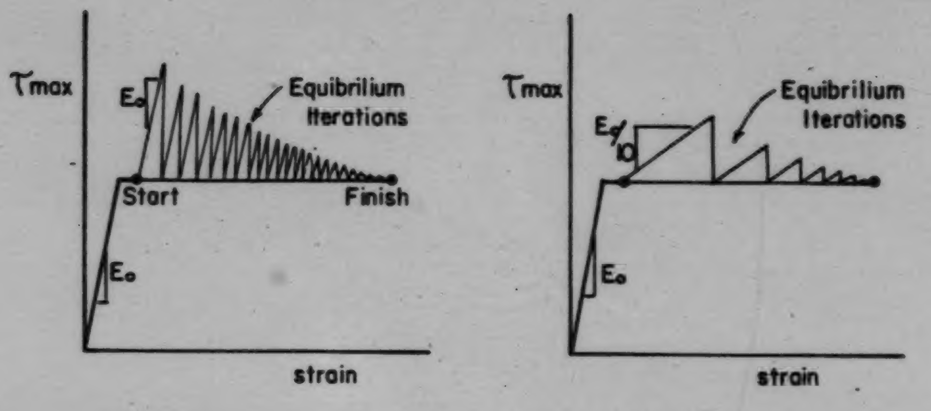
τ_{max}
E_o
Equibrilium Iterations
Start
Finish
E_o
strain
τ_{max}
$E_o/10$
Equibrilium Iterations
E_o
strain

(a) Constant Elastic Stiffness (b) Reduced Elastic Stiffness

(A) EFFECT ON REDUCTION OF ELASTIC STIFFNESS FOR ELEMENTS ALREADY IN YIELDED STATE.

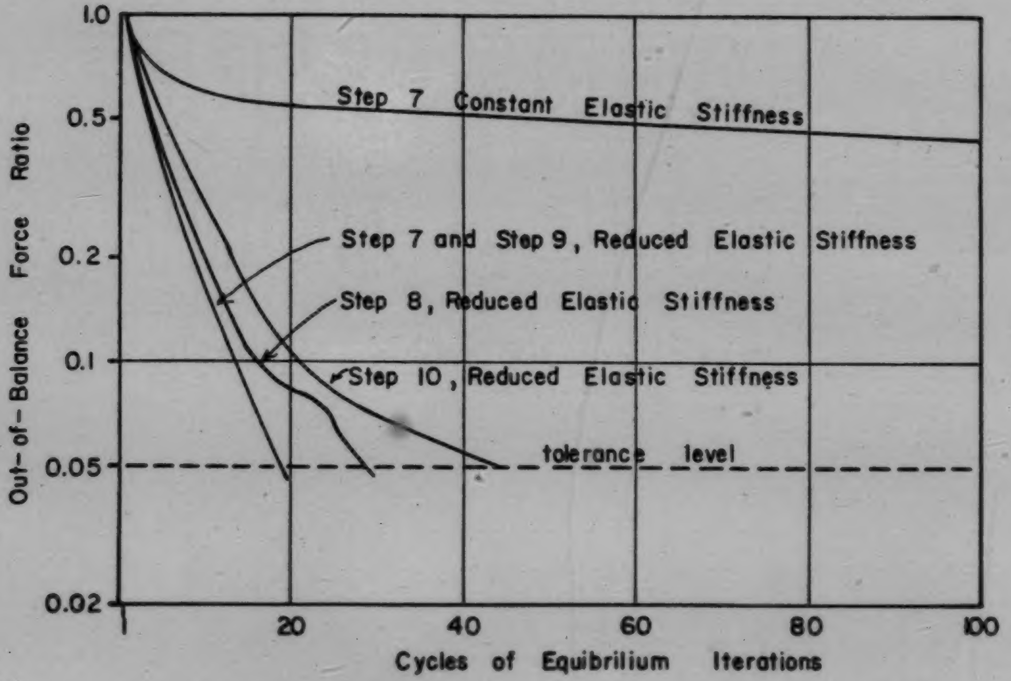

FIGURE 6.19 IMPROVED CONVERGENCE TECHNIQUE

and 15 thereafter.

The convergence characteristics shown on Figure 6.19 have some irregular or changed curvatures. In step 8, the kink in the curve is due to propagation of yielding into the adjoining shearband element. Propagation is detected in this stepwise fashion because of stress sampling at the element Gauss points. The decreased convergence rate in step 10 (the last portion of unloading) is due to tensile yielding which developed in the upper region of the sliding block. This is noticeable here because of the lack of mesh refinement. The analogy in field behaviour would be the opening of a joint sub-parallel with the excavation face.

Stage I of excavation was designed to set suitable initial conditions for studying the response of the slope to subsequent excavations. Results from Stage I were carefully examined and Figure 6.20 shows the pattern of displacements along the shearband. Other results will be presented and discussed in relation to Stage II of excavation.

Stage II Elastoplastic Analysis:

Figure 6.21 shows the stresses along the boundaries of the Stage II excavation, existing after Stage I was completed. There is a sharp "peak" in the value of σ_x in the shearband. This was ignored and a linear extrapolation of the σ_x distribution adopted instead, because boundary stresses were obtained by a nodal averaging procedure, and in the above instance the influence of higher stress levels

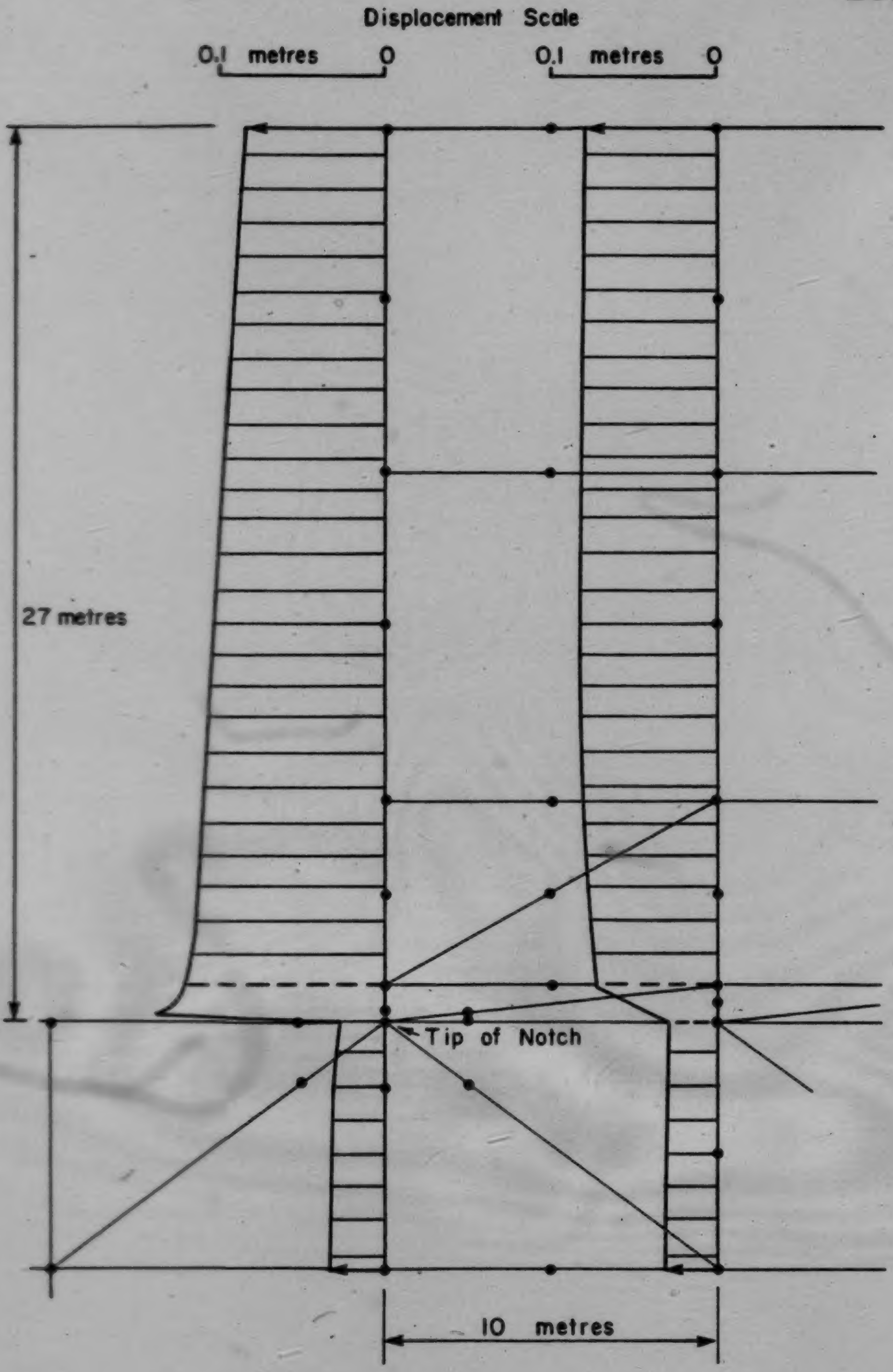
Displacement Scale
0.1 metres 0
0.1 metres 0
27 metres
Tip of Notch
10 metres

FIGURE 6.20 HORIZONTAL DISPLACEMENTS FOR STAGE I ELASTOPLASTIC ANALYSIS.

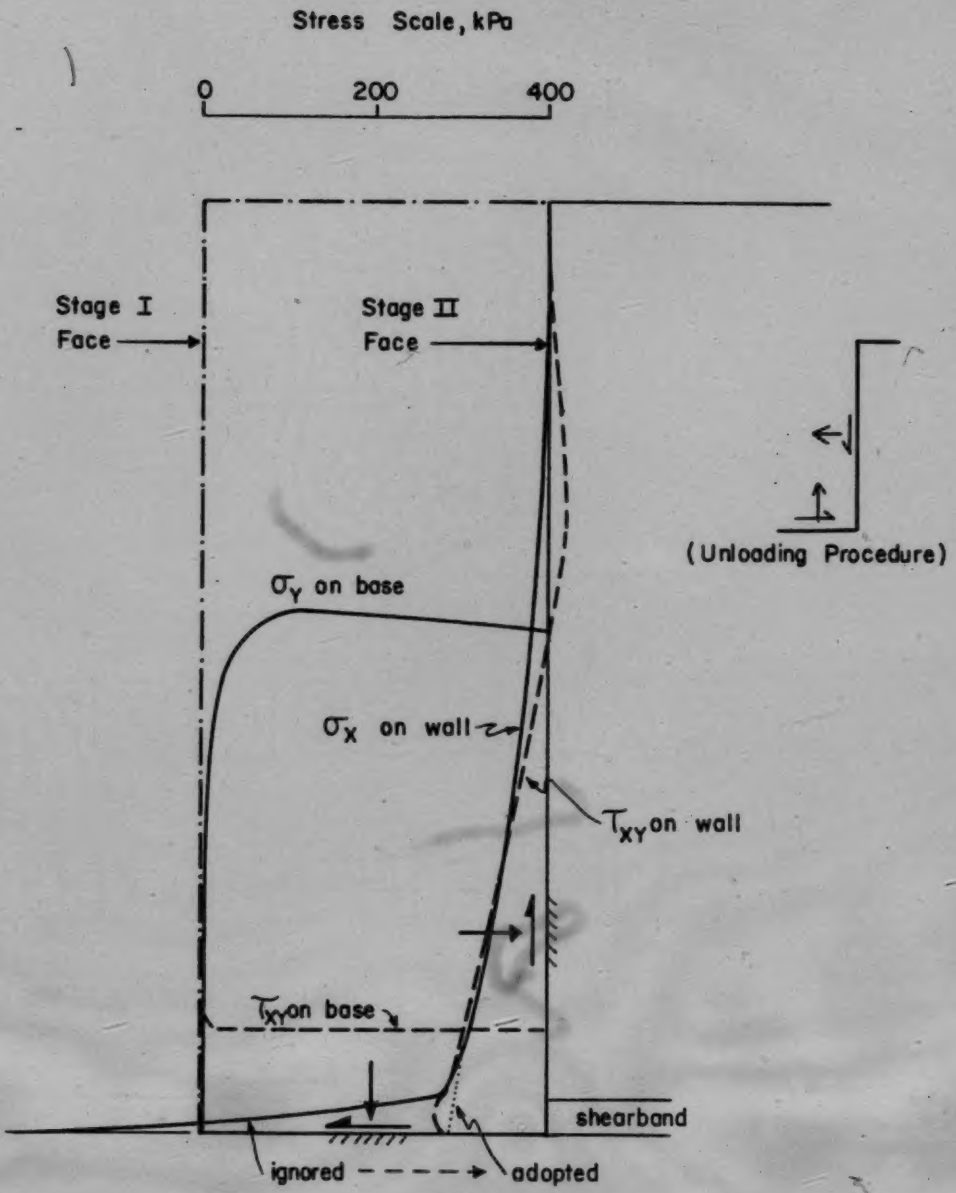
Stress Scale, kPa
0
200
400
Stage I
Face
Stage II
Face
(Unloading Procedure)
σ_Y on base
σ_X on wall
τ_{XY} on wall
τ_{XY} on base
shearband
ignored
adopted

FIGURE 6.21 BOUNDARY STRESSES FOR STAGE II UNLOADING.

below the shearband had to be filtered out.

Forces equal and opposite to these stresses had to be calculated for the Stage II excavation simulation. Six elements were removed from the mesh. The quarter-point nodes surrounding the previous shearband tip were moved back to their midside location, and those midside nodes adjacent to the new shearband tip were moved to their respective quarterpoints in order to represent the new position of the singularity.

Stresses, strains, and displacements for the remaining elements and nodes were saved from the Stage I analysis. This resulted in unavoidable approximations in the Stage II analysis. Some nodes would undergo incremental displacements from different geometrical locations than they occupied for Stage I. Likewise, the Gauss points of distorted-node elements are in different positions physically from their undistorted locations. Strictly speaking, corrections and adjustments should have been made to allow for these geometrical problems. A more pragmatic approach was decided upon: using a series of Stage II elastic tests, the errors arising from lack of correction for node-position changes were evaluated. Only a localized region was affected and the stress error in this region never exceeded 10%. Likewise, the displacement errors were found to be less than 4%. Given the local nature of the errors and their small relative magnitude, it was decided to accept the approximations without further concern.

Stresses along the upper Gauss points of the shearband and horizontal strains from the uppermost Gauss points of the sliding block are shown in Figure 6.22. This figure also shows these quantities at the end of the Stage I excavation. Figure 6.22 thus summarizes the incremental response of the pit wall and shearband to the passing of the planer. Note that the horizontal strain increment is closely related to the stress changes that occurred along the shearband.

The pattern of incremental horizontal displacements, if plotted in a similar manner to those in Figure 6.20, show the same essential block slip motion with discrete shearing of the shearband. The relative slip displacements across the 1 metre thick shearband were 25 millimetres at the new face and 10 millimetres at a distance of 10 metres behind the new face.

Selected incremental displacement vectors are plotted in Figure 6.23. These show small settlement tendencies for about 22 metres below the upper surface. Net heave occurred along the base of the shearband, implying compression of the 5 metre zone above the shearband base.

Stage I and Stage II Nonlinear Elastic Analysis:

Unloading procedures for the nonlinear elastic analyses were the same as for the elastoplastic analyses, except that only single loading steps were used. This caused problems in controlling the shearband stresses in the yielded portion of the band. The pattern of discrete shearing of the band, and

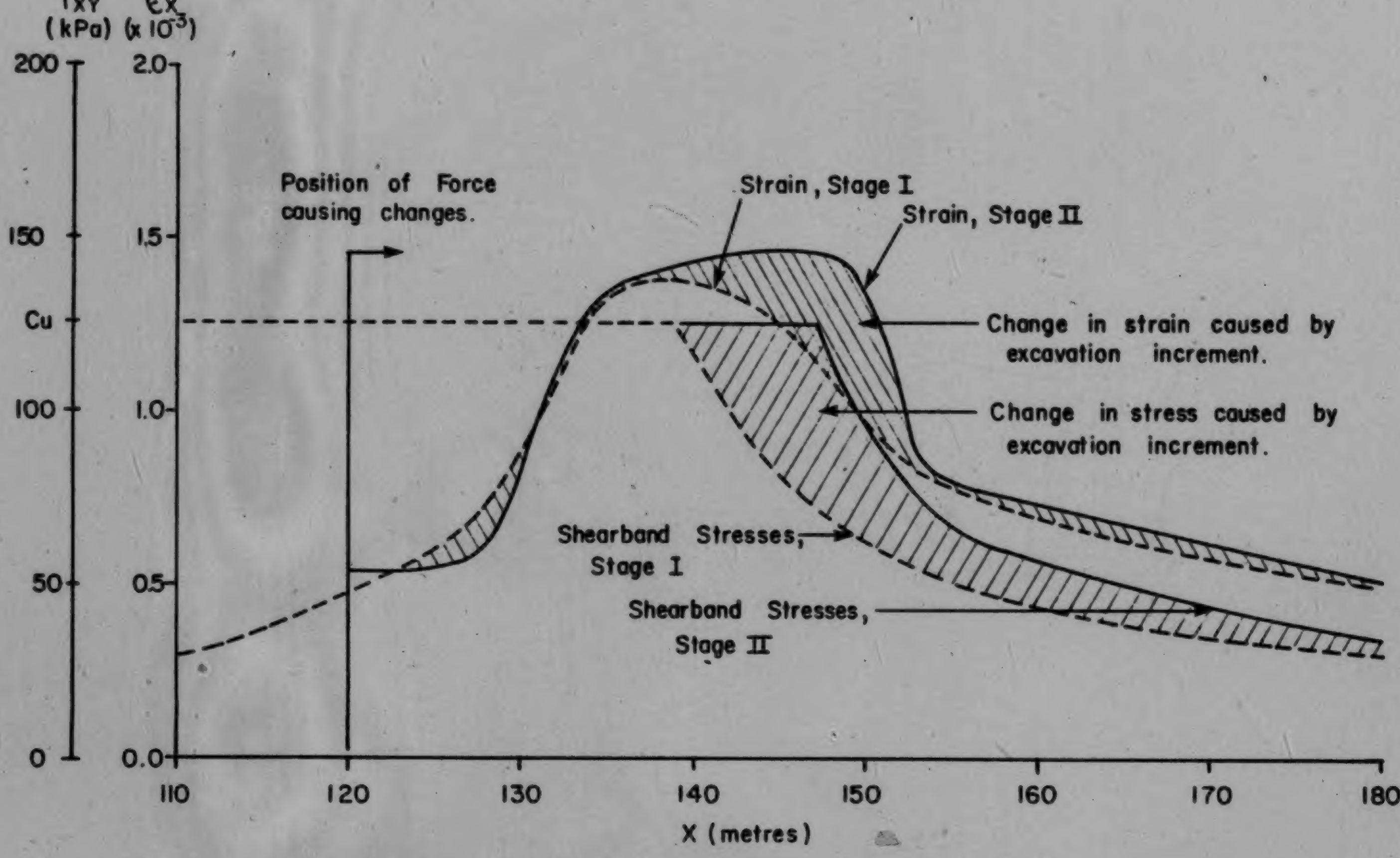

FIGURE 6.22 STRESS-DEFORMATION RESPONSE TO EXCAVATION INCREMENT, CRD ELASTOPLASTIC ANALYSIS.

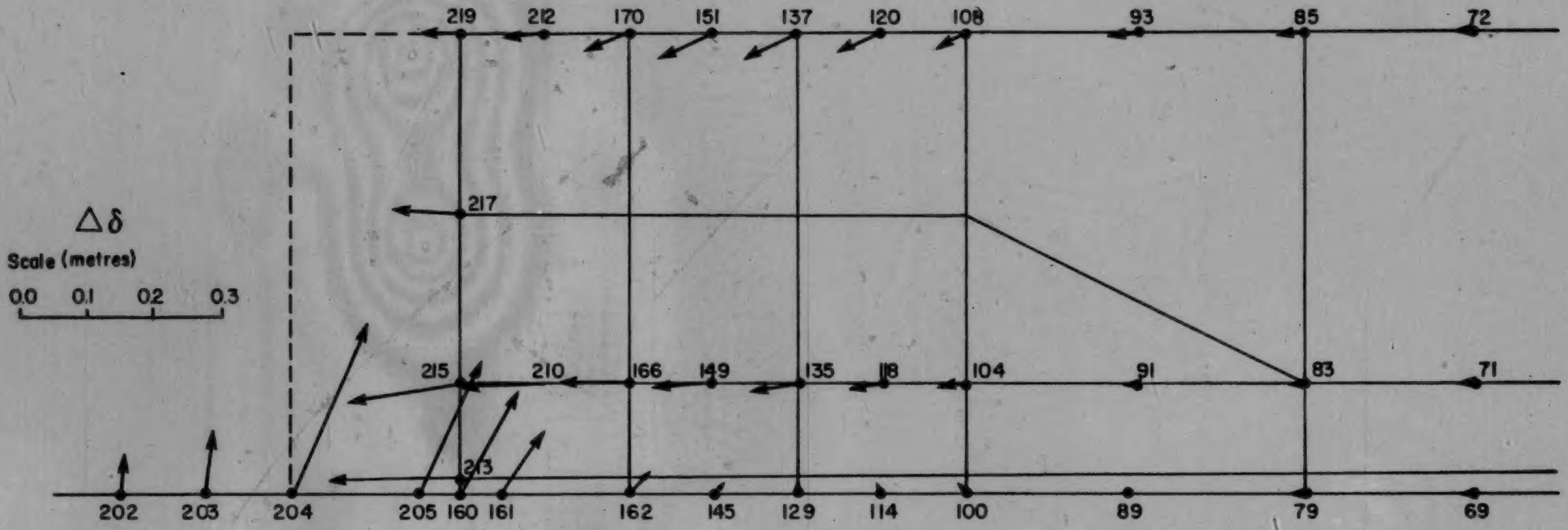
219
212
170
151
137
120
108
93
85
72
217
$\Delta\delta$
Scale (metres)
0.0
0.1
0.2
0.3
215
210
166
149
135
118
104
91
83
71
213
202
203
204
205
160
161
162
145
129
114
100
89
79
69

FIGURE 6.23 INCREMENTAL DISPLACEMENTS FOR EXCAVATION STEP, ELASTOPLASTIC ANALYSIS

block motion above the band, was maintained but smaller displacements were computed. Similar unloading forces for Stage II excavation resulted.

Considerable difficulties were encountered in controlling the stresses in the yielded portion of the shearband. The results were very sensitive to the Gv values, which were chosen automatically for stress adjustment. However, a deliberate effort was being made to obtain a viable solution with a single load step, although some attempts were made to use partial unloading steps as for the elastoplastic analysis. The everriding concern was to use the nonlinear analysis as a direct ("one-shot") tool, mainly to see how well it could be made to perform in relation to the sophistication, expense, and exaggerated preparation time of the elastoplastic analysis.

Figure 6.24 shows the stress-deformation results obtained using nonlinear elastic analysis, which may be compared directly with those of Figure 6.22 for the elastoplastic analysis. The strains are almost 50% smaller and the strain increment is not so sharply concentrated at the zone of shearband yield propagation. The stresses are not very satisfactory, but if the stresses for the zones of shearband yielding indicated by the elastoplastic analysis are averaged, the results are quite satisfactory.

Selected incremental displacement vectors are plotted in Figure 6.25, which may be compared directly with those of Figure 6.23 for the elastoplastic analyses. The displacement

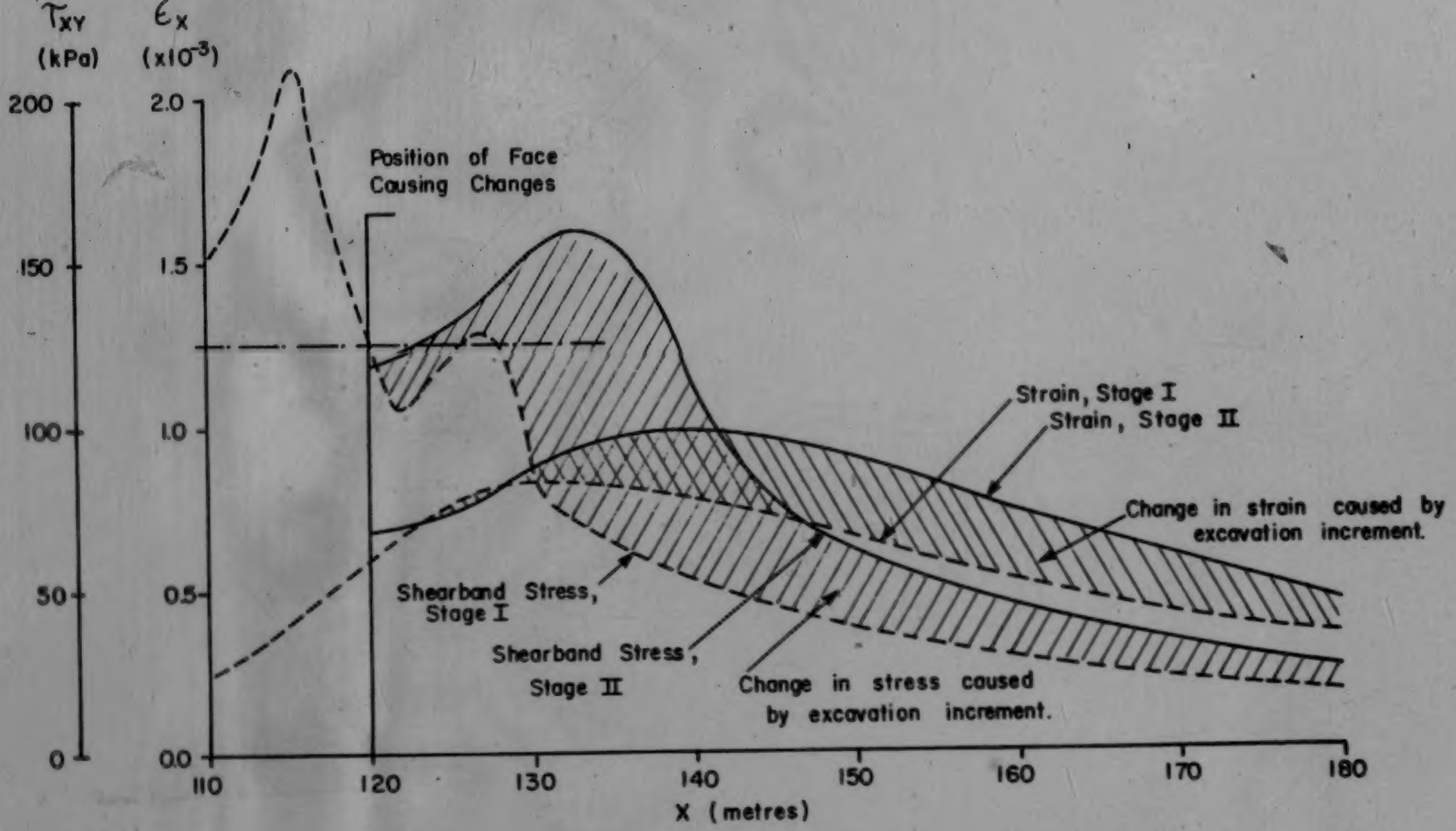

FIGURE 6.24 STRESS-DEFORMATION RESPONSE TO EXCAVATION INCREMENT, NONLINEAR ELASTIC ANALYSIS.

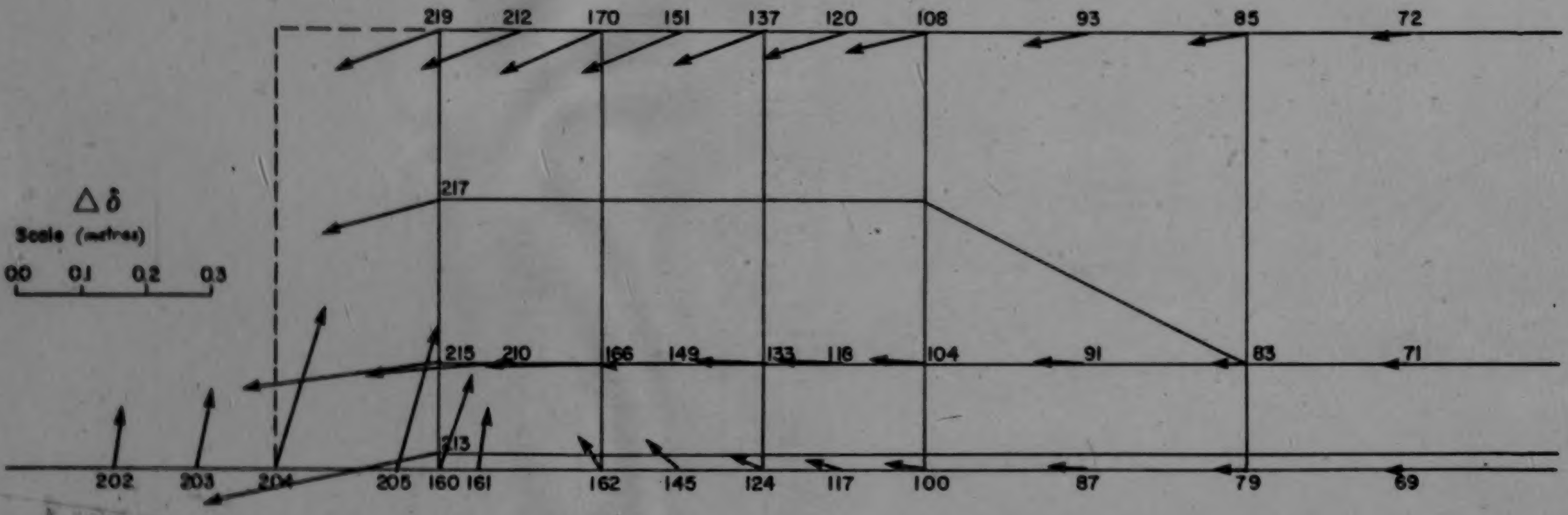
Δδ
Scale (metres)
0.0 0.1 0.2 0.3
219 212 170 151 137 120 108 93 85 72
217
215 210 166 149 133 116 104 91 83 71
213
202 203 204 205 160 161 162 145 124 117 100 87 79 69

FIGURE 6.25 INCREMENTAL DISPLACEMENTS FOR EXCAVATION STEP, NONLINEAR ELASTIC ANALYSIS.

increments are generally a little larger and heave is shown to extend for a distance of 7 or 8 metres above the base of the shearband. Relative slips of 42 millimetres at the new face, and 15 millimetres at a distance of 10 metres behind the new face, were calculated.

For comparison, a typical nonlinear elastic load increment required about 20 CPU seconds on the Amdahl 470 V/7. This is at least an order of magnitude cheaper than one partial load step of elastoplastic analyses. Given comparable (large) preparation times, the computational advantage of the nonlinear elastic approach is obvious.

6.5 CONCLUSIONS REGARDING BEHAVIOUR

A number of aspects of the field measurements deserve detailed interpretation. Discussion here will be restricted to those aspects which can be addressed with a minimum of speculation. In order of importance, these are:

1. Proving or disproving the hypothesis that only residual-strength sliding took place,
2. Examining the performance of the elastoplastic and nonlinear elastic models,
3. Assessing the influence of time-dependent processes.

Did Progressive Failure Occur?

Figure 6.26A is a schematic view of the interpretation advanced by Burland *et.al.* (1977) on the basis of field measurements. This interpretation was based on modelling the excavation process as quasi-continuous, with the total strains and stresses at any point being a reflection of the effects of a continuously advancing face. The discrete zone of large strain-rate was assumed to correspond to the postpeak weakening portion of the shearband yield model. Superimposed on Figure 6.26A are the increments of shear stress and horizontal extension strain associated with 10 metres of excavation of the face (this can easily be calculated from the figure). In terms of increments of stress and strain, it is not easy to explain a positive change of strain with a negative change of stress. Therefore the explanation advanced by Burland *et.al.* (1977), which seems plausible in terms of total stress and strain patterns and a quasi-continuous excavation process, does not appear to be entirely consistent in terms of discrete increments of response.

Figure 6.26B is an equivalent schematic view of the predictions of the residual strength finite element analysis. The increase in strain-rate is associated with the immediate prepeak elastic zone. Expressed in terms of shear stress and horizontal extension strain increments, which are also shown superimposed, there is a much more consistent relationship of positive and negative increments. The decrease in horizontal extension strain which can be noted

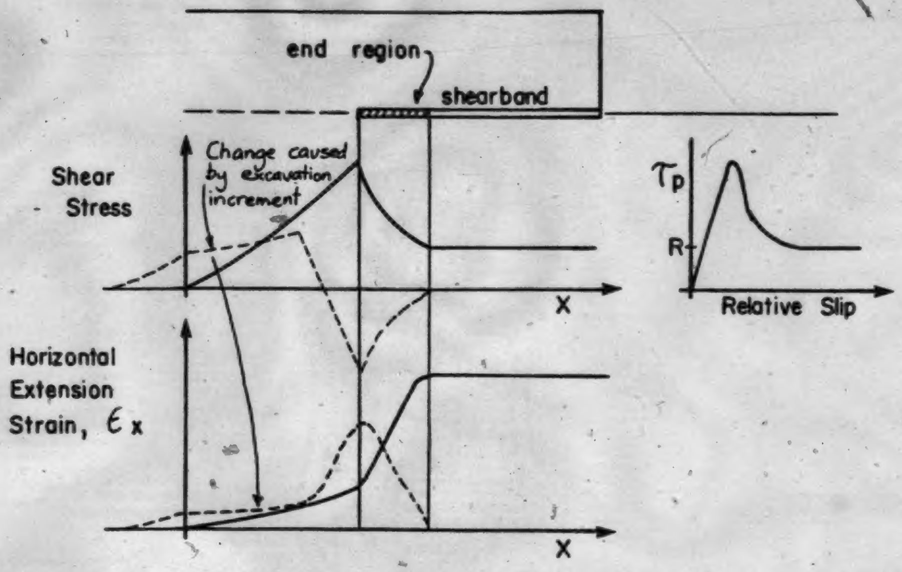
end region
shearband
Change caused by excavation increment
Shear Stress
X
τ_p
R
Relative Slip
Horizontal Extension Strain, ϵ_x
X

(A) INFERRED BY BURLAND *et. al.* (1977)

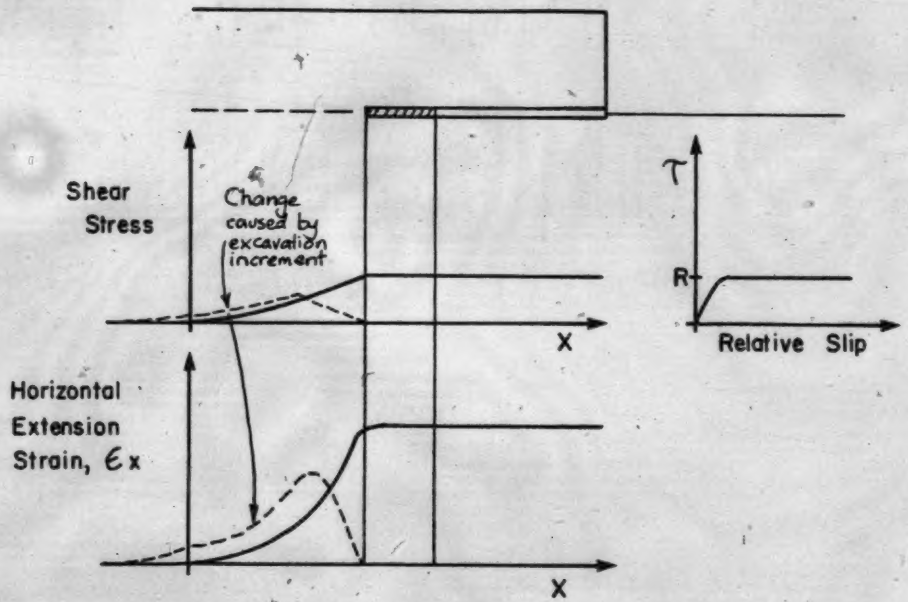
Shear Stress
Change caused by excavation increment
X
τ
R
Relative Slip
Horizontal Extension Strain, ϵ_x
X

(B) PREDICTED BY FINITE ELEMENT ANALYSIS

FIGURE 6.26 SCHEMATIC INTERPRETATIONS OF RESPONSE

in Figure 6.22 close to the free face has been ignored in Figure 6.26B because it is believed to have been caused by horizontal stress concentrations in the first stage of the finite element analysis. These would not exist with more complex material models, nor in reality.

Figures 20 and 22 from Burland *et.al.* (1977) can be reinterpreted in terms of deformation increments. Using the displacement histories from points 28 and 29 of the field study, differentiating to obtain strains, and then noting the strain change with distance from the face, it is possible to represent the increment of horizontal extension strain measured in the field. It should be noted that only two points have been treated in this fashion; with more field points the resultant data would be more scattered but more fully representative of field conditions. For the purposes herein,the data from these two points can be used as a basis for representing field response since the differentiations of displacement were published for these two points only, whereas for any other points the differentiations would have to be approximated from published displacements. It is not thought that the sparsity of utilized field data represents too great a lack of generality.

Figure 6.27 shows the resulting incremental horizontal extension strain and shear stress patterns calculated by finite element analysis assuming both residual and softened peak strengths. Also shown are the incremental strains derived from the field study.

There is a surprising coincidence both in magnitude, form, and position with respect to the excavated face, between the measured and predicted behaviour. Of particular note, however, is the relationship between the magnitude of incremental shear stress and incremental strain along the shearband. Although a constant yield stress was used on the shearband, the *increment* of shear stress resembles the classical peak-residual strain weakening curve proposed in the field interpretation.

On the basis of Figure 6.27, which presents the relationship between incremental shearband stress and incremental extensional strain in the sliding block above the shearband, the hypothesis of "residual strength" control of behaviour is ***tentatively*** *confirmed.*

For comparison, equivalent results are shown on Figure 6.27 for the elastoplastic analysis assuming an undrained shear strength equal to the softened peak strength. The pattern of response is sufficiently different in detail that there can be little doubt that only residual-level strength was being mobilized in the field.

The overall extensional displacement increments calculated using the two strength assumptions are of interest. Although the yielded zone in the softened peak strength case was significantly smaller than in the residual strength case, the softened peak strength case lead to incremental displacements about five times larger. No

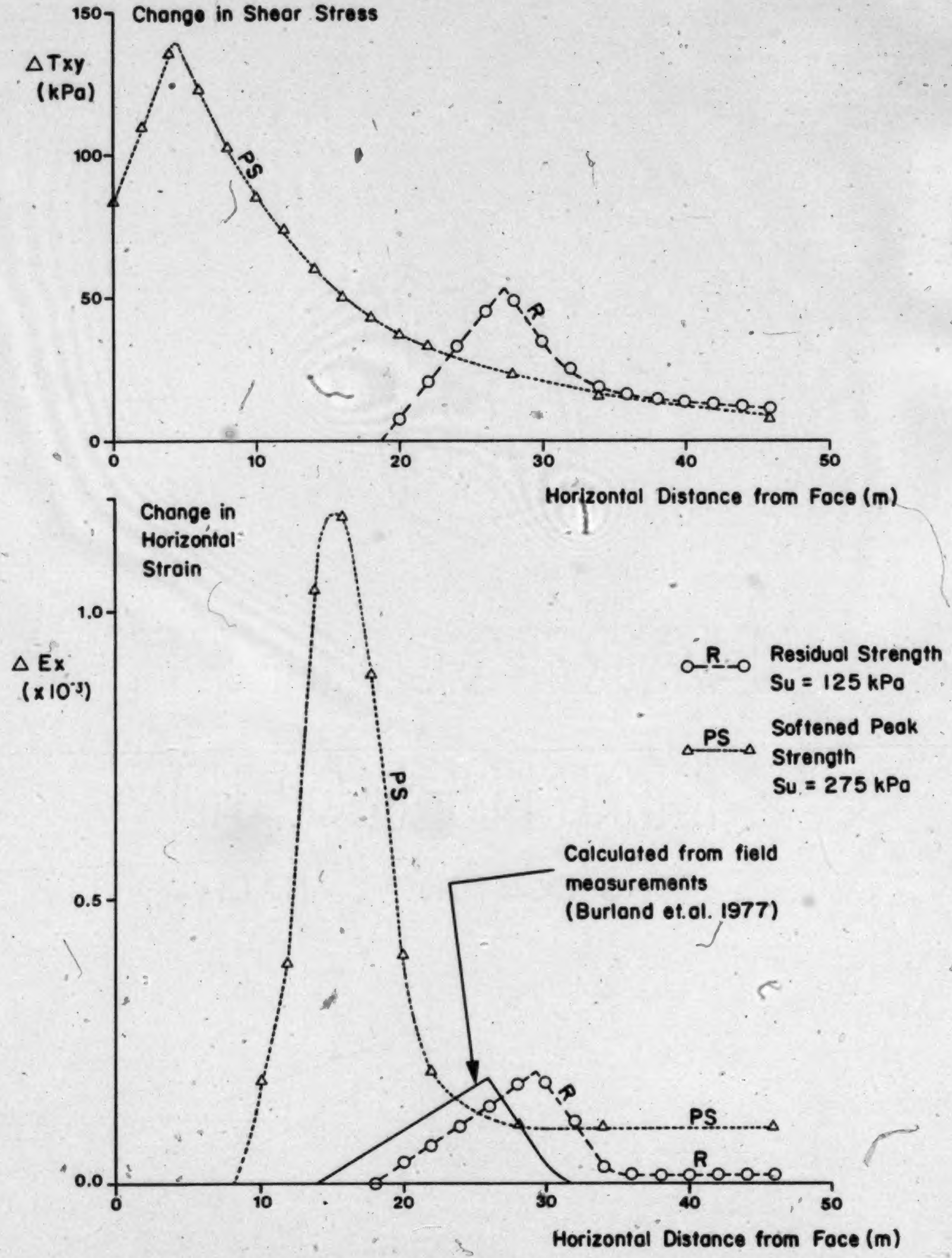

FIGURE 6.27 COMPARISON OF MEASURED AND PREDICTED INCREMENTAL BEHAVIOUR OF PIT WALL.

variations in the elastic parameters can explain such differences of displacement magnitude: the differences can best be explained as a function of the different stress fields above the shearband.

It is concluded that, for a variety of reasons such as flexural slip during lateral straining, progressive failure did not occur in the Saxon Clay Pit wall.

Performance of the Finite Element Models:

Comparison of Figures 6.22 and 6.24 suggests that the elastoplastic analysis can be accepted while the nonlinear elastic analysis cannot. This does not mean that nonlinear elastic analysis is generally inapplicable to such problems, however. When the analysis was carried out, the elastoplastic model was used first. Considerable effort was involved in controlling numerical convergence by careful examination and interpretation of a large number of partial load increments. The preparation time involved was estimated to be 2 man-months, not including 1 man-year of experience obtained by the time the reported computations were undertaken. A very deliberate attempt was therefore made to use the nonlinear elastic analysis as a "one-shot" convenience tool, to explore the practicality of undertaking detailed analysis of this class of problem cheaply. Even so, about 3 man-weeks of preparation time was involved, not including about 6 man-months of experience already obtained with the Gardiner Dam analysis (Chapter 7).

Given the differences in intended scope of the two procedures, it is hardly surprising that the elastoplastic results are more valuable. Some explanation of the limitations of the analysis is in order, otherwise the results of Figure 6.27 are too appealing.

Firstly, no facility was available for considering natural lithological variations, nor were any time-dependent processes explicitly included. However, a successful prediction of a very limited portion of the field data was undertaken. One should conclude that some of the success of the predictions is indeed fortuitous. On the other hand, an alternative and more easily understandable approach to interpretation of the field data has been proposed, and vindicated. The incremental shearband stress and sliding-block strain patterns are simple and consistent. On an incremental basis, the "active zone" (a better term, at this point, than "end region") *appears* to be experiencing strain-weakening.

The greatest value of the finite element analysis, it is concluded, is the capability it provides to quantify processes. A sensitivity study of the various controlling parameters of this problem, namely

1. strength parameters;
2. deformation parameters; and
3. ground stress state,

should be undertaken at this stage. It is suspected that the Young's modulus for the sliding block is too low, and for an equivalent shearband length a higher modulus would require a higher value of Ko. The greatest uncertainty surrounds the use of undrained shear strength, implicitly assuming a constant material effective stress condition at yield. Time and effort weigh very much against undertaking such a study.

Perhaps of more immediate interest would be the incremental shearband stress and sliding block strains associated with a strain-weakening strength model. The PPP model (Chapter 3) could be used directly, but more difficult numerical convergence problems are forecast unless a more efficient equilibrium-iteration algorithm is employed. Some form of variable-stiffness procedure could be devised at this point with little additional difficulty.

An observation from the one-dimensional studies should now be recalled. The CW and CWX models had quite different post-peak characteristics, and undoubtedly produced differences in the detail of strain destribution above the shearband. However, they predicted essentially the same relationships among the three components listed above and the shearband length.

Two conclusions arise. Firstly, the relationships among the components of a progressive failure problem are complex. Given the lack of precision in identifying material parameters, it is difficult to imagine obtaining a unique solution to any progressive failure problem. Secondly, finite element analyses are essential to an understanding of the detailed deformational response of any problem involving discrete zones of localized shearing. It appears that difficult and expensive elastoplastic techniques are necessary if such analyses are to be carried out realistically.

Influence of Time-Dependent Processes:

Excavation of the Saxon Clay Pit wall was, in detail, a three-dimensional time-dependent process. An incremental, two-dimensional analysis appears to provide satisfactory predictions of performance. Time-dependent processes set aside in the above studies include:

1. Detailed consideration of pore pressure changes, both as a function of position and time with respect to excavation and also as a function of stress changes associated with shearband propagaton;
2. Influence of strain-rate on the strength attainable by material under the field conditions prevailing.

Pore Pressure Effects: Alternative analytical procedures have been developed for directly accounting for coupled stress-diffusion problems (Cleary, 1976 and 1977). These may not yet have sufficient detail to treat elastoplastic shearbands adequately, but the potential exists. The pore pressure changes which could be expected included reponse to changes in hydrostatic and deviatoric stress, unsteady drainage towards moving boundaries, and diffusion of any excess pressures. The number of material parameters required to describe these processes is large.

Also, the descriptions are approximate in nature, and the range of natural variability sufficiently great to make pursuit of such details almost pointless.

On this basis, there is much simple common sense in adopting undrained strength behaviour at this stage of analysis. Palmer and Rice (1973) referred to three time scales for diffusion effects. In the first case, the shearband advances rapidly in comparison to any time scales for diffusion. This is true "undrained" response which, if coupled to induced negative pore pressure changes at the shearband "end zone", implies a higher slip resistance and stiffer elastic response than in a drained situation. On another time scale, the speed of propagation is slow enough to allow no induced pore pressure changes in the shearzone, but still rapid enough to permit overall "undrained" response. Again, stiffer propagation results. Lastly, for wholly drained behaviour, shearband response is softest.

Burland *et.al.* (1977) provided some consolidation test data for the Oxford clay, as well as for Kellaways sand and clay (draft version of final paper). Typical Cv values for the Lower Oxford Clay were 0.5 to 1.0 m^2/year. For the Kellaways sand and clay, values were 20.0 and 1.0 m^2/year respectively. For a shearband 1 metre thick directly overlying the Kellaways sand, the longest drainage path is 1 metre and an estimate for 90% dissipation would be 6 months to one year. If such a simple approach was representative, then only partial drainage would occur during a typical excavation increment. There is no means by which the laboratory values could be related to any field measurements.

Strain-Rate Effects on Strength: Kaiser (1979) discussed how a strain-weakening material could display different apparent strengths depending on the stress-history as well as time-history of shearing. The strain rates mobilized in the field are difficult to assess, because of the uncertainty of relating multiple discrete slips to some measure of strain. It is probably more appropriate to think of the shearzone as a complex mechanism composed of different elements which, under changing conditions, assume or relinquish the role of "weakest links". This was alluded to by Burland *et.al.* (1977) in their discussion of stick-slip phenomena observed within the Saxon Clay Pit shearzone. There are, unfortunately, no means by which the time-dependent strength can be further quantified at present.

Summary:

One-dimensional models and two-dimensional finite element analyses have been applied to the behaviour of a propagating shearzone at the Saxon Clay Pit.

The one-dimensional analyses demonstrated the relationships between the various components of progressive failure, or even residual-strength shearzone slip. Discrepancies between different models arose because of different assumptions and the material parameters chosen. These models were not capable of explaining the deformation patterns observed in the field measurements.

Finite element analyses were carried out to test the hypothesis that only residual-strength shearzone slip developed. Incremental deformation patterns corresponded remarkably well with field measurements. Although these analyses may have been too simplistic, there is circumstantial evidence from the one-dimensional studies to suggest that the computed shearband behaviour is insensitive to the details of constitutive modelling of the shearing in the band. Elastoplastic analyses carry high overhead costs (preparation time, development time) and are expensive computationally. They are probably more reliable to use, however, than nonlinear elastic analyses. For equivalent levels of detail in results, the material parameters required for elastoplastic analysis are more practical and meaningful.

The behaviour of the Saxon Clay Pit shearzone was no doubt influenced by a number of simultaneous time-dependent processes. It is not possible to quantify the effects of these to any degree. Until this becomes possible, no analysis can confidently claim to have fully explained field behaviour. This research has identified an incremental deformation mechanism which appears to be more reasonable than that proposed by the original investigators. In no manner does this reflect on the field study, for it represents the finest example available where progressive failure processes have been considered.

7. SHEARBAND BEHAVIOUR IN GARDINER DAM FOUNDATIONS

Gardiner Dam was constructed on the South Sasktchewan River in south-central Saskatchewan, between 1958 and 1968. Bedrock consists of overconsolidated clay shale and sandstone, materials which were known to pose unusual and difficult foundation and stability problems. Geotechnical performance of the dam and associated works was described by Jaspar and Peters (1979), whose work forms the basis of the review in this Chapter.

Continuing cyclic deformations of the embankment and foundation caused some concern, particularly as movements were concentrated along foundation shearzones with a history of previous movements. A deformation analysis using the NLCP nonlinear elastic finite element computer program was carried out by Morgenstern and Simmons (1980) for the Prairie Farm Rehabilitation Administration, the present operators of the dam. This finite element study is also reviewed in this Chapter.

The deformation analysis was able to clarify the nature of the recurring load-deformation mechanism. This has some important implications for stability design, which is usually based on limit-equilibrium analysis.

7.1 REVIEW OF FIELD BEHAVIOUR

Geology:

Foundation materials consist of units of the late Cretaceous Bearpaw Formation. Typical materials are fine grained, weakly cemented clayey sandstones; dark grey clay shale with bentonite layers and lenses; and clayey sandstones. The bentonite seams are between 13 and 100 mm thick. Upland areas are mantled with clay till, glaciolacustrine silts and clays, and glaciofluvial sands. The river channel contains as much as 33m of alluvial sands and silts.

Postdepositional bedrock features include bedding-plane shears thought to have been induced as a consequence of solution-subsidence faulting of deeper-seated evaporites. Glacial loading and unloading may have induced further shears.

Main valley slopes and side valleys display widespread slumping. Disturbed slump material has undergone extensive shearing and weakening.

Stress reduction is known to produce the following characteristics in the clay shale: shearzones (along bentonite-rich seams), softening, slickensiding, and shrinkage cracking.

Embankment Design:

Original design was based upon site investigations and experience from other sites having similar conditions. The structure consists of a main river valley embankment, and a smaller subsidiary embankment across Coteau Creek, to the west. The spillway, power tunnels, and outlet works are situated in the main west abutment, which forms the ridge between the two valley embankments. A simplified view of the layout is given in Figure 7.1.

After construction commenced, it became necessary to revise designs because of stability problems encountered with soft weathered shale. Embankment slopes had to be substantially flattened. This proved to be satisfactory until construction was well advanced.

Foundation displacements were then experienced in weak shale zones at three locations: the river section; main east abutment; and Coteau Creek section. Additional slope flattening, closely controlled fill placement, and more extensive berming were required to complete the embankments. It appeared that old shearzones had been reactivated under the east abutment and Coteau Creek sections, but that a previously unnoticed shearzone developed as a result of construction of the main section.

The final embankment cross-sections for the three areas of concern are also shown in Figure 7.1.

Performance Monitoring:

As a consequence of the foundation conditions, much reliance was placed upon field observation of performance, and a very comprehensive suite of monitoring instrumentation

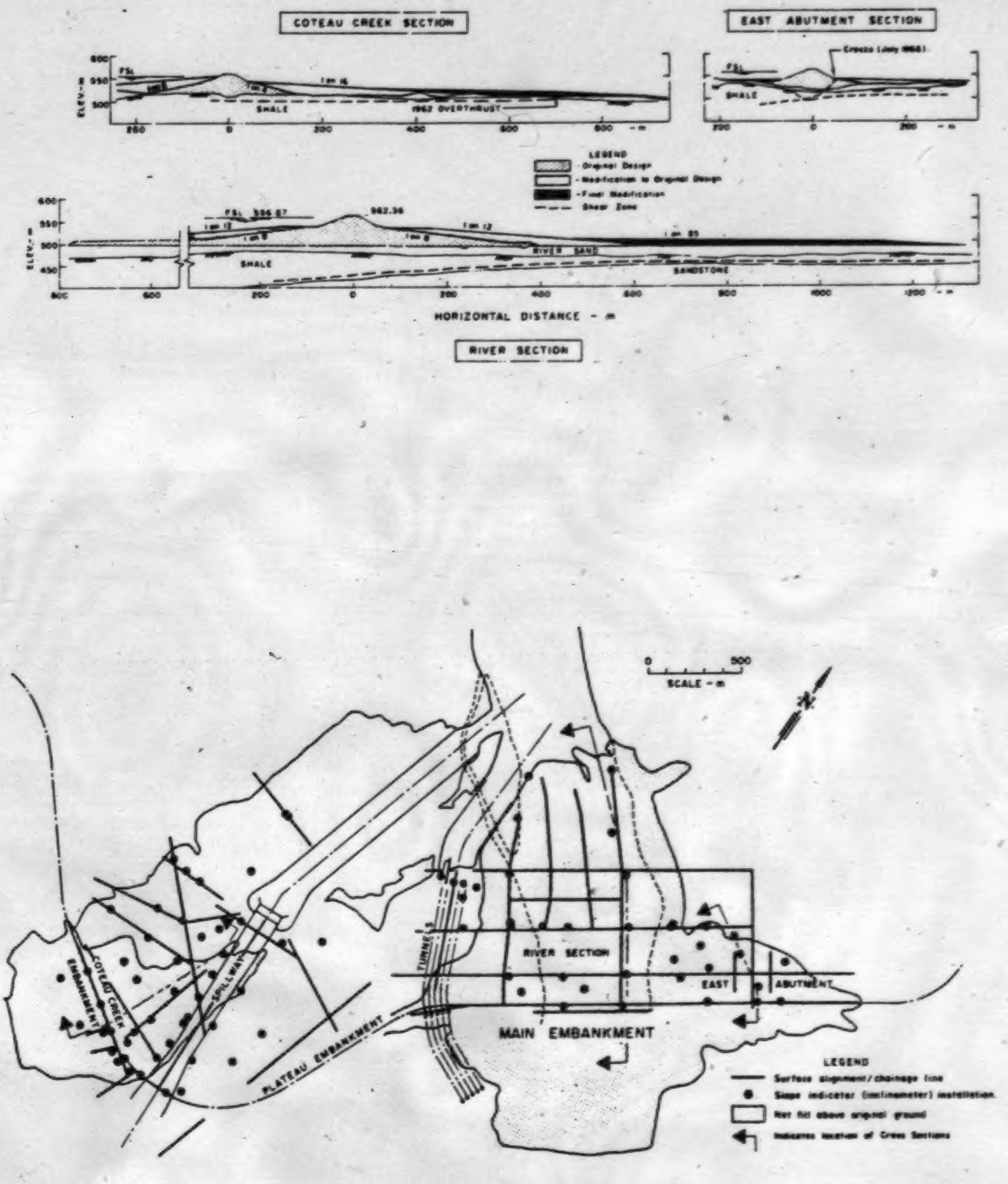
COTEAU CREEK SECTION
EAST ABUTMENT SECTION
FSL
1 on 16
SHALE
1962 OVERTHRUST
Crezzo (July 1966)
ELEV.- m
600
550
500
450
200
0
400
600
800
900
1000
1200
- m
LEGEND
Original Design
Modification to Original Design
Final Modification
Shear Zone
FSL 556.87
562.36
1 on 12
1 on 8
1 on 85
RIVER SAND
SANDSTONE
HORIZONTAL DISTANCE - m
RIVER SECTION
SCALE - m
500
COTEAU CREEK EMBANKMENT
SPILLWAY
PLATEAU EMBANKMENT
TUNNELS
RIVER SECTION
EAST ABUTMENT
MAIN EMBANKMENT
LEGEND
Surface alignment/chainage line
Slope indicator (inclinometer) installation
Net fill above original ground
Indicates location of Cross Sections

FIGURE 7.1 GENERAL LAYOUT OF GARDINER DAM (after Jaspar and Peters, 1979)

was installed. Figure 7.1 also shows the location of some instrumentation for monitoring embankment movements.

Piezometers were very widely installed. Those measuring pore pressure response in the shale foundation, particularly the shearzones, show a very high level of response and virtually no dissipation since construction was completed.

Construction and Postconstruction Performance:

The detailed descriptions of Jaspar and Peters (1979) deserve to be carefully read in this regard. Summaries of deformation- and pore-pressure-time relationships were provided for all three areas of concern. A pattern of yearly incremental displacements was noted in all areas. These were non-recoverable shearzone slips related to the increase of reservoir level as snowmelt runoff accumulated each spring. The slips were definitely related to the water thrust changes: creep movements at more-or-less constant reservoir level were small in comparison with the slips associated with change in reservoir level. Figure 7.2 is a summary of postconstruction movements for selected inclinometer locations.

It is important to recognize two key issues concerning the postconstruction behaviour. Firstly, no postimpoundment deformation measurements are available from the upstream parts of the embankments. This means that virtually no inferences can be made about the overall embankment motions. Secondly, the postconstruction movements are largest near

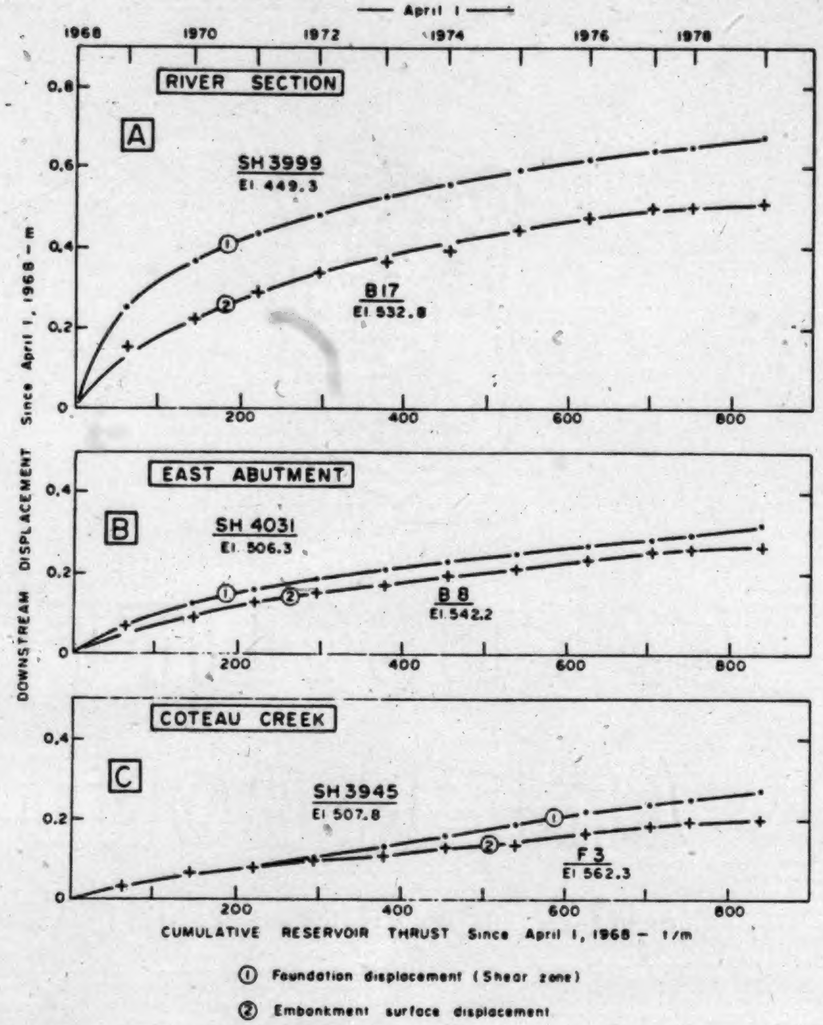

FIGURE 7.2 SELECTED POSTCONSTRUCTION DISPLACEMENTS.
(after Jaspar and Peters, 1979)

the maximum embankment heights, and are much smaller beneath the embankment toes. This implies some form of cumulative compression of the downstream portion of the embankment.

From Figure 7.2, it is obvious that the Coteau Creek shearzone slips are the only ones showing no general decrease with time. Mainly for this reason, the Coteau Creek embankment was chosen for detailed deformation analysis. It was hoped that the indications of this study, at the likely most critical part of the structure, could be extended to the other locations. Figure 7.3 is a summary of performance at the Coteau Creek section. The average slip under the embankment centreline is approximately 0.027 metres per year.

7.2 FINITE ELEMENT ANALYSIS PROCEDURES

The purpose of the deformation analysis was to simulate the ongoing displacement patterns of the prototype. These patterns are known to result from highly localized nonlinear behaviour. It was thus necessary not only to simulate ongoing behaviour, but also to reconstruct each and every stage of behaviour as faithfully as possible. Failure to account for the full deformation history would invalidate the analysis, because of the highly path-dependent nature of nonlinear behaviour.

The stages of behaviour to be reconstructed were:

1. Foundation preparation;

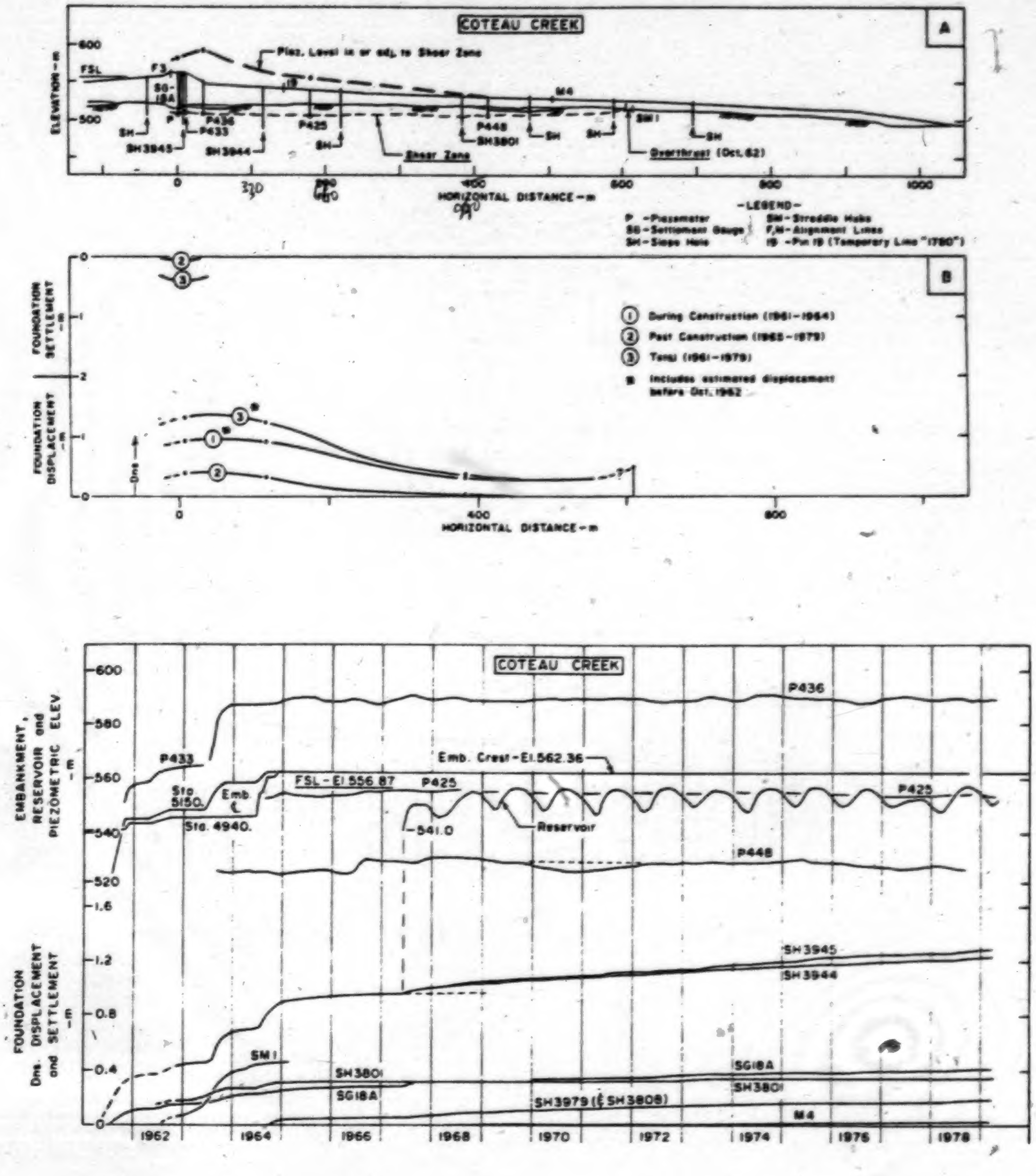

FIGURE 7.3 COTEAU CREEK SECTION PERFORMANCE SUMMARY (after Jaspar and Peters, 1979)

2. Embankment construction;
3. First filling of the reservoir; and
4. Cyclic reservoir operation.

Each of these stages presents analytical difficulties. Additionally, the long, low, flat geometry of the structure provides difficulties for mesh discretization. Central to all the analyses, however, is the problem of defining suitable deformation parameters for the various material constitutive behaviours.

Each of these "general" aspects will now be discussed. Subsequent sections of this Chapter describe the two basic phases of the analysis: deformation-matching of construction behaviour and simulation of load cycling.

Before any of these matters are discussed, however, it is necessary to address the question of total and effective stress analysis of the embankment and foundation.

Total Stress and Effective Stress Analyses:

Deformations should ideally be analysed on an effective stress basis. This requires coupling of total stress and pore pressure analysis (Law, 1975) but the processes are not routine. Complexities are introduced which create difficulties in obtaining representative material parameters.

Analysis in terms of total stresses is the only practical alternative, and is reasonable here in light of material behaviour. Other studies (Morgenstern and Kaiser,

1980) suggest that in the core and foundation there have been only minor pore pressure changes since the end of construction. It was deemed satisfactory to carry out total stress analyses, with appropriate shear strengths governing the deformation response. Effective stress behaviour can be inferred by reference to appropriate seepage analysis or measured pore pressures.

Mesh design:

Figure 7.4 is a simplified cross-section of the Coteau Creek embankment, and Figure 7.5 shows part of the finite element mesh. Noteworthy are the different material zones, and the non-rectangular element shapes these necessitated. The optional midside nodes were omitted wherever possible in order to minimise the core storage requirements for the overall mesh. Some detail of the distribution of nodes is given in Figure 7.6.

The foundation boundary was chosen to be 50 feet below the shearzone, since at this depth rigidity and fixity could be expected. Lateral boundaries were dictated by the need to isolate the upstream embankment from lateral strain effects (1000 feet upstream was assumed to be satisfactory) and provision for the full extent of the downstream shearzone. Since the shearzone cropped-out about 2000 feet downstream, the total mesh comprised 622 nodes and 251 elements. Greater mesh refinement would have been valuable in the critically stressed region beneath the embankment centreline, but this

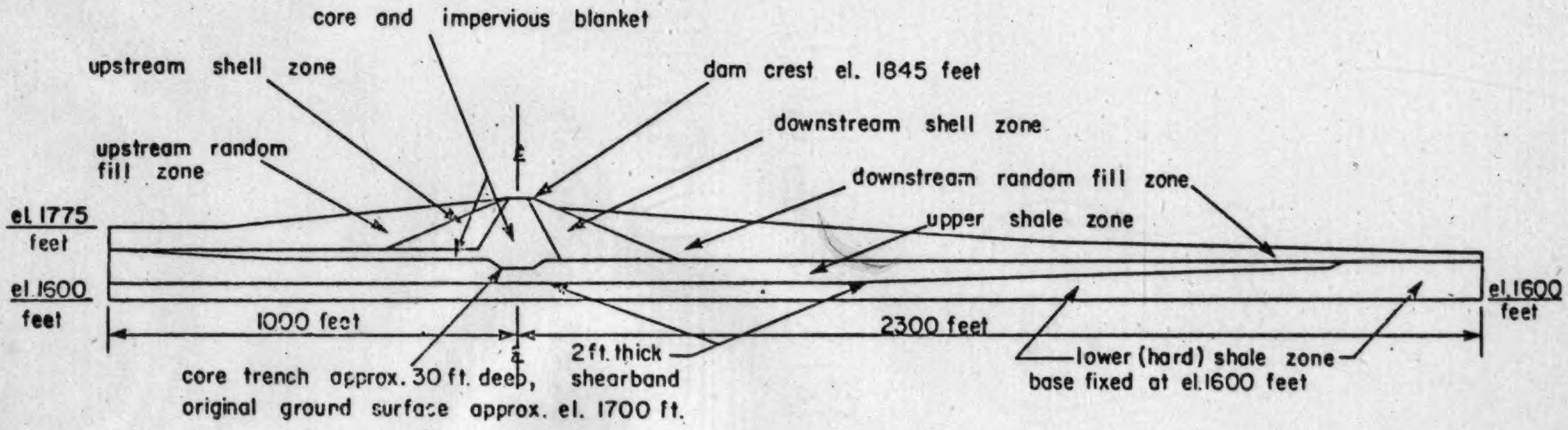
core and impervious blanket
upstream shell zone
dam crest el. 1845 feet
downstream shell zone
upstream random fill zone
downstream random fill zone
upper shale zone
el. 1775 feet
el. 1600 feet
el. 1600 feet
1000 feet
2300 feet
2 ft. thick shearband
core trench approx. 30 ft. deep, original ground surface approx. el. 1700 ft.
lower (hard) shale zone base fixed at el. 1600 feet

FIGURE 7.4 ADOPTED CROSS-SECTION, COTEAU CREEK STA. 169+50

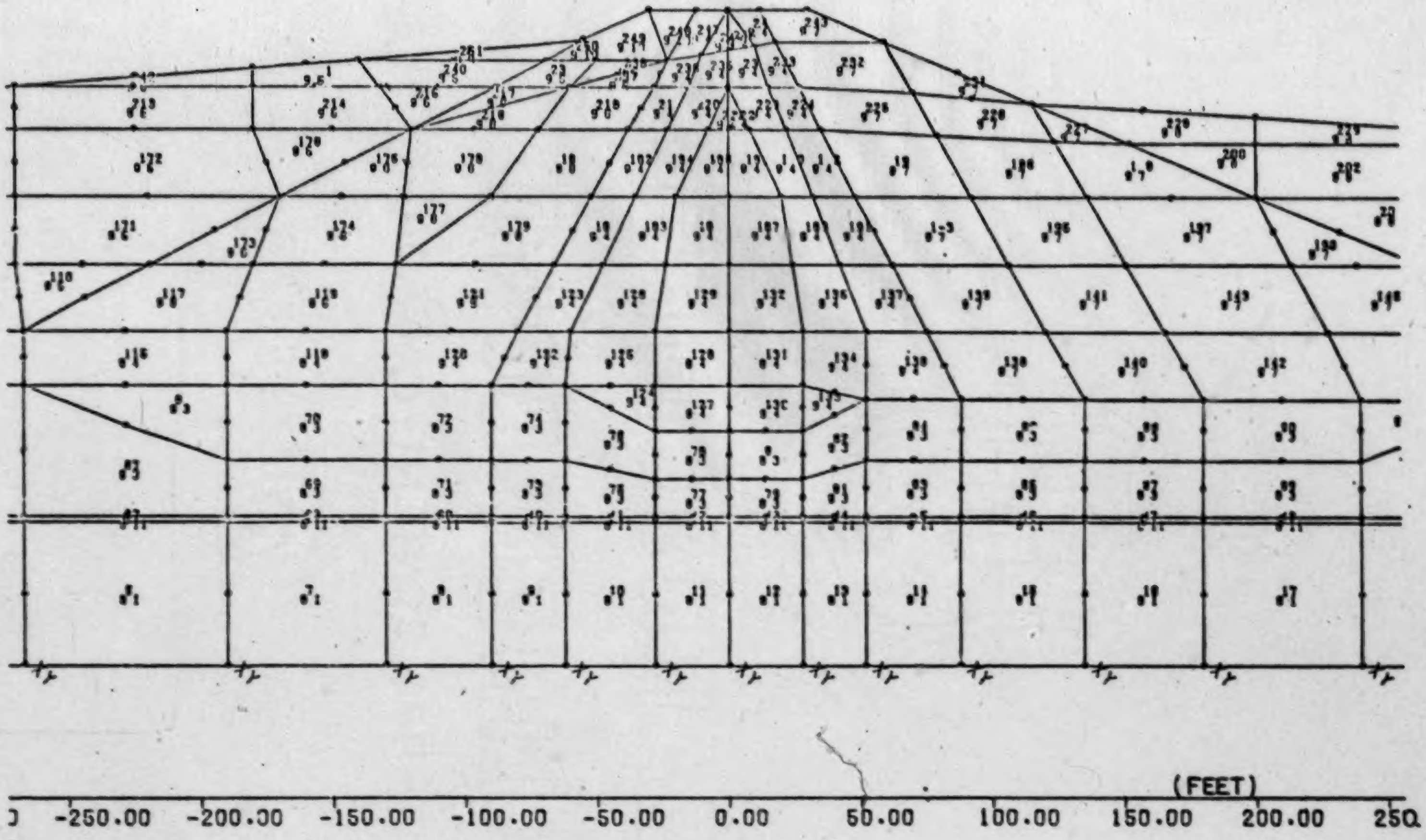
(FEET)
0
-250.00
-200.00
-150.00
-100.00
-50.00
0.00
50.00
100.00
150.00
200.00
250.

FIGURE 7.5 FINITE ELEMENT MESH DETAIL SHOWING ELEMENTS.

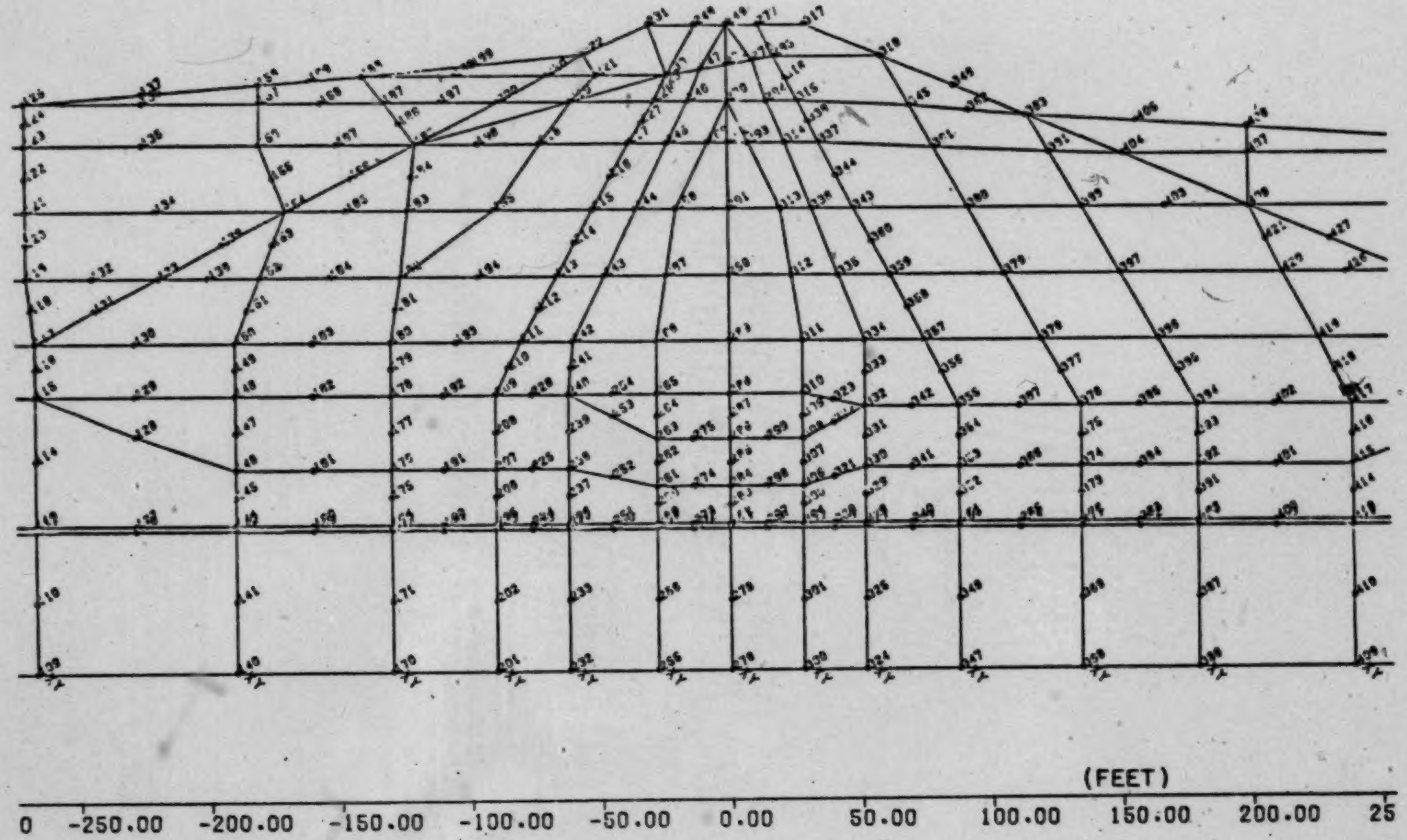
(FEET)
0
-250.00
-200.00
-150.00
-100.00
-50.00
0.00
50.00
100.00
150.00
200.00
25

FIGURE 7.6 FINITE ELEMENT MESH DETAIL SHOWING NODES.

would have been too expensive in terms of core storage and computation procedures.

Selection of Material Model Parameters:

At the outset of the analysis, it was expected that significant zones of material would be at or close to maximum strength mobilization. Therefore, adequate strength and representative nonlinear deformaton parameters had to be selected. There are tremendous ranges of material properties in Gardiner Dam, and it was therefore anticipated that contrasts between certain materials in restricted portions of the dam could dominate the outcome of the analysis. On the other hand, only the hyperbolic nonlinear elastic constitutive model (Duncan and Chang, 1970, see Chapter 3) was well-proven enough to warrant adoption. Each of the materials was examined in turn, to define material parameters. Background experience (Duncan *et.al*. 1978) was available to guide parameter selection.

Shale Bedrock: The undisturbed shale is hard and stiff. Mass strength was not known, and mass deformability could only be estimated from field rebound measurements. Experience with similar materials elsewhere was a good guide for selecting properties.

Shale Bedrock Above Shearzone: Material above the shearzone was typified as weathered and weakened, all or much having at some stage been involved in mass movements. It is probable that the foundation spreading experienced during construction created highly stressed zones and shears oblique to bedding. The *operational* strength and deformability were therefore assessed by initially assigning "intact" shale properties, and then reducing these until suitable behaviour was observed in the analytical model. Considerable judgement was required in this regard.

Shearzone: The shearzone was idealized as a 2 feet thick shearband. Conventional nonlinear behaviour was simulated by assigning the same properties as for the shale bedrock above the shearzone. The exceptional weakness and low stiffness of bedding plane shearing was simulated using the transverse-isotropic model (see Chapter 3). Considerable experience was available for assessing the parameters governing bedding plane shearing.

Compacted Shale: Oedometer test results were available. However, this material was only one component of the random fill zones, whose behaviour is not fully characterized by oedometer tests. No detailed attention was paid to compacted shale within the random fill zones.

Core and Upstream Blanket: These were formed from till, for which a variety of drained and undrained test data were available. A typical stress path in the core corresponds reasonably well to conditions in conventional triaxial tests, for which the hyperbolic nonlinear elastic model works quite well. Deformation studies for other projects (for example, Skermer, 1975, for Mica Dam) have demonstrated that triaxial test moduli are usually lower than operational moduli. Considerable judgement was therefore required to select deformation parameters, but strength parameters were known reasonably well.

Sand and Gravel Shells: Little test information and no deformation properties were available. Construction reports enabled reasonable estimates of strength and deformability to be made. In the shells, stress paths typically are proportional loading, for which the hyperbolic model is not ideally siuted.

Random Fill Berms: These upstream and downstream zones consist of variable and randomly placed spoil and other materials. Little is known of their current composition, strength, and deformation characteristics. Typical stress paths involve proportional loading, but part of the downstream zone may function as a zone of passive resistance with the maximum compressive stress rotating towards horizontal. Any suitably weak and nonlinear parameters could be selected.

Summary: Although the shortcomings of the hyperbolic nonlinear model for non-triaxial stress paths (Eisenstein and Law, 1979) have been established, and no single nonlinear technique seems preferable for embankment analysis (Cathie and Dungar, 1978), the hyperbolic model was adopted generally because of convenience and experience with its use (Soriano *et.al.* 1976). Initial strength and deformation parameters were chosen, and embankment construction was simulated in order to refine parameter selection.

Foundation Preparation and Embankment Construction:

Simulation of construction behaviour was felt to be the best means for checking performance of the finite element model, as the original structure was well instrumented.

In order to simulate construction of the embankment, stresses and displacements had to be evaluated in steps as layers of fill were added. The initial stresses in the shale foundation, and the effects of core trench excavation had first to be specified, due to the nonlinear behaviour and expected stress concentrations under the embankment crest. Overburden stress were calculated from the original ground surface assuming a ratio of original horizontal to vertical stress of 1.0 and a unit weight of 125 pcf. Ideally a large number of fill layer additions would be made: in this case one (initial) unload followed by three fill construction lifts were used, owing to economic and mesh refinement constraints. The excavation and construction sequence is shown in Figure 7.7. Details of the construction analysis are given in Section 7.3.

First Filling of the Reservoir:

First filling of the reservoir to Full Supply Level (FSL) is an incremental loading process similar to that of adding fill. However, water impounded by the embankment has a number of influences on the structure which had to be considered in the finite element model:

1. Hydrostatic Forces: the water may be considered either

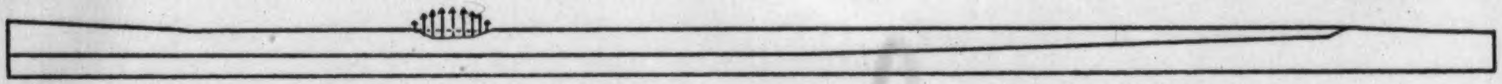

STAGE 1: Original Ground Stresses, Remove Core Trench Material

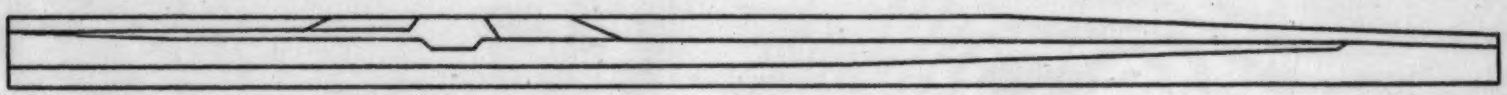

STAGE 2: Add First Layer of Fill (Approx. el. 1750 ft.)

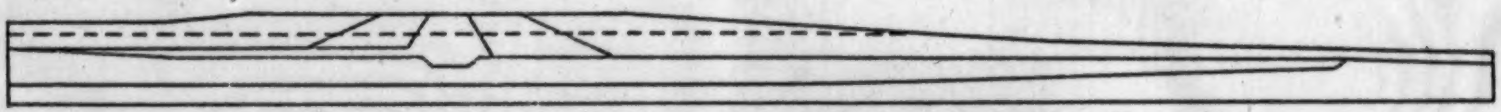

STAGE 3: Add Second Layer of Fill (Approx. el. 1800 ft.)

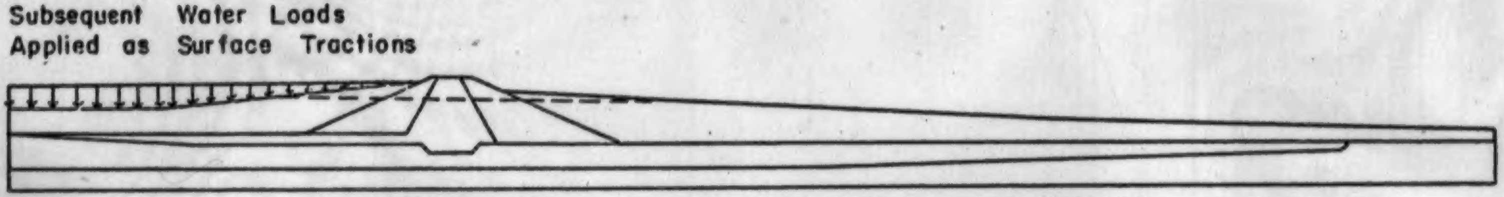

Subsequent Water Loads
Applied as Surface Tractions

STAGE 4: Add Third Layer of Fill (To crest el. 1845 ft.)

FIGURE 7.7 CONSTRUCTION LOADING PROCEDURE.

as a material having zero shear stiffness, very high bulk stiffness, and self-weight; or as a distribution of surface pressures against suitable surfaces representing flow barriers.

2. Infiltration and Seepage: material which offers little barrier to water percolation is rapidly made bouyant, resulting in weakening and stiffness reduction.

In the original structure, effective stress changes accompanying first filling could be expected to have caused significant deformations. The development of steady-state seepage in the core and blanket may take many years during which there is an adjustment of pore pressures, and again the effective stress changes may cause significant changes in deformation patterns (Squier, 1970). The time scale of these processes may be considered *undrained* in some materials and *drained* in others.

The sequence of effects of impounding has been examined by many writers (Nobari and Duncan, 1971; Eisenstein, 1974; Law, 1975; and Stewart, 1979). Analysis of the various effects is complex and there is a general lack of suitably documented field experience.

For this study, the key element of reservoir filling to be considered was the deformation pattern along the shearband. Stress distributions in the embankment were not likely to be critical unless zones of tensile stress became too pronounced. The upstream random-fill zone consists of rather ill-defined distributions of both pervious and relatively impervious materials. Appreciable infiltration in selected zones might be realistic over the time scale of impounding, elsewhere little water penetration would be possible.

Figure 7.8 shows two possible loading schemes to simulate the effects of impounding. One considers the random fill to be impervious and the other, pervious. The "impervious" scheme was adopted for the following reasons:

1. Simplicity: extra complexity always tends to cloud the interpretation of results;
2. Potential Numerical Problems: introduction of the "pervious" model, it was feared, might lead to increased tension zones in the random fill.

A series of numerical experiments indicated that zones of appreciable tension tended to occur within the random fill. Displacement patterns obtained with the *impervious* loading scheme were satisfactory even in this event.

Cyclic Reservoir Operation:

An essential aspect of the entire study was whether or not an apparently satisfactory model could reproduce the pattern of deformation response to cyclic reservoir operation. Complete details of the reservoir and embankment movement histories were available so that this loading sequence could be evaluated with confidence.

Loading at all steps prior to the reduction of reservoir level consists of a general increase in confining

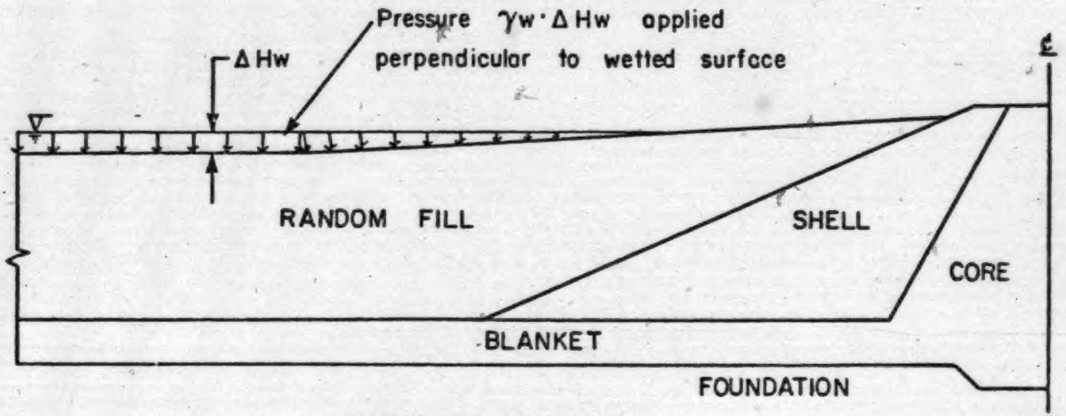
Pressure $\gamma w \cdot \Delta Hw$ applied
perpendicular to wetted surface
ΔHw
℄
RANDOM FILL
SHELL
CORE
BLANKET
FOUNDATION
℄

IMPERVIOUS SCHEME

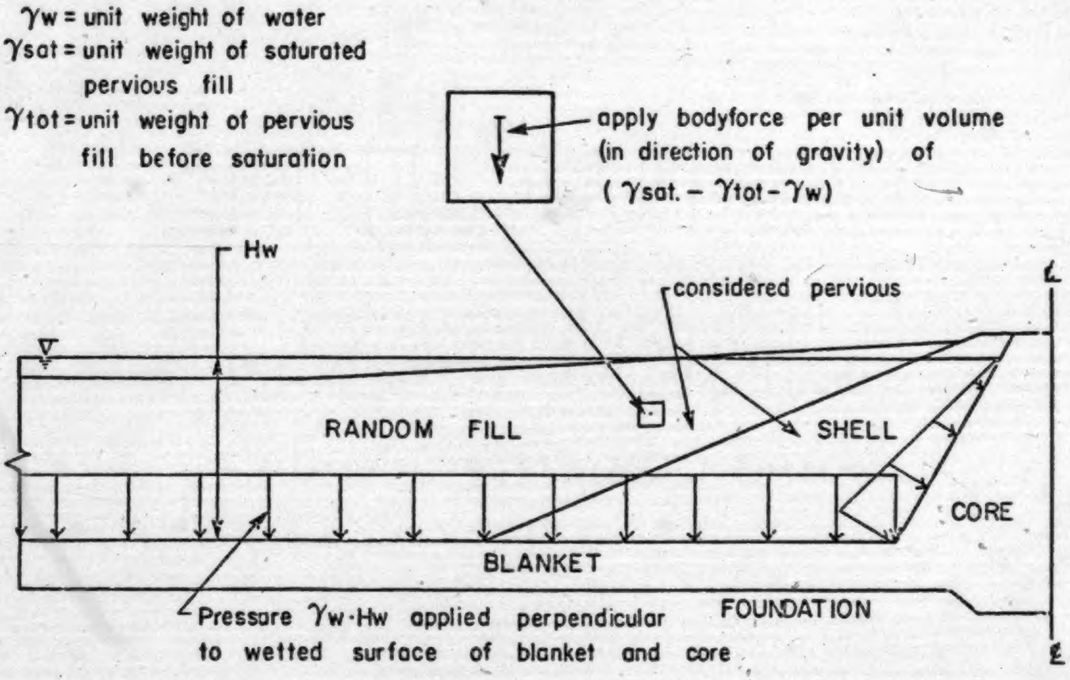
γw = unit weight of water
γsat = unit weight of saturated pervious fill
γtot = unit weight of pervious fill before saturation
apply bodyforce per unit volume
(in direction of gravity) of
$(\gamma sat. - \gamma tot - \gamma w)$
Hw
considered pervious
℄
RANDOM FILL
SHELL
CORE
BLANKET
FOUNDATION
Pressure $\gamma w \cdot Hw$ applied perpendicular
to wetted surface of blanket and core
℄

PERVIOUS SCHEME

FIGURE 7.8 LOADING SCHEMES FOR SIMULATING RESERVOIR IMPOUNDING.

pressure and proportional increase in deviator stress. In the shearband, local regions were expected to be stressed to yield, with substantial softening of deformation response in order to accommodate induced shearing. Material response during lowering of the water to the Low Water Level (LWL) constitutes an entirely different stress-state change. Unloading consists of a reversal of forces due to incremental water pressures on the upstream face. In the embankment and foundation, the typical stress changes associated with this would be pseudo-elastic unloading. The unload/reload cycle thus consists of two distinctly different processes, with unloading being considerably stiffer and more linear in nature.

Without any clear test information on the nonlinear unloading response of the Gardiner Dam materials, a simple acceptable unloading model was established by evaluating an initial tangent modulus at zero deviator stress, at the average confining pressure in each material zone. Experimental evidence from elsewhere suggested that the cyclic stress-strain response of relatively weak material might be as indicated in Figure 7.9, which also illustrates the response that the adopted model simulates. It should be noted that this model does not stiffen with cyclic behaviour.

Selection of appropriate parameters for reloading was a contentious issue. On the one hand, field experience indicated significant, reproducible incremental deformations

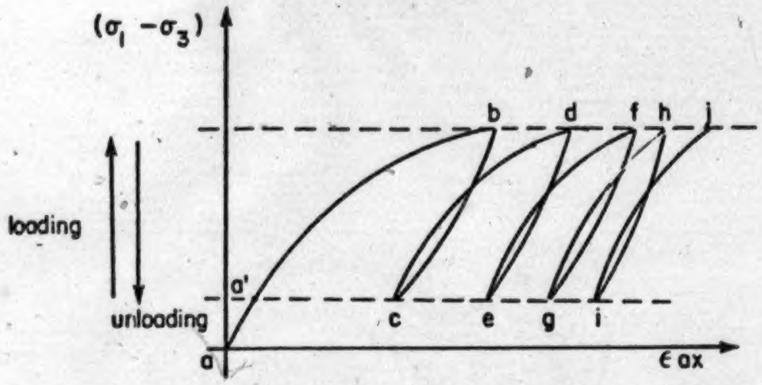
$(\sigma_1 - \sigma_3)$
loading
unloading
b
d
f
h
j
a'
c
e
g
i
a
ϵ_{ax}

SCHEMATIC CYCLIC LOADING TRIAXIAL TEST

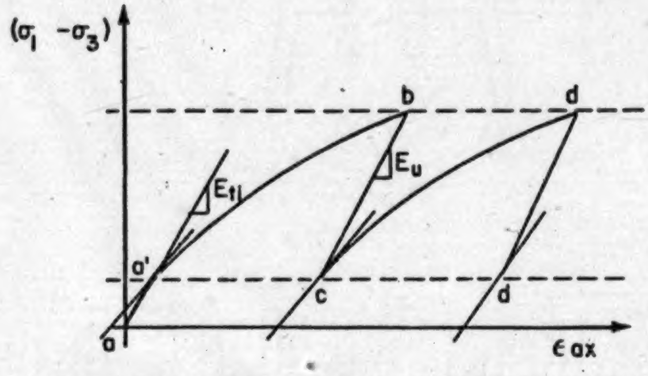
$(\sigma_1 - \sigma_3)$
b
d
E_{ti}
E_u
a'
c
d
a
ϵ_{ax}

SIMULATED CYCLIC LOAD BEHAVIOUR USING CONSTANT HYPERBOLIC MODEL PARAMETERS IN LOADING (ADOPTED FOR THIS STUDY)

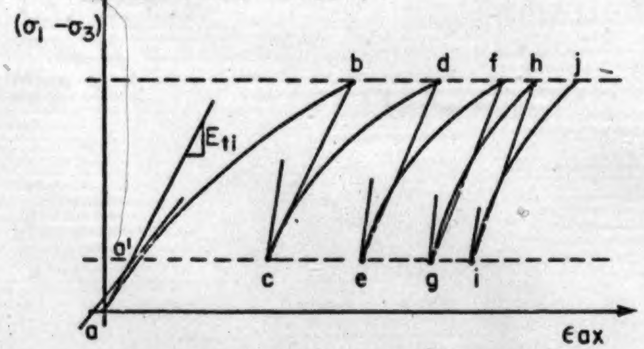
$(\sigma_1 - \sigma_3)$
b
d
f
h
j
E_{ti}
a'
c
e
g
i
a
ϵ_{ax}

SIMULATED CYCLIC LOAD BEHAVIOUR USING VARIABLE HYPERBOLIC MODEL PARAMETERS FROM TEST DATA FOR EACH CYCLE

FIGURE 7.9 SCHEMATIC LOADING/RELOADING RESPONSE.

during loading. On the other hand, any elastic cyclic load model would indicate reloading with no net incremental movement over a cycle. Clearly, the process to be simulated was a relatively stiff unloading and a progressively softer nonlinear reloading. This was handled conveniently using the hyperbolic nonlinear elastic model, as shown in Figure 7.9. The stiffness of the reloading cycle is most open to revision should cyclic tests be carried out on the materials. It was thought to be prudent in the analysis by retaining the original loading stiffness and accepting conservatively large deformations.

The model predictions for cyclic loading are thus not intended to represent predictions of actual movements. Rather, the predictions are consistent with a model developed under reasonable and critically evaluated circumstances. The expected deviation of such a model from the prototype can be assessed knowing that the model is as complex as necessary without *any* unsubstantiated modifications or changes.

7.3 SIMULATION OF CONSTRUCTION

During this phase of the analysis, material parameter values were modified in a manner consistent with knowledge of each material's likely response characteristics. This was necessary in order to calibrate the model against measured field behaviour. Table 7.1 shows the parameter values selected, with the original choices shown in parentheses. The various considerations which lead to these modifications are now described.

Sequential Construction:

The core-trench unloading step was necessary in order to approximate expected local stress concentrations adjacent to the excavation. Weakening and yielding of the shearband was anticipated to start in this region, so it was necessary to be as precise as modelling permitted.

During construction, the actual extent and character of shearzone movement was not fully identified. However, using three lifts was felt to represent a satisfactory compromise between excessive computational costs and acceptable numerical results. The shearband *had* to experience shear failure and significant rigid body motion of overlying material during construction. Modelling by horizontal layers did not exactly match constructed profiles, but this was not felt to be a serious matter particularly regarding postconstruction behaviour.

Figure 7.10 shows horizontal and vertical movement patterns calculated using the originally selected parameters.

The vertical displacements did not duplicate field settlement data from crossarm gauges for the following reason. Each fill increment was about 50 feet thick and so large deformations occurred at the top of each added layer.

TABLE 7.1

MATERIAL PARAMETERS FOR LOADING ANALYSES (see note ⓒ)

MATERIAL	HYPERBOLIC MODEL						SHEARBAND MODEL						
	K	n	c (ksf)	Ø	R_f	ν	E	g_f	n	ν_{VH}	ν_{HH}	c (ksf)	Ø
LOWER SHALE	2500 (1000)	0.1 (0.1)	15.0 (20)	0.0 (18.0)	0.8 (0.9)	0.4 (0.4)	not applicable						
UPPER SHALE	1750 (600)	0.1 (0.1)	2.5 (2.0)	0.0 (18.0)	0.8 (0.9)	0.4 (0.4)	not applicable						
SHEARBAND	1750	0.1	2.5	0.0	0.7	0.4	NOTE Ⓐ (2500)	250 (2.5)	1.0 (2.0)	0.4 (0.25)	0.4 (0.35)	1.0 (0.0)	0.0 (10.0)
CORE AND BLANKET	312.5 (0.6)	0.7 (0.7)	1.0 (1.0)	24.5 (24.5)	0.8 (0.8)	0.4 (0.4)	not applicable						
RANDOM FILL	3125 (0.2)	07 (1.0)	0.0 (0.0)	25.0 (25.0)	0.8 (0.9)	0.4 (0.15)	not applicable						
SHELLS	1250 (3.3)	0.19 (0.19)	0.0 (0.0)	35.0 (35.0)	0.76 (0.76)	NOTE Ⓑ "	not applicable						

NOTES

A E_v values computed using hyperbolic model parameters shown.

B Poissons ratio allowed to vary using G=0.33, F=0.15, d=14.0 following data in Soriano et.al. (1976). Approximate value 0.33.

C Values shown in parentheses were initial parameters, chosen at start of project. The final parameters indicated were selected after assessment of model performance during embankment construction simulation.

D For all materials, γ=125 pcf. For foundation materials, K_o=1.0.

E All parameters are described in Simmons (1980b)

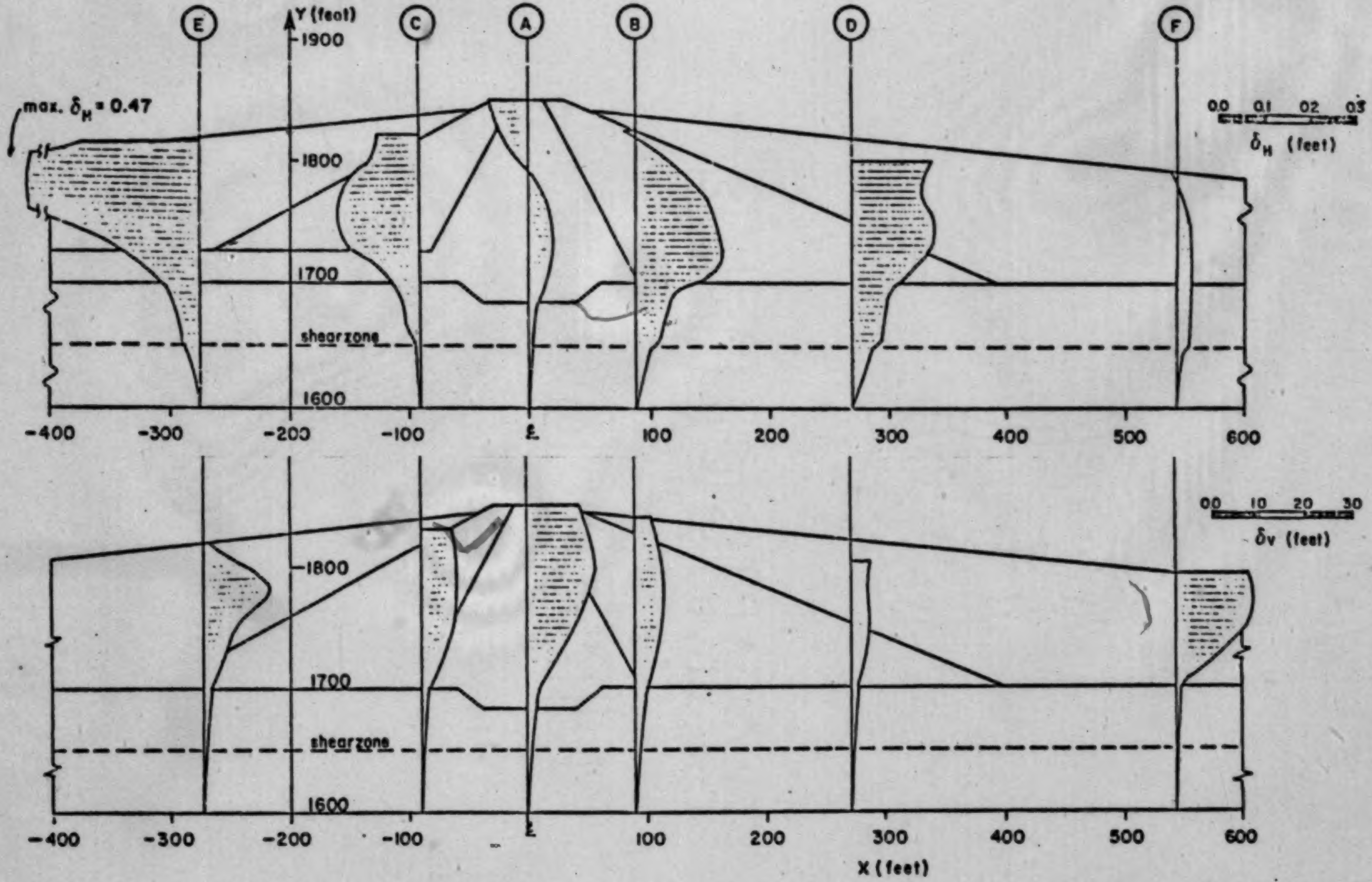

FIGURE 7.10 DISPLACEMENT PATTERNS FOR FIRST TRIAL CONSTRUCTION.

However, crossarm gauge arms are zeroed at the time of installation, so that the top of any fill increment implicitly registers zero movement. The finite element results can be corrected to coincide with the method of field measurement, and by doing so the deformations were in reasonably good agreement with field data. As a general rule, the corrections were not made subsequently because it was the relative pattern of deformations, rather than close actual comparison with field data, which was important.

The dominant rigid-body style of slip on the shearband was not reproduced in the original analyses. The major material property controlling this response was found to be the operational modulus of the foundation shale, above and including the shearband. The magnitude of operational axial strain necessary to accommodate the spreading of the materials above the shearband meant that the operational modulus had to be low and representative of yield. Since yielding is controlled by the operating deviator stress, it was found that the strength of the upper shale had to be reduced to about 17% of that of the lower shale in order to modify response sufficiently.

It was decided to always specify undrained shear strength as the operational strength control in subsequent analyses. This seemed appropriate in light of the field behaviour of these materials. Since the upper shale was more weathered and had probably been incorporated in mass movements in the past, it was quite reasonble to accept a significant reduction of operational strength in this material.

Tension Removal Procedures:

The final end-of-construction analysis did contain locally excessive tensions in the random fill and shell zones. It was necessary to accept this rather than to pursue somewhat elusive refinements to the material response parameters. A tension-reduction procedure was developed, based upon the method of Zienkiewicz *et.al.* 1968. The option of using this procedure was exercised when felt necessary in subsequent analyses.

End-of-Construction (EOC) Results:

Parameters for the final EOC analysis are also given in Table 7.1. A tension-reduction adjustment was carried out. Selected deformation profile lines were used as the basis for assessment of deformations for this stage and subsequent stages of the analysis. Locations of these lines are shown in Figure 7.11.

Figure 7.12 shows the pattern of horizontal movements at the selected profile lines. Comparison with Figure 7.10 demonstrates that the desired patterns of discrete, intense shear along the shearband and essentially rigid-body motion above the shearband were successfully simulated. A tendency for upstream-directed movement of higher elevations of fill material may be noted: this is a consequence of the low

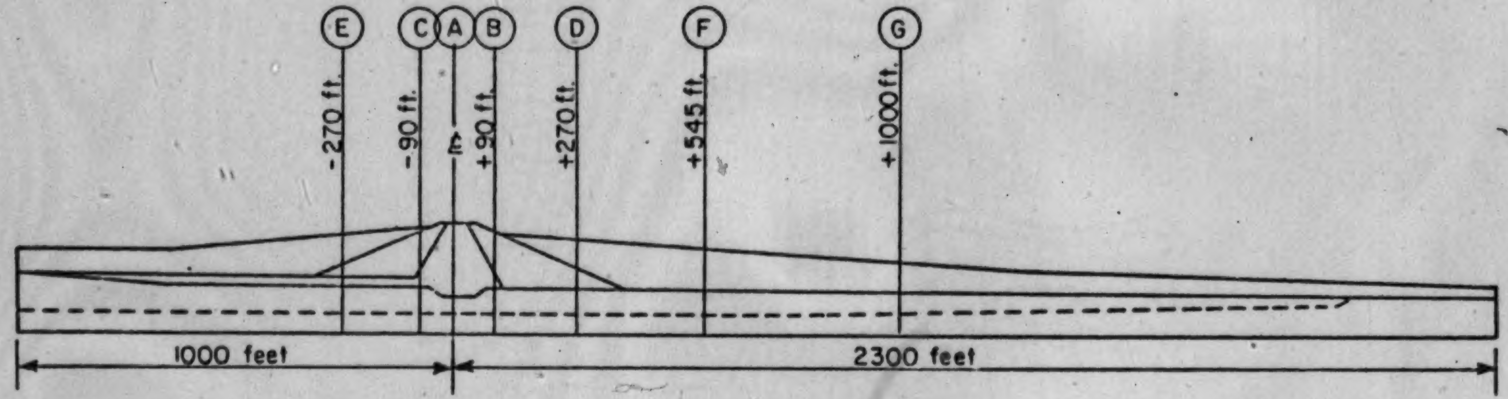
E
C
A
B
D
F
G
-270 ft.
-90 ft.
℄
+90 ft.
+270 ft.
+545 ft.
+1000 ft.
1000 feet
2300 feet

FIGURE 7.11 LOCATIONS OF MOVEMENT MEASUREMENT LINES.

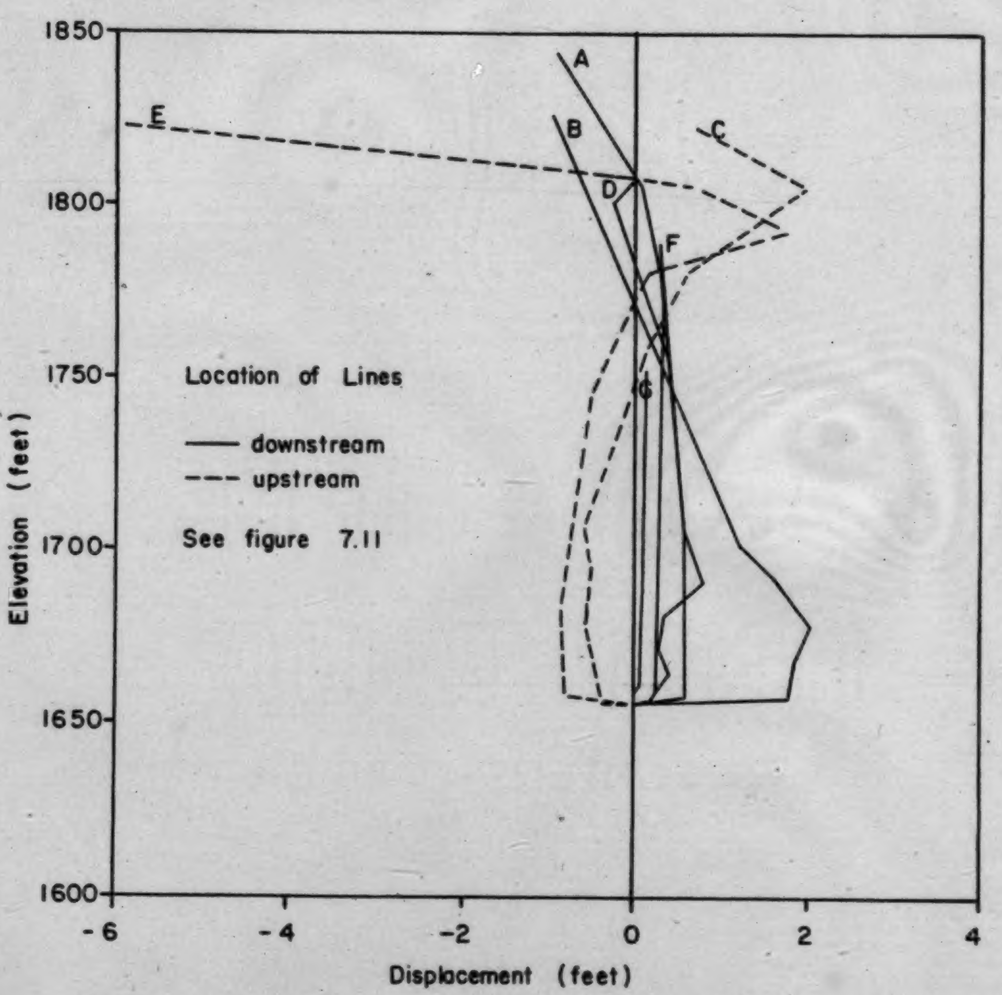

FIGURE 7.12 TOTAL HORIZONTAL MOVEMENT PREDICTIONS TO END-OF-CONSTRUCTION.

values of (isotropic) stiffness adopted for the random fill zones.

The shearband stress state at EOC is indicated in Figure 7.13 by a plot of normalized shear stress as a function of horizontal distance along the band. The normalizing parameter Su is the bedding plane shear strength of 1000 psf. There are two points at each X-location, representing upper and lower stress sampling points for the shearband elements. Two such points having significantly different stresses are a measure of numerical instability or lack of mesh refinement.

Locally more severe numerical instability is indicated in the region of greatest slip movement. The stresses arise from differentiation of the element displacement field and therefore do not have the same order of accuracy. The points are deliberately not connected in Figure 7.13 in order for the reader to use individual best judgement in smoothing the data. At one location, element stresses exceed the strength by about 20%, which reflects a lack of detail in the mesh and is not considered serious. While the numerical accuracy of individual data points may be questioned, *there is no doubt in concluding that non-uniform spreading of the embankment increased the tendency for downstream slip without any effects of reservoir thrust.*

Also noteworthy from Figure 7.13 is the fact that some downstream-directed shear stress was generated in the shearband upstream of the embankment axis. The reason for

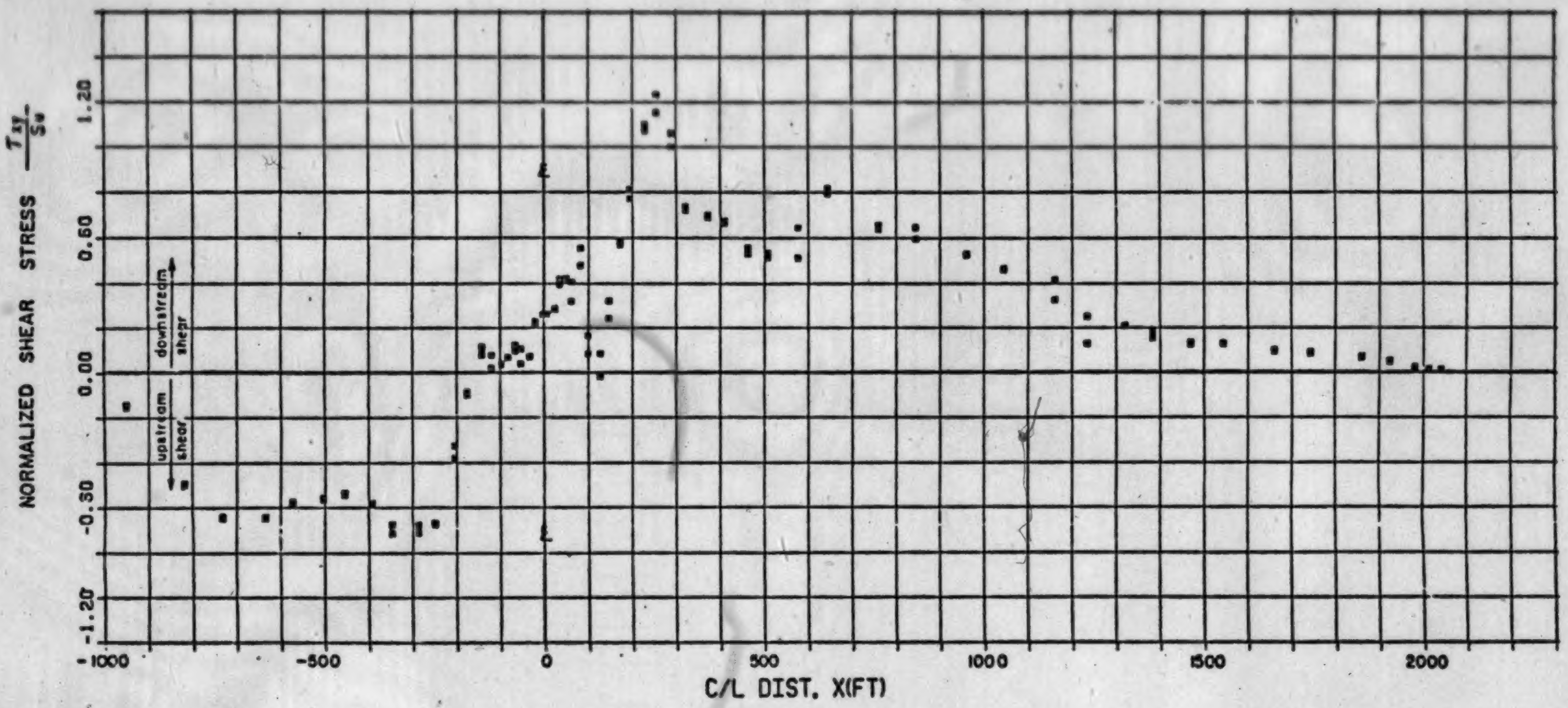

FIGURE 7.13 SHEARBAND STRENGTH MOBILIZATION PREDICTIONS FOR E.O.C.

this is that load is transferred directly from the embankment to the downstream foundation through stiff shell material, whereas this does not occur upstream of the centreline. The net result is a more direct downstream thrust under construction loading. Other likely reasons for this behaviour, such as full restraint of shearing at the upstream extremity of the mesh and reduced stiffness of material above the downstream portion of the shearband, proved not to contribute significantly.

In terms of mobilized total stress friction angles, the maximum smoothed value is about 3°. Depending upon pore pressures within the shearband at the time, this still represents very low strength of the insitu shearzone.

Figure 7.14 shows the development of shearband slip during construction. *It is obvious that the major proportion of all deformation up to EOC occurred during the last construction step*, due to the addition of the relatively small fill volume above elevation 1800 feet. This history is consistent with that of the prototype, and can be expected when weak materials are stressed close to yielding where incremental deformation moduli are very low.

7.4 SIMULATION OF OPERATION

Three phases of operation had to be considered:

1. First Reservoir Filling;
2. Cyclic Reservoir Operation; and

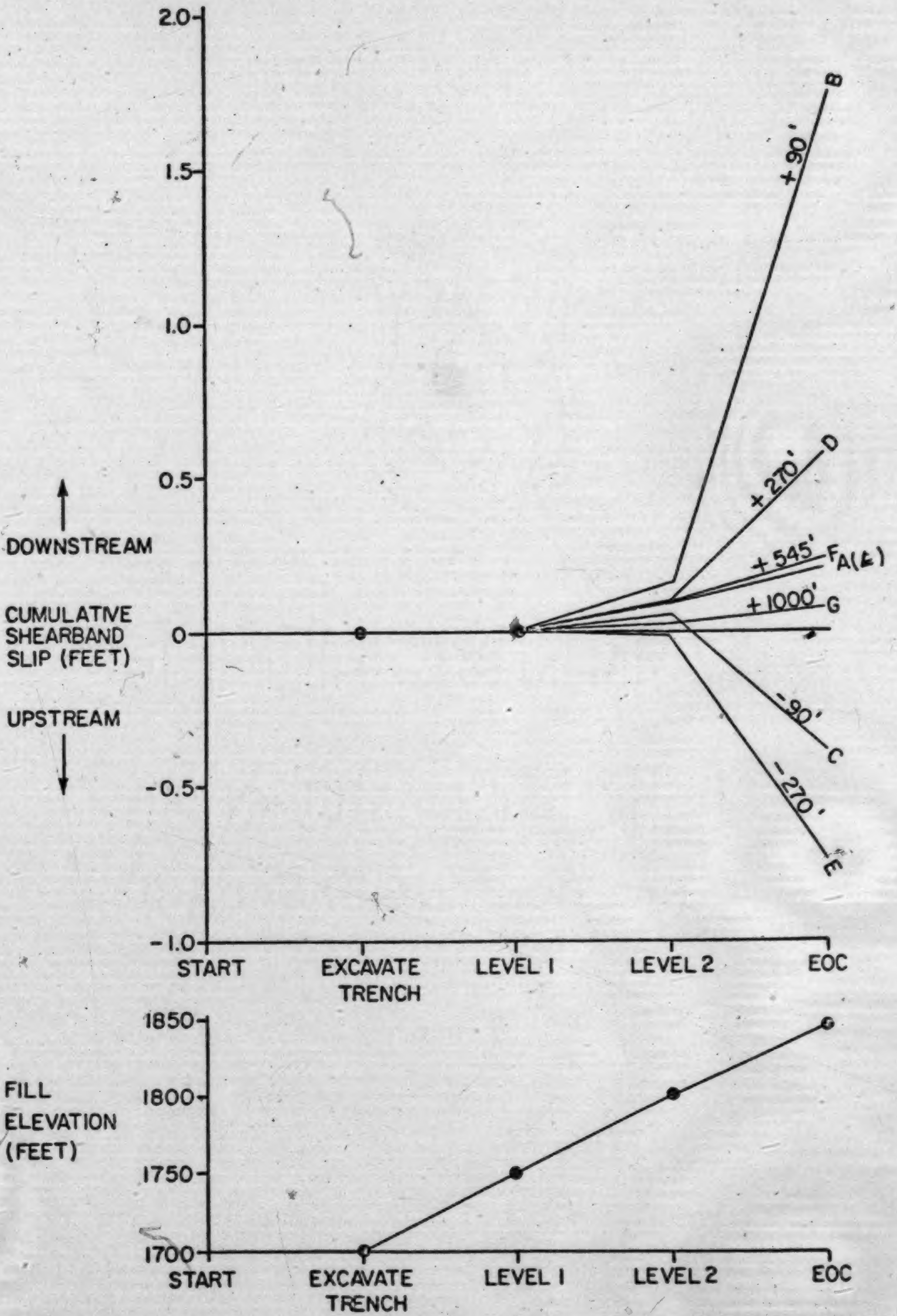

FIGURE 7.14 SHEARBAND SLIP PREDICTIONS DURING CONSTRUCTION

3. Mechanisms for Reducing Shearband Slip.

First Reservoir Filling:

Two analyses of impounding were made, considering both the "as-is" and "tension-adjusted" EOC results. For the "as-is" case, water loads were applied in two steps:

a. from EOC (water entry level, el. 1775 feet) to Low Water Level (LWL, el. 1800 feet);

b. from EOC to Full Supply Level (FSL, el. 1827 feet). For the "tension-adjusted" case, only the step from EOC to FSL was recalculated.

Incremental embankment movements due to impounding (EOC to FSL) are shown on Figure 7.15 for the "tension-adjusted" case. A pattern of shearband slip with essentially rigid-body motion of overlying material was obtained. Some tendency for the upstream random fill zone to restrain downstream movement of the higher fill zones upstream is evident in the pattern for line E.

Figure 7.16 shows the incremental shearband slip during impounding as a function of horizontal distance along the band. Obviously, most of the slip occurs during the higher reaches of water level, in accordance with field measurements (Jaspar and Peters, 1979). The effect of the tension adjustment is not large, but as might be expected there is less upstream restraint and hence a tendency for more slippage to occur upstream.

Shearband strength mobilization is shown in Figure 7.17 for the "tension-adjusted" case. By comparison with Figure

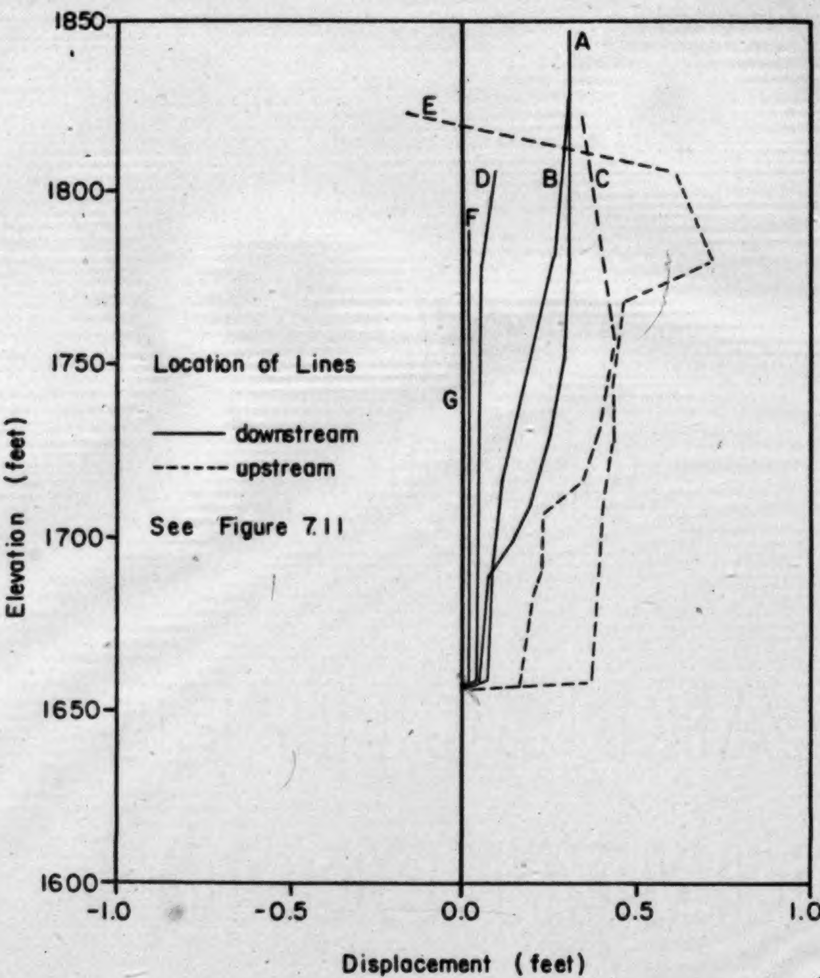

FIGURE 7.15 INCREMENTAL HORIZONTAL MOVEMENT PREDICTIONS DURING IMPOUNDING.

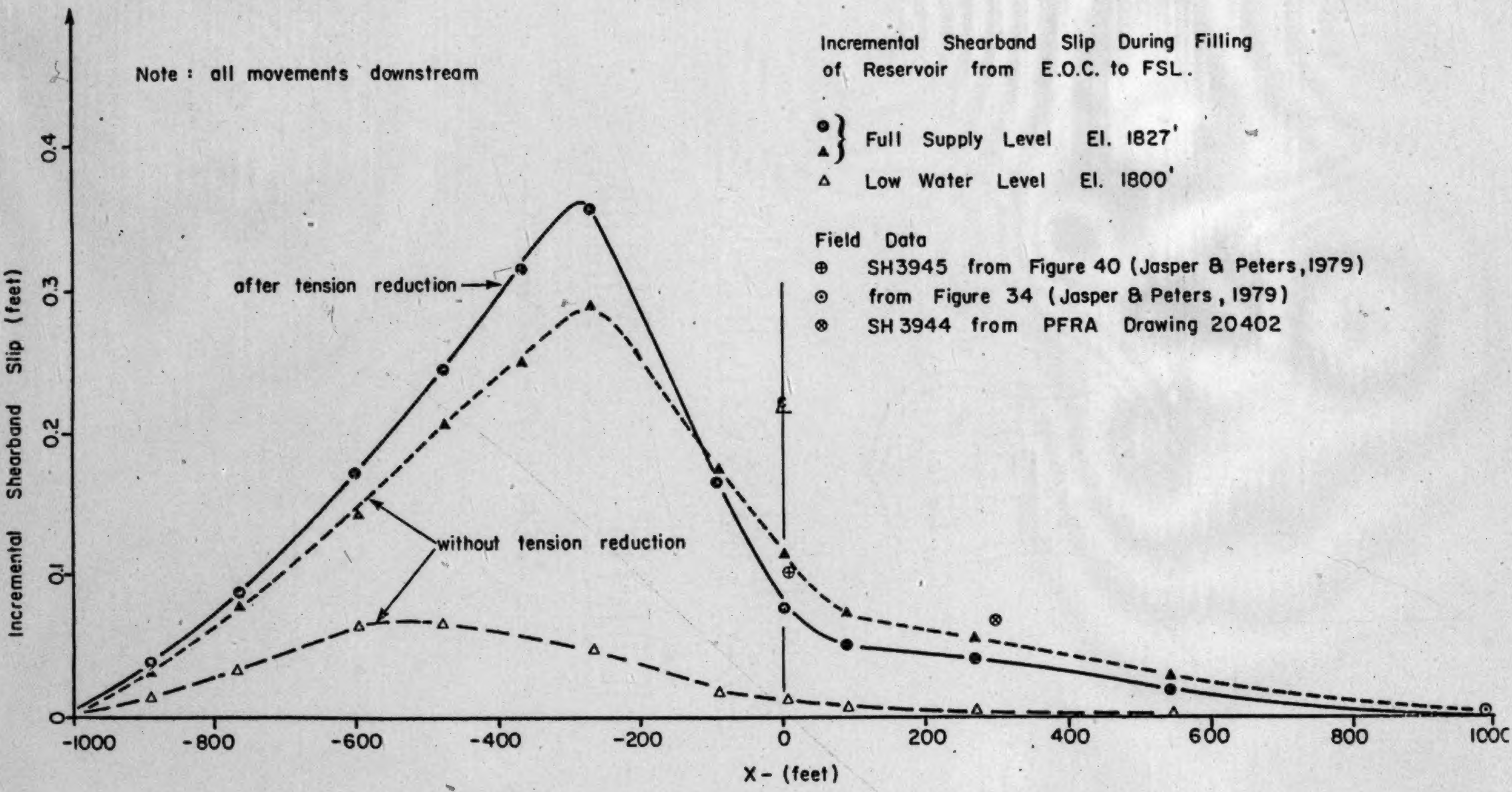

FIGURE 7.16 SHEARBAND SLIP PREDICTIONS DURING IMPOUNDING.

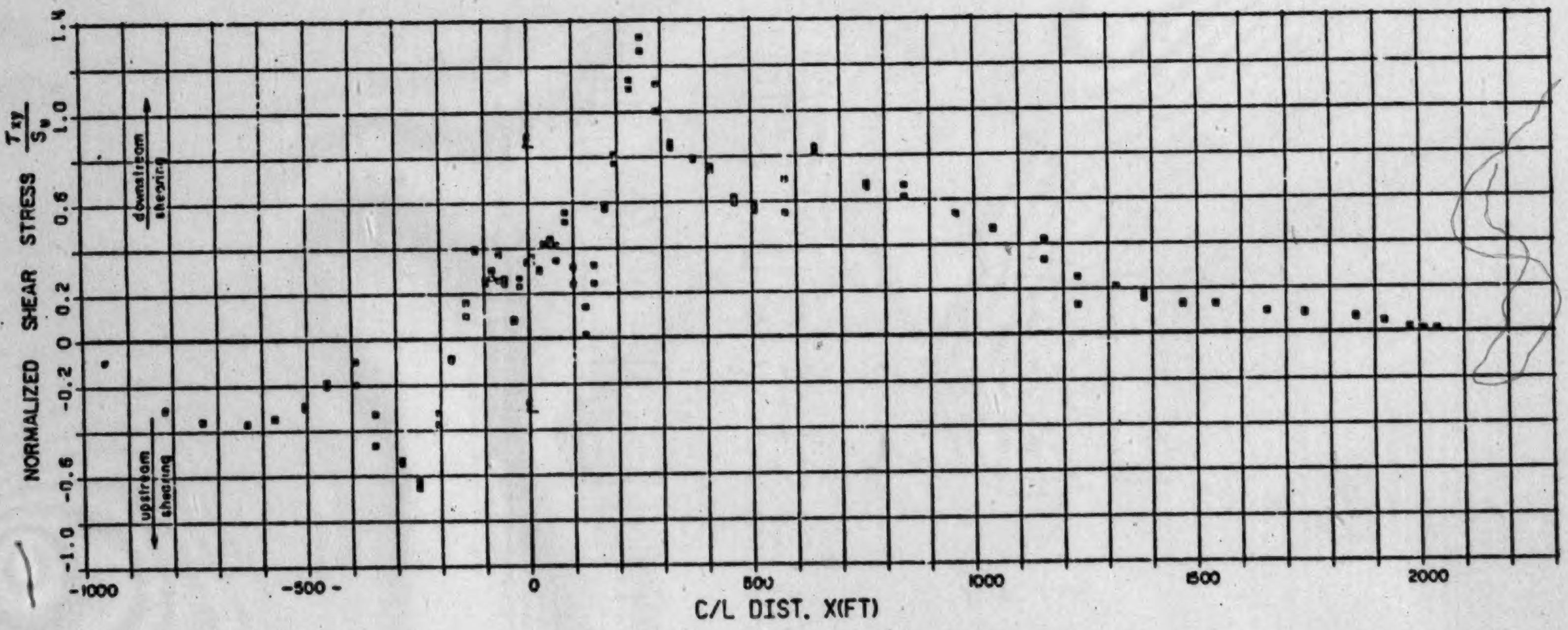

Su = 1.0 Ksf, shearband shearing

FIGURE 7.17 SHEARBAND STRENGTH MOBILIZATION PREDICTIONS FOR IMPOUNDING.

7.13, downstream strength mobilization is somewhat higher while upstream mobilization has been reduced significantly. Without a rather exhaustive investigation it was not possible to tell whether the EOC upstream shear was transferred downstream entirely along the band or carried to some extent by extra compression and principal stress rotation in the upper foundation and fill.

The mobilized total stress friction angles have a maximum smoothed value between 3° and 4°, not significantly different from the EOC case.

It is concluded that impounding of the reservoir was modelled quite successfully despite local zones of unsatisfactory tensile stress. There is excellent agreement with measured field behaviour. Reservoir loading apparently has little influence on the shearband beyond about 800 feet downstream, as noted in the field studies.

Cyclic Reservoir Operation:

Careful and complete field records of seasonal reservoir fluctuations and corresponding shearzone slip have enabled a good correlation to be made between reservoir level (expressed as hydrostatic thrust) and slip magnitude (Jaspar and Peters, 1979).

Cyclic response of the embankment materials was simulated in the simplest reasonable manner by maintaining nonlinear parameters during loading and constant linear parameters during unloading. The parameters for the loading portion are given in Table 7.1 while those for linear elastic unloading are given in Table 7.2. This does not consider incremental stiffening with cyclic loading, and should lead to overestimation of cyclic slip. Four cycles were analysed (FSL to LWL, LWL to FSL again constituted one cycle). Both "as-is" and "tension-adjusted" calculations were made.

The cumulative shearband slip over the four cycles is shown in Figure 7.18 for the "as-is" case. Each line refers to a movement profile location as noted in Figure 7.11. At load cycle 3, an attempt was made to control some excessive stress oscillations in two shearband elements by specifying reduced stiffness. The results at cycle 3 thus represent a sensitivity study and indicate a range of acceptable response. No reason could be established for the behaviour of line A at cycle 2. Incremental slips for the "tension-adjusted" analysis were consistently near 80% of those for the "as-is" analysis.

Typical slip increments during a load cycle are shown in Figure 7.19, and the average slip per cycle is presented as a function of location along the shearband in Figure 7.20. The slip movements are quite consistent, apart from the one anomaly noted at line A, and are of the same order of magnitude as those experienced by the prototype. The field data were averaged over many years of observation, because actual reservoir cycles were less regular than those imposed on the model.

TABLE 7.2

LINEAR ELASTIC PARAMETERS FOR "UNLOADING" ANALYSES

MATERIAL	E(ksf)	V	K(ksf)	G(ksf)
LOWER SHALE	6625	0.4	11041	2366
UPPER SHALE	4424	0.4	7374	1580
SHEARBAND (SLIP MODE) *	4424	0.4	7374 (AS FOR LOADING) *	1580
CORE, BLANKET	1207	0.4	2012	431
RANDOM FILL	1207	0.4	2012	431
SHELLS	3115	0.33	3054	1171

NOTE: 1. * The slip mode was introduced in some unloading analyses in an attempt to control shear stress reversals which lead to reloading. The material possessed a hyperbolic modulus model for obtaining incremental K, G and the g_f factor was allowed to vary from 250 to control shear stresses.

2. Based roughly on tangent moduli for stress-strain curves at average confining pressure for each material.

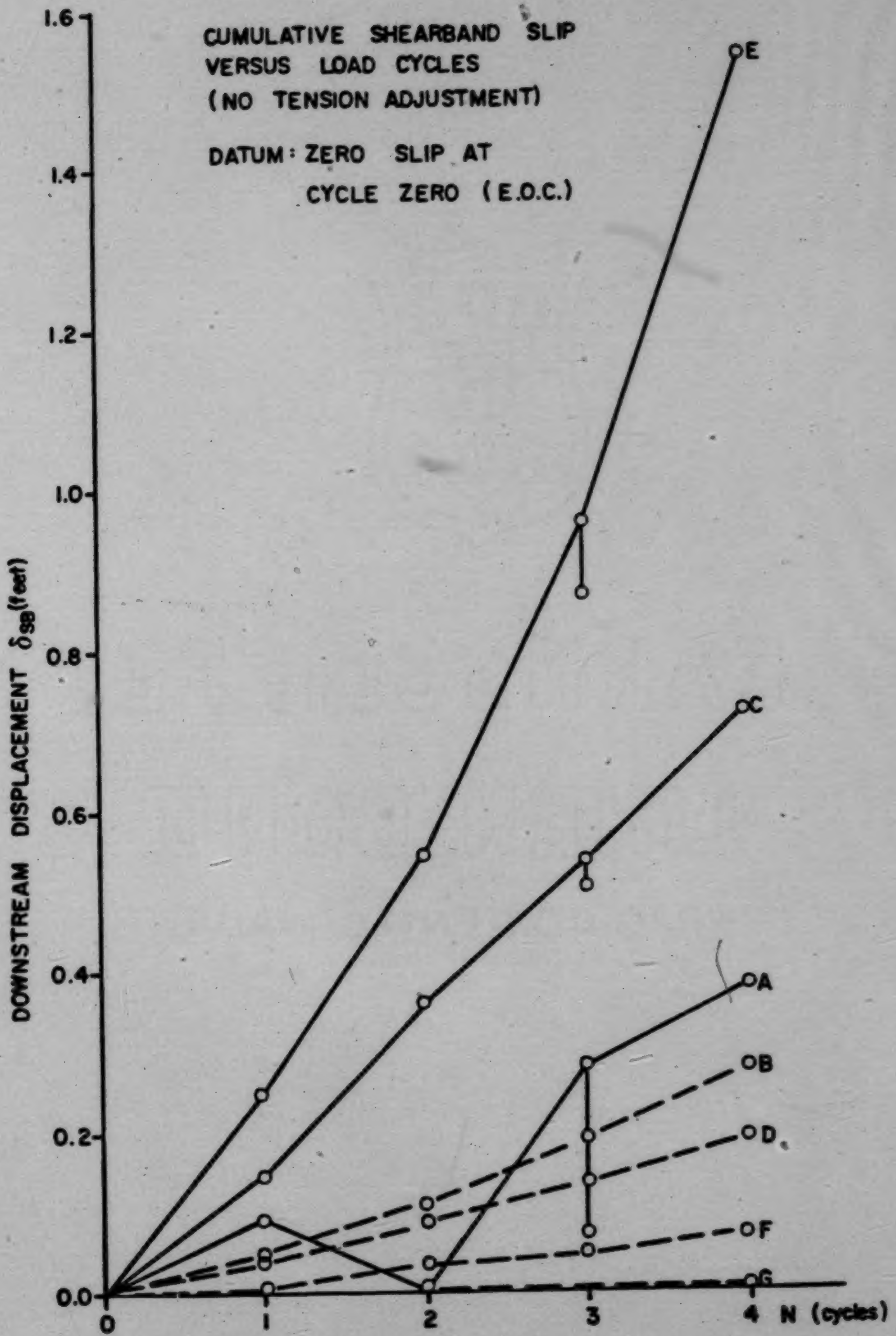

FIGURE 7.18 PREDICTIONS OF CUMULATIVE SLIP FOR CYCLIC LOADING.

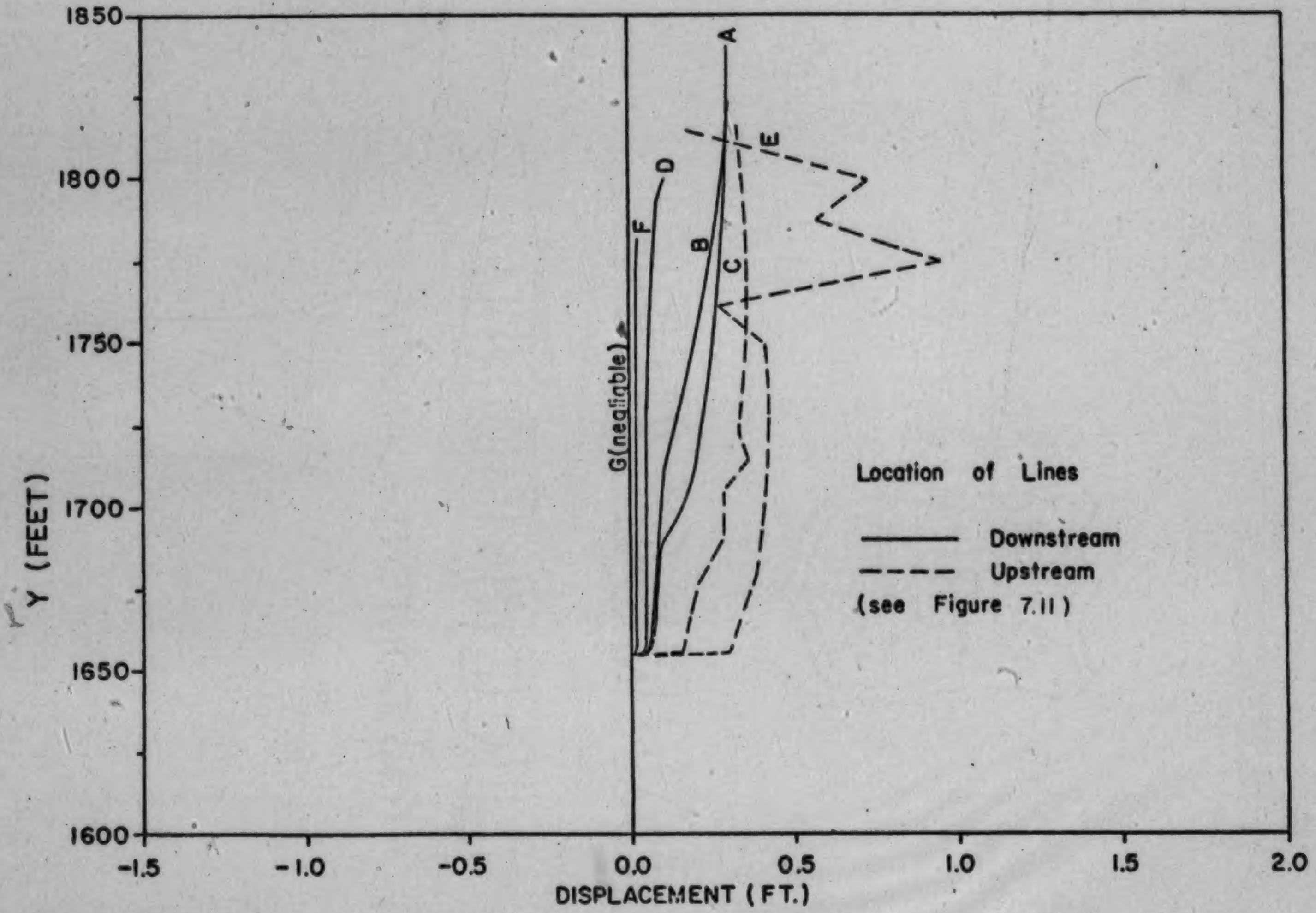

FIGURE 7.19 TYPICAL SHEARBAND SLIP PREDICTION FOR RESERVOIR LOAD CYCLE.

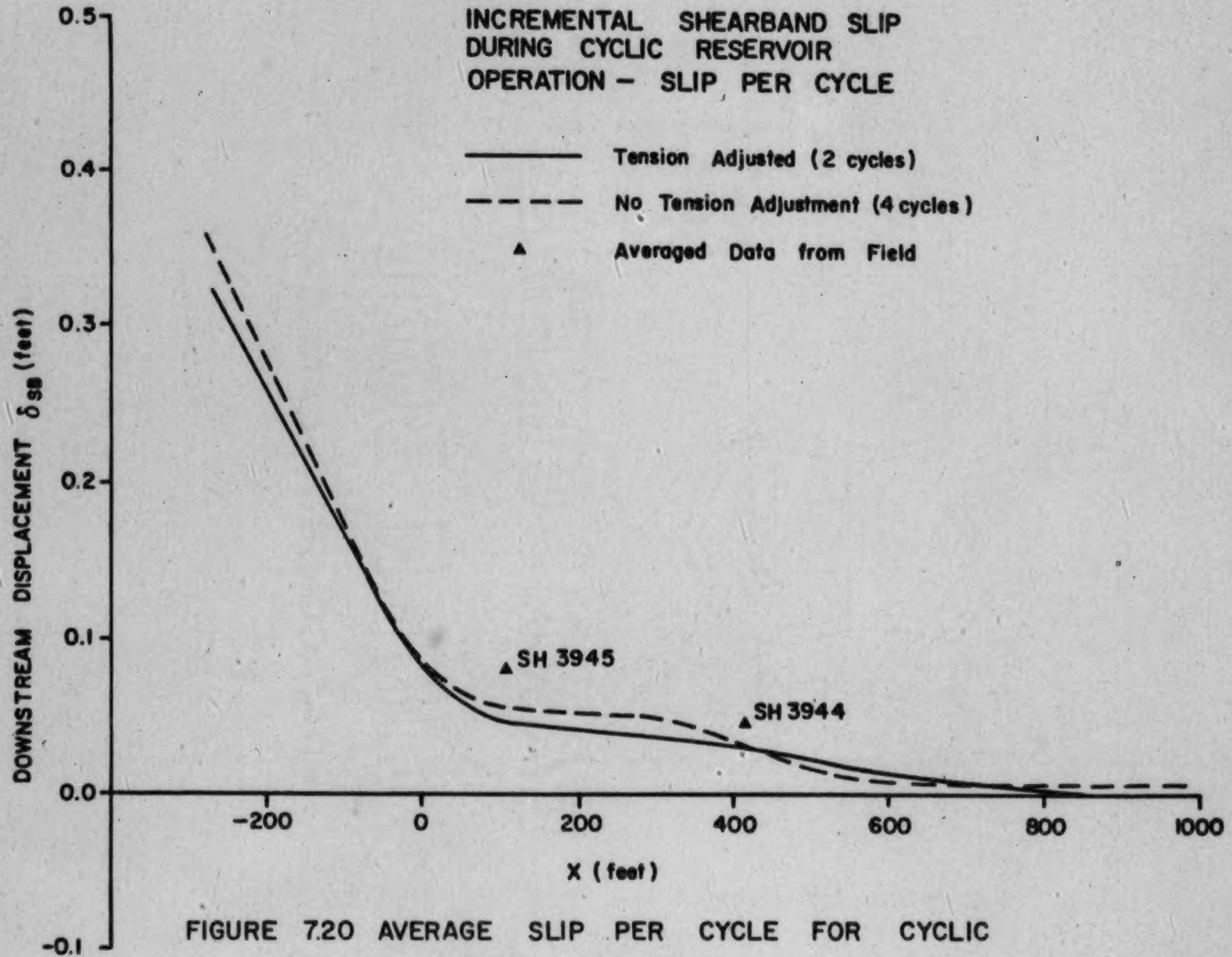

FIGURE 7.20 AVERAGE SLIP PER CYCLE FOR CYCLIC RESERVOIR LOADING.

Numerical accuracy of the stresses deteriorated with cyclic loading. Some effects of the accumulated deformations on the stress state were expected, and ideally these would serve to predict whether cyclic slip increments increased or decreased with time for a given constitutive behaviour. Because of the numerical difficulties encountered, successful simulation was limited to four cycles. *It would not be reasonable to use the results in Figure 7.18 as a basis for predicting longer-term movements, because of the increasing effects of inaccuracies in the stress calculations.*

The numerical capabilities of the model were extended as far as possible by the cyclic load analysis. It was concluded that a more detailed numerical model wih a more refined mesh would be necessary to extend studies of the cyclic load mechanism.

The results show that a cyclic reloading mechanism was responsible for cumulative slippage along the shearzone. *It may be inferred that if the reservoir were to fluctuate between lower operational levels, similar slip movements might be expected although the magnitudes would probably be significantly reduced.*

Mechanisms for Reducing Shearband Slip:

An earlier stability study using limit-equilibrium methods was carried out for Gardiner Dam (Morgenstern and Kaiser, 1978). It was indicated that the *Factors of Safety* could be increased by excavation of portion of the crest and upstream fill, as indicated in Figure 7.21.

It is normal practice to associate increases in Factor of Safety with decreased movements. Once the influence of the soft random fill zone was observed in the finite element analysis, the possible beneficial effects of replacing some random fill with much stiffer material was also raised as a matter for investigation.

Excavation of the crest zone. The removal of crest material was achieved by removing the appropriate elements and applying forces to neutralize the stresses along the new crest surface. (The reservoir was first unloaded to LWL). Cyclic loading was carried out on the modified crest, and incremental slips are compared in Figure 7.22 with incremental slips calculated for the original profile. The overall magnitudes are comparable but the patterns are distinctly different. This can be explained as follows. The incremental nonlinear elastic moduli in the shearband were reduced when the confining stress was decreased by crest unloading, the effect being most pronounced in the critically stressed regions. Thus, further slippage could proceed most easily in the regions where yielding had already occurred. This may not completely reflect field behaviour but is consistent with previous assumptions and so constitutes a valid extension of the model. *It was conluded that the magnitude of shearband slip is primarily a function of the magnitude of cyclic loading, caused by nonlinear and*

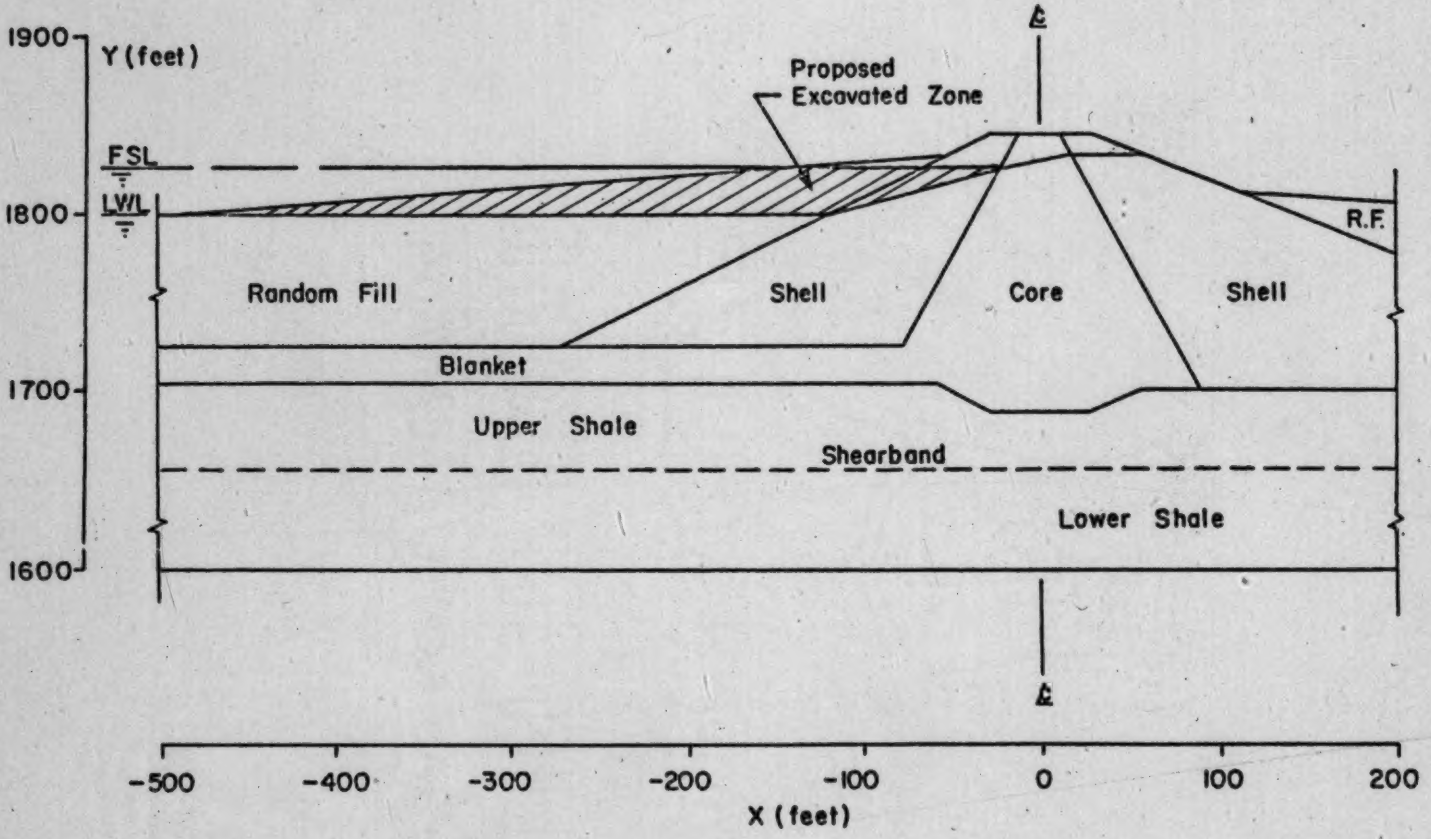
Y (feet)
1900
1800
1700
1600
FSL
LWL
℄
Proposed
Excavated Zone
R.F.
Random Fill
Shell
Core
Shell
Blanket
Upper Shale
Shearband
Lower Shale
℄
-500
-400
-300
-200
-100
0
100
200
X (feet)

FIGURE 7.21 GEOMETRY OF CREST MODIFICATION.

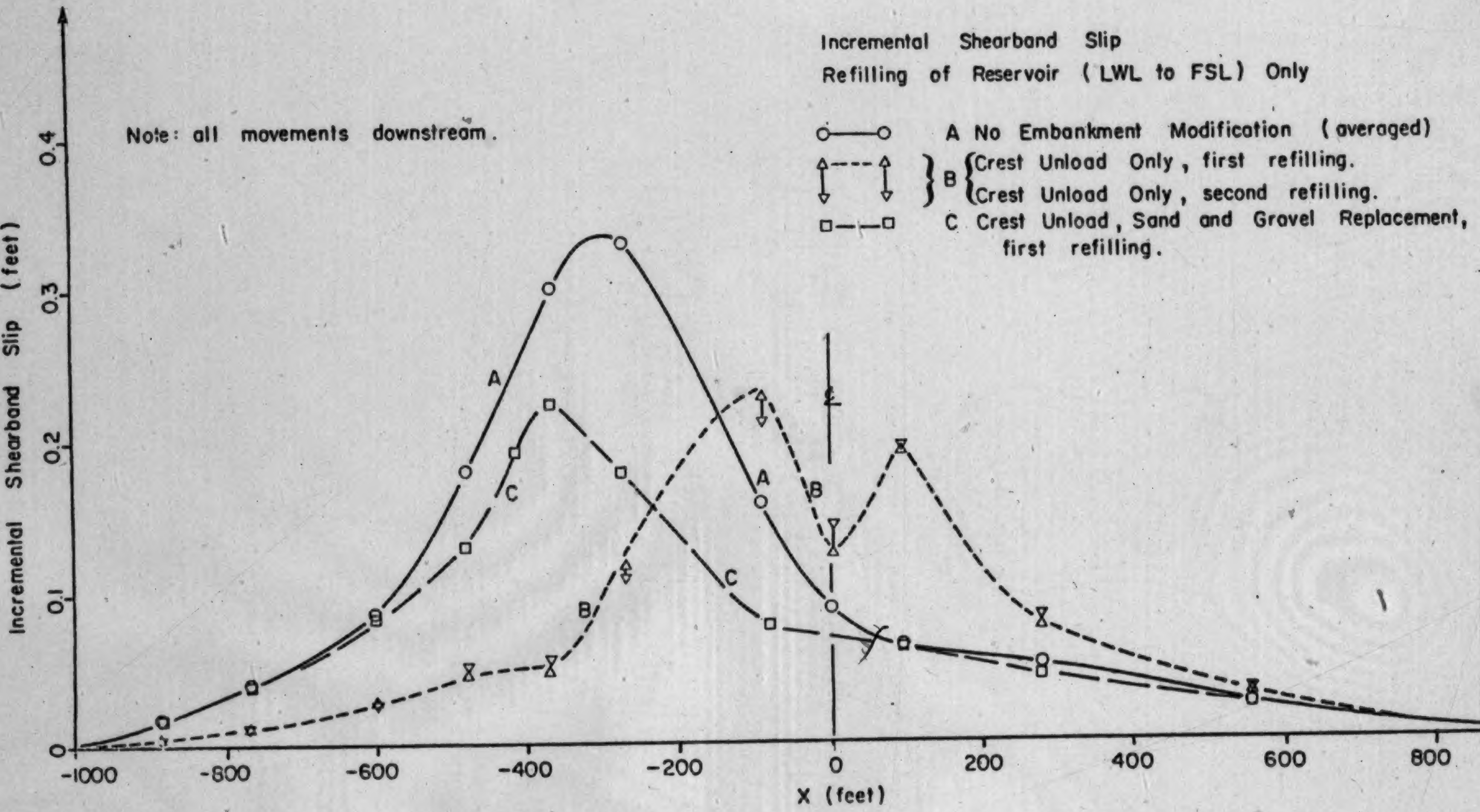

FIGURE 7.22 AVERAGE SLIP PER CYCLE FOR MODIFIED CREST.

hysteretic load-unload response. Unless cyclic loading were to mobilize only the stiffest, initial elastic part of the stress-strain curve, there would still be significant cumulative deformations. The magnitudes of movements are dictated by the level of strength mobilization during loading.

Replacement with strong, stiff fill. The replacement of the excavated zone (Figure 7.21) was simulated by replacing the excavated elements but assigning sand and gravel (shell zone) material properties to them. It was expected that shearband response would be stiffened due to the increased confining pressure. Limit-equilibrium analyses would then show an increase in Factor of Safety associated with stronger material, possibly offset by decreases due to the increment of driving force. As happened during original construction simulation, the additional load produced further shearband slip, with a maximum of about 1.5 feet of slip predicted 90 feet downstream of centreline. Spreading of the foundation occurred again, with some upstream slip occurring upstream of centreline, but predominantly downstream movements. Incremental shearband slip for refilling the reservoir to FSL are also shown on Figure 7.22. Clearly, the pattern of incremental slip is unaffected by the nature of the uppermost fill, except for some restraint in the upstream areas associated with development of localized tensile stress again. *The model predicted incremental slips comparable in magnitude to those* *experienced during original construction, when replacement fill was added at the crest. These predictions are probably of an unacceptable magnitude.*

7.5 SUMMARY AND CONCLUSIONS

This study has shown that a reasonable model of the Coteau Creek embankment was capable of reproducing deformations similar to those observed in the prototype under conditions of fill placement, impounding, and reservoir operation.

Some numerical problems arose during the analysis. Numerical instability of some critically stressed portions of the shearband proved difficult to control. Zones of tensile stress developed in the upstream random fill zone and along some interfaces of shell and random fill. Reasonable attempts were made to overcome these problems and better performance would be obtained with greater mesh refinement and more detailed constitutive models.

Reliable prediction of deformation behaviour over many load cycles proved to be beyond the capabilities of the present analysis, so there is no indication that the magnitudes of shearband slip would either increase or decrease with time. However, the model was sufficiently accurate to identify clearly the pattern of response to cyclic reservoir operation.

The primary cause of shearzone slip is incremental reservoir loading acting upon materials which undergo nonlinear, hysteretic deformation at high levels of strength mobilization. Field measurements correlating reservoir level with slip magnitude have been confirmed by the model.

Simulation of crest unloading showed that cyclic response was largely unaffected by such modifications. This is at variance with the conclusions of limit equilibrium stability analysis. It was argued, with the stability analysis, that cyclic deformations would be greatly reduced if the modified structure had a Factor of Safety at FSL the same as that for the original structure at LWL. This argument is misleading, being based on the incomplete view that since sustained movements did not occur at LWL, the Factor of Safety at LWL was sufficient to keep slip movements small. When the overall Factor of Safety is low and critical elements of the soil mass have yielded, it is not advisable to relate deformation patterns to Factor of Safety on an empirical basis.

A strong correspondence was obtained between reservoir level and shearband slip magnitude. This was supported by field measurements. *It is concluded that reservoir cycling would cause some incremental slip, no matter what levels of reservoir were involved.* Clearly, the *magnitude* of the increments would depend very much on the actual limits of reservoir water level.

It is strongly suspected that the Coteau Creek shearzone pinches out a few hundred feet upstream of the embankment axis. This can be inferred from an air photograph (Jaspar and Peters, 1979). Therefore, the magnitudes of computed upstream movements may be much larger than is realistic. It would be possible to model the shearband with increasing strength upstream of centreline in order to pinch it out at a given location, should such an investigation be considered worthwhile in the future.

8. SUMMARY, CONCLUSIONS, AND RECOMMENDATIONS

The principal conclusion of this research is that analysis of shearband yielding which involves controlled location (bedding) and non-weakening stress-strain behaviour is now feasible. Two case history analyses have demonstrated the numerical capability which now exists to predict yielding of presheared surfaces.

Conclusions from this research concern four major issues:

1. Comments on perfomance of the numerical models;
2. Discussion of the role of deformation analysis in design for progressive failure problems;
3. Conclusions as to areas most warranting further research; and
4. Recommendations resulting from this research.

8.1 PERFORMANCE OF THE NUMERICAL MODELS

Appropriate analytical procedures have been developed only for non-weakening materials. As described in Chapter 5, the postpeak weakening material models are fairly simple and straightforward by themselves. The Stress Dilatancy model is satisfactory for processes within a defined shearzone; but the Post Peak Plasticity model, being more phenomenological, can simulate more generally a zone within which a shearzone is controlling response. However, the numerical procedures for obtaining equilibrium solutions for heterogeneous deformation modes are immature.

Certain features of the numerical models are unashamedly approximate, and it may well be that simpler and more convenient means of stating and achieving the same objectives can readily be found. It was the intention of this research to make the complexities of nonlinear analysis as accessible as possible, and this has been a prime motivation for all the procedures undertaken.

The elastoplastic approach is considered to be far superior to the nonlinear elastic approach for obtaining stable numerical behaviour when shearband yield is simulated. However the equilibrium iteration procedure is expensive, making nonlinear elastic analysis a more economical tool.

One important conclusion stands out in connection with the models. Numerical analysis is an art, and like any other art demands patience, skill, and experience. Practical geotechnical engineering is usually far removed from the realms of numerical analysis, and unfortunately this leads to too great an emphasis on results rather than what is involved in getting the results. There are difficulties in "bridging the gap" from analysis to practice, and the writer's efforts in developing the models have had this concern always in mind. No apologies are therefore made to the analytical purists or those who deal solely with the results, as it is felt that this thesis contains much material which bridges the gap.

8.2 ROLE OF DEFORMATION ANALYSIS

Speaking solely in terms of problems which involve yielding of shearbands, the case history analyses in this thesis illustrate the unique value of numerical analysis in evaluating field performance. From a *design* point of view, it is now felt that a controlled-location deformation analysis can assume the rightful role of informing designers of the consequences of various options they may exercise.

The role of microstructural processes is so dominant in shearband yielding that analysis must take into account all of the known or suspected geological factors applicable to a given site or situation. The analyst must either be familiar with geological processes, or be interfaced *effectively* with others who are geologically aware.

In many cases, lack of data or funding will preclude full-scale deformation analysis. The simpler one-dimensional models allow for effective manipulation of the various parameters at play, and are a necessary prerequisite to deformation analyses in any event. There are still difficulties in applying limit equilibrium analysis to shearband problems. Deformation performance, and hence tolerance to failure, is not simply related to the standard means by which Factors of Safety are used in design, as borne out by the Gardiner Dam analysis. Each form of analysis is appropriate in its own context. The problem of progressive failure is as much a problem of human insight as it is an unapproachable physical process.

There is still no satisfactory means for dealing with shearzone development or progressive failure in uncontrolled situations. The classical retaining wall problem is a prime example of such a situation. Fortunately, analyses which do not recognize shearband behaviour still appear to offer good predictions of response (Evgin, 1981). It is tempting to conclude that under uncontrolled conditions, shearband modes do not dominate overall structural deformations as they do for problems of controlled locations. Were this the case, however, there is no reason why shearbands should occur at all in uncontrolled conditions. Clearly, much research work still remains to clarify this aspect of shearband behaviour.

8.3 AREAS MOST WARRANTING FURTHER RESEARCH

Numerical Procedures:

Quite obviously, *improved convergence procedures* have to be developed for handling shearband strain weakening. It is likely that the most satisfactory procedures would involve tangential, rather than constant initial, stiffness during equilibrium iteration.

Localization inception and propagation are at present "grey areas". The mathematical problems are formidable, and it is not yet possible to simplify the present state-of-the-art to practically oriented techniques.

Tensile yielding has long been recognized in analysis of geotechnical problems. The procedures for dealing with tension reduction are crude and converge slowly. Amongst a number of possible remedies, it is suggested that substructuring, with suitable orthotropic material models, be employed to prevent cyclic recurrence of tensile stress in equilibrium iterations.

Progressive Failure:

The progressive failure problem is intimately related to conditions causing delayed failure. There is no field evidence as yet for first-time slides involving true progressive failure, but the evidence for geologically controlled delayed failure has been found frequently. Case history experience must be developed both to confirm present understanding of these problems, and to further develop rational design approaches to progressive failure.

Dilatancy:

Most dense-structural earth materials dilate during yielding, particularly when stress paths involve unloading. Discussion in this thesis has been confined largely to problems of progressive failure in slopes. It must not be forgotten that other equally demanding progressive failure problems exist, however. A prime example is the behaviour of locked sands. The Stress Dilatancy model could be expected to clarify many of the attempts made to evaluate *in situ* strengths for such materials. However, such developments await more stable computational procedures.

8.4 RECOMMENDATIONS FOR FUTURE WORK

Firstly, it is recommended that more attention be paid to obtaining economical, converged numerical solutions. This should not involve substantial modifications to the computer programs already available.

Secondly, it is recommended that a Stress-Dilatancy model be used in conjunction with diffusion relationships to enable the relationship between dilatancy and temporary "locking" of yielding zones to be explored. This has immediate goals in locked sand research, but longer-term goals in developing understanding of tectonic faulting processes.

Thirdly, every possible effort should be extended in applying the analytical methods outlined in this thesis to field problems. This demands equal effort in describing and documenting significant case histories. A wide variety of problems, not merely progressive failure in clay shales, demands more of such practically oriented numerical analysis.

REFERENCES

Aamodt, B. and Bergan, P.G. 1975. "Numerical Techniques in linear and nonlinear fracture mechanics". In "Computational Fracture Mechanics", E.F. Rybicki and S.E. Benzley eds., A.S.M.E., New York, pp. 199-216.

Arthur, J.R.F., Dunstan, T., Al-Ani, Q.A.J.L., and Assadi, A. 1977. "Plastic deformation and failure in granular media". Geotechnique, Volume 27, Number 1, pp. 53-74.

Atkinson, J.H. and Bransby, P.L. 1978. "The Mechanics of Soils: an introduction to Critical State Soil Mechanics". McGraw-Hill, London, 375pp.

Barden, L. and Khayatt, A.J. 1966. "Incremental strain rate ratios and strength of sand in the triaxial test". Geotechnique, Volume 16, No. 4, pp. 338-357.

Barlow, J. 1976. "Optimal stress locations in finite element models". International Journal for Numerical Methods in Engineering, Volume 10, pp. 243-251.

Barsoum, R. 1976. "On the use of isoparametric finite elements in linear fracture mechanics". International Journal for Numerical Methods in Engineering, Volume 10, pp. 25-37.

Barsoum, R.S. 1977. "Triangular quarter-point elements as elastic and perfectly-plastic crack tip elements". International Journal for Numerical Methods in Engineering, Volume 11, No. 1, pp. 85-98.

Barton, N.R. 1971. "Progressive failure of excavated rock slopes". In "Stability of Rock Slopes", Proceedings of the Thirteenth U.S. Symposium on Rock Mechanics, Illinois, pp.139-170.

Barton, N. 1976. "The shear strength of rock and rock joints". International Journal of Rock Mechanics and Mining Sciences and Geomechanics Abstracts, Volume 13, pp. 255-279.

Bathe, K.-J., Wilson, E.L., and Iding, R.H. 1974. "NONSAP A Structural Analysis Program for Static and Dynamic Response of Nonlinear Systems". Report No. UC SESM 74-3, Structural Engineering Laboratory, University of California, Berkeley.

Bathe, K.-J. and Wilson, E.L. 1976. "Numerical Methods in Finite Element Analysis". Prentice-Hall, New Jersey. 528 pp.

Bathe, K.-J. 1978. "ADINA. A Finite Element Program for Automatic Dynamic Incremental Nonlinear Analysis". Report 82448-1, Mechanical Engineering Department, Massachusetts Institute of Technology. Revised second edition.

Bazant, Z.P. 1976. "Instability, ductility, and size effect in strain-softening concrete". Journal of the Engineering Mechanics Division, A.S.C.E., Volume 102, No. EM2, pp. 331-344.

Bazant, Z.P. and Cedolin, L. 1979. "Blunt crack band propagation in finite element analysis". Journal of the Engineering Mechanics Division, A.S.C.E., Volume 105, No. EM2, pp. 297-315.

Bieniawski, Z.T. 1967. "Mechanism of brittle fracture of rock". International Journal of Rock Mechanics and Mining Sciences, Volume 4, pp. 395-430.

Bieniawski, Z.T., Denkhaus, H.G., and Vogler, U.W. 1969. "Failure of fractured rock". International Journal of Rock Mechanics and Mining Sciences, Volume 6, pp.323-341.

Bishop, A.W. 1967. "Progressive failure - with special reference to the mechanism causing it". Proceedings of the Geotechnical Conference, Oslo, Norwegian Geotechnical Institute, Volume II, pp. 143-149.

Bishop, A.W. 1971. "The influence of progressive failure on the choice of method of stability analysis". Geotechnique, Volume 21, No. 2, pp. 168-172.

Bjerrum, L. 1967. "Progressive failure in slopes of overconsolidated plastic clay and clay shales". Journal of the Soil Mechanics and Foundations Division, A.S.C.E., Volume 93, Number SM5, pp. 3-49.

Bridgwater, J. 1980. "On the wirth of failure zones". Geotechnique, Volume 30, No. 4, pp. 533-536.

Brooker, E.W. and Ireland, H.O. 1965. "Earth pressures at rest related to stress history". Canadian Geotechnical Journal, Volume 2, Number 1, pp. 1-15.

Bruce, I. 1978. "The Field Estimation of Shear Strength on Rock Discontinuities". Ph.D. thesis, Department of Civil Engineering, University of Alberta.

Burland, J.B., Longworth, T.I., and Moore, J.F.A. 1977. "A study of ground movement and progressive failure caused by a deep excavation in Oxford Clay". Geotechnique, Volume 27, Number 4, pp. 557-591.

Bushnell, D. 1977. "A strategy for the solution of problems involving large deflections, plasticity, and creep". International Journal for Numerical Methods in Engineering, Volume 11, pp. 683-708.

Byerlee, J.D. and Summers, R. 1976. "A note on the effect of fault gouge thickness on fault stability". International Journal of Rock Mechanics and Mining Sciences and Geomechanics Abstracts, Volume 13, pp. 35-36.

Byerlee, J.D., Mjachkin, V., Summers, R., and Voevoda, O. 1978. "Structures developed in fault-gouge during stable sliding and stick-slip". Tectonophysics, Volume 44, pp. 161-171.

Byrne, P.M. and Grigg, R. 1980. "OILSTRESS - A computer program for analysis of stresses and deformations in oilsand". Soil Mechanics Series No. 42, Department of Civil Engineering, University of British Columbia.

Cathie, D.N. and Dungar, R. 1978. "Evaluation of finite element predictions for constructional behaviour of a rockfill dam". Proceedings of the Institution of Civil Engineers, Volume 65, Part 2, September, pp. 551-568.

Chowdury, R.N. 1978. "Propagation of failure surfaces in natural slopes". Journal of Geophysical Research, Volume 83, Number B12, pp. 5983-5988.

Christian, J.T. and Whitman, R.V. 1969. "A one-dimensional model for progressive failure". Proceedings, Seventh International Conference on Soil Mechanics and Foundation Engineering, Mexico City, Volume 2, pp. 541-545.

Christian, J.T., Hagmann, A.J., and Marr, W.A. Jr. 1977. "Incremental plasticity analysis of frictional soils". International Journal for Numerical and Analytical Methods in Geomechanics, Volume 1, No. 4, pp. 343-375.

Cleary, M.P. 1976. "Continuously distributed dislocation model for shear bands in softening materials". International Journal for Numerical Methods in Engineering, Volume 10, pp. 679-702.

Cleary, M.P. 1977. "Fundamental solutions for a fluid-saturated porous solid". International Journal of Solids and Structures, Volume 13, pp. 785-806.

Cleary, M.P. and Bathe, K.-J. 1979. "On tractable constitutive relations and numerical procedures for structural analysis in masses of geological materials". Proceedings of the Third International Conference on Numerical Methods in Geomechanics, Aachen, Volume 1, pp. 15-29.

Cleary, M.P., Bathe, K.-J., and Dong, J.L. 1979. "On tractable contitutive descriptions for analysis of geological materials". Special lecture preprints, 1979 ADINA Conference, available from Department of Mechanical Engineering, Massachusetts Institute of Technology.

Clough, R.W. and Woodward, R.J. III. 1967. "Analysis of embankment stresses and deformations". Journal of the Soil Mechanics and Foundations Division, A.S.C.E., Volume 93, No. SM4, pp. 529-549.

Cobbold, P.R. 1977a. "Description and origin of banded deformation structures. I. Regional strain, local perturbations, and deformation bands". Canadian Journal of Earth Sciences, Volume 14, pp. 1721-1731.

Cobbold, P.R. 1977b. "Description and origin of banded deformation structures. II. Rheology and the growth of banded perturbations". Canadian Journal of Earth Sciences, Volume 14, pp. 2510-2523.

Cook, R.D. 1974. "Concepts and Applications of Finite Element Analysis". Wiley, New York. 402 pp.

Cornforth, D.H. 1964. "Some experiments on the influence of strain conditions on the strength of sand". Geotechnique, Volume 14, No. 2, pp. 143-167.

Cramer, H., Wunderlich, W., Kutter, H.K., and Rahn, W. 1979. "Finite element analysis of stress distribution, induced fracture, and post-failure behaviour along a shearzone in rock". Proceedings of the THird International Conference on Numerical Methods in Geomechanics, Aachen, Volume 2, pp. 505-513.

Crouch, S.L. 1976. "Solution of plane elasticity problems by the Displacement Discontinuity Method. I. Infinite body solution; II. Semi-infinite body solution". International Journal for Numerical Methods in Engineering, Volume 10, pp. 301-343.

Dang, M.T. and Magnan, J.P. 1977. "Application des modeles elastoplastiques de l'Universite de Cambridge au calcul du comportement d'un remblai experimental sur sols mous". Rapport de recherche LPC No74, Laboratoire Central des Ponts et Chaussees, France.

Davis, E.H. 1969. "Theories of plasticity and the failure of soil masses". Chapter 6 in "Soil Mechanics Selected Topics", I.K. Lee ed., Butterworth, London.

Davis, E.H. and Booker, J.R. 1974. "The significance of the rate of plastic work in elasto-plastic analysis". Research Report R242, School of Civil Engineering, University of Sydney, Australia.

de Josselin de Jong, G. 1959. "Statics and Kinematics in the Failable Zone of a Granular Material". Waltman, Delft.

de Josselin de Jong, G. 1976. "Rowe's stress-dilatancy relation based on friction". Geotechnique, Volume 26, No. 3, pp. 527-534.

Desai, C.S. 1974. "A consistent finite element technique for work-softening behaviour". Proceedings of the International Conference on Computational Methods in Nonlinear Mechanics, J.T. Oden *et.al.* eds., Austin, Texas, pp. 969-978.

Desai, C.S. and Abel, J.F. 1972. "Introduction to the Finite Element Method". Van Nostrand Reinhold, New York. 477 pp.

Desai, C.S. and Christian, J.T. 1977. "Numerical Methods in Geotechnical Engineering". McGraw Hill, New York, 783 pp.

Dong, J.L. 1980. "Analyses of Deformation and Failure in Geological Materials". M.Sc. dissertation, Department of Mechanical Engineering, Massachusetts Institute of Technology.

Drescher, A. and de Josselin de Jong, G. 1972. "Photoelastic verification of a mechanical model for the flow of a granular material". Journal of the Mechanics and Physics of Solids, Volume 20, pp. 337-351.

Drescher, A. 1976. "An experimental investigation of flow rules for granular materials using optically sensitive glass particles". Geotechnique, Volume 26, Number 4, pp. 591-601.

Drucker, D.C. and Prager, W. 1952. "Soil mechanics and plastic analysis of limit design". Quarterly of Applied Mechanics, Volume 10, pp. 157-165.

Duncan, J.M. and Chang, C.-Y. 1970. "Nonlinear analysis of stress and strain in soils". Journal of the Soil Mechanics and Foundations Division, A.S.C.E., Volume 96, No. SM5, pp. 1629-1653.

Duncan, J.M., Byrne, P., Wong, K.S., and Mabry, P. 1978. "Strength, Stress-Strain, and Bulk Modulus Parameters for Finite Element Analyses of Stresses and Movements in Soil Masses". Report Number UCB/GT/78-02 to National Science Foundation, College of Engineering, Office of Research Services, University of California, Berkeley, California, 76 pp., appendix.

Edmond, J.M. and Paterson, M.S. 1972. "Volume changes during the deformation of rocks at high pressures". International Journal of Rock Mechanics and Mining Sciences and Geomechanics Abstracts, Volume 9, pp. 161-182.

Eisenstein, Z. 1974. "Application of finite element method to analysis of earth dams". State-of-the-Art Report, First Brazilian Seminar on Application of the Finite Element Method in Soil Mechanics, Universidade Federal do Rio de Janiero, 71pp.

Eisenstein, Z. and Law, S.T.C. 1979. "The role of constitutive laws in analysis of embankments". Contribution to Geotechnical Engineering Number 10-1979, Department of Civil Engineering, University of Alberta, Edmonton, Alberta.

Elwi, A.A. and Murray, D.W. 1979. "A 3D hypoelastic concrete constitutive relationship". Journal of the Engineering Mechanics Division, A.S.C.E., Volume 105, No. EM4, pp. 623-641.

Elwi, A. 1981. User manual for FEPARCS. Department of Civil Engineering, University of Alberta, Edmonton, Alberta.

Evgin, E. 1981. "Evaluation of an Elasto-Plastic Model". Ph.D. thesis, Department of Civil Engineering, University of Alberta, Edmonton, Alberta.

Evgin, E. and Eisenstein, Z. 1980. "Re-evaluation of work-hardening model". Preprint 80-545, A.S.C.E. Convention and Exposition, Florida, 14 pp.

Gates, R.H. 1972. "Progressive failure model for clay shale". Proceedings of the Symposium on Applications of the Finite Element Method in Geotechnical Engineering, Vicksburg, Mississippi, U.S. Army Corps of Engineers, Waterways Experiment Station, pp. 327-348.

Geertsma, J. 1976. "Numerical treatment of some geomechanical problem areas in oil and natural gas production". Numerical Methods in Geomechanics, C.S. Desai ed., A.S.C.E., New York, Volume II, pp. 759-772.

Ghaboussi, J., Wilson, E.L., and Isenberg, J. 1973. "Finite element for rock joints and interfaces". Journal of the Soil Mechanics and Foundations Division, A.S.C.E., Volume 99, No. SM10, pp. 833-848.

Goodman, R.E., Taylor, R.L., and Brekke, T.L. 1968. "A model for the mechanics of jointed rock". Journal of the Soil Mechanics and Foundations Division, A.S.C.E., Volume 94, No. SM3, pp. 637-659.

Goodman, R.E. and Dubois, J. 1972. "Duplication of dilatancy in analysis of jointed rock". Journal of the Soil Mechanics and Foundations Division, A.S.C.E., Volume 98, No SM4, pp. 399-422.

Green, G.E. and Bishop, A.W. 1969. "A note on the drained strength of sand under generalized strain conditions". Geotechnique, Volume 19, No. 1, pp. 144-149.

Gudehus, G. and Wichter, L. 1977. "Case study of a landslide in jointed and layered red marl". Proceedings of the International Symposium on Geotechnics of Structurally Complex Formations, Capri, Italy, Volume I, pp. 269-280.

Hibbit, H.D. 1977. "Some properties of singular isoparametric elements". International Journal for Numerical Methods in Engineering, Volume 11, pp. 180-184.

Hill, R. 1950. "The Mathematical Theory of Plasticity". Clarendon Press, Oxford.

Hinton, E., Scott, F.C., and Ricketts, R.E. 1975. "Local least squares stress smoothing for parabolic isoparametric elements". International Journal for Numerical Methods in Engineering, Volume 9, pp. 235-238.

Hoeg, K. 1972. "Finite element analysis of strain softening clay". Journal of the Soil Mechanics and Foundations Division, A.S.C.E., Volume 98, No. SM1, pp. 43-58. See also discussion and closure in same publication: Lo and Lee, Volume 98, No. SM9, pp. 981-983; and Hoeg, Volume 99, No. SM12, pp. 1167-1168.

Hoeg, K., Christian, J.T., and Whitman, R.V. 1968. "Settlement of strip load on elastic-plastic soil". Journal of the Soil Mechanics and Foundations Division, A.S.C.E, Volume 94, No. SM2, pp. 431-445.

Holzhausen, G. 1977. "Axial and subaxial fracturing of Chelmsford Granite in uniaxial compression tests". Proceedings of the Eighteenth U.S. Symposium on Rock Mechanics, Keystone, Colorado, pp. 3B7-1 to 3B7-7.

Horne, M.R. 1965. "The behaviour of an assembly of rotund, rigid, cohesionless particles", Parts I and II. Proceedings of the Royal Society of London, Volume 286 Series A, pp. 62-97.

Houlsby, G.T. and Wroth, C.P. 1980. "Strain and displacement discontinuities in soil". Journal of the Engineering Mechanics Division, A.S.C.E., Volume 106, Number EM4, pp. 753-771.

Ingraffea, A.R. 1977. "Discrete Fracture Propagation in Rock: Laboratory Tests and Finite Element Analysis". Ph.D. thesis, Department of Civil Engineering, University of Colorado at Boulder, Colorado.

Jaeger, J.C. and Gay, N.C. 1974. "Behaviour of lightly confined granular material". International Journal of Rock Mechanics and Mining Sciences and Geomechanics Abstracts, Volume 11, pp. 295-301.

James, P.M. 1970. "Time Effects and Progressive Failure in Clay Slopes". Ph.D. thesis, Department of Civil Engineering, Imperial College, University of London, England.

Jaspar, J.L. and Peters, N. 1979. "Foundation performance of Gardiner Dam". Canadian Geotechnical Journal, Volume 16, Number 4, pp. 758-788.

Kaiser, P.K. 1979. "Time-Dependent Behaviour of Tunnels in Jointed Rock Masses". Ph.D. thesis, Department of Civil Engineering, University of Alberta, Edmonton, Alberta.

Kaiser, P.K. and Morgenstern, N.R. 1981. "Phenomenological model for rock with time-dependent strength". International Journal of Rock Mechanics and Mining Sciences and Geomechanics Abstracts, Volume 18, pp. 153-165.

Kawamoto, T. and Takeda, N. 1979. "An analysis of progressive failure in rock slopes". Proceedings of the Third International Conference on Numerical Methods in Geomechanics, Aachen, Federal Republic of Germany, Volume 2, pp. 797-808.

Kenney, T.C. 1967. "The influence of mineral composition on the residual strength of natural soils". Proceedings of the Geotechnical Conference, Oslo, Norwegian Geotechnical Institute, Volume I, pp. 123-129.

Kondner, R.L. 1963. "Hyperbolic stress-strain response: cohesive soils". Journal of the Soil Mechanics and Foundations Division, A.S.C.E., Volume 89, No. SM1, pp. 115-143.

Kovari, K. 1977. "Micromechanics model of progressive failure in rock and rock-like materials". Proceedings of the International Symposium on Geotechnics of Structurally Complex Formations, Capri, Italy, Volume I, pp. 307-316.

Kovari, K. 1979. "Models for the interpretation of plastic and brittle behaviour of rocks". Proceedings of the Third International Conference on Numerical Methods in Geomechanics, Aachen, Federal Republic of Germany, Volume 2, pp. 533-544.

Krahn, J. and Morgenstern, N.R. 1979. "The ultimate frictional resistance of rock discontinuities". International Journal of Rock Mechanics and Mining Sciences and Geomechanics Abstracts, Volume 16, pp. 127-133.

Krishnayya, A.V.G. 1973. "Analysis of Cracking of Earth Dams". Ph.D. thesis, Department of Civil Engineering, University of Alberta, Edmonton, Alberta.

Kulhawy, F.H. and Duncan, J.M. 1970. "Nonlinear finite element analysis of stresses and movements in Oroville Dam". Research Report TE-70-2, College of Engineering, University of California, Berkeley. 69 pp.

Ladanyi, B. and Archambault, G. 1970. "Simulation of shear behaviour of a jointed rock mass". Proceedings of the 11th U.S. Symposium on Rock Mechanics, A.I.M.E., pp. 83-104.

Lade, P.V. and Duncan, J.M. 1975. "Elastoplastic stress-strain theory for cohesionless soil". Journal of the Geotechnical Division, A.S.C.E., Volume 101, No. GT10, pp. 1037-1053.

Landes, J.D. and Begley, J.A. 1976. "A fracture mechanics approach to creep crack growth". Special Technical Publication 590, A.S.T.M., New York, pp. 128-148.

Law, K.T. and Lumb, P. 1978. "A limit equilibrium analysis of progressive failure in the stability of slopes". Canadian Geotechnical Journal, Volume 15, pp. 113-122.

Law, S.T.C. 1975. "Deformations of Earth Dams During Construction". Ph.D. thesis, Department of Civil Engineering, University of Alberta, Edmonton, Alberta.

Lawn, B.R. and Wilshaw, T.R. 1975. "Fracture of Brittle Solids". Cambridge University Press, Cambridge, United Kingdom, 204pp.

Lee, K.L. 1970. "Comparison of plane strain and triaxial tests on sand". Journal of the Soil Mechanics and

Foundations Division, A.S.C.E., Volume 96, No. SM3, pp. 901-923.

Leussink, H. and Wittke, W. 1963. "Difference in triaxial and plane strain shear strength, theoretical and experimental investigations". Special Technical Publication 361, A.S.T.M., New York, pp. 77-89.

Lo, K.Y. 1972. "An approach to the problem of progressive failure". Canadian Geotechnical Journal, Volume 9, pp. 407-429.

Lo, K.Y. and Lee, C.F. 1973. "Stress analysis and slope stability in strain-softening materials". Geotechnique, Volume 23, pp. 1-11.

Maltman, A.J. 1977. "Some microstructures of experimentally deformed argillaceous sediments". Tectonophysics, Volume 39, pp. 417-436.

Mandl, G. and Fernandez Luque, R. 1970. "Fully developed plastic shear flow of granular materials". Geotechnique, Volume 20, No. 3, pp. 277-307.

Mandl, G., de Jong, L.N.J., and Maltha, A. 1977. "Shear zones in granular material". Rock Mechanics, Volume 9, pp. 95-144.

MARC Analysis Research Corporation, 1973. User manual for MARC computer program. Volumes 1-8, Palo Alto, California.

Meyer, C. 1973. "Solution of linear equations - state of the art". Journal of the Structures Division, A.S.C.E., Volume 99, No. ST7, pp. 1507-1526.

Meyer, C. 1975. "Special problems related to linear equation solvers". Journal of the Structures Division, A.S.C.E., Volume 101, No. ST4, pp. 869-890.

Morgenstern, N.R. 1977. "Slopes and excavations in heavily over-consolidated clays". Section 3 of "Slopes and Excavations - State of the Art", with co-reporters G. Blight, N. Janbu, and D. Resendiz. Proceedings of the Ninth International Conference on Soil Mechanics and Foundation Engineering, Tokyo, Japan.

Morgenstern, N.R. 1979. "Geotechnical behaviour of clay shales - an overview". General Report to Session II on Behaviour of Natural and Compacted Shales, International Symposium on Soil Mechanics, Oaxaca, Mexico, Mexican Society for Soil Mechanics, 14pp. Preprint.

Morgenstern, N.R. and Tchalenko, J.S. 1967a. "Microscopic structures in kaolin subjected to direct shear". Geotechnique, Volume 17, No. ?, pp. 309-328.

Morgenstern, N.R. and Tchalenko, J.S. 1967b. "Microstructural observations on shear zones from slips in natural clays". Proceedings of the Geotechnical Conference, Oslo, Norwegian Geotechnical Institute, Volume I, pp. 147-152.

Morgenstern, N.R. and Kaiser, P.K. 1978. "Analyses of the stability of Gardiner Dam South Saskatchewan River Project". Report to Chief Engineer, Prairie Farm Rehabilitation Administration, Regina, Saskatchewan, 29pp.

Morgenstern. N.R. and Kaiser, P.K. 1980. "Seepage Analysis for the River Section of Gardiner Dam South Saskatchewan River Project". Report to Chief Engineer, Prairie Farm Rehabilitation Administration, Regina, Saskatchewan, 33pp.

Morgenstern, N.R. and Simmons, J.V. 1980. "A Deformation Analysis of Gardiner Dam South Saskatchewan River Project". Report to Chief Engineer, Prairie Farm Rehabilitation Administration, Regina, Saskatchewan, 98pp., addendum.

Muller-*Salzburg*, L. and Malina, H. 1968. "Schubspannungsverteilung im Progressiven Bruch" ("Distribution of shear stresses in a progressive failure surface"). Felsmechanik u. Ingenieurgeologie, Volume 6, pp. 216-224. (*in German*).

Nayak, G.C. and Zienkiewicz, O.C. 1972. "Elasto-plastic stress analysis - a generalization for various constitutive relations including strain softening". International Journal for Numerical Methods in Engineering, Volume 5, pp. 113-135.

Nobari, E.S. and Duncan, J.M. 1971. "Effects of Reservoir Filling on Stresses and Movements in Earth and Rockfill Dams". Geotechnical Engineering Report Number TE-72-1, Department of Civil Engineering, University of California, Berkeley, California, 186pp.

Oda, M. 1972a. "Initial fabrics and their relationship to mechanical properties of granular material". Soils and Foundations, Volume 12, No. 1, pp. 17-37.

Oda, M. 1972b. "The mechanism of fabric changes during compressional deformation of sand". Soils and Foundations, Volume 12, No. 2, pp. 1-18.

Oda, M. 1972c. "Deformational mechanism of sand in triaxial compression tests". Soils and Foundations, Volume 12, No. 4, pp. 45-63.

Oda, M. and Konishi, J. 1974a. "Microscopic deformation mechanism of granular material in simple shear". Soils and Foundations, Volume 14, No. 4, pp. 25-38.

Oda, M. and Konishi, J. 1974b. "Rotation of principal stresses in granular material during simple shear". Soils and Foundations, Volume 14, No. 4, pp. 39-53.

Oda, M., Koishikawa, I., and Higuchi, T. 1978. "Experimental study of anisotropic shear strength of sand by plane strain test." Soils and Foundations, Volume 18, No. 1, pp. 25-38.

Palmer, A.C. and Rice, J.R. 1973. "The growth of slip surfaces in the progressive failure of over-consolidated clay". Proceedings of the Royal Society of London, Series A, Volume 332, pp. 527-548.

Pande, G.N. and Sharma, K.G. 1979. "On joint/interface elements and associated problems of numerical ill-conditioning". International Journal for Numerical and Analytical Methods in Geomechanics, Volume 3, No. 3, pp. 293-300.

Pariseau, W.G. 1979. "A finite element approach to strain softening and size effects in rock mechanics." Proceedings of the Third International Conference on Numerical Methods in Geomechanics, Aachen, Volume II, pp. 545-558.

Parkin, A.K. 1964. "The Application of Discrete Unit Models to Studies of the Shear Strength of Granular Materials". Ph.D. thesis, University of Melbourne, Australia.

Peano, A., Pasini, A., Riccioni, R. and Sardella, L. 1978. "Adaptive approximations in finite element structural analysis". Istituto Sperimentale Modelli e Strutture, Bergamo, Publication 114, 10 pp.

Peano, A. and Riccioni, R. 1978. "Automated discretization error control in finite element analysis". Istituto Sperimentale Modelli e Strutture, Bergamo, Publication 115, 20 pp.

Peano, A., Szabo, B.A. and Mehta, A.K. 1979. "Self-adaptive finite elements in fracture mechanics". Istituto Sperimentale Modelli e Strutture, Bergamo, Publication 120, 12 pp.

Peng, S. and Johnson, A.M. 1972. "Crack growth and faulting in cylindrical specimens of Chelmsford Granite".

International Journal of Rock Mechanics and Mining Sciences, Volume 9, pp. 37-86.

Poulos, H.G. and Davis, E.H. 1974. "Elastic Solutions for Soil and Rock Mechanics". Wiley, New York, 411 pp.

Poulos, S.J. "The steady state of deformation". Journal of the Geotechnical Engineering Division, A.S.C.E., Volume 107, No. GT5, pp. 553-562.

Prevost, J.-H. 1974. "Soil Stress-Strain-Strength theories based on plasticity theory". Ph.D. thesis, Stanford University, California.

Prevost, J.-H. and Hoeg, K. 1975. "Soil mechanics and plasticity analysis of strain softening". Geotechnique, Volume 25, pp. 279-297.

Ramsay J.G. and Graham, R.H. 1970. "Strain variations in shear belts". Canadian Journal of Earth Sciences, Volume 7, pp. 786-813.

Rennie, B.C. 1959. "On the strength of sand". Journal of the Australian Mathematical Society, Volume 1, Part I, pp. 71-79.

Rice, J.R. 1968. "A path-independent integral and the approximate analysis of strain concentration by notches and cracks". Journal of Applied Mechanics, Volume 35, pp. 379-386.

Rice, J.R. 1976. "Elastic-plastic fracture mechanics". In "The Mechanics of Fracture", A.M.D. Volume 19, A.S.M.E., New York, pp. 23-53.

Rice, J.R. and Cleary, M.P. 1976. "Some basic stress-diffusion solutions for fluid-saturated elastic porous media with compressible constituents". Reviews of Geophysics and Space Physics, Volume 14, No. 2, pp. 227-241.

Rice, J.R. and Simons, D.A. 1976. "The stabilization of spreading shear faults by coupled deformation-diffusion effects in fluid-infiltrated porous solids". Journal of Geophysical Research, Volume 81, No. B10, pp. 5322-5334.

Rice, J.R. and Rudnicki, J.W. 1979. "Earthquake precursory effects due to pore fluid stabilization of a weakened fault zone". Journal of Geophysical Research, Volume 84, No.B5, pp. 2177-2193.

Rice, J.R. and Rudnicki, J.W. 1980. "A note on some features of the theory of localization". International Journal of Solids and Structures, Volume 16, pp. 597-605.

Roscoe, K.H. 1970. "The influence of strains in Soil Mechanics". Tenth Rankine Lecture, Geotechnique, Volume 20, No. 2, pp. 129-180.

Roscoe, K.H., Bassett, R.H., and Cole, E.R.L. 1967. "Principal axes observed during simple shear of sand". Proceedings of the Geotechnical Conference, Oslo, Norwegian Geotechnical Institute, Volume 1, pp. 231-237.

Roscoe, K.H. and Burland, J.B. 1968. "On the generalized stress-strain behaviour of 'wet' clay", in "Engineering Plasticity", Heyman and Leckie eds., pp. 535-609.

Rowe, P.W. 1962. "The stress-dilatancy relation for static equilibrium of an assembly of particles in contact". Proceedings of the Royal Society of London, Volume 269 Series A, pp. 500-527.

Rowe, P.W. 1963. "Stress-dilatancy, earth pressures, and slopes". Journal of the Soil Mechanics and Foundations Division, A.S.C.E., Volume 89, No. SM3, pp. 37-61.

Rowe, P.W. 1969. "The relation between the shear strength of sands in triaxial compression, plane strain, and direct shear". Geotechnique, Volume 19, No. 1, pp. 75-86.

Rowe, P.W. 1972. "Theoretical meaning and observed values of deformation parameters in soil". Stress Strain Behaviour of Soil, R.H.G. Parry ed., Foulis and Company, London, pp. 143-194.

Rowe, P.W., Oates, D.B., and Skermer, N.A. 1963. "The stress-dilatancy performance of two clays". Laboratory Shear Testing of Soils, A.S.T.M. Special Technical Publication No. 361, pp. 134-143.

Rowe, P.W., Barden, L., and Lee, I.K. 1964. "Energy components during the triaxial cell and direct shear tests". Geotechnique, Volume 14, No. 3, pp. 247-261.

Rowe, R.K. and Davis, E.H. 1977. "Application of the finite element method to the prediction of collapse loads". Research Report R310, School of Civil Engineering, University of Sydney, 37 pp, 31 fig.

Rowe, R.K. and Pells, P.J.N. 1980. "A theoretical study of pile/rock socket interaction". Research Report R368, University of Sydney, School of Civil Engineering. 24 pp, 20 fig.

Rudnicki, J.W. 1977. "The inception of faulting in a rock mass with a weakened zone". Journal of Geophysical Research, Volume 82, No. B5, pp. 844-854. Corrections to some results given by Rice and Rudnicki (1979).

Rudnicki, J.W. and Rice, J.R. 1975. "Conditions for the localization of deformation in pressure-sensitive, dilatant materials". Journal of the Mechanics and Physics of Solids, Volume 23, pp. 371-394.

Sandhu, R.S. 1973. "Finite element analysis of stresses, deformations, and progressive failure of non-homogeneous fissured rock." Ohio State University Research Foundation, published as Report AD 768 648 by National Technical Information Service, Washington. 220 pp.

Sangha, C.M., Talbot, C.J., and Dhir, R.K. 1974. "Microfracturing of a sandstone in uniaxial compression". International Journal of Rock Mechanics and Mining Sciences and Geomechanics Abstracts, Volume 11, pp. 107-113.

Schofield, A.N. and Wroth, C.P. 1968. "Critical State Soil Mechanics". McGraw-Hill, London.

Shih, C.F., de Lorenzi, H.G., and German, M.D. 1976. "Crack extension modelling with singular quadratic isoparametric elements". International Journal of Fracture, Volume 12, pp. 647-651.

Sibson, R.H. 1981. "Controls on low-stress hydro-fracture dilatancy in thrust, wrench, and normal fault terrains". Nature, Volume 289, pp. 665-667.

Simmons, J.V. 1980a. Preliminary documentation for ESB programs: Elastoplastic finite element analysis with mesh plotting and partial generation aids. Department of Civil Engineering, University of Alberta, Edmonton, Alberta.

Simmons, J.V. 1980b. Preliminary documentation for NLCP programs: Nonlinear construction-style finite element analysis with data processing utilities. Department of Civil Engineering, University of Alberta, Edmonton, Alberta.

Skempton, A.W. 1964. "Long term stability of clay slopes". Geotechnique, Volume 14, Number 2, pp. 77-102.

Skempton, A.W. 1966. "Some observations on tectonic shear zones". Proceedings of the First Congress of the International Society for Rock Mechanics, Lisbon, Volume 1, pp. 329-335.

Skempton, A.W. 1970. "First-time slides in over-consolidated clays". Geotechnique, Volume 20, pp. 320-324.

Skermer, N.A. 1975. "Mica Dam Embankment Stress Analysis". Journal of the Geotechnical Engineering Division, A.S.C.E., Volume 101, Number GT3, March, pp. 229-242.

Smith, I.M. 1972. "Plane plastic deformation of soil". Stress Strain Behaviour of Soil, R.H.G. Parry ed., Foulis and Company, London, pp. 548-563.

Soriano, A., Duncan, J.M., Wong, K. and Simon, J.-M. 1976. "Finite Element Analyses of Stresses and Movements in Birch Dam". Contract Report S-76-2, U.S. Army Corps of Engineers, Waterways Experiment Station, Vicksburg, Mississippi, 100 pp.

Squier, L.R. 1970. "Load transfer in earth and rockfill dams". Journal of the Soil Mechanics and Foundations Division, A.S.C.E., Volume 96, Number SM1, pp. 213-233.

Stewart, R.A. 1979. "Pore Pressures in Earth Dams During Impounding". M.Sc. thesis, Department of Civil Engineering, University of Alberta, Edmonton, Alberta.

Stroud, M.A. 1971. "The Behaviour of Sand at Low Stress Levels in the Simple-Shear Apparatus". Ph.D. thesis, Cambridge University.

Stuart, W.D. 1979. "Strain softening prior to two-dimensional strike-slip earthquakes". Journal of Geophysical Research, Volume 84, No. B3, pp. 1063-1070.

Sture, S. 1976. "Strain Softening Behaviour of Geologic Materials and its Effect on Structural Response". Ph.D. thesis, University of Colorado at Boulder.

Sture, S. and Ko, H.-Y. 1978. "Strain-softening of brittle geologic materials". International Journal for Numerical and Analytical Methods in Geomechanics, Volume 2, pp. 237-253.

Tapponnier, P. and Brace, W.F. 1976. "Development of stress-induced microcracks in Westerly Granite". International Journal of Rock Mechanics and Mining Sciences and Geomechanics Abstracts, Volume 13, pp. 103-112.

Tada, H., Paris, P.C., and Irwin, G.R. 1973. "The Stress Analysis of Cracks Handbook". Del Research Corporation, Hellertown, Pennsylvania.

Taylor, D.W. 1948. "Fundamentals of Soil Mechanics". Wiley, New York.

Tchalenko, J.S. 1968. "The evolution of kink-bands and the development of compression textrures in sheared clays". Tectonophysics, Volume 6, pp. 159-174.

Tchalenko, J.S. 1970. "Similarities between shear zones of different magnitudes". Bulletin of the Geological Society of America, Volume 81, pp. 1625-1640.

Tchalenko, J.S. and Ambrayseys, N.N. 1970. "Structural analysis of the Dasht-e-Bayaz (Iran) earthquake fractures". Bulletin of the Geological Society of America, Volume 81, pp. 41-60.

Terzaghi, K. 1936. "Stability of slopes in natural clays". Proceedings of the First International Conference on Soil Mechanics and Foundation Engineering, Cambridge, Massachusetts, Volume 1, pp. 161-165.

Terzaghi, K. and Peck, R.B. 1948. "Soil Mechanics in Engineering Practice". Wiley and Sons, New York, First Edition.

Thornton, C. 1979. "The conditions for failure of a face-centred cubic array of uniform rigid spheres". Geotechnique, Volume 29, No. 4, pp. 441-459.

Thurber Consultants Limited, 1979. "Computer model for stress-strain analysis of oilsand". Report to Canadian Department of Energy, Mines, and Natural Resources.

Tracey, D.M. and Cook, T.S. 1977. "Analysis of power-type singularities using finite elements". International Journal for Numerical Methods in Engineering, Volume 11, pp. 1225-1233.

Trollope, D.H. 1968. "The mechanics of discontinua or clastic me problems". Chapter 9 of "Rock Mechanics in Engineering Practice", K.G. Stagg and O.C. Zienkiewicz, eds., Wiley, London, pp. 275-320.

Trollope, D.H. 1973. "Sequential failures in strain softening soils". Proceedings of the Eighth International Conference on Soil Mechanics and Foundation Engineering, Moscow, U.S.S.R., Paper 4/38, pp. 227-232.

Trollope, D.H. and Burman, B.C. 1980. "Physical and numerical experiments with granular wedges". Geotechnique, Volume 30, Number 1, pp. 137-157.

Tse, R. 1979. "Studies of the Strength of Rough Rock Surfaces in Direct Shear". M.Sc. thesis, Department of Civil Engineering, University of Alberta.

Vardoulakis, I., Goldscheider, M., and Gudehus, G. 1978. "Formation of shear bands in sand bodies as a bifurcation problem". International Journal for Numerical and Analytical Methods in Geomechanics, Volume

2, pp. 99-128.

Vermeer, P.A. 1980. "Formulation and Analysis of Sand Deformation Problems". Report Number 195, Geotechnical Laboratory, Department of Civil Engineering, Delft Institute of Technology, The Netherlands, 142pp.

Wong, K.S. 1978. "Elasto-Plastic Finite Element Analysis of Passive Earth Pressure Tests". Ph.D. thesis, Department of Civil Engineering, University of California, Berkeley. 373 pp.

Yamamoto, Y. and Tokuda, N. 1971. "A note on convergence of finite element solutions". International Journal for Numerical Methods in Engineering, Volume 3, pp. 485-493.

Zienkiewicz, O.C., Valliappan, S., and King, I.P. 1968. "Stress analyses of rock as a 'no tension' material". Geotechnique, Volume 18, No. 1, pp. 56-66.

Zienkiewicz, O.C., Best, B., Dullage, C. and Stagg, K.G. 1970. "Analysis of nonlinear problems in rock mechanics with particular reference to jointed rock systems". Proceedings of the Second Congress of the International Society for Rock Mechanics, Belgrade, Volume 3, pp. 501-509.

Zienkiewicz, O.C., Humpheson, C., and Lewis, R.W. 1975. "Associated and non-associated visco-plasticity and plasticity in soil mechanics". Geotechnique, Volume 25, No. 4, pp. 671-689.

APPENDIX A

One-Dimensional Strain-Weakening Progressive Failure Model
(CWX Model)

(Refer to Section 3.1 and Figure 3.4 of Text)

Symbols

σ = horizontal stress (uniform with depth)

δ = horizontal relative displacement
(position with respect to original position)

σ_i = initial horizontal stress

L = horizontal distance

τ = shear stress on shearband

A.1 Residual Zone (① to ②, Figure 3.4)

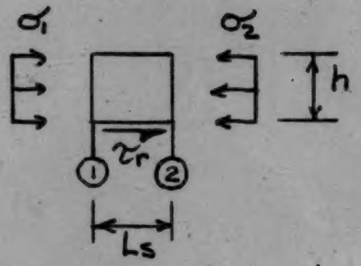

Equilibrium: $\tau_r L_s = h(\sigma_2 - \sigma_1)$ ....(A.1)

Alternatively, $\tau . dx = -h \frac{d\sigma}{dx} . dx$

ie $\frac{d\sigma}{dx} = -\frac{\tau}{h}$ ....(A.2)

here, $\tau \equiv \tau_r$

therefore $d\sigma = -\frac{\tau_r}{h} . dx$

integrating, $\sigma = C - \frac{\tau_r}{h} . x$

and $C = \sigma_1$

Therefore, (A.1) and (A.2) are equivalent

Consider deformations above shearband

$$\epsilon = \frac{d\delta}{dx}$$

and
$$\epsilon = -\frac{\Delta\sigma}{E} = (\sigma_i - \sigma)/E$$

Therefore
$$\frac{d\delta}{dx} = \frac{\sigma_i - \sigma}{E} \qquad \text{....(A.3)}$$

Now $$d\delta = \frac{1}{E}(\sigma_i\,dx - \sigma\,dx)$$
$$= \frac{1}{E}\left(\sigma_i\,dx - \left(-\frac{\tau_r}{h}x + \sigma_1\right)dx\right) \text{ from (A.2)}$$

ie $$d\delta = \frac{1}{E}\left(\sigma_i - \sigma_1 + \frac{\tau_r}{h}x\right)dx$$

Integrating,
$$\delta = \frac{1}{E}\int(\sigma_i - \sigma_1)\,dx + \frac{1}{E}\int\frac{\tau_r}{h}x.dx$$
$$= \frac{1}{E}\left[(\sigma_i - \sigma_1)x + \frac{\tau_r}{2h}x^2\right] + C$$

When $x = x_1 = 0$, $\delta = \delta_1$ and when $x = x_2$, $\delta = \delta_2$
Also, $x_2 = -L_s$, so substitution gives
$$\delta_2 = \frac{1}{E}\left[(\sigma_i - \sigma_1).-L_s + \frac{\tau_r}{2h}.L_s^2\right] + \delta_1$$

However, $\delta_2 = \delta_r$ and $L_s = \frac{h}{\tau_r}(\sigma_2 - \sigma_1)$ from (A.1)

Therefore $$\delta_1 = \delta_r + \frac{h(\sigma_2 - \sigma_1)}{E\,\tau_r}\left(\sigma_i - \left(\frac{\sigma_1 + \sigma_2}{2}\right)\right) \qquad \text{....(A.4)}$$

A.2 Post-Peak Zone (② to ③, Figure 3.4)

from (A.2) $$d\sigma = -\frac{\tau}{h}.dx$$

Now, $$\frac{\tau_p - \tau}{\tau_p - \tau_r} = \frac{\delta - \delta_p}{\delta_r - \delta_p}$$

giving
$$\left.\begin{aligned} \tau &= \tau_p - (\delta - \delta_p)R \\ \text{with}\quad R &= (\tau_p - \tau_r)/(\delta_r - \delta_p) \end{aligned}\right\} \qquad \text{....(A.5)}$$

Therefore $$\frac{d\sigma}{dx} = -\frac{\tau_p}{h} + (\delta - \delta_p)\frac{R}{h}$$

Combining with (A.3) in terms of dx,
$$(\delta - \delta_p)R\,d\delta - \tau_p\,d\delta = \frac{h}{E}(\sigma_i\,d\sigma - \sigma.d\sigma)$$

Integrating,
$$R\frac{\delta^2}{2} - R\delta_p\delta - \tau_p\delta = \frac{h}{E}\left(\sigma_i\sigma - \frac{\sigma^2}{2}\right) + C$$

When $x = x_3$, $\delta = \delta_p$ and $\sigma = \sigma_3$, therefore

$$\frac{R}{2}\delta_p^2 - (\tau_p + R\delta_p)\delta_p = \frac{h}{E}\left(\sigma_i\sigma_3 - \frac{\sigma_3^2}{2}\right) + C$$

which evaluates C

Substituting,

$$\frac{R}{2}(\delta^2 - \delta_p^2) - (\tau_p + R\delta_p)(\delta - \delta_p) = \frac{h}{E}\left(\sigma_i\sigma - \sigma_i\sigma_3 + \frac{\sigma_3^2}{2} - \frac{\sigma^2}{2}\right)$$

This may be rearranged as follows,

$$\sigma^2 - 2\sigma_i\sigma + A = 0 \qquad \text{.... (A.6)}$$

where

$$A = \frac{2E}{h}\left(\frac{R}{2}(\delta^2 - \delta_p^2) - (\tau_p + R\delta_p)(\delta - \delta_p)\right) + 2\sigma_i\sigma_3 - \sigma_3^2 \qquad \text{.... (A.7)}$$

The solution for (A.6) is

$$\sigma = \sigma_i \pm \sqrt{\sigma_i^2 - A} \qquad \text{.... (A.8)}$$

Section A.4 shows that this expression is always proper in the post-peak zone. The realistic root within the post-peak zone is

$$\sigma = \sigma_i - \sqrt{\sigma_i^2 - A} \qquad \text{.... (A.9)}$$

At ②, $\delta = \delta_r$ and $\sigma = \sigma_2$ giving

$$\sigma_2 = \sigma_i - \sqrt{\sigma_i^2 - A_2}$$

Substituting in (A.7) for the values at ②,

$$A_2 = \frac{2E}{h}\left[\frac{R}{2}(\delta_r^2 - \delta_p^2) - (\tau_p + R\delta_p)(\delta_r - \delta_p)\right] + 2\sigma_i\sigma_3 - \sigma_3^2$$

which after rearrangement and simplification gives

$$A_2 = -\frac{E}{h}(\tau_p + \tau_r)(\delta_r - \delta_p) + 2\sigma_i\sigma_3 - \sigma_3^2$$

Substituting for A_2 in the above then gives

$$\sigma'_2 = \sigma'_i - \sqrt{\frac{E}{h}(\tau_p+\tau_r)(\delta_r-\delta_p) + (\sigma'_i-\sigma'_3)^2} \quad \ldots (A.10)$$

A.3 Linear Zone (③ to ④, Figure 3.4)

From (A.2) $\quad d\sigma = -\frac{\tau}{h} \cdot dx$

Here, $\quad \tau = \frac{\tau_p}{\delta_p} \cdot \delta$

Therefore $\quad d\sigma = \frac{-\tau_p}{h\delta_p} \cdot \delta . dx$

Combining with (A.3) in terms of dx,

$$-\frac{h\delta_p}{\tau_p} \cdot \frac{d\sigma'}{\delta} = \frac{E\, d\delta}{\sigma'_i - \sigma'}$$

$$(\sigma'_i - \sigma')\, d\sigma' = -\frac{E}{h} \cdot \frac{\tau_p}{\delta_p} . \delta . d\delta$$

Integrating,

$$\left(\sigma'_i\sigma' - \frac{\sigma'^2}{2}\right) = \frac{-\tau_p E}{\delta_p h} \cdot \frac{\delta^2}{2} + \frac{c}{2}$$

When $\sigma' = \sigma'_i$, $\delta \Rightarrow 0$ and so

$$\sigma'^2_i - \frac{\sigma'^2_i}{2} = \frac{c}{2}, \quad \text{or} \quad c = \sigma'^2_i$$

Therefore $\quad \sigma'_i\sigma' - \frac{\sigma'^2}{2} = -\frac{\tau_p E}{\delta_p h} \cdot \frac{\delta^2}{2} + \frac{\sigma'^2_i}{2}$

or, $\quad -(\sigma'_i - \sigma')^2 = -\frac{\tau_p E}{\delta_p h} \cdot \delta^2$

and $\quad \delta\sqrt{\frac{\tau_p E}{\delta_p h}} = (\sigma'_i - \sigma') \quad \ldots (A.11)$

When $\delta = \delta_p$, $\sigma' = \sigma'_3$ and

$$\sigma'_3 = \sigma'_i - \sqrt{\frac{\tau_p \delta_p E}{h}} \quad \ldots (A.12)$$

Rearranging (A.12) gives

$$(\sigma_i - \sigma_3)^2 = \frac{\tau_p \delta_p E}{h}$$

Referring back to the Post-Peak Zone, (A.10) becomes

$$\sigma_2 = \sigma_i - \sqrt{\frac{E}{h}} \cdot \sqrt{\tau_p \delta_p + (\tau_p + \tau_r)(\delta_r - \delta_p)} \qquad \text{....(A.13)}$$

A.4 Proof that Equation (A.8) is always proper

Equation (A.8) $\sigma = \sigma_i \pm \sqrt{\sigma_i^2 - A}$

for this to be proper,

$$\sigma_i^2 \geqslant A$$

ie $\sigma_i^2 \geqslant \frac{2E}{h}\left[\frac{R}{2}(\delta^2 - \delta_p^2) - (\tau_p + R\delta_p)(\delta - \delta_p)\right] + 2\sigma_i\sigma_3 - \sigma_3^2$

ie $\sigma_i^2 \geqslant \frac{2E}{h}\left[\frac{R}{2}(\delta^2 - \delta_p^2) - (\tau_p + R\delta_p)(\delta - \delta_p)\right]$ ....(A.14)

At ③, $\delta = \delta_p$ and the RHS of (A.14) $\rightarrow 0$

Since $\sigma_i > \sigma_3$ the LHS > RHS for (A.14) at ③

At ②, $\delta = \delta_r$ and the RHS of (A.14) becomes

$$\text{RHS} = \frac{2E}{h}\left[\frac{1}{2}\left(\frac{\tau_p - \tau_r}{\delta_r - \delta_p}\right)(\delta_r^2 - \delta_p^2) - \left[\tau_p + \delta_p\left(\frac{\tau_p - \tau_r}{\delta_r - \delta_p}\right)\right](\delta_r - \delta_p)\right]$$

after extensive simplification, this becomes

RHS $= \frac{E}{h}(\tau_p + \tau_r)(\delta_p - \delta_r)$; that is, the RHS is always negative at ②.

It may also be deduced that the RHS must also be negative between ③ and ②. Since the LHS is always positive, then Equation (A.8) is always proper.

A.5 Displacements in the Post-Peak Zone (② to ③)

(A.3) gives $$\frac{d\delta}{dx} = \frac{\sigma_i' - \sigma'}{E}$$

(A.9) gives $$(\sigma_i' - \sigma') = \sqrt{\sigma_i'^2 - A}$$

Substituting for A from (A.6)

$$\frac{d\delta}{dx} = \frac{1}{E}\sqrt{\sigma_i' - 2\sigma_i'\sigma_3 + \sigma_3^2 - \frac{2E}{h}\left[\frac{R}{2}(\delta^2-\delta_p^2) - (\tau_p + R\delta_p)(\delta - \delta_p)\right]}$$

$$= \frac{1}{E}\sqrt{(\sigma_i' - \sigma_3')^2 - \frac{2E}{h}\left[\frac{R}{2}(\delta^2-\delta_p^2) - (\tau_p + R\delta_p)(\delta - \delta_p)\right.}$$

from (A.12)

$$(\sigma_i' - \sigma_3)^2 = \frac{\tau_p\delta_p E}{h}$$

so $$\frac{d\delta}{dx} = \frac{1}{E}\cdot\sqrt{\frac{E}{h}}\cdot\sqrt{\tau_p\delta_p - R\delta^2 + R\delta_p^2 + 2\tau_p\delta + 2R\delta_p\delta - 2\tau_p\delta_p - 2R\delta_p^2}$$

$$= \frac{1}{\sqrt{Eh}}\cdot\sqrt{-\delta_p(\tau_p + R\delta_p) + 2(\tau_p + R\delta_p)\delta - R\delta^2}$$

Let $C = (\tau_p + R\delta_p)$

so $$\frac{d\delta}{dx} = \frac{1}{\sqrt{Eh}}\cdot\sqrt{-C\delta_p + 2C\delta - R\delta^2}$$

or $$\frac{d\delta}{dx} = \sqrt{\frac{R}{Eh}}\cdot\sqrt{-\frac{C}{R}\delta_p + \frac{2C}{R}\delta - \delta^2} \qquad \text{....(A.14)}$$

Since $(\delta + a)^2 = \delta^2 + 2a\delta + a^2$ where "a" is as yet undefined

$-(\delta + a)^2 = -\delta^2 - 2a\delta - a^2$

Introducing a quantity "d" which is also yet to be defined,

$d^2 - (\delta + a)^2 = d^2 - a^2 - 2a\delta - \delta^2$

Compare this RHS with $\left(-\frac{C}{R}\delta_p + \frac{2C}{R}\delta - \delta^2\right)$

Clearly, $(d^2 - a^2) = -\frac{c}{R}\delta_p$ and $-2a = \frac{2c}{R}$

Therefore, $a = -\frac{c}{R}$ and $a^2 = \frac{c^2}{R^2}$

so that $d^2 = \frac{c^2}{R^2} - \frac{c}{R}\delta_p$

that is, $d^2 = \frac{c}{R}\left(\frac{c}{R} - \delta_p\right)$

Now (A.14) becomes

$$\frac{d\delta}{dx} = \sqrt{\frac{R}{Eh}} \cdot \sqrt{d^2 - (\delta + a)^2}$$

Replace δ by $s = \delta + a$

$$\frac{ds}{dx} = \frac{d\delta}{dx} \quad \text{and so}$$

$$\frac{ds}{dx} = \sqrt{\frac{R}{Eh}} \cdot \sqrt{d^2 - s^2}$$

$$\text{or,} \quad \frac{ds}{\sqrt{d^2 - s^2}} = \sqrt{\frac{R}{Eh}} \cdot dx$$

Integrating LHS (CRC Standard Math Tables, 23rd Ed., p.412)

$$\int \frac{ds}{\sqrt{d^2 - s^2}} = \sin^{-1}\frac{s}{|d|} \qquad (d^2 > s^2)$$

Integrating RHS

$$\int \sqrt{\frac{R}{Eh}} \cdot dx = \sqrt{\frac{R}{Eh}} \cdot x + K$$

Provided $d^2 > s^2$, therefore,

$$\sqrt{\frac{R}{Eh}} \cdot x + K = \sin^{-1}\frac{\delta + a}{|d|} \qquad \ldots\ldots (A.15)$$

$$a = -\frac{c}{R} \qquad = -\left(\frac{\tau_p}{R} + \delta_p\right)$$

$$|d| = \sqrt{\frac{c}{R}\left(\frac{c}{R} - \delta_p\right)} = \sqrt{\frac{\tau_p}{R}\left(\frac{\tau_p}{R} + \delta_p\right)}$$

Therefore $(\delta + a) \quad = \delta - \left(\delta_p + \frac{\tau_p}{R}\right)$

Since $\delta_p + \frac{\tau_p}{R} = \delta_a > \delta_r$, and $\delta_a \rightarrow \delta_r$ as $\tau_R \rightarrow 0$,

then $\sin^{-1}\frac{(\delta - \delta_a)}{|d|}$ is negative and is the same as $-\sin^{-1}\frac{(\delta_a - \delta)}{|d|}$

Equation (A.15) becomes

$$\sqrt{\frac{R}{Eh}} + K \quad = -\sin^{-1}\frac{\delta_a - \delta}{d}$$

($|d|$ can be replaced by d now)

It is known that when $x = x_3$, $\delta = \delta_p$

and when $x = x_2$, $\delta = \delta_r$

Therefore $\sqrt{\frac{R}{Eh}}\,(x_2 - x_3) \quad = \sin^{-1}\left(\frac{\delta_a - \delta_p}{d}\right) - \sin^{-1}\left(\frac{\delta_a - \delta_r}{d}\right)$

and, since $L_p = (x_2 - x_3)$, we obtain

$$\left.\begin{aligned} L_p &= \sqrt{\frac{Eh}{R}}\left[\sin^{-1}\left(\frac{\delta_a - \delta_p}{d}\right) - \sin^{-1}\left(\frac{\delta_a - \delta_r}{d}\right)\right] \\ \text{where } d &= \sqrt{\frac{\tau_p}{R}\left(\frac{\tau_p}{R} + \delta_p\right)} \\ \text{and } \delta_a &= \left(\frac{\tau_p}{R} + \delta_p\right) \end{aligned}\right\} \quad \ldots (A.16)$$

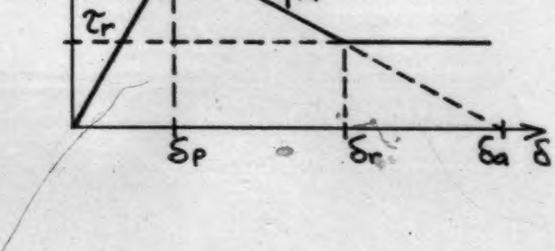

APPENDIX B

CRD (Constant-Rate-of-Dilation) Elastoplastic Model

(Refer to Section 3.3 and Figure 3.7 of Text)

B.1 Elastic Portion of Behaviour

Isotropic Elasticity $\dot{\underset{\sim}{\sigma}} = [D]\, \dot{\underset{\sim}{\epsilon}}^{E}$

in full,

$$\begin{Bmatrix} \dot{\sigma}_x \\ \dot{\sigma}_y \\ \dot{\tau}_{xy} \end{Bmatrix} = \begin{bmatrix} K+\frac{4G}{3} & K-\frac{2G}{3} & 0 \\ K-\frac{2G}{3} & K+\frac{4G}{3} & 0 \\ 0 & 0 & G \end{bmatrix} \begin{Bmatrix} \dot{\epsilon}_{xx} \\ \dot{\epsilon}_{yy} \\ \dot{\gamma}_{xy} \end{Bmatrix}^{E}$$

inverting,

$$\begin{Bmatrix} \dot{\epsilon}_{xx} \\ \dot{\epsilon}_{yy} \\ \dot{\gamma}_{xy} \end{Bmatrix}^{E} = \frac{3}{4G\,(G+3K)} \begin{bmatrix} K+\frac{4G}{3} & -(K-\frac{2G}{3}) & 0 \\ -(K-\frac{2G}{3}) & K+\frac{4G}{3} & 0 \\ 0 & 0 & \frac{4(G+3K)}{3} \end{bmatrix} \begin{Bmatrix} \dot{\sigma}_x \\ \dot{\sigma}_y \\ \dot{\tau}_{xy} \end{Bmatrix}$$

Here, the Bulk Modulus is $K = \frac{E}{3(1-2\nu)}$

the Shear Modulus is $G = \frac{E}{2(1+\nu)}$

the Young's Modulus is E

the Poisson's ratio is ν

B.2 Plastic Portion of Behaviour

Yield Function: $\tau = c + \sigma_n \tan\phi$ (Mohr-Coulomb)
(this assumes that σ_n is compressive)

A tension-positive sign convention is used herein.

Rewriting the yield function in terms of the principal stresses (with σ_1 being the most tensile, σ_3 the least tensile)

$$\frac{\sigma_1 - \sigma_3}{2} = c\cos\phi - \frac{\sigma_1 + \sigma_3}{2}\sin\phi \qquad \text{.....(B.1)}$$

From Figure 3.7B, the components of Equation (B.1) are

$$\frac{\sigma_1 - \sigma_3}{2} = \sqrt{\left(\frac{\sigma_x - \sigma_y}{2}\right)^2 + \tau_{xy}^{\;2}}$$

$$\frac{\sigma_1 + \sigma_3}{2} = \frac{\sigma_x + \sigma_y}{2}$$

Substituting in the yield function gives

$$\sqrt{\left(\frac{\sigma_x - \sigma_y}{2}\right)^2 + \tau_{xy}^2} = c.\cos\phi - \left(\frac{\sigma_x + \sigma_y}{2}\right)\sin\phi$$

Expanding this, we get the final form

$$\sigma_x^{\,2}(1-\sin^2\phi) + \sigma_y^{\,2}(1-\sin^2\phi) - 2\sigma_x\sigma_y(1+\sin^2\phi) + 4c(\sigma_x+\sigma_y)\sin\phi\cos\phi + 4\tau_{xy}^2 - 4c^2\cos^2\phi = 0$$

which is in the form

$$f(\sigma_x, \sigma_y, \tau_{xy}, c, \phi) = 0 \qquad \text{....(B.2)}$$

For yielding, $\dot{f} = 0$ implies $\frac{\partial f}{\partial \sigma_{ij}}\dot{\sigma}_{ij} = 0$

Here, $b_1\dot{\sigma}_x + b_2\dot{\sigma}_y + b_3\dot{\tau}_{xy} = 0$

or $\underset{\sim}{b}^T\dot{\underset{\sim}{\sigma}} = 0$ ....(B.3)

and

$$\left.\begin{aligned} b_1 &= 2\sigma_x(1-\sin^2\phi) - 2\sigma_y(1+\sin^2\phi) + 4c\sin\phi\cos\phi \\ b_2 &= 2\sigma_y(1-\sin^2\phi) - 2\sigma_x(1+\sin^2\phi) + 4c\sin\phi\cos\phi \\ b_3 &= 8\tau_{xy} \end{aligned}\right\} \qquad \text{....(B.4)}$$

Flow Rule: (i) Principal Axes of Stress and Strain Increment coincide

(ii) constant Dilatancy Rate $\dot{\epsilon}_v^p = D\dot{\gamma}_{max}^p$ (see Figure 3.7C)

Using global-axis strain increment components, and from the Mohr Circle of Strain Increments (Figure 3.7C)

$$\dot{\epsilon}^{P}_{XX} = \frac{D}{2}\dot{\gamma}^{P}_{max} + \frac{\dot{\gamma}^{P}_{max}}{2}\cos 2\beta = \frac{\dot{\gamma}^{P}_{max}}{2}\left(D + \cos 2\beta\right)$$

$$\dot{\epsilon}^{P}_{YY} = \frac{D}{2}\dot{\gamma}^{P}_{max} - \frac{\dot{\gamma}^{P}_{max}}{2}\cos 2\beta = \frac{\dot{\gamma}^{P}_{max}}{2}\left(D - \cos 2\beta\right)$$

$$\frac{\dot{\gamma}^{P}_{XY}}{2} = \frac{\dot{\gamma}^{P}_{max}}{2}\sin(-2\beta) = -\frac{\dot{\gamma}^{P}_{max}}{2}\sin 2\beta$$

The angles β and α coincide and may be interchanged.

From the Mohr Circle of Stress (Figure 3.7B)

$$\tan 2\alpha = -\tan(-2\alpha) = \frac{-2\tau_{XY}}{\sigma_X - \sigma_Y}$$

The radius of the Mohr Circle of Stress is

$$\tau_{max} = \sqrt{\left(\frac{\sigma_X - \sigma_Y}{2}\right)^2 + \tau_{XY}{}^2}$$

therefore

$$\cos 2\alpha = \frac{\sigma_X - \sigma_Y}{2\tau_{max}}$$

$$\sin 2\alpha = \frac{-\tau_{XY}}{\tau_{max}}$$

Substituting and rearranging,

$$\left.\begin{aligned} \begin{Bmatrix} \dot{\epsilon}^{P}_{XX} \\ \dot{\epsilon}^{P}_{YY} \\ \dot{\gamma}^{P}_{XY} \end{Bmatrix} &= \frac{\dot{\gamma}_{max}}{4\tau_{max}} \begin{bmatrix} \sigma_X - \sigma_Y + 2D\tau_{max} \\ -\sigma_X + \sigma_Y + 2D\tau_{max} \\ 4\tau_{XY} \end{bmatrix} \\ \text{or, } \quad \underset{\sim}{\dot{\epsilon}}^{P} &= g\,\underset{\sim}{a} \end{aligned}\right\} \quad \ldots (B.5)$$

B.3 Incremental Elastoplastic Response

$$\underset{\sim}{\dot{\epsilon}} = \underset{\sim}{\dot{\epsilon}}^{E} + \underset{\sim}{\dot{\epsilon}}^{P}$$

$$[D]\,\underset{\sim}{\dot{\epsilon}} = \underset{\sim}{\dot{\sigma}} + [D]\,\underset{\sim}{\dot{\epsilon}}^{P} \quad \text{(substituting elastic form)}$$

substituting from (B.5)

$$[D]\,\dot{\underset{\sim}{\epsilon}} = \dot{\underset{\sim}{\sigma}} + g\,[D]\,\underset{\sim}{a}$$

Premultiplying both sides by $\underset{\sim}{b}^T$ and observing Equation (B.3) gives

$$\underset{\sim}{b}^T[D]\,\dot{\underset{\sim}{\epsilon}} = g\,\underset{\sim}{b}^T[D]\,\underset{\sim}{a}$$

or,

$$g = \frac{\underset{\sim}{b}^T[D]\,\dot{\underset{\sim}{\epsilon}}}{\underset{\sim}{b}^T[D]\,\underset{\sim}{a}} \qquad \ldots.(B.6)$$

The parameter g can thus be calculated from the current stress state and the total strain increment.

g should equal $\dfrac{\dot{\gamma}^p_{max}}{4\tau_{max}}$ and be $\geqslant 0$, and if these conditions are satisfied the remaining parts of the increment can be accepted.

These are,

$$\dot{\underset{\sim}{\epsilon}}^p = g\,\underset{\sim}{a}$$

$$\dot{\underset{\sim}{\sigma}} = [D]\,(\dot{\underset{\sim}{\epsilon}} - \dot{\underset{\sim}{\epsilon}}^p) \qquad \ldots.(B.7)$$

B.4 Treatment of σ_θ in axisymmetric problems

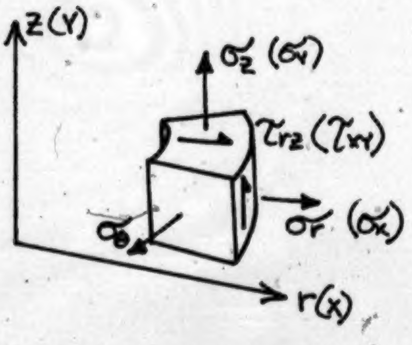

Assume $\Delta\sigma_\theta$ is an isotropic elastic response to $\Delta\sigma_z$, $\Delta\sigma_r$

$$\dot{\epsilon}_\theta = \frac{1}{E}\left(\dot{\sigma}_\theta - \nu(\dot{\sigma}_x + \dot{\sigma}_y)\right) \qquad \ldots.(B.8)$$

Assume $\dot{\epsilon}_\theta = 0$; not necessarily true but a simplification here,

Therefore $\dot{\sigma}_\theta = \nu(\dot{\sigma}_x + \dot{\sigma}_y) \qquad \ldots.(B.9)$

with $\nu = \dfrac{3K - 2G}{6K + 2G} \qquad \ldots.(B.10)$

APPENDIX C

SD (Stress-Dilatancy) Elastoplastic Model

(Refer to Section 3.4 and Figures 3.7, 3.8 of Text)

C.1 Elastic Portion of Behaviour

Same as for the CRD model, Appendix B

C.2 Plastic Portion of Behaviour

Stress - Dilatancy Formulation

Current Void Ratio e
Current Mean Principal Stress p

For current stress conditions, the maximum dilatancy rate is λ_{max} and for the current void ratio, the instantaneous dilatancy rate is

$$\left.\begin{aligned} \lambda = \frac{\dot{\varepsilon}_v^{\,p}}{\dot{\gamma}^{\,p}_{max}} &= \lambda_{max}\left(\frac{e_{max}-e}{e_{max}-e_{min}}\right)^{n} \\ &\text{for } e_{min} \leqslant e < e_{max} \\ &= 0 \\ &\text{for } e \geqslant e_{max} \end{aligned}\right\} \quad \ldots (C.1)$$

Here,

$$\left.\begin{aligned} \lambda_{max} &= \lambda_{max_0}\left(\frac{p-p_{cv}}{p_0-p_{cv}}\right)^{m} \\ &\text{for } 0 \geqslant p \geqslant p_{cv} \\ &= 0 \\ &\text{for } p \leqslant p_{cv} \end{aligned}\right\} \quad \ldots (C.2)$$

The parameters e_{max}, e_{min}, λ_{max_0}, p_0, p_{cv}, m, n, are used in the description of material response

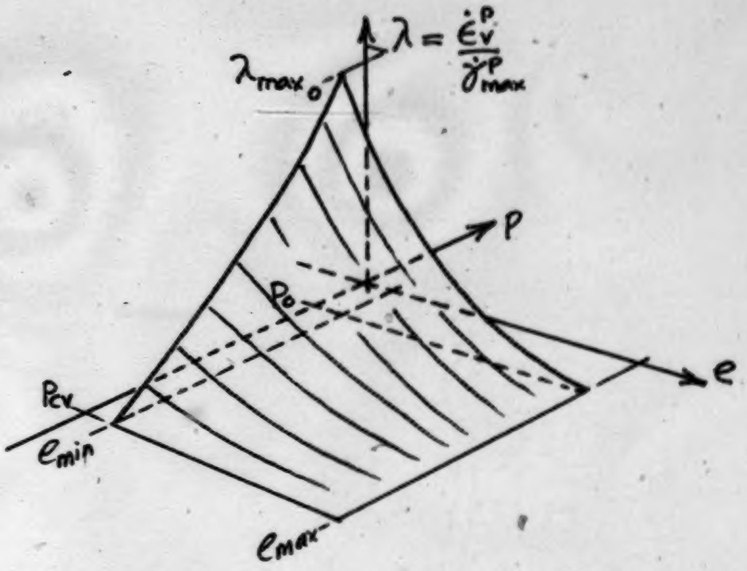

The Stress-Dilatancy relationship for plane strain is

$$R = D.K_{cv} \qquad \text{.... (C.3)}$$

where $K_{cv} = \tan^2(45 + \frac{\phi_{cv}}{2}) = \frac{1 + \sin\phi_{cv}}{1 - \sin\phi_{cv}}$

$$D = \frac{1+\lambda}{1-\lambda} \qquad (\lambda > 0)$$

$$= 1.0 \qquad (\lambda = 0)$$

Now $\quad R = \frac{\sigma_3'}{\sigma_1'}$ (tension-positive convention)

Therefore $\quad \sigma_3' = DK_{cv}\sigma_1'$ (from this point onwards, the primes on the stress components will be implied, though not written)

The Yield Function is $\sigma_3 = \frac{1+\lambda}{1-\lambda} K_{cv}\sigma_1$

$$\text{or,} \quad \sigma_3 - \lambda\sigma_3 - K_{cv}\sigma_1 - \lambda K_{cv}\sigma_1 = 0 \qquad \text{.... (C.4)}$$

For small increments,

$$\dot{\sigma}_3 - \dot{\lambda}\sigma_3 - \lambda\dot{\sigma}_3 - K_{cv}\dot{\sigma}_1 - \dot{\lambda}K_{cv}\sigma_1 - \lambda K_{cv}\dot{\sigma}_1 = 0$$

$$\text{ie,} \quad \dot{\sigma}_3(1-\lambda) - \dot{\sigma}_1 K_{cv}(1+\lambda) - \dot{\lambda}(\sigma_3 + K_{cv}\sigma_1) = 0 \qquad \text{.... (C.5)}$$

Equation (C.5) has to be expressed in terms of cartesian stress components and strain changes

$$\dot{\lambda} = \frac{d\lambda}{de} \cdot \dot{e} \quad \text{(ignore effects of changes in p)}$$

$$\dot{e} = \dot{\epsilon}_v (1+e_0)$$

and $$\dot{\epsilon}_v^p = \lambda \dot{\gamma}^p_{max}$$

Assume that plastic strains dominate the strain increment, so that $\dot{\epsilon}_v \doteqdot \dot{\epsilon}_v^p$

Then, $$\dot{\lambda} = \frac{d\lambda}{de} (1+e_0) \lambda \dot{\gamma}^p_{max}$$

also, $$\sigma_1 = \frac{\sigma_x + \sigma_y}{2} + \tau_{max}$$

$$\sigma_3 = \frac{\sigma_x + \sigma_y}{2} - \tau_{max}$$

$$\sigma_3 / \sigma_1 = R$$

Substituting for these terms and their derivatives gives

$$(1-\lambda)\left[\frac{\dot{\sigma}_x + \dot{\sigma}_y}{2} - \tau_{max}\right] - K_{cv}(1+\lambda)\left[\frac{\dot{\sigma}_x + \dot{\sigma}_y}{2} + \tau_{max}\right] - \dot{\lambda}(\sigma_3 + K_{cv}\sigma_1) = 0$$

After rearrangement, this gives

$$\dot{\sigma}_x (1-R) + \dot{\sigma}_y (1-R) - 2\tau_{max}(1+R) - \frac{2\lambda}{1-\lambda} \cdot \frac{d\lambda}{de} (1+e_0) \dot{\gamma}^p_{max} (\sigma_3 + K_{cv}\sigma_1) = 0 \quad \ldots .(C.6)$$

Now reduce $\dot{\tau}_{max}$, $\tau_{max} = \sqrt{U}$ therefore $\dot{\tau}_{max} = \frac{1}{2\sqrt{U}} \dot{U}$

$$\dot{\tau}_{max} = \frac{1}{2\tau_{max}} \Delta \left[\left(\frac{\sigma_x - \sigma_y}{2}\right)^2 + \tau_{xy}^2\right]$$

where Δ is an operator

This gives $$-2(1+R)\dot{\tau}_{max} = \frac{-(1+R)}{2\tau_{max}} (\sigma_x - \sigma_y)(\dot{\sigma}_x - \dot{\sigma}_y) - \frac{2(1+R)}{\tau_{max}} \tau_{xy} \dot{\tau}_{xy}$$

which can be substituted in Equation (C.6) to give

$$\dot{\sigma}_x\left[(1-R)-\frac{(1+R)}{2\tau_{max}}(\sigma_x-\sigma_y)\right] + \dot{\sigma}_y\left[(1-R)+\frac{(1+R)}{2\tau_{max}}(\sigma_x-\sigma_y)\right]$$

$$+\dot{\tau}_{xy}\left[\frac{-2(1+R)}{\tau_{max}}\tau_{xy}\right] = \frac{2\lambda}{(1-\lambda)}\cdot\frac{d\lambda}{de}(1+e_0)(\sigma_3+K_{cv}\sigma_1)\,\dot{\gamma}^p_{max} \quad \ldots.(C.7)$$

Let

$$Q = \left(\frac{1+R}{2\tau_{max}}\right) \quad \ldots.(C.8)$$

$$S = \frac{2\lambda}{(1-\lambda)}\,\frac{d\lambda}{de}(1+e_0)(\sigma_3+K_{cv}\sigma_1) \quad \ldots.(C.9)$$

Equation (C.7) becomes

$$\dot{\sigma}_x\left[(1-R)-Q(\sigma_x-\sigma_y)\right] + \dot{\sigma}_y\left[(1-R)+Q(\sigma_x-\sigma_y)\right] + \dot{\tau}_{xy}\left[-4Q\tau_{xy}\right]$$

$$= S\dot{\gamma}^p_{max} \quad \ldots.(C.10)$$

That is, $\langle b_1\ b_2\ b_3\rangle\dot{\underset{\sim}{\sigma}} = S\dot{\gamma}^p_{max}$ as required

Here,

$$b_1 = 1-R-Q(\sigma_x-\sigma_y)$$

$$b_2 = 1-R+Q(\sigma_x-\sigma_y)$$

$$b_3 = -4Q\tau_{xy}$$

$$\tau_{max} = \sqrt{\left(\frac{\sigma_x-\sigma_y}{2}\right)^2+\tau_{xy}^2}$$

These provide the required yield function relationship.

Flow Rule : The instantaneous dilatancy rate $\lambda = \frac{\dot{\epsilon}^p_v}{\dot{\gamma}^p_{max}}$ can be obtained from the current void ratio. The rest of the formulation follows that for the CRD model material. Equation (B.5) becomes

$$\left.\begin{aligned}&\begin{Bmatrix}\dot{\epsilon}^p_{xx}\\ \dot{\epsilon}^p_{yy}\\ \dot{\gamma}^p_{xy}\end{Bmatrix} = \frac{\dot{\gamma}^p_{max}}{4\tau_{max}}\begin{Bmatrix}\sigma_x-\sigma_y+2\lambda\tau_{max}\\ -\sigma_x+\sigma_y+2\lambda\tau_{max}\\ 4\tau_{xy}\end{Bmatrix}\\ &\text{or, } \dot{\underset{\sim}{\epsilon}}^p = g\underset{\sim}{a}\end{aligned}\right\} \quad \ldots.(C.11)$$

C.3 Incremental Elastoplastic Response

$$\begin{aligned}
\dot{\underset{\sim}{\epsilon}} &= \dot{\underset{\sim}{\epsilon}}^{E} + \dot{\underset{\sim}{\epsilon}}^{P} \\
[D]\,\dot{\underset{\sim}{\epsilon}} &= \dot{\underset{\sim}{\sigma}} + [D]\,\dot{\underset{\sim}{\epsilon}}^{P} \\
&= \dot{\underset{\sim}{\sigma}} + g[D]\,\underset{\sim}{a}
\end{aligned}$$

Premultiplying by $\underset{\sim}{b}^T$ gives

$$\underset{\sim}{b}^T[D]\dot{\underset{\sim}{\epsilon}} = S\dot{\gamma}^{P}_{max} + g\,\underset{\sim}{b}^T[D]\underset{\sim}{a}$$

or,
$$g = \frac{\underset{\sim}{b}^T[D]\dot{\underset{\sim}{\epsilon}} - S\dot{\gamma}^{P}_{max}}{\underset{\sim}{b}^T[D]\underset{\sim}{a}} \qquad \ldots.(C.12)$$

Equation (C.12) requires an iterative solution since $\dot{\gamma}^{P}_{max}$ is not known in advance. Several approximate starting procedures can be used:

(a) start with $\dot{\gamma}^{P}_{max} = 0$ and iterate
(b) start with $\dot{\gamma}^{P}_{max} = \dot{\gamma}_{max}$ and iterate
(c) assume that $\dot{\gamma}^{P}_{max} = \dot{\gamma}_{max}$, no iteration.

The performance of the model has been found to be insensitive to the procedure used, and (c) was adopted.

Once (C.12) is evaluated, equation (B.7) applies.

For axisymmetric analysis, similar assumptions were made for $\dot{\sigma}_\theta$.

APPENDIX D

PPP (Post-Peak-Plasticity) Elastoplastic Model

(Refer to Section 3.5 and Figures 3.7, 3.11 of Text)

D.1 Elastic Portion of Behaviour

Same as for the CRD model, Appendix B

D.2 Plastic Portion of Behaviour

Plastic behaviour consists of two phases

(a) Peak-Residual Transition, $0 < \gamma^p_{max} < GPR$

(b) Residual Strength, $\gamma^p_{max} \geq GPR$

Residual Strength Behaviour

This is the same as for the CRD model, with the following parameters:

$$\left.\begin{aligned} c &= c_r \\ \phi &= \phi_r \\ D &= \frac{\dot{\epsilon}^p_v}{\dot{\gamma}^p_{max}} = 0 \end{aligned}\right\} \quad \ldots.(D.1)$$

Peak-Residual Transition

Accumulated Plastic Shear Strain $GPT = \Sigma\, \dot{\gamma}^p_{max}$;

Shear Strain for Peak-Residual Transition GPR ;

Derivable Strength Index

$$DSI = \left(1 - \frac{GPT}{GPR}\right)^{DSIX} \quad \ldots.(D.2)$$

where DSIX is a suitable exponent ;

Instantaneous Strength

$$\left.\begin{aligned} c &= c_r + DSI\,(c_p - c_r) \\ \phi &= \phi_r + DSI\,(\phi_p - \phi_r) \end{aligned}\right\} \ldots.(D.3)$$

Instantaneous Dilatancy Rate

$$D = DSI \cdot D_p \qquad \text{....(D.4)}$$

Instantaneous Tensile Strength

$$tenst = DSI \cdot t_p \qquad \text{....(D.5)}$$

Yield Function:

$$\frac{\partial f}{\partial \sigma_{ij}} \dot{\sigma}_{ij} + \frac{\partial f}{\partial c} \dot{c} + \frac{\partial f}{\partial \phi} \dot{\phi} = 0$$

$$\text{thus} \quad \langle b_1 \; b_2 \; b_3 \rangle \dot{\underset{\sim}{\sigma}} = b_4 \dot{c} + b_5 \dot{\phi} \qquad \text{....(D.6)}$$

The yield function is given by Equation (B.2), Appendix B, so using the instantaneous values of c and ∅ gives

$$\left.\begin{aligned} b_1 &= 2\sigma'_x (1 - \sin^2\phi) - 2\sigma'_y (1 + \sin^2\phi) + 4c \cos\phi \sin\phi \\ b_2 &= -2\sigma'_x (1 + \sin^2\phi) + 2\sigma'_y (1 - \sin^2\phi) + 4c \cos\phi \sin\phi \\ b_3 &= 8 \tau_{xy} \end{aligned}\right\}$$

....(D.7)

$$b_4 = -\frac{\partial f}{\partial c} = 4(\sigma'_x + \sigma'_y) \sin\phi \cos\phi - 8c \cos^2\phi \qquad \text{....(D.8)}$$

$$\begin{aligned} b_5 = -\frac{\partial f}{\partial \phi} &= 2 \sin\phi \cos\phi ({\sigma'_x}^2 + {\sigma'_y}^2 + 2\sigma'_x \sigma'_y - 4c^2) \\ &\quad + 4c(\sigma'_x + \sigma'_y)(\sin^2\phi - \cos^2\phi) \qquad \text{....(D.9)} \end{aligned}$$

The changes in c and ∅ are, from Equation (D.3),

$$\left.\begin{aligned} \dot{c} &= \dot{DSI}\,(c_p - c_r) \\ \dot{\phi} &= \dot{DSI}\,(\phi_p - \phi_r) \end{aligned}\right\} \qquad \text{....(D.10)}$$

Now $\dot{DSI} = \Delta(U)^{DSIX}$ where $U = 1 - \frac{GPT}{GPR}$

and Δ is an operator

Therefore,

$$\dot{DSI} = -\frac{DSIX}{GPR}\left(1 - \frac{GPT}{GPR}\right)^{(DSIX-1)} \dot{\gamma}^{p}_{max} \qquad \text{...(D.11)}$$

D.3 Incremental Elastoplastic Response

Residual Strength Behaviour

This is the same as for the CRD model, with the parameters given in Equation (D.1)

Peak – Residual Transition

$$\begin{aligned}
\dot{\underset{\sim}{\epsilon}} &= \dot{\underset{\sim}{\epsilon}}^{E} + \dot{\underset{\sim}{\epsilon}}^{P} \\
[D]\,\dot{\underset{\sim}{\epsilon}} &= \dot{\underset{\sim}{\sigma}} + [D]\,\dot{\underset{\sim}{\epsilon}}^{P} \\
\underset{\sim}{b}^{T}[D]\,\dot{\underset{\sim}{\epsilon}} &= b_4\dot{c} + b_5\dot{\phi} + g\,\underset{\sim}{b}^{T}[D]\,\underset{\sim}{a}
\end{aligned}$$

from which $$g = \frac{\underset{\sim}{b}^{T}[D]\,\dot{\underset{\sim}{\epsilon}} - (b_4\dot{c} + b_5\dot{\phi})}{\underset{\sim}{b}^{T}[D]\,\underset{\sim}{a}} \qquad \ldots(D.12)$$

Here, the equation for g is a function of the unknown value $\dot{\gamma}^{p}_{max}$. An iterative procedure was used to calculate $\dot{\gamma}^{p}_{max}$ by initially assuming $\dot{\gamma}^{p}_{max} = \dot{\gamma}_{max}$.

Once (C.12) is evaluated, equation (B.7) applies.

For axisymmetric analysis, similar assumptions were made for $\dot{\sigma}_{\theta}$.